



UNIVERSIDADE ESTADUAL DE CAMPINAS
Faculdade de Engenharia Elétrica e de Computação

Denis Gustavo Fantinato

**New Methods for Adaptive Equalization
Based on Information Theoretic Learning**

*Novas Metodologias de Aprendizado
Baseado na Teoria da Informação
para Equalização Adaptativa*

Campinas
2017

Denis Gustavo Fantinato

**New Methods for Adaptive Equalization
Based on Information Theoretic Learning**

*Novas Metodologias de Aprendizado Baseado na
Teoria da Informação para Equalização Adaptativa*

Thesis presented to the School of Electrical and Computer Engineering of the University of Campinas in partial fulfillment of the requirements for the degree of Doctor in Electrical Engineering, in the area of Computer Engineering.

Tese apresentada à Faculdade de Engenharia Elétrica e de Computação da Universidade Estadual de Campinas como parte dos requisitos exigidos para a obtenção do título de Doutor em Engenharia Elétrica, na Área de Engenharia de Computação.

Supervisor/*Orientador*: Prof. Dr. Romis Ribeiro de Faissol Attux

Co-Supervisor/*Co-orientadora*: Profa. Dra. Aline de Oliveira Neves Panazio

Este exemplar corresponde à versão final da tese defendida pelo aluno Denis Gustavo Fantinato, e orientada pelo Prof. Dr. Romis Ribeiro de Faissol Attux

Ficha catalográfica
Universidade Estadual de Campinas
Biblioteca da Área de Engenharia e Arquitetura
Luciana Pietrosanto Milla - CRB 8/8129

F218n Fantinato, Denis Gustavo, 1985-
New methods for adaptive equalization based on Information Theoretic Learning / Denis Gustavo Fantinato. – Campinas, SP : [s.n.], 2017.

Orientador: Romis Ribeiro de Faissol Attux.
Coorientador: Aline de Oliveira Neves Panazio.
Tese (doutorado) – Universidade Estadual de Campinas, Faculdade de Engenharia Elétrica e de Computação.

1. Processamento de sinais. 2. Aprendizado de máquina. 3. Teoria da informação. I. Attux, Romis Ribeiro de Faissol, 1978-. II. Panazio, Aline de Oliveira Neves. III. Universidade Estadual de Campinas. Faculdade de Engenharia Elétrica e de Computação. IV. Título.

Informações para Biblioteca Digital

Título em outro idioma: Novas metodologias de aprendizado baseado na Teoria da Informação para equalização adaptativa

Palavras-chave em inglês:

Signal processing

Machine learning

Information theory

Área de concentração: Engenharia de Computação

Titulação: Doutor em Engenharia Elétrica

Banca examinadora:

Romis Ribeiro de Faissol Attux [Orientador]

Magno Teófilo Madeira da Silva

Charles Casimiro Cavalcante

João Marcos Travassos Romano

Rafael Ferrari

Data de defesa: 31-03-2017

Programa de Pós-Graduação: Engenharia Elétrica

COMISSÃO JULGADORA - TESE DE DOUTORADO

Candidato: Denis Gustavo Fantinato - RA: 060111

Data da Defesa: 31 de março de 2017

Título da Tese: “Novas Metodologias de Aprendizado Baseado na Teoria da Informação para Equalização Adaptativa”

Prof. Dr. Romis Ribeiro de Faissol Attux (Presidente, FEEC/UNICAMP)

Prof. Dr. Magno Teófilo Madeira da Silva (EP/USP)

Prof. Dr. Charles Casimiro Cavalcante (GTEL/UFC)

Prof. Dr. João Marcos Travassos Romano (FEEC/UNICAMP)

Prof. Dr. Rafael Ferrari (FEEC/UNICAMP)

A ata de defesa, com as respectivas assinaturas dos membros da Comissão Julgadora, encontra-se no processo de vida acadêmica do aluno.

*To my beloved fiancée, Raíssa,
To my admired parents, Célia and Wanderlei,
and to my favorite sister, Debora.*

Acknowledgements

First and foremost, I would like to thank God, to whom I owe everything.

Secondly, I would like to enormously thank my parents, Célia and Wanderlei, for their unconditional support during my Ph. D.; together with my sister, Debora, they provided the love, affection and tranquility necessary for all decisions I take.

I am thankful to my beloved fiancée, Raíssa, for having accepted to follow this journey together with me; for the love and happiness that you always give me.

I am very grateful to Romis, who is an exceptional supervisor and friend. With great kindness, patience, commitment and competence, he has been during my entire academic life an excellent professor example that I wish to follow in my career.

To my co-supervisor Aline, for the guidance, patience and friendship. Although relatively far, she was always present for positive discussions and, mainly, to motivate the continuity of our work.

Thanks to the committee members, Prof. Magno Silva, Prof. Charles Cavalcante, Prof. João Marcos and Prof. Rafael Ferrari, for their valuable suggestions that enormously contributed to the improvement of this manuscript.

I am also grateful to all my colleagues and friends of DSPCom laboratory for all interesting discussions: Marcos, Michele, Viking, Gaúcho, Cássio, Sergio, Bulhões, Luisa, Zanetti, Delai, T. Novaes, Patrick, Vinícius, Monacér and David; and the (not so) recent professors: Gremista, Levy, Daniel, T., Kazuo, Krummen, Sarah, Kenji, Marco and Suyama.

I owe great thanks for Prof. Christian Jutten and Prof. Bertrand for kindly receiving me in their research group at GIPSA-lab; for the indispensable support of Prof. Leonardo Tomazeli and for the friendship of Fardin, Bahram, Rafael Assato, Georges and Anton.

Thanks to Celi, Noêmia, Camila and the employees of FEEC for the direct and indirect support.

Finally, thanks to FAPESP for the financial support during the regular Ph. D. period and to the BEPE-FAPESP program that allowed my Ph. D. sandwich at GIPSA-lab.

“Le savant n’étudie pas la nature
parce que cela est utile;
il l’étudie parce qu’il y prend plaisir
et il y prend plaisir parce qu’elle est belle.
Si la nature n’était pas belle,
elle ne vaudrait pas la peine d’être connue, la vie
ne vaudrait pas la peine d’être vécue”

Henri Poincaré, “Science et méthode”

Abstract

In signal processing, statistically dependent signals carry valuable information to solve problems of various natures. Based on the classical second-order statistical framework, however, their statistical characterization is limited to a certain degree of partiality. In view of this, in this work, a more extensive extraction of the information regarding statistical dependence is proposed via the use of methods based on Information Theoretic Learning (ITL) allied to a multivariate perspective.

Focusing on the statistical temporal dependence, this approach is applied to three important problems within the signal processing area: blind channel equalization with temporally-structured sources, supervised equalization using Infinite Impulse Response (IIR) filters, and nonlinear Blind Source Separation (BSS) problems. In each case, the results led to relevant contributions, including the extension of the ITL paradigm to the multivariate perspective and also to the use of metaheuristics as optimization strategies, instead of the traditional gradient-based methods.

The developed study opens new possibilities for the statistical processing of videos, images and speech data in complex scenarios; in communications, it becomes possible to deal with messages subject to statistically dependent coding schemes.

Keywords: Information Theoretic Learning, Temporal Structured Data, Channel Equalization, Blind Source Separation, Infinite Impulse Response Filters, Post-Nonlinear Mixtures.

Resumo

Sinais dotados de dependência estatística portam informações relevantes para a solução de problemas no contexto de processamento de sinais. Porém, de acordo com o ferramental clássico baseado em estatísticas de segunda ordem, a caracterização probabilística desses sinais é limitada a certo grau de parcialidade. Tendo isso em vista, propõe-se nesta tese de doutorado a extração mais extensiva da informação sobre a dependência estatística, sendo utilizadas para isto as metodologias de Aprendizado Baseado na Teoria da Informação (ITL, do inglês *Information Theoretic Learning*) combinadas a uma perspectiva multivariada dos dados.

Com particular interesse na dependência estatística temporal, esta abordagem é aplicada em três relevantes problemas dentro da área de processamento de sinais: equalização cega de canais com fontes dotadas de estrutura temporal, equalização supervisionada com filtros de Resposta ao Impulso Infinita (IIR, do inglês *Infinite Impulse Response*) e Separação Cega de Fontes (BSS, do inglês *Blind Source Separation*) no contexto não linear. Em cada caso, os resultados levaram a relevantes contribuições, incluindo a extensão do paradigma de ITL para a perspectiva multivariada e o uso de metaheurísticas como estratégia de otimização em vez dos tradicionais métodos baseados no gradiente.

O estudo desenvolvido abre novas possibilidades para o processamento estatístico de vídeos, imagens e dados de fala em cenários complexos; no contexto de comunicações, torna-se possível lidar com mensagens sujeitas a esquemas de codificação com dependência estatística.

Palavras-chave: Aprendizado Baseado na Teoria da Informação, Dados Dotados de Estrutura Temporal, Equalização de Canais, Separação Cega de Fontes, Filtros com Resposta ao Impulso Infinita, Modelo de Misturas Post-Nonlinear.

List of Figures

1.1	Triad of fundamental elements in signal processing problems.	30
1.2	Diagram of a general filtering structure.	31
1.3	Finite impulse response filter.	32
1.4	FIR filter block.	33
1.5	Infinite impulse response filter.	34
1.6	Stability regions for IIR filters.	35
1.7	Radial-Basis Function Network.	37
4.1	Block diagram of a communication system.	61
4.2	Equation-error formulation - Copy operation.	69
4.3	Output-error formulation - Simplified gradient components.	72
4.4	Mixing and separating systems in the PNL model.	85
5.1	Block diagram of the communication system assumed in the classical theorem.	91
5.2	Non- <i>i.i.d.</i> source as the result of a filtering process over an <i>i.i.d.</i> signal.	95
5.3	Source with temporal structure: Communication system block diagram.	95
5.4	Distribution of $p_S(v)$ for pre-coder $P(z)$	99
5.5	Source distribution for pre-coder with $L_c = 2$	103
5.6	System of equations - Intersection.	106
5.7	Cross-kurtosis for colored Gaussian Source.	112
5.8	Scenario 1 - Solutions for FIR $C(z)$ - BGR theorem extensions.	116
5.9	Scenario 1 - Contours for covariance and cross-kurtosis matching - Solutions for FIR $C(z)$	116
5.10	Scenario 1 - Solutions for IIR $C(z)$ - BGR theorem extensions.	117
5.11	Scenario 1 - Contours for covariance and cross-kurtosis matching - Solutions for IIR $C(z)$	118
5.12	Scenario 2 - Solutions for FIR $C(z)$ - BGR theorem extensions.	119
5.13	Scenario 2 - Contours for covariance and cross-kurtosis matching - Solutions for FIR $C(z)$	120

5.14	Scenario 2 - Solutions for IIR $C(z)$ - BGR theorem extensions.	120
5.15	Scenario 2 - Contours for covariance and cross-kurtosis matching - Solutions for IIR $C(z)$	121
6.1	Block diagram of a communication system with non- <i>i.i.d.</i> source.	124
6.2	Integration of the joint PDF over the plane.	125
6.3	Scenario 1 - PMF of the <i>i.i.d.</i> and pre-coded signal.	139
6.4	Scenario 1 - Analytical instances associated with the source s_n	139
6.5	Scenario 1 - Cost values: $N_s \times M$	140
6.6	Histogram of the noisy samples of s_n	141
6.7	Scenario 1 - Cost values: $N_s \times M$ for noisy samples (SNR 5 dB).	142
6.8	Scenario 2 - Histograms of the PDFs of the <i>i.i.d.</i> and pre-coded signal. . .	143
6.9	Scenario 2 - Analytical instances associated with the source s_n	144
6.10	Scenario 2 - Cost values: $N_s \times M$	145
6.11	Scenario 2 - Cost values: $N_s \times M$ for noisy samples (SNR 5 dB).	146
6.12	Scenario 1 - Cost values: $\sigma \times N_s$ and $M = 2$, with and without noise. . . .	148
6.13	Scenario 1 - \hat{J}_{MQD-D} in function of σ (SNR of 5 dB).	148
6.14	Scenario 1 - Cost values: $\sigma \times M$ and $N_s = 200$, with and without noise. . .	149
6.15	Scenario 2 - Cost values: $\sigma \times N_s$ and $M = 2$, with and without noise. . . .	150
6.16	Scenario 2 - \hat{J}_{MQD-C} in function of σ	151
6.17	Scenario 2 - Cost values: $\sigma \times M$ and $N_s = 200$, with and without noise. . .	151
6.18	Measured values for QISI and HISI.	154
6.19	Eye diagram for the optimal cases of QISI and of HISI.	155
6.20	Cost Surface - Scenario 1: Analytical instances associated with the source s_n	156
6.21	Cost Surface - Scenario 1: Surface contours for $M = 1$ and $M = 2$	157
6.22	Cost Surface - Scenario 1: \hat{J}_{cor} and \hat{J}_{MQD-D} costs for $M = 2$ and $\sigma = 0.3$. .	158
6.23	Cost Surface - Scenario 2: Analytical instances associated with the source s_n	160
6.24	Cost Surface - Scenario 2: Surface contours for $M = 1$ and $M = 2$	161
6.25	Costs Surfaces - Scenario 3: Source distribution and its estimation from samples.	163
6.26	Cost Surfaces - Scenario 3: Estimation of the source statistics.	163
6.27	Cost Surface - Scenario 3: Surface contours for $M = 1$ and $M = 2$	164
6.28	Discrete Sources - Scenario 1 - Mean HISI/QISI performance for the best solution found by the DE.	167
6.29	Discrete Sources - Scenario 1 - Algorithms QISI performance for $M = 1$ and $M = 2$	168
6.30	Adaptive kernel size σ	169

6.31	Discrete Sources - Scenario 1 - Algorithms QISI performance for varying σ and for $M = 1$ and $M = 2$	169
6.32	QISI x SNR - Gaussian and impulsive noise ($M = 4$).	170
6.33	Discrete Sources - Scenario 2 - IIR equalizer.	171
6.34	Continuous Sources - Scenario 1: Laplacian source.	173
6.35	Continuous Sources - Scenario 1: Algorithms QISI performance for $M = 1$ and $M = 2$	174
6.36	Continuous Sources: Algorithms QISI performance for varying σ and for $M = 1$ and $M = 2$	174
6.37	Laplacian Source: IIR equalizer.	175
6.38	Image processing: (a) original; (b) received; recovered by (c) the CR, (d) the MCK, (e) the correntropy-based and (f) the MQD-C approach.	176
6.39	Image processing: Estimation of the source statistics.	177
7.1	Block diagram of a communication system with an IIR equalizer.	182
7.2	Equation-Error Formulation - Scenario 1 - MSEE Surface contours.	193
7.3	Equation-Error Formulation - Scenario 1 - ITL costs surface contours for $\sigma = 3$, $M = 0$ and SNR of 10 dB.	193
7.4	Equation-Error Formulation - Scenario 1: ITL costs surface contours for $\sigma = 0.7$, $M = 0$ and SNR of 10 dB.	194
7.5	Equation-Error Formulation - Scenario 1: ITL costs surface contours for $\sigma = 0.7$, $M = 2$ and SNR of 10 dB.	195
7.6	Equation-Error Formulation - Scenario 1: QISI Performance of the LMS-based algorithms for $M = 0$ and $M = 2$ and SNR of 10 dB.	196
7.7	Equation-Error Formulation - Scenario 1: QISI Performance σ sweep.	197
7.8	Equation Error - Scenario 1: QISI \times SNR ($M = 0$).	197
7.9	Equation-Error Formulation - Scenario 2: QISI \times SNR for $M = 0$	199
7.10	Equation-Error Formulation - Scenario 2: QISI \times SNR for $M = 3$	200
7.11	Equation-Error Formulation - Scenario 3: QISI \times SNR for $M = 0$	202
7.12	Equation-Error Formulation - Scenario 3: QISI \times SNR for $M = 3$	203
7.13	Output-Error Formulation - Scenario 1 - MSOE Surface contours.	205
7.14	Output-Error Formulation - Scenario 1: ITL costs surface contours for $\sigma = 3$, $M = 0$ and SNR of 10 dB.	206
7.15	Output-Error Formulation - Scenario 1: ITL costs surface contours for $\sigma = 1.2$, $M = 0$ and SNR of 10 dB.	207
7.16	Output-Error Formulation - Scenario 1: ITL costs surface contours for $\sigma = 1.2$, $M = 2$ and SNR of 10 dB.	208
7.17	Output-Error Formulation - Scenario 1: PLR and RPE algorithms Performance - σ sweep ($M = 0$).	209

7.18	Output-Error Formulation - Scenario 1: PLR and RPE algorithms Performance - σ sweep ($M = 2$).	210
7.19	Output-Error Formulation - Scenario 1: QISI Performance of the PLR- and RPE-based algorithms for $M = 0$ and SNR of 10 dB.	211
7.20	Output-Error Formulation - Scenario 1: QISI Performance of the PLR- and RPE-based algorithms for $M = 2$ and SNR of 10 dB.	212
7.21	Output-Error Formulation - Scenario 1: QISI \times SNR for $M = 0$.	213
7.22	Output-Error Formulation - Scenario 1: QISI \times SNR for $M = 2$.	215
7.23	Output-Error Formulation - Scenario 2: QISI \times SNR for Gaussian noise and $M = 0$.	217
7.24	Output-Error Formulation - Scenario 2: QISI \times SNR for impulsive noise and $M = 0$.	218
7.25	Output-Error Formulation - Scenario 2: QISI \times SNR for Gaussian noise and $M = 2$.	220
7.26	Output-Error Formulation - Scenario 2: QISI \times SNR for impulsive noise and $M = 2$.	221
7.27	Output-Error Formulation - Scenario 3: QISI \times SNR for Gaussian noise and $M = 0$.	222
7.28	Output-Error Formulation - Scenario 3: QISI \times SNR for impulsive noise and $M = 0$.	223
7.29	Output-Error Formulation - Scenario 3: QISI \times SNR for Gaussian noise and $M = 2$.	225
7.30	Output-Error Formulation - Scenario 3: QISI \times SNR for impulsive noise and $M = 2$.	226
8.1	Mixing and separating systems in the PNL model.	231
8.2	Number of delays: equations and solutions.	244
8.3	Mean and Best Performance - Analytical Costs.	245
8.4	Cost Comparison and Correlation matrices.	246
8.5	Estimated Costs: Scatter plots.	248
8.6	Estimated Costs: $s(n) \times y(n)$ plots.	249

List of Tables

5.1	Permutations of $P(z)$ and required responses for the combined channel+equalizer system $C(z)$	99
5.2	Permutations of $P(z)$ and associated multivariate distribution.	102
5.3	Permutations of $P(z)$ and associated covariance matrices.	107
5.4	Permutations of $P(z)$ and associated cross-kurtosis $k_S(m)$	111
5.5	Summary of the Extensions.	114
6.1	Permutations of $P(z)$ and associated correntropy values for m from 0 to 3.	126
6.2	Solutions performance measures for the scenario 1.	159
6.3	Solutions performance measures for scenario 2.	162
6.4	Solutions performance measures for scenario 3.	165
6.5	Image Processing - MSE values for the CR, MCK, cor and MQD-C criteria.	177
7.1	Mean QISI performance for several number of delays M	198
7.2	Scenario 2: Mean QISI performance for Gaussian noise and for $M = 0$ and $M = 3$	201
7.3	Scenario 2: Mean QISI performance for impulsive noise and for $M = 0$ and $M = 3$	201
7.4	Scenario 3: Mean QISI performance for Gaussian noise and for $M = 0$ and $M = 3$	203
7.5	Scenario 3: Mean QISI performance for impulsive noise and for $M = 0$ and $M = 3$	204
7.6	Output-Error Formulation: Algorithms Parameters for $M = 0$ and $M = 2$	210
7.7	Output-Error Formulation - Scenario 1: Mean QISI performance for $M = 0$ and $M = 2$ (SNR level of 10 dB).	212
7.8	Output-Error Formulation - Scenario 2: Mean QISI performance for $M = 0$	219
7.9	Output-Error Formulation - Scenario 2: Mean QISI performance for $M = 2$	219
7.10	Output-Error Formulation - Scenario 3: Mean QISI performance for $M = 0$	224
7.11	Output-Error Formulation - Scenario 3: Mean QISI performance for $M = 2$	227

8.1 Performance in terms of SIR [dB]	248
--	-----

Acronym List

AMUSE	Algorithm for Multiple Unknown Signals Extraction
ANN	Artificial Neural Networks
AWGN	Additive White Gaussian Noise
BD	Block Diagonalization
BGR	Benveniste-Goursat-Ruget
BPSK	Binary Phase-Shift Keying
BSS	Blind Source Separation
CM	Constant Modulus
CMA	Constant Modulus Algorithm
cor	Correntropy
corEE	Correntropy - Equation-Error
corOE	Correntropy - Output-Error
CR	Correlation Retrieval
DD	Decision-Directed
DE	Differential Evolution
DFE	Decision Feedback Equalizer
FIR	Finite Impulse Response
GMI	Gaussian Mutual Information
HISI	Entropy-based Intersymbol Intereference
HOS	Higher-Order Statistics
HS	Shannon's Entropy
HSEE	Shannon's Entropy - Equation-Error
HSEO	Shannon's Entropy - Output-Error
HR	Rényi's Entropy
HSEE	Rényi's Entropy - Equation-Error
HSEO	Rényi's Entropy - Output-Error
ICA	Independent Component Analysis
<i>i.i.d.</i>	independent and identically distributed
IIR	Infinite Impulse Response

IP	Information Potential
ISI	Intersymbol Interference
ITL	Information Theoretic Learning
KL	Kullback-Leibler
<i>kurt</i>	Kurtosis
LMS	Least-Mean-Square
LQ	Linear-Quadratic
MCK	Matching of Cross-Kurtosis
MI	Mutual Information
MIMO	Multiple-Inputs Multiple-Outputs
MQD	Multivariate Quadratic Divergence
MQD-D	Multivariate Quadratic Divergence for Discrete Distribution
MQD-C	Multivariate Quadratic Divergence for Continuous Distribution
MQDEE	Multivariate Quadratic Divergence - Equation-Error
MQDOE	Multivariate Quadratic Divergence - Output-Error
MSE	Mean-Squared Error
MSEE	Mean-Squared Equation-Error
MSOE	Mean-Squared Output-Error
PAM	Pulse Amplitude Modulation
PDF	Probability Density Function
PLR	Pseudolinear Regression
PMF	Probability Mass Function
PNL	Post-Nonlinear
QAM	Quadrature Amplitude Modulation
QD	Quadratic Divergence
QISI	Quadratic Intersymbol Interference
RBF	Radial-Basis Function
RPE	Recursive Prediction Error
RV	Random Variable
RD	Rényi's entropy of the p -order Dispersion
SIR	Signal-to-Interference Ratio
SOBI	Second-Order Blind Identification
SOMI	Second-Order Mutual Information
SOMIq	Second-Order Mutual Information - Quadratic
SOS	Second-Order Statistics
SNR	Signal-to-Noise Ratio
SW	Shalvi-Weinstein
TDSEP	Temporal Decorrelation Separation
ZF	Zero-Forcing

Notation

Symbol	Meaning
Scalars, Vectors, Matrix and Functions	
a	scalar
\mathbf{a}	vector
\mathbf{A}	matrix
\mathbf{I}	identity matrix
$(\cdot)^*$	complex conjugate
$(\cdot)^T$	vector or matrix transpose
$(\cdot)^H$	vector or matrix Hermitian transpose
$f(\cdot), g(\cdot)$	function
$\nabla f(\cdot)$	gradient vector of $f(\cdot)$
$\hat{(\cdot)}$	estimate of a scalar, vector or matrix
$\ \mathbf{a}\ $	Euclidean norm of vector \mathbf{a}
$(\cdot)^{\odot a}$	Hadamard power of a
$\log(\cdot)$	natural logarithm operator
$\det(\cdot)$	determinant operator
Spaces and Sets	
\mathbb{R}	set of real numbers
\mathbb{C}	set of complex numbers
\mathcal{A}	general set symbol
Probability and Statistics	
X	random variable
\underline{X}	set of random variables
$E[\cdot]$	mathematical expectation operator
$p_X(v)$	probability mass function of RV X , with $v \in \mathbb{R}$
$f_X(v)$	probability density function of RV X
$p_{\underline{X}}(\mathbf{v})$	multivariate/joint probability mass function of the set of RVs \underline{X}
$f_{X,Y}(\mathbf{v})$	multivariate/joint probability density function of the set of RVs \underline{X}

Contents

Introduction	23
I Foundations	29
1 Statistical Adaptive Filters	30
1.1 Adaptive Filters	31
1.1.1 Linear Filters	32
1.1.2 Nonlinear Filters	35
1.2 Conclusion	38
2 Information Theoretic Learning	40
2.1 Information Theory - Fundamentals	41
2.2 Non-Parametric Density Estimators	42
2.2.1 The Parzen Window Method	43
2.2.2 The Multivariate Kernel Density Estimator	45
2.3 The ITL Criteria	46
2.3.1 Uncertainty Measures	47
2.3.2 Similarity Measures	49
2.4 Conclusion	52
3 Optimization Methods	53
3.1 Gradient-Based Optimization	54
3.1.1 The Approximate Gradient	55
3.2 Metaheuristics	56
3.2.1 Differential Evolution	57
3.3 Conclusion	59
4 Statistical and Adaptive Signal Processing Problems	60
4.1 Channel Equalization	60

4.2	Supervised Equalization	62
4.2.1	Finite Length Equalizers	63
4.2.2	Infinite Length Equalizers	68
4.3	Unsupervised Equalization	73
4.3.1	The Theoretical Pillars in Blind Equalization	74
4.3.2	Bussgang Techniques	75
4.3.3	The Shalvi-Weinstein Algorithm	77
4.3.4	ITL Criteria	78
4.3.5	Correntropy	80
4.4	Blind Source Separation	81
4.4.1	The Linear Case	82
4.4.2	The Nonlinear Case	85
4.5	Conclusion	87

II Contributions 89

5 Theoretical Conditions for Blind Equalization in the Context of a Temporally Structured Source 90

5.1	Recapitulation: The Classical Theorems for Channel Equalization	91
5.1.1	The Benveniste-Goursat-Ruget Theorem	92
5.1.2	Shalvi-Weinstein Theorem	93
5.2	Extension of the Classical Theorems for Sources with Temporal Structure .	95
5.2.1	Extension of the BGR Theorem - Univariate Distributions	96
5.2.2	Extension of the BGR Theorem - Multivariate Distributions	99
5.2.3	Extension of the SW Theorem	108
5.3	Summary of the Extensions	113
5.4	Test Scenarios	113
5.4.1	Scenario 1 - Non-Gaussian Source	115
5.4.2	Scenario 2 - Colored Gaussian Source	118
5.5	Conclusions	122

6 Methods for Blind Channel Equalization in the Context of a Temporally Structured Source 123

6.1	Background on Colored Blind Channel Equalization	123
6.1.1	Motivation for Further Investigation	125
6.2	Criteria for Colored Channel Equalization	127
6.2.1	The Cost Functions	127
6.2.2	Gradient-Based Optimization	135
6.3	Estimation Issues	138

6.3.1	The Number of Samples vs. Dimensionality	138
6.3.2	The Kernel Size	147
6.4	Methodology - Optimization and Performance	152
6.5	Cost Surfaces	155
6.5.1	Cost Surfaces - Scenario 1	156
6.5.2	Cost Surfaces - Scenario 2	159
6.5.3	Cost Surfaces - Scenario 3	162
6.6	Performance Analysis	165
6.6.1	Discrete Source - Scenario 1	166
6.6.2	Discrete Sources - Scenario 2 - IIR Filtering	170
6.6.3	Continuous Source - Scenario 1	172
6.6.4	Continuous Source - Scenario 2: Image Processing	175
6.7	Conclusions	178
7	Adaptive IIR Equalization Based on Information Theoretic Learning	181
7.1	Supervised Equalization Using IIR Equalizers	182
7.2	ITL Criteria for Adaptive IIR Filtering	183
7.2.1	Multivariate Shannon's Entropy	184
7.2.2	Multivariate Rényi's Entropy	185
7.2.3	Multivariate Correntropy	186
7.2.4	Matching of Multivariate Distributions	187
7.3	Novel ITL Algorithms for Adaptive IIR Filters	188
7.3.1	Gradient of ITL Criteria	188
7.3.2	LMS-Based Algorithms - Equation-Error Formulation	189
7.3.3	PLR-Based Algorithms - Output-Error Formulation	189
7.3.4	RPE-Based Algorithm - Output-Error Formulation	190
7.4	Performance Analysis - Equation-Error Formulation	191
7.4.1	Equation-Error Formulation - Scenario 1	192
7.4.2	Equation-Error Formulation - Scenario 2	199
7.4.3	Equation-Error Formulation - Scenario 3	201
7.5	Performance Analysis - Output-Error Formulation	204
7.5.1	Output-Error Formulation - Scenario 1	205
7.5.2	Output-Error Formulation - Scenario 2	216
7.5.3	Output-Error Formulation - Scenario 3	222
7.6	Conclusions	227
8	Blind Separation of Temporally Structured Sources in Post-Nonlinear Mixtures	230
8.1	The Post-Nonlinear Mixing Model	231
8.1.1	Time-Dependent Sources in the PNL Model	232

8.1.2	A Special Case: The Cubic Nonlinearity	234
8.2	Classical Joint Diagonalization of Correlation Matrices	237
8.2.1	The Analytical BD Cost Function	238
8.3	Second-Order Mutual Information Measure	239
8.3.1	The Quadratic SOMI Cost	241
8.4	Identifiability and Bounds	241
8.4.1	Blind Identifiability	242
8.4.2	Bounds on the Number of Delays	242
8.5	Performance Analysis	244
8.5.1	Performance Using the Analytical Costs	245
8.5.2	Performance Using Estimated Costs	247
8.6	Conclusion	250

9 Conclusions

Introduction

In signal processing problems, the statistical characterization of signals and systems is known to provide efficient mathematical tools to carry out complex tasks. As a well studied topic, its theoretical background sums up results from more than two centuries in areas like statistical inference, linear filtering and information theory [Romano et al., 2010], in which a classical approach is the assumption of linear models and Gaussian distributed and statistically independent signals.

However, the recent increase of the amount of available data and the associated complexity contributed to the rise of new problems – as well as the redefinition of the traditional ones – for which the classical assumptions might not be sufficient. In fact, for nonlinear systems and/or signals in which the statistical information cannot be easily characterized by a limited set of statistical moments (even higher-order statistics), the classical statistical framework may lead to a performance far from that ideally attainable. Examples of this assertion emerge in applications related to audio and speech signals, images and non-Gaussian noise (like the impulsive, uniform and Laplacian noises) [Wang and Bovik, 2009; LeBlanc et al., 1994; Axford et al., 1998]. In the additional case of violation of the signal statistical independence assumption, there exists an unavoidable demand for theoretically-based methodologies to turn possible the treatment of the messages with inherent statistical dependence [Comon and Jutten, 2010].

Particularly, statistically dependent signals are of major interest in this Ph.D. thesis, where special attention will be dedicated to the information regarding the temporal structure. Sometimes called temporal dependence, this information is not easily extracted from the statistical measures belonging to the classical approaches, i.e., only a partial portion of the information can be exploited by them. In that sense, a promising option comes from the methods belonging to the research field known as Information Theoretic Learning (ITL), whose objective is to provide the extraction of the statistical information in a more complete fashion. This will be the central theme of the present thesis, i.e., the use of the temporal structure of the signals within the ITL paradigm to solve signal processing problems. More specifically, the channel equalization and the nonlinear Blind Source Separation (BSS) problems will be considered.

Due to the nature of the tackled problems, the study is carried out according to a multivariate perspective, which will lead to relevant contributions in the area, among which we cite: in the blind equalization problem, a theoretical basis will be provided in order to establish the necessary statistical conditions for performing equalization in a class of temporally structured sources; for supervised equalization, the use of the temporal dependence information on a recursive equalizer will lead to an improvement on the achieved performance; and, for the nonlinear BSS problem, an extended temporal formulation will provide further insight to solve a particular mixture case with the use of the Second-Order Statistics (SOS).

Perspectives on the Use of the Temporal Structure of Data

The historical preference for statistically independent source signals is justified by the fact that the distortion effects caused by intermediate systems can be successfully nullified through the recovery of this condition, which is usually not a difficult task. Statistically independent sources also present other convenient mathematical features, which can be exploited in order to obtain simpler methods to restore the information [Godard, 1980; Shalvi and Weinstein, 1993; Comon and Jutten, 2010]. For this reason, the option for these type of sources is a common sense in diverse fields, mainly regarding unsupervised approaches [Romano et al., 2010].

Although this assumption can be successfully used in a wide range of practical problems, there still remains a gap when considering the case of inherently dependent sources. Such type of sources naturally occurs in analog discrete-time signal processing (e.g., in audio-related scenarios), videos (due to pixel correlation), or as a result of channel coding in communications. In view of their large occurrence in signal processing problems, they are far from belonging to a neglected group of signals.

In fact, the temporal dependence of the signals can be used in a beneficial manner, since they carry valuable information about the sources. For instance, the knowledge of the temporal structure would be able to provide, at each time instant, the information about other probable past and future occurrences. From the Information Theory perspective, the statistical dependence is able to reduce the uncertainty about the events [Cover and Thomas, 1991]. In that sense, their effective manipulation opens an horizon to the direct statistical processing of the present day media, such as images, audio and speech data. In the context of communications, besides the extension to a broader communication model encompassing signals that have inherent temporal dependence, it becomes possible to deal with messages subject to general coding schemes, even at symbol level. This would open possibilities to the emergence of novel statistically dependent modulation/demodulation

schemes. Additionally, the own temporal structure printed by the source coding scheme can be used for system deconvolution.

These perspectives motivate us in the use of ITL measures/entities capable of encompassing the statistical dependence present on the signals of interest, which shall be of great significance for solving the aforementioned problems.

Objectives and Thesis Organization

The present thesis sums up the results obtained during the regular Ph.D. research period, focused on the channel equalization problem as well as during the Ph.D. sandwich made by the student, carried out in the context of the nonlinear BSS problem.

The document is structured in two parts: the first one provides the fundamental background on channel equalization and nonlinear BSS, including the basic elements to solve a signal processing task, which comprises the filtering structure, the criterion and the optimization method; the second part presents the contributions on the two problems using the concepts and definitions introduced in the previous part. A more detailed content of each chapter is described in the following.

- In Chapter 1, a selection of linear and nonlinear filtering structures are presented and their main features are discussed, such as the tradeoff between flexibility and complexity.
- Chapter 2 presents the main aspects regarding the criterion, followed by an introduction on the concepts of the ITL field. As the main theme of this thesis, the most promising ITL criteria are also presented, including the extension of the Parzen window method for multivariate densities.
- To complete the triad – filtering structure, criterion and optimization method –, Chapter 3 discusses the main techniques involved in the optimization process in the signal processing area, from which a special attention is dedicated to the gradient-based methods and the metaheuristics.
- Using the elements of the previous chapters, Chapter 4 provides an overview on the main methods applied in the channel equalization and the blind source separation problems. Besides a brief historical perspective, it is also discussed how the ITL methods are inserted in each problem. Finally, to conclude the foundations part, the promising investigative lines are pointed out.
- The contributions part begins with Chapter 5, which presents a novel and detailed theoretical basis for solving the blind channel equalization problem with a

temporally-structured source. The statistical conditions are established by resorting to important theorems in the literature and by some empirical results, revealing the need for using multivariate densities in this context.

- Based on the previous theoretical analysis, Chapter 6 introduces the novel criteria – including an ITL-based approach that uses the concept of multivariate density matching – for the blind channel equalization problem with a temporally structured source. The performances of the criteria are evaluated in a set of representative scenarios and compared with that of the state-of-the-art method.
- Chapter 7 treats the supervised channel equalization problem through the exclusive use of linear Infinite Impulse Response (IIR) filters. The problem is analyzed from the perspective of the equation-error and output-error formulations, whose ITL-based methods – like entropy and correntropy – can be successfully applied. In this case, the extraction of the temporal dependence is made through the extension of these ITL criteria to the multivariate domain.
- In Chapter 8, a special case within the nonlinear BSS problem is investigated. A temporal-extended formulation is followed in order to encompass the statistical temporal dependence of the sources. Using the definition of the ITL metric named Mutual Information (MI) and with the hypothesis of colored multivariate Gaussian sources, a criterion based on Second-Order Statistics (SOS) is proposed.
- Having presented the contributions, the thesis is concluded in Chapter 9, where the final considerations and the future perspectives are presented.

Publications

During the Ph.D. research period, the following works were published.

- Works published in Journals:
 1. **Fantinato, D. G.**, Neves, A., and Attux, R. Analysis of a Novel Density Matching Criterion within the ITL Framework for Blind Channel Equalization. *Journal on Circuits, Systems and Signal Processing*, v. 34 (543), 1–29, 2017.
 2. Silva, D. G., **Fantinato, D. G.**, Canuto, J., Duarte, L. T., Neves, A., Suyama, R., Montalvão Filho, J., and Attux, R. An Introduction to Information Theoretic Learning, Part I: Foundations. *Journal of Communication and Information Systems*, 2016.

-
3. Silva, D. G., **Fantinato, D. G.**, Canuto, J., Duarte, L. T., Neves, A., Suyama, R., Montalvão Filho, J., and Attux, R. An Introduction to Information Theoretic Learning, Part II: Applications. *Journal of Communication and Information Systems*, 2016.
 4. Boccato, L., **Fantinato, D. G.**, Silva, D. G., Ferrari, R., Neves, A., and Attux, R. Analysis of ITL Criteria in the Context of Channel Equalization. *Journal of Communication and Information Systems*, 2016.
- Book Chapter:
 1. Attux, R., Boccato, L., **Fantinato, D. G.**, Montalvão Filho, J., Neves, A., Suyama, R., Nose-Filho, K., and Silva, D. G. *Bio-Inspired and Information-Theoretic Signal Processing*. Chapter 17 of the book entitled “Signals and Images: Advances and Results in Speech, Estimation, Compression, Recognition, Filtering, and Processing.” Editors: R. Coelho, V. Nascimento, R. de Queiroz, J. M. Romano, C. Cavalcante; CRC Press, 2015.
 - Conference Publications:
 1. **Fantinato, D. G.**, Duarte, L. T., Zanini, P., Rivet, B., Attux, R., and Jutten, C. A Joint Second-Order Statistics and Density Matching-Based Approach for Separation of Post-Nonlinear Mixtures. *Proceedings of the 13th International Conference on Latent Variable Analysis and Signal Separation (LVA/ICA)*, 2017.
 2. **Fantinato, D. G.**, Duarte, L. T., Rivet, B., Ehsandoust, B., Attux, R., and Jutten, C. Gaussian Processes for Source Separation in Overdetermined Bilinear Mixtures. *Proceedings of the 13th International Conference on Latent Variable Analysis and Signal Separation (LVA/ICA)*, 2017.
 3. **Fantinato, D. G.**, Silva, D. G., Neves, A., and Attux, R. Blind Channel Equalization of Coded Data over Galois Fields, *submitted to IEEE International Workshop on Machine Learning for Signal Processing (MLSP)*, 2017.
 4. **Fantinato, D. G.**, Ando, R. A., Neves, A., Duarte, L. T., Jutten, C., and Attux, R. A Quadratic Divergence-Based Independence Measure Applied to Linear-Quadratic Mixtures. *Proceedings of the XXXIV Simpósio Brasileiro de Telecomunicações*, 2016.
 5. Alvarez, S., Attux, R., **Fantinato, D. G.**, Montalvão Filho, J., and Silva, D.G. An Immune-Inspired, Dependence-Based Approach to Blind Inversion of Wiener Systems. *Proceedings of the European Symposium on Artificial Neural Networks, Computational Intelligence and Machine Learning*, 2016.

6. Suyama, R., Attux, R., **Fantinato, D. G.**, and Romano, J. M. T. Some Reflections on the 35 Years of the Constant Modulus Criterion, *Proceedings of the XXXIII Simpósio Brasileiro de Telecomunicações (SBrT)*, Juiz de Fora, 2015.
7. **Fantinato, D. G.**, Neves, A., and Attux, R. Preliminary Results on Rényi's Entropy-Based Blind IIR Filtering, *Anais do VI Simpósio de Processamento de Sinais da UNICAMP (Intern Conference)*, 2015.
8. **Fantinato, D. G.**, Boccato, L., Neves, A., Attux, R. Multivariate PDF Matching via Kernel Density Estimation. *Proceedings of the IEEE Symposium Series on Computational Intelligence*, 150–157, 2014.
9. **Fantinato, D. G.**, Attux, R., Suyama, R., Neves, A., and Romano, J. M. T. A Volterra Filtering Approach for the Polynomial Formulation of the Constant Modulus Criterion. *Proceedings of the International Telecommunications Symposium*, 2014.
10. Boccato, L., Silva, D. G., **Fantinato, D. G.**, Ferrari, R., and Attux, R. A Comparative Study of Non-MSE Criteria in Nonlinear Equalization. *Proceedings of the International Telecommunications Symposium*, 2014.

Awards

The following work was granted the *Best Paper Award* in the Symposium Series on Computational Intelligence (SSCI), 2014:

- **Fantinato, D. G.**, Boccato, L., Neves, A., and Attux, R. Multivariate PDF Matching via Kernel Density Estimation, *Proceedings of the IEEE Symposium Series on Computational Intelligence (SSCI)*, 2014.

Part I

Foundations

Chapter 1

Statistical Adaptive Filters

In signal processing, a given task can be efficiently carried out when the following triad works with great synergy: (i) the filtering structure, (ii) the adaptation criterion and (iii) the optimization method, as illustrated in Fig. 1.1. In this chapter, the focus will be on the first one.

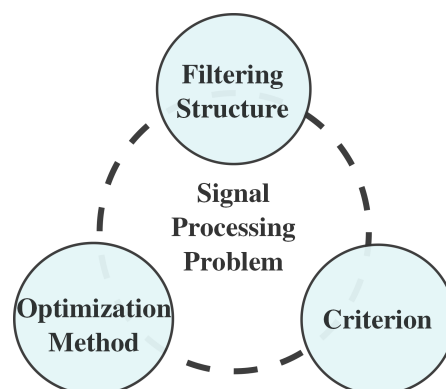


Figure 1.1: Triad of fundamental elements in signal processing problems.

The filtering structure has as its *raison d'être* the extraction of information about a quantity of interest from the available data [Haykin, 1996]. In other words, the filter must process the input data (or signal) and be flexible enough to provide the information of interest in the form of an output signal. Fig. 1.2 illustrates the general form of a filtering structure, where the number of inputs/outputs may vary according to the application.

Before assuming the form of an analog or digital device, the filter is defined by means of a mathematical model that establishes a mapping of the input space to the output space. The filter can be dynamically controlled in any level, but, generally, adaptation is carried out by a set of free parameters (hence the name adaptive filter) [Haykin, 1996; Coelho et al., 2015]. Particularly, in situations where signals and/or systems may vary from time to time or can even be unknown, the use of a filter whose coefficients are variable – i.e., an adaptive filter – is crucial to obtain a good performance.

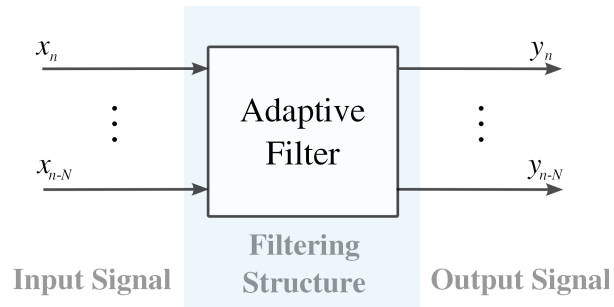


Figure 1.2: Diagram of a general filtering structure.

There are many practical instances in which it is relevant to perform filtering. Communications, control, radar and seismic [Romano et al., 2010] are examples of areas where the filter performs the role of fundamental tool for processing the information in its various forms.

In this thesis, we are mainly concerned with the processing of the statistical content of data or, more specifically, we are interested on the existence of a temporal structure. Since the filter plays a key role as an effective modifying agent of the statistical properties (i.e., it is able to modify the statistical structure of the signals), the correct choice of its structure and properties will be of fundamental importance to carry out the task at hand. In the following, we present the filters that figure as fundamental elements in signal processing.

1.1 Adaptive Filters

The systems or structures that are capable of extracting from data the information about a quantity of interest receive the name of *filters*. They can be divided into two main classes: linear and nonlinear. Basically, the filter is linear if its input and output obey the superposition principle, i.e., if input x_1 produces output $f(x_1)$ and input x_2 produces output $f(x_2)$, then the input $x_1 + x_2$ must produce the output $f(x_1 + x_2) = f(x_1) + f(x_2)$. In addition to that, for any scalar a , $f(ax_1) = af(x_1)$ must hold. In summary,

$$f(ax_1 + bx_2) = af(x_1) + bf(x_2), \quad (1.1)$$

where both outputs $f(ax_1 + bx_2)$ and $af(x_1) + bf(x_2)$ are equivalent. Otherwise, if the superposition principle is not obeyed, the filter is nonlinear.

It is worth pointing out that, as a rule, in this thesis, the signals are assumed to be stationary discrete-time stochastic processes and the filters discrete-time structures.

1.1.1 Linear Filters

Linear digital filters are the simplest processing structures and can be divided into two types: Finite Impulse Response (FIR) and Infinite Impulse Response (IIR) filters. The main difference between them is that FIR filters are feedforward structures while IIR filters rely on the existence of a feedback loop.

Finite Impulse Response Filters

The emblematic FIR filter is the most basic signal processing system. Its importance is the result of a vast theoretical framework developed in areas like linear estimation theory [Gauss, 1809; Kolmogorov, 1939; Wiener, 1949], adaptive filtering algorithms [Widrow, 1971; Godard, 1974] and signal processing applications [Lucky, 1965; Godard, 1980].

The linear FIR filter is defined by a set of tap coefficients that weight present and past samples of an input signal. In the adaptive case, the coefficients or weights of the filter can be adapted along the time samples. Its structure can be seen in Fig. 1.3.

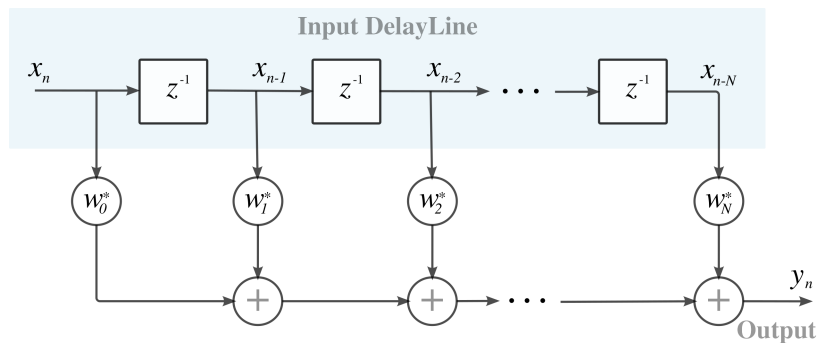


Figure 1.3: Finite impulse response filter.

Mathematically, the output of the FIR filter of order L_w – and with L_w+1 coefficients – can be expressed, using a vector notation, as

$$\begin{aligned}
 y_n &= \begin{bmatrix} w_0^* & w_1^* & \cdots & w_{L_w}^* \end{bmatrix} \begin{bmatrix} x_n \\ x_{n-1} \\ \vdots \\ x_{n-L_w} \end{bmatrix} \\
 &= \mathbf{w}^H \mathbf{x}_n,
 \end{aligned} \tag{1.2}$$

where \mathbf{w} is the vector with the tap weights, \mathbf{x}_n the input vector and y_n the output signal at time instant n ; the superscript H denotes Hermitian transpose (the operation of transposition combined with complex conjugation), and the asterisk $(\cdot)^*$ denotes complex conjugation.

An FIR filter can also be described by means of its transfer function (or the Z-transform

of its impulse response) [Oppenheim et al., 1997], i.e.:

$$W(z) = w_0^* + w_1^* z^{-1} + \dots + w_{L_w}^* z^{-L_w}, \quad (1.3)$$

where the roots of this polynomial in function of z are called *zeros*. Since a filter can be totally characterized, up to a scale factor, by the number of zeros and its values, its graphical representation is reduced to the simple block shown in Fig. 1.4.

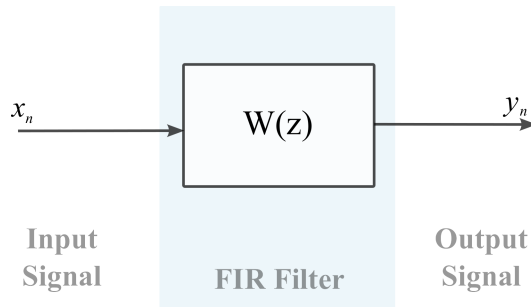


Figure 1.4: FIR filter block.

Infinite Impulse Response Filters

IIR filters are linear structures as well, but endowed with feedback loops. They were intensively studied along the decades of 70 to 90 [Horvath Jr., 1976; Johnson Jr., 1984; Goodwin and Sin, 1984; Treichler, 1985; Long et al., 1987; Regalia, 1994], with applications in system identification, adaptive control, linear prediction, channel equalization and echo cancellation. Later, in the beginning of the 2000s, some efforts were aimed at the use of evolutionary algorithms/metaheuristics for training IIR filters, which showed to be a more robust alternative than the gradient-based methods [Chen, 2000; Krusienski and Jenkins, 2004; Chen and Luk, 2010].

IIR systems are attractive due to two main reasons: *(i)* they are linear structures with low complexity and *(ii)* they are able to perfectly compensate other linear systems – even when the number of the IIR coefficients are insufficient, they tend to present an improved performance in comparison with an adaptive FIR filter with the same number of coefficients. It is important to remark that these features are consequence of the feedback loop within the IIR structure, which allows the achievement of a infinite impulse response from only a finite number of parameters [Shynk, 1989].

Notwithstanding, the same feedback loops that guarantee an improved performance for the IIR filters also contribute to the emergence of a nonlinear relationship between the filter output and its coefficients, which, on its turn, may provoke a behavior that demands special attention in order to keep the system stable. In that sense, the task of using IIR filters is still a challenge.

IIR filters are composed of two parts: the feedforward and the feedback parts, as shown in Fig. 1.5. Mathematically, the filter output can be expressed as

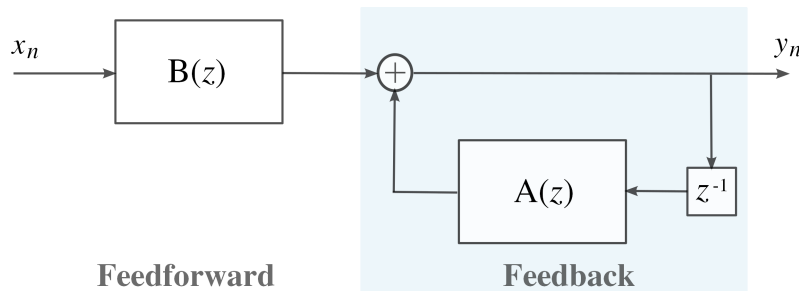


Figure 1.5: Infinite impulse response filter.

$$y_n = \sum_{i=0}^{L_b} b_i x_{n-i} + \sum_{j=1}^{L_a} a_j y_{n-j}, \quad (1.4)$$

where L_b and L_a are the order of the feedforward and the feedback parts, respectively. Alternatively, using a vector notation,

$$y_n = \boldsymbol{\theta}^T \boldsymbol{\phi}_n, \quad (1.5)$$

where $\boldsymbol{\theta} = [b_0 \ b_1 \ \dots \ b_{L_b} \ a_1 \ \dots \ a_{L_a}]^T$ and $\boldsymbol{\phi}_n = [x_n \ x_{n-1} \ \dots \ x_{n-L_b} \ y_{n-1} \ \dots \ y_{n-L_a}]^T$. Note that the feedback loop only operates on the delayed versions of y_n .

Using the Z-transform at (1.4), it results

$$Y(z) = \frac{B(z)}{1 - A(z)} X(z), \quad (1.6)$$

where the numerator $B(z)$ is a polynomial in function of z , whose roots are named *zeros* and are associated with the feedforward part, and the denominator $1 - A(z)$ is a polynomial whose roots are called *poles* [Oppenheim et al., 1997] and are associated with the feedback part.

In order to guarantee the IIR filter stability, its poles must be located within the region limited by the unit circle, as illustrated in Fig. 1.6(a). Alternatively, the stable region can also be identified by the *stability triangle* [Shynk, 1989]. For $L_a = 2$, the stability triangle is as depicted in Fig. 1.6(b). Each point within the triangle area can be mapped to another point within the unit circle. If the point falls below the dashed line, the poles will form complex conjugate pairs.

When the poles of the IIR filter are outside the unit circle, the output signal will grow in modulus indefinitely (the system is not *Bounded-Input Bounded-Output* [Proakis and Manolakis, 1996]). Generally, this case is not desired and additional care might be necessary to avoid that it happens.

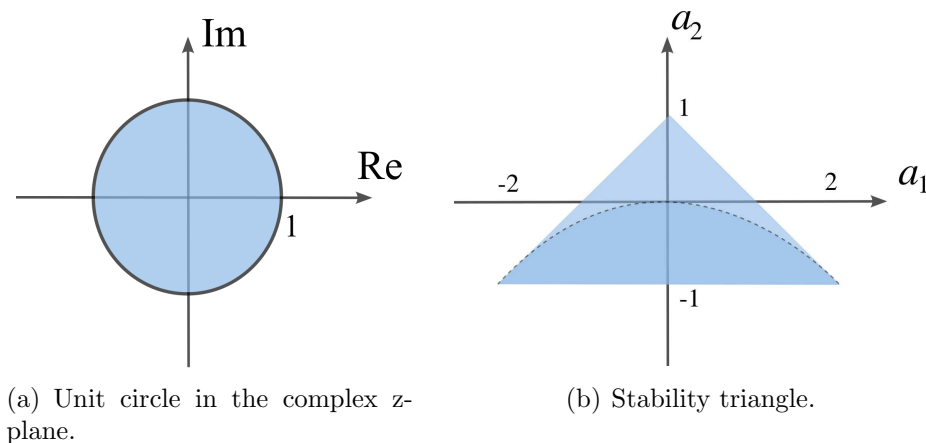


Figure 1.6: Stability regions for IIR filters.

Other important aspect in IIR filters is the already mentioned emergence of a nonlinear relationship between the filter coefficients and the output y_n . In fact, a recursive expansion of the delayed outputs of y_n in Eq. (1.4) would reveal terms with the product of the coefficients b_i and a_j , for $i = 0, \dots, L_b$ and $j = 1, \dots, L_a$. This feature exposes the nonlinear essence of the IIR structure, implemented by means of a linear framework.

1.1.2 Nonlinear Filters

Linear filters present advantages like structural simplicity and mathematical tractability, however, they may be unsatisfactory when extracting the information about the signals of interest in complex scenarios. In that sense, the use of nonlinear filtering structures is an interesting alternative, since they are able to provide more flexible mappings of the data.

An infinite set of mappings or filters do not obey the superposition principle, giving rise to a number of classes among the nonlinear structures. In that sense, the analysis of these structures in a general context is not trivial. However, certain classes of nonlinear filters share an important feature: their structure encompasses the universal approximation capability [Park and Sandberg, 1991]. For instance, this is the case of the polynomial filters and the Radial-Basis Function neural network. Both of them are able to approximate any given continuous function with any expected learning error [Park and Sandberg, 1991; Haykin, 1998].

Polynomial Filters

In signal processing applications, the use of polynomial filters was the starting point of a more widespread adoption of nonlinear models. The initial efforts can be traced to the decades of 70 and 80, in the context of equalization and echo cancellation [Agazzi et al., 1982; Benedetto et al., 1979; Biglieri et al., 1984; Thomas, 1971].

The main advantage of the polynomial filters is to represent general functions in terms of a linear combination of other functions. This idea is closely related to the Volterra series [Mathews and Sicuranza, 2000], where, in analogy with the Taylor series [Oppenheim et al., 1997], a given continuous function can be expressed by its polynomial expansion:

$$\begin{aligned}
 y_n = & w_0 + \sum_i w_1(i)x_{n-i} + \sum_i \sum_j w_2(i,j)x_{n-i}x_{n-j} \\
 & + \sum_i \sum_j \sum_k w_3(i,j,k)x_{n-i}x_{n-j}x_{n-k} + \dots
 \end{aligned} \tag{1.7}$$

where $w(i, \dots, k)$ are the weights or the Volterra kernels and x_n and y_n are the input and output of the system, respectively. Basically, the series is based on the idea of representing the system response in terms of polynomial components, which contain products of different delayed versions of the input signal.

Usually, a truncated version of the Volterra series is adopted to avoid excessively large filters. For instance, a system with two inputs, say x_n and x_{n-1} , is of the form:

$$\begin{aligned}
 y_n = & \begin{bmatrix} w_0 & w_1(1) & w_2(0,0) & w_2(0,1) & w_2(1,1) \end{bmatrix} \begin{bmatrix} x_n \\ x_{n-1} \\ x_n^2 \\ x_n x_{n-1} \\ x_{n-1}^2 \end{bmatrix} \\
 = & \mathbf{w}^T \boldsymbol{\xi}_n,
 \end{aligned} \tag{1.8}$$

where $\boldsymbol{\xi}_n$ is the vector of expanded terms of x_n and x_{n-1} in the Volterra domain. The key factor of this polynomial filter is that, although the input-output relationship is nonlinear, the structure is linear with respect to the free parameter vector \mathbf{w} .

From the standpoint of parameter adaptation, the linear free parameters \mathbf{w} allow the emergence of methods whose complexity is close to that of FIR filters, which is certainly a positive feature [Romano et al., 2010].

Radial-Basis Function Neural Network

Artificial Neural Networks (ANNs) are nonlinear adaptive signal processing devices whose original purpose was to model the nervous systems of living beings [Haykin, 1998]. The beginning of the studies on this topic can be attributed to the seminal works of McCulloch and Pitts [McCulloch and Pitts, 1943] and Frank Rosenblatt [Rosenblatt, 1958] in pattern recognition. Later, an extension of the Rosenblatt's work gave rise to the so-called Multilayer Perceptron (MLP) [Werbos, 1974; Haykin, 1998], an ANN structured in multiple layers and composed of nonlinear processing units (called neurons). In this case, each neuron could be defined by the values of the synaptic weights and by a nonlinear

memoryless activation function. Finally, in 1988, Broomhead and Lowe [Broomhead and Lowe, 1988] introduced a new multilayer structure, the Radial-Basis Function (RBF) network, a fundamental neural approach for function approximation [Park and Sandberg, 1991].

By rule, RBF networks are composed of one input layer, one hidden layer and a linear output layer, which linearly combines the output of the activation functions. The model is described by Fig. 1.7.

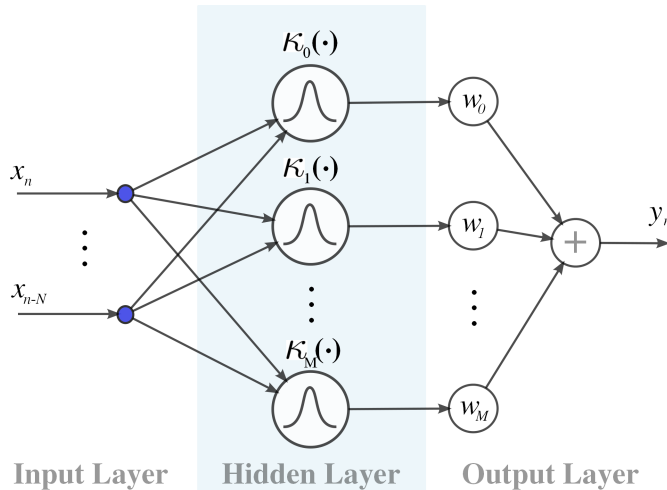


Figure 1.7: Radial-Basis Function Network.

Mathematically, the output of the RBF network can be expressed as follows:

$$\begin{aligned}
 y_n &= \begin{bmatrix} w_0 & w_1 & \dots & w_M \end{bmatrix} \begin{bmatrix} \kappa_0(\mathbf{x}_n) \\ \kappa_1(\mathbf{x}_n) \\ \vdots \\ \kappa_M(\mathbf{x}_n) \end{bmatrix} \\
 &= \mathbf{w}^T \boldsymbol{\kappa}_n,
 \end{aligned} \tag{1.9}$$

where $\mathbf{x}_n = [x_n \ x_{n-1} \ \dots \ x_{n-N}]^T$ is the input vector, $\boldsymbol{\kappa}_n$ is the vector with the $M+1$ responses of the hidden neurons for input \mathbf{x}_n , $\kappa_i(\cdot)$ is the i -th radial-basis activation function, for $i = 0, \dots, M$, and, as usual, $\mathbf{w} = [w_0 \ w_1 \ \dots \ w_M]$ is the vector with the linear weights.

The nonlinear activation functions $\kappa_i(\cdot)$ must be radially symmetric about a center vector (hence the name radial-basis function) and compliant with other mild conditions on its shape. If these conditions are satisfied, an RBF network with enough hidden neurons can approximate any continuous function on a compact subset with arbitrary precision [Park and Sandberg, 1991]. Although this result guarantees the universal function approximation, it does not reveal how many neurons are necessary in the hidden layer. In practical terms, the number of neurons in the design of an RBF network is a

trade-off between computational cost and performance.

Generally, the radial-basis function is a multidimensional Gaussian function:

$$\kappa_i(\mathbf{x}_n) = \exp\left(-(\mathbf{x}_n - \mathbf{c}_i)^T \boldsymbol{\Sigma}_i^{-1} (\mathbf{x}_n - \mathbf{c}_i)\right), \quad (1.10)$$

where \mathbf{c}_i is the center vector of the RBF and $\boldsymbol{\Sigma}_i$ is the positive definite and diagonal matrix

$$\boldsymbol{\Sigma}_i = \begin{bmatrix} \sigma_{i1}^2 & 0 & \cdots & 0 \\ 0 & \sigma_{i2}^2 & \ddots & \vdots \\ \vdots & \ddots & \ddots & 0 \\ 0 & \cdots & 0 & \sigma_{iN}^2 \end{bmatrix}, \quad (1.11)$$

being σ_{ij}^2 , for $i = 0, \dots, M$ and $j = 0, \dots, N$, the variances or dispersion factors. Although not the common option, the case in which the off-diagonal elements of $\boldsymbol{\Sigma}_i$ are not null can also be adopted when dealing with statistically dependent data.

The common approach for training the RBF networks is performed in two stages: (i) first, the center vectors and the dispersion factors are defined according to heuristic or unsupervised methods (e.g., randomly picking inputs as centers and assuming a single dispersion factor for all centers, such as $\sigma^2 = d_{max}/\sqrt{2M+2}$, being d_{max} the maximum Euclidean distance between centers [Haykin, 1998]); (ii) for the second stage, there remains a linear combination problem in function of the free parameters \mathbf{w} to be solved, where, again, the complexity will be comparable to that of FIR filters.

1.2 Conclusion

This chapter introduced some linear and nonlinear structures that can be employed to process or filter the statistical information underlying the data and to provoke modifications in its temporal structure.

In the linear case, the fundamental concepts of the FIR and IIR filters were introduced. Both filters present a feedforward weighting structure, however, the IIR filter contains an additional feedback loop, which is capable of increasing the performance of the filter in comparison with an FIR structure, but also demands special attention to avoid unstable behavior.

In the nonlinear domain, we presented two structures which share the property of universal function approximation: polynomial filters and RBF networks. In both cases, the nonlinearities are result of mappings of the input signal to a higher dimensional (nonlinear) space, followed by linear transformations in this space. This approach is particularly convenient because, besides encompassing nonlinear properties, the structure is linear with respect to the free parameters, thus reducing the complexity of parameter adaptation.

In any case, the design of a filter may require some structural choices that are not always simple to deal with. Questions like “the filter should be linear or nonlinear?”, “does it need a feedback loop?” or “when using an ANN, how many neurons are necessary?” are unavoidable and the answer must take into account a trade-off between simplicity (computational cost) and efficiency. In fact, the choice of the filter concerns the complexity of the problem at hand and the criterion it must satisfy, as we will see in the next chapter.

Chapter 2

Information Theoretic Learning

After a careful choice of the filtering structure to be employed in the signal processing problem, the next step is to define an adaptation (or performance) criterion. This mathematical entity is responsible for reliably translating the rationale of the entire framework according to the problem at hand so that the desired objective can be achieved [Romano et al., 2010; Attux et al., 2015].

The criterion is composed of a cost function, a mathematical expression that encompasses the general objectives of the problem and the optimization information (maximization or minimization). For instance, a criterion can be defined as the minimization of a given cost $J(\mathbf{w})$ with respect to the filter coefficients \mathbf{w} , i.e.,

$$\min_{\mathbf{w}} J(\mathbf{w}) . \quad (2.1)$$

In signal processing, the cost function generally involves (explicitly or implicitly) the statistical information about the signals of interest, which, in a number of practical applications, may be the most reliable information within range.

Interestingly, the research branch known as Information Theoretic Learning (ITL) [Principe, 2010] focuses on the study of criteria and methods capable of extracting the signal statistical information in a manner as complete as possible, using concepts and measures from Information Theory [Cover and Thomas, 1991], like entropy and Mutual Information (MI). The relevance of these entities can be justified in terms of their probabilistic structure, which allows a more extensive statistical characterization than that provided by second or even specific higher-order moments. In that sense, its application in signal processing problems – like blind source separation [Comon and Jutten, 2010] and channel equalization [Romano et al., 2010] – is already known to be very effective [Comon and Jutten, 2010; Principe, 2010; Santamaría et al., 2006]. Particularly, this topic constitutes the main theme of the present thesis, whose features will be crucial while extracting the temporal information about the underlying signals. Hence, a special attention will be dedicated to it.

Nonetheless, before proceeding with the discussion about the ITL criteria, it is convenient to firstly introduce the fundamental aspects on Information Theory and the entities that established a close connection with the signal processing area and gave rise to the ITL research field, as presented in the following.

2.1 Information Theory - Fundamentals

Differently from many other theories that gradually formed their *corpus* from several contributions along the years, the Information Theory was entirely conceived in a single and remarkable work of Claude Elwood Shannon, a celebrated researcher from the 20th century. The work entitled “A Mathematical Theory of Communication” [Shannon, 1948] provided an insightful and careful study, from which important theoretical bounds on communication devices could be derived.

It is not preposterous to state that the development of the Information Theory is consequence of a key element defined by Shannon: the entropy. The importance of this entity comes from its brilliant interpretation as a measure of uncertainty and, mainly, of information. Mathematically, for discrete random variables (RVs), the entropy can be defined as [Cover and Thomas, 1991]:

$$H^S(X) = - \sum_{v \in \mathcal{A}_X} p_X(v) \log(p_X(v)), \quad (2.2)$$

where $p_X(v)$ is the Probability Mass Function (PMF) of the RV X and \mathcal{A}_X is the alphabet of all possible occurrences of X ; for continuous variables, the entropy extension (also called differential entropy [Cover and Thomas, 1991]) is intuitive:

$$H^S(X) = - \int f_X(v) \log(f_X(v)) dv, \quad (2.3)$$

where $f_X(v)$ is the Probability Density Function (PDF) of the continuous RV X . In both discrete and continuous cases, the entropy can be viewed as a measure of the average amount of information required to describe the RV [Cover and Thomas, 1991]. Based on this, Shannon proves a theorem that establishes the entropy of the source as a limit to the achievable efficiency of any coding process [Shannon, 1948; Silva et al., 2016].

Besides that, Shannon also makes use of a measure of the amount of information one RV brings about another RV. This quantity is called Mutual Information (MI) and can be defined as [Cover and Thomas, 1991]:

$$I(X; Y) = H^S(X) + H^S(Y) - H^S(X, Y), \quad (2.4)$$

where $H^S(X, Y)$ is the joint entropy, defined as

$$H^S(X, Y) = - \sum_{\mathbf{v} \in \mathcal{A}_X, \mathcal{A}_Y} p_{X,Y}(\mathbf{v}) \log(p_{X,Y}(\mathbf{v})), \quad (2.5)$$

being $p_{X,Y}(\mathbf{v})$ the joint PMF associated with the discrete RVs X and Y ; or, for continuous RVs,

$$H^S(X, Y) = - \int_D f_{X,Y}(\mathbf{v}) \log(f_{X,Y}(\mathbf{v})) d\mathbf{v}, \quad (2.6)$$

where $f_{X,Y}(\mathbf{v})$ is the joint PDF of the continuous RVs X and Y and $D \subseteq \mathbb{R}^2$. Shannon refers to the MI as the “rate of actual transmission” and uses it to obtain an astonishing result: the definition of the bound on the channel capacity, i.e., the limit of the rate of information production at the source for which there always exists a coding system capable of giving rise to an arbitrarily small error rate [Shannon, 1948; Silva et al., 2016].

The immense importance of the results reached by Shannon contributed to make Information Theory a research field *per se* and have attracted the attention of several researchers, who extended its concepts and elements (specially the entropy and the mutual information) beyond their original scope. In signal processing, the link with Information Theory can be traced back to the development of Independent Component Analysis (ICA) and of applications related to BSS, in which were used, for instance, the idea of quantification of statistical independence with the aid of the MI and the concepts like information flow in a given system [Hyvärinen et al., 2001; Héroult et al., 1985]. In the context of channel equalization, the notion of entropy and of RVs comparisons (similar to the MI) [Principe, 2010] is explored to mitigate the distortions caused by the channel. Particularly, in this case, the adopted entropy is based on a generalized measure of information – an extended version of the original definition in Eq. (2.3) – allied to the use of non-parametric density estimators, which resulted in the first referred ITL method.

In fact, the use of these non-parametric density estimators became a special trend within the ITL field, and, for this reason, we present their definition in the following, considering both the cases of univariate and multivariate density estimators.

2.2 Non-Parametric Density Estimators

From the definitions of entropy and MI, the requirement of the distribution knowledge is essential to translate the notion of information. However, in many practical cases, the probabilistic distribution is not available and must be estimated from data samples.

In the case in which the distributions are not based on parametrized classes of probability distributions, the non-parametric estimators can be employed, i.e., they make no prior assumption of the RVs being assessed. Although there are a number of non-parametric methods that can be used, the standard approach within the ITL field is the Parzen

window method [Parzen, 1962; Principe, 2010]. The preference for this choice is justified by two main reasons: firstly, this method allied with certain Information Theory entities can lead to simplified estimators (as will be seen) and, secondly, they are differentiable, a useful property for deriving gradient-based algorithms.

2.2.1 The Parzen Window Method

In 1962, Parzen proposed a method whose objective was to obtain density estimates from a data set [Parzen, 1962]. The fundamental component in his formulation were the kernel functions, which, although not originally aimed for statistical purposes, showed to be perfectly suitable for the derivation.

The kernel functions are known to be particularly useful for solving nonlinear problems, given their ability of performing inner product operations, represented by $\langle \cdot, \cdot \rangle$, in a potentially much higher-dimensional feature space with a linear structure, which, under the perspective of the input space, results in nonlinear operations over the data. Very interestingly, these operations can be implicitly performed in the input (or data) space, without the need of nonlinear mappings, i.e., the inner product formulation is implicitly performed in the higher-dimensional feature space but the data and the operations are completely executed in the input space [Principe, 2010].

To clarify this kernel paradigm, suppose the nonlinear mapping:

$$\begin{aligned} \Phi : S &\rightarrow H \\ \mathbf{x} &\rightarrow \Phi(\mathbf{x}), \end{aligned} \tag{2.7}$$

where the data $\{\mathbf{x}_1, \mathbf{x}_2, \dots, \mathbf{x}_n\} \subset S$ are mapped into a potentially much higher-dimensional feature space H (an allusion to the reproducing kernel Hilbert space) by the nonlinear function $\Phi(\cdot)$. From this, it is possible to prove that there exists a real-valued bivariate kernel function $\kappa(\mathbf{x}_i, \mathbf{x}_j)$, non-negative definite and symmetric (the Mercer's conditions [Vapnik, 1995]), such that

$$\kappa(\mathbf{x}_i, \mathbf{x}_j) = \langle \Phi(\mathbf{x}_i), \Phi(\mathbf{x}_j) \rangle. \tag{2.8}$$

In words, Eq. (2.8) reveals that the application of the kernel function over the data, $\kappa(\mathbf{x}_i, \mathbf{x}_j)$, in the input space S corresponds to an inner product of the nonlinearly mapped data in the higher-dimensional feature space H (the so-called “kernel trick”) [Principe, 2010]. This elegant idea allows us to implicitly deal with nonlinear transformations Φ by using only the kernel functions. Hence, the nonlinear mapping Φ is not even necessary to be known. However, the effective nonlinear mapping Φ is directly related with the choice of the kernel function [Aronszajn, 1943].

Besides the Mercer's conditions [Vapnik, 1995], a kernel function must also fulfill the

following properties to be used for density estimation [Principe, 2010], i.e.:

$$\begin{aligned}
 (i) \quad & \kappa(x) \geq 0; \\
 (ii) \quad & \int_{\mathbb{R}} \kappa(x) dx = 1; \\
 (iii) \quad & \lim_{x \rightarrow \infty} |x\kappa(x)| = 0.
 \end{aligned} \tag{2.9}$$

Generally, the used kernel functions for density estimation are symmetric and normalized, with peak at the sample. If the aim is to develop gradient-based methods, it is also desirable that the kernels be continuous and differentiable.

Based on these kernel properties, Parzen proposed the estimation of the PDF associated with the continuous RV X , $f_X(v)$, from a window of N samples (realizations of X): assuming that N independent and identically distributed (*i.i.d.*) samples $\{x_1, \dots, x_N\}$ are available, the PDF $f_X(v)$ can be estimated by [Parzen, 1962]:

$$\hat{f}_X(v) = \frac{1}{N} \sum_{i=1}^N \kappa_{\sigma} \left(\frac{v - x_i}{\sigma} \right), \tag{2.10}$$

where $\kappa_{\sigma}(\cdot)$ is an arbitrary kernel function and σ is the kernel size.

A common option in the literature is the use of the Gaussian kernel function $G_{\sigma^2}(\cdot)$, which can be defined as [Principe, 2010]:

$$G_{\sigma^2}(v - x_i) = \frac{1}{\sqrt{2\pi}\sigma} \exp \left(\frac{-|v - x_i|^2}{2\sigma^2} \right), \tag{2.11}$$

where the kernel size σ plays the role of a smoothing factor and $|\cdot|$ is the absolute value operator. The preference for this choice is justified by the large occurrence of Gaussian distributed RVs in practical scenarios and, mainly, by the simplification properties it holds. For instance, the integral of the product of two Gaussian kernel functions leads to another Gaussian kernel evaluated at the samples difference:

$$\int G_{\sigma^2}(v - x_i) G_{\sigma^2}(v - x_j) dv = G_{2\sigma^2}(x_i - x_j). \tag{2.12}$$

This property shall be particularly useful for us, as we will see later.

Note that the Parzen window method considers *i.i.d.* samples, but, in practice, statistically dependent samples can be considered, with certain impact on the estimation, depending on the “degree” of dependence. In these cases, the Gaussian kernel also shows to be a favorable choice, since the product of Gaussian functions treat the samples independently, contributing to the reduction of the estimation error [Scott, 2015].

2.2.2 The Multivariate Kernel Density Estimator

The work of Parzen [Parzen, 1962] was limited to univariate densities and, indeed, within the ITL field, the use of the Parzen window method for univariate PDF density estimation is the standard approach due to its greater mathematical simplicity. However, the multivariate (or joint) PDF estimation can also be a promising or even necessary approach – e.g., on the MI estimation, given by Eq. (2.4). In fact, the generalization of the Parzen window method for multivariate densities was introduced by Cacoullos [1966] and later applied to some practical problems [Silverman, 1978; Scott, 2015]. In our work, the manipulation of multivariate densities will be of fundamental importance to extract the temporal structure underlying the signals of interest.

Basically, from the temporal perspective, the estimation of the multivariate PDFs can be stated as follows: assume that $\mathbf{x}_n = [x_n \ x_{n-1} \ \dots \ x_{n-M}]^T$ is the vector composed of signal x_n at time instant n plus M of its delayed versions, being associated with the vector of RVs $\underline{X} = \{X_n, X_{n-1}, \dots, X_{n-M}\}$ (note that, in this case, the RV is not required to be *i.i.d.*). Thus, similarly to the Parzen window method, from a window of N vector samples $\{\mathbf{x}_1, \dots, \mathbf{x}_N\}$, the estimate of the multivariate PDF $f_{\underline{X}}(\mathbf{v})$ is

$$\hat{f}_{\underline{X}}(\mathbf{v}) = \frac{1}{N} \sum_{i=1}^N \kappa_{\sigma} \left(\frac{\mathbf{v} - \mathbf{x}_i}{\sigma} \right), \quad (2.13)$$

where $\kappa_{\sigma}(\cdot)$ is the multivariate kernel function, since it operates on vectors (instead of samples, as in Eq. (2.10)), and σ is the kernel size. Since this estimate is very similar to Eq. (2.10), we will refer to it as the multivariate Parzen window method.

Just like the univariate case, the multivariate kernel function must satisfy the Mercer's conditions – i.e., to be non-negative definite and symmetric – and, to be suitable for PDF estimation, it must also fulfill the moments constraints [Scott, 2015]:

$$\begin{aligned} (i) \quad & \int_D \kappa(\mathbf{v}) \, d\mathbf{v} = 1; \\ (ii) \quad & \int_D \mathbf{v} \kappa(\mathbf{v}) \, d\mathbf{v} = \mathbf{0}; \\ (iii) \quad & \int_D \mathbf{v} \mathbf{v}^T \kappa(\mathbf{v}) \, d\mathbf{v} = \mathbf{I}_{M+1}; \end{aligned} \quad (2.14)$$

where $D \subseteq \mathbb{R}^{(M+1)}$ and \mathbf{I}_{M+1} is the identity matrix of dimension $M+1$. If $\kappa(\mathbf{v})$ is indeed a multivariate kernel function, then the two last expressions are very informative about the marginal kernels: the expression (ii) states that the mean values of the marginal kernels are all null; while expression (iii) affirms that the marginal kernels are pair-wisely uncorrelated and each of them present unit variance. Hence, the multivariate kernel functions are symmetric and normalized, typically with peak on the sample.

For reasons similar to the univariate Gaussian kernel, the multivariate Gaussian kernel occupies a special place among all the multivariate kernel functions. Mathematically, it can be defined as

$$G_{\Sigma}(\mathbf{v} - \mathbf{x}_i) = \frac{1}{\sqrt{(2\pi)^{M+1} \det(\Sigma)}} \exp \left[\frac{-1}{2} (\mathbf{v} - \mathbf{x}_i)^T \Sigma^{-1} (\mathbf{v} - \mathbf{x}_i) \right], \quad (2.15)$$

where $\Sigma = \sigma^2 \mathbf{I}_{M+1}$ is the covariance matrix and $\det(\cdot)$ is the determinant operator. Since it is continuous and differentiable, the multivariate Gaussian kernel is an attractive option to be used in optimization techniques based on the stochastic gradient.

Other important advantage of the multivariate Gaussian kernel is the analogous property of the integral of the product of two Gaussian functions, which results in

$$\int_D G_{\Sigma}(\mathbf{v} - \mathbf{x}_i) G_{\Sigma}(\mathbf{v} - \mathbf{x}_j) d\mathbf{v} = G_{2\Sigma}(\mathbf{x}_i - \mathbf{x}_j). \quad (2.16)$$

This property shall be very useful for the study of the multivariate case.

It is important to mention that the multivariate case might suffer from the so-called “curse of dimensionality”, in which it is stated that the higher the dimension the larger must be the number of samples necessary to obtain reliable density estimates [Scott, 2015]. This fact, allied to the increment on the computational cost it engenders, may have caused certain aversion to this approach. However, as we intend to show, the “curse of dimensionality” is not severe and, with the huge computational power available nowadays, the performance gain provided by the multivariate perspective is worth its costs.

In the following, we will show how the kernel methods are applied to the ITL criteria. However, since the standard approach focus on the use of the univariate Parzen window method, the derivation will be limited to this case. The application of the multivariate kernel density estimator will be addressed later, starting from Chapter 5.

2.3 The ITL Criteria

Shannon has introduced the concept of uncertainty with his entropy definition and, later on 1976, Alfred Rényi proposed a generalization of this idea in [Rényi, 1976]. Nonetheless, the effective use of the entropy as a criterion for the channel equalization problem only occurred on the beginning of the 2000’s [Erdogmus and Principe, 2002a,b; Santamaría et al., 2002a; Sala-Alvarez and Vázquez-Grau, 1997; Principe, 2010], where a Rényi’s entropy estimator was accomplished through the use of the Parzen window method. This first approach opened way to other similar approaches [Santamaría et al., 2002b; Lázaro et al., 2003a, 2005; Santamaría et al., 2006], forming a set of methods that later was classified as belonging to the ITL field, whose objective was the application of the Information Theory concepts in machine learning problems. It is possible to state

that the research on this topic was mainly concentrated on the research group led by Prof. José C. Príncipe, but also counted with important contributions of other groups, like that of Silva et al. [2005] and of Cavalcante and Romano [2005], responsible for using the Parzen window method in the Shannon's entropy and in information theoretic similarity measures.

Although the term ITL is commonly associated with the use of the Parzen window method, in the big picture, any use of the entities and concepts belonging to the Information Theory applied to a filtering task might be classified as an ITL method as well [Silva et al., 2016]. Following this line of reasoning, the beginning of the ITL field can be traced back to the 80's, when Information Theory concepts were massively used on ICA and/or BSS problems [Hyvärinen et al., 2001; Comon and Jutten, 2010], but without relying on the specific use of the Parzen window estimator.

In the present thesis, we also pursue the wide perspective of the ITL definition, whose criteria are directly involved with the notion of information about the variables of interest. As we have seen from entropy and MI definitions presented in Section 2.1, the information concept makes indispensable use of the distributions associated with the signals of interest, which, from a statistical perspective, is an instance containing all statistical moments, including higher-order statistics (HOS). In that sense, the ITL criteria encompass a richer statistical content in comparison with the classical approaches that are generally based on second-order statistics (SOS), which might be crucial when dealing with non-Gaussian distributions, temporally dependent sources, recurrent and nonlinear structures. These aspects allows, at least in theory, the achievement of formulations in a more general standpoint [Erdogmus and Principe, 2006].

The wide scope in which the instances of the information concept can be applied is undoubtedly vast, even if only the signal processing area is considered. This contributed to the emergence of several ITL criteria, but we will restrain ourselves to a small but representative set of them, which we roughly classified in measures of uncertainty and of similarity.

2.3.1 Uncertainty Measures

The uncertainty measures, as described by Shannon, are directly related to the notion of information. Within the ITL framework, we highlight the Shannon's and the Rényi's entropy.

Shannon's Entropy

The employment of the Shannon's entropy in signal processing problems was firstly addressed to ICA methods, in which kernel density estimators were employed [Ahmad and Lin, 1976] as well as further approximations in an attempt to reduce the computational

complexity [Comon and Jutten, 2010]. Particularly, in the context of the classification problem, the approximation followed by Silva et al. [2005] used a simple formulation allied to the use of the Parzen window estimator, as presented in the following.

Recalling the entropy definition for continuous RV given by Eq. (2.3), a sample mean is used instead of the expectation operator in the work of Silva et al. [2005], which results in:

$$\hat{H}^S(X) = \frac{-1}{N_x} \sum_{i=1}^{N_x} \log(f_X(x_i)), \quad (2.17)$$

where N_x is the number of samples of the signal x_n used for estimation. Note that the PDF is assessed only based on the sample values. Using the Parzen window method for univariate PDF estimation – given by Eq. (2.10) – and with Gaussian kernel functions, we obtain the following relation

$$\hat{J}_{HS} = -\frac{1}{N_x} \sum_{i=1}^{N_x} \log \left(\frac{1}{N_x} \sum_{j=1}^{N_x} G_{\sigma^2}(x_i - x_j) \right), \quad (2.18)$$

which is the Shannon’s entropy estimator via the use of the Parzen window method. As a cost function, it can be considered in several signal processing problems: for equalization purposes, the estimated Shannon’s entropy is usually a cost function that must be minimized, in order to reduce the uncertainty introduced by the channel [Principe, 2010]; however, for the BSS problem, the cost can be sometimes maximized, e.g., to increase the information flow [Hyvärinen et al., 2001].

Rényi’s Entropy

The proposal that vigorously contributed to establish and unify the ITL methods was introduced through the combination of the quadratic Rényi’s entropy and the Parzen window method for PDF estimation [Santamaría et al., 2002; Principe, 2010], an arrangement that presents the advantage of being differentiable, a property necessary for online adaptive algorithms based on the stochastic gradient.

Rényi’s entropy can be viewed as a generalization of Shannon’s entropy, since it preserves, to a certain extent, the properties of uncertainty. Sometimes called the order- α Rényi’s entropy, it can be defined as

$$H_\alpha^R(X) = \frac{1}{1-\alpha} \log \left(\int f_X^\alpha(v) dv \right), \quad (2.19)$$

where $\alpha \geq 0$ and $\alpha \neq 1$. Note that, differently from the Shannon’s entropy, the PDF only exists in the argument of the logarithm function. Interestingly, it is possible to show that, for $\alpha \rightarrow 1$, Rényi’s entropy becomes Shannon’s entropy [Principe, 2010].

For estimation purposes, the case in which $\alpha = 2$ – the quadratic Rényi’s entropy –

is usually preferred, since it leads to simpler relations when combined with the Parzen window method. Indeed, using a Gaussian kernel function, the quadratic Rényi's entropy can be written as

$$\begin{aligned}
\hat{J}_{HR} &= -\log \int_{-\infty}^{\infty} \left(\frac{1}{N_x} \sum_{i=1}^{N_x} G_{\sigma^2}(v - x_i) \right)^2 dv \\
&= -\log \frac{1}{N_x^2} \int_{-\infty}^{\infty} \left(\sum_{i=1}^{N_x} \sum_{j=1}^{N_x} G_{\sigma^2}(v - x_j) G_{\sigma^2}(v - x_i) \right) dv \\
&= -\log \frac{1}{N_x^2} \sum_{i=1}^{N_x} \sum_{j=1}^{N_x} \int_{-\infty}^{\infty} G_{\sigma^2}(v - x_j) G_{\sigma^2}(v - x_i) dv \\
&= -\log \left(\frac{1}{N_x^2} \sum_{i=1}^{N_x} \sum_{j=1}^{N_x} G_{2\sigma^2}(x_j - x_i) \right),
\end{aligned} \tag{2.20}$$

where the result given by Eq. (2.12) was used in the last step. Since the logarithm function $\log(\cdot)$ is monotonic, it can be disregarded in optimization problems, since the null-gradient points are not influenced by this change. In addition, the negative sign can also be discarded, with the proviso that the optimization direction must be inverted, i.e., if the objective is the maximization of the cost \hat{J}_{HR} , by disregarding the negative sign and the logarithm function, the resulting cost must be minimized. In literature, the argument of the logarithm is called quadratic Information Potential estimator (or simply IP) [Principe, 2010].

2.3.2 Similarity Measures

There exists a vast number of similarity measures which, in the context of ITL, aim at a most extensive information comparison among RVs, like Rényi's divergence, Cauchy-Schwarz divergence and quadratic MI [Principe, 2010; Principe et al., 2000]. For us, three of them shall be very useful: the MI, the Quadratic Divergence (QD) and the correntropy.

Mutual Information

In signal processing, the MI metric defined in Eq. (2.4) is particularly known for its application in ICA methods as a measure that exploits the degree of statistical independence between variables.

From a more generic standpoint, the MI can be viewed as a special case of the Kullback-Leibler (KL) divergence, which is a measure of dissimilarity between two distributions, i.e.:

$$D_{KL}(X||Y) = \int f_X(v) \log \left(\frac{f_X(v)}{f_Y(v)} \right) dv, \tag{2.21}$$

where $f_X(v)$ and $f_Y(v)$ are the two densities being compared. The KL divergence is zero

if and only if $f_X(v) = f_Y(v)$. If one considers the comparison between the joint density $f_{X,Y}(\mathbf{v})$ and the product $f_X(v_1)f_Y(v_2)$, the resulting KL divergence is exactly the MI measure, which can be written as

$$\begin{aligned}
 I(X;Y) &= \int_D f_{X,Y}(\mathbf{v}) \log \left(\frac{f_{X,Y}(\mathbf{v})}{f_X(v_1)f_Y(v_2)} \right) d\mathbf{v} \\
 &= \int_D f_{X,Y}(\mathbf{v}) (\log(f_{X,Y}(\mathbf{v})) - \log(f_X(v_1)) - \log(f_Y(v_2))) d\mathbf{v} \\
 &= - \int_D f_{X,Y}(\mathbf{v}) \log(f_X(v_1)) d\mathbf{v} - \int_D f_{X,Y}(\mathbf{v}) \log(f_Y(v_2)) d\mathbf{v} \\
 &\quad + \int_D f_{X,Y}(\mathbf{v}) \log(f_{X,Y}(\mathbf{v})) d\mathbf{v} \\
 &= H^S(X) + H^S(Y) - H^S(X, Y),
 \end{aligned} \tag{2.22}$$

where $\mathbf{v} = [v_1 \ v_2]^T$ and $D \subseteq \mathbb{R}^2$.

Since the MI can be decomposed in instances of the Shannon's entropy, MI estimation is usually reduced to the estimation of the marginal entropies $H^S(X)$ and $H^S(Y)$, which was already discussed. For the joint entropy $H^S(X, Y)$, approximations or special properties are usually explored [Comon and Jutten, 2010]. Other possibility is its estimation via multivariate kernels, but this discussion will be left for an opportune moment.

The Quadratic Divergence

An alternative measure for dissimilarity between PDFs is the QD measure. Differently from the KL divergence, the QD measure is symmetric with respect to the RVs, and can be considered as a distance measure. Interestingly, this idea also establishes connections with the notion of MI [Principe, 2010]. Its application is focused on the unsupervised channel equalization, since it leads to simpler estimators in comparison with the MI/KL divergence when combined with the Parzen window method [Santamaría et al., 2002b; Lázaro et al., 2005].

Mathematically, the QD measure can be defined as [Principe, 2010]:

$$\begin{aligned}
 QD(X||Y) &= \int (f_X(v) - f_Y(v))^2 dv \\
 &= \int f_X^2(v)dv + \int f_Y^2(v)dv - 2 \int f_X(v)f_Y(v)dv .
 \end{aligned} \tag{2.23}$$

Note that, similarly to the estimation of the quadratic Rényi's entropy, there emerge terms with the densities to the power of two, in which the Parzen window method can be applied satisfactorily. Assuming Gaussian kernel functions, the QD measure can be

estimated as [Lázaro et al., 2005]

$$\begin{aligned} \hat{J}_{QD} &= \frac{1}{N_x^2} \sum_{i=1}^{N_x} \sum_{j=1}^{N_x} G_{2\sigma^2}(x_j - x_i) + \frac{1}{N_y^2} \sum_{i=1}^{N_y} \sum_{j=1}^{N_y} G_{2\sigma^2}(y_j - y_i) \\ &\quad - \frac{2}{N_x N_y} \sum_{i=1}^{N_x} \sum_{j=1}^{N_y} G_{2\sigma^2}(y_j - x_i), \end{aligned} \quad (2.24)$$

where N_x and N_y are the number of samples used in the window for the RVs X and Y , respectively. If it is desired to match the PDFs $f_X(v)$ and $f_Y(v)$, then the criterion becomes the minimization of the cost \hat{J}_{QD} .

Correntropy

Other emblematic ITL entity for measuring similarity is the one called correntropy, which can be viewed as a generalized correlation function [Principe, 2010; Santamaría et al., 2006]. It differs from the previous methods for taking into account a kernel function $\kappa_\sigma(\cdot)$ in its definition:

$$\begin{aligned} v_{X,Y} &= \int_D \kappa_\sigma(\mathbf{v}) f_{X,Y}(\mathbf{v}) d\mathbf{v} \\ &= E_{X,Y}[\kappa_\sigma(\mathbf{v})], \end{aligned} \quad (2.25)$$

where $E_{X,Y}[\cdot]$ denotes expectation over the joint space $D \subseteq \mathbb{R}^2$. Depending on the chosen kernel function, different statistical moments about the RVs are considered. For instance, when Gaussian kernels are used, only even moments are encompassed in the measure – as can be shown through a Taylor series expansion [Principe, 2010].

Assuming a Gaussian kernel for the kernel function, the correntropy becomes [Principe, 2010]

$$\begin{aligned} v_{X,Y} &= \int_D G_\sigma(v_1 - v_2) f_{X,Y}(\mathbf{v}) d\mathbf{v} \\ &= \int G_\sigma(\xi) f_\Xi(\xi) d\xi \end{aligned} \quad (2.26)$$

where $\mathbf{v} = [v_1 \ v_2]^T$ and $\xi = v_1 - v_2$. Using a sample mean instead of the statistical expectation, the correntropy estimator becomes

$$\hat{v}_{X,Y} = \frac{1}{N} \sum_{i=1}^N G_{\sigma^2}(x_i - y_i), \quad (2.27)$$

where N is the number of differences $x_i - y_i$. When $x_i - y_i$ approaches zero, the kernel function value tends to its peak; hence, if it is desired to match the RVs X and Y , the maximization of the correntropy estimator can be used as a criterion.

It is worth mentioning that the correntropy main features are its lower computational cost and its lower sensitivity to the kernel size σ parameter in comparison with the other

ITL approaches. It also presents interesting relations to the correlation function and the estimated quadratic Rényi's entropy, hence the name [Principe, 2010]. Correntropy has been successfully used in a variety of applications, among which we cite time series analysis, channel equalization, robust regression and blind source separation [Santamaría et al., 2006; Li et al., 2007; Singh and Principe, 2009; Gunduz and Principe, 2009; Principe, 2010].

2.4 Conclusion

In this chapter, we focused on the optimization criterion, an entity whose purpose is to express the general objectives of the problem in mathematical terms. In signal processing problems, the adoption of some statistical properties of the underlying signals is usual. Particularly, the criteria belonging to the ITL framework are of special interest here, since they aim at the extraction of the signal statistical information in a manner as complete as possible, using concepts and measures from Information Theory. These entities are also known for their direct manipulation of the signal distributions, allowing a more extensive statistical characterization than that of the classical second-order moments.

In practical scenarios, the distributions associated with the signals might not be easily obtained, being usually estimated from samples. In that sense, we presented the Parzen window method, which is the standard approach for PDF estimation within the ITL framework. This method encompasses the use of kernel functions, which presents interesting properties, such as the implicit operations in a potentially much higher-dimensional feature space – also known as the kernel trick. The extension of the Parzen window method to the multivariate case was also presented; however, in ITL, the univariate perspective is the common choice due to their reduced computational complexity. In light of this, a selection of the relevant ITL criteria was presented, being classified into uncertainty and similarity measures. In the first class, Shannon's and Rényi's entropy estimators were defined, and, in the second class, the mutual information, the quadratic divergence and the correntropy. Although they share similar concepts, each criterion follows a particular characterization of the signals, which can be more or less suitable, depending on the problem at hand. The presentation of the ITL criteria was limited to the univariate perspective, but we highlight that their multivariate extension will be addressed later, since it shall be very useful when extracting the temporal information about the signals, one of our main objectives in this work.

After choosing the filtering structure (Chapter 1) and the criterion, the next step is to define the optimization method, as will be discussed in the next chapter.

Chapter 3

Optimization Methods

Having defined the filtering structure and the adaptation criterion, it is possible to choose a suitable optimization method. An optimization methodology is responsible for efficiently adapting the parameters of the chosen filtering structure, in order to determine an optimum solution with respect to the criterion at hand.

The optimization process can be performed by means of an algorithm with finite steps to achieve the optimal solution, or with iterative convergence to a solution [Haykin, 1996], or, yet, by means of metaheuristics, which can perform a more extensive search for the solution [Blum and Roli, 2003]. In view of these possibilities, there are a number of optimization methods, whose features may vary depending on the type of focused cost function(s). For example, the cost function can be unimodal or multimodal (when there are one or multiple solutions), and the optimization process may involve one or more cost functions (criteria) at once – i.e., it is said to be single- or multi-objective [De Castro and Von Zuben, 2005].

For some specific classes of unimodal and single-objective problems, a finite-step algorithm can be used [Ruggiero and Lopes, 1997], but a wider class of problems can be addressed with iterative convergence methods, like gradient-based strategies; however, for multimodal cost functions, global convergence is not guaranteed [Haykin, 1996]. In these cases, a broader search strategy, like that provided by metaheuristics, can be an interesting alternative, although it is usually associated with a higher computational cost [Blum and Roli, 2003].

In signal processing, the most popular techniques for optimization are undoubtedly the gradient-based algorithms and, more recently, the metaheuristics [Haykin, 1996; De Castro and Von Zuben, 2005]. In this thesis, these approaches will also be of great importance and the details will be presented in the next sections.

3.1 Gradient-Based Optimization

Gradient-based optimization methods – also known as *gradient-descent* or *steepest-descent* [Murray, 1972] – are iterative methods, being the updates of the filter coefficients at each iteration corrections in the opposite direction of the gradient. Since the negative of the gradient of a function points towards its maximum decrease, this approach can be employed in minimization tasks (in maximization problems, the direction of the positive gradient is adopted, being the approach called *steepest-ascent* [Haykin, 1996]). It is required, however, that the objective (or cost) function be continuous and differentiable for all possible configurations of the parameters.

Mathematically, the update of the filter coefficients at iteration n can be expressed as

$$\mathbf{w}_{n+1} = \mathbf{w}_n - \mu \nabla_{\mathbf{w}} J(\mathbf{w}_n), \quad (3.1)$$

where $\nabla J(\mathbf{w}_n)$ is the gradient vector of the cost function evaluated with respect to \mathbf{w}_n , the filter coefficients at time instant n , and μ is a positive real-valued parameter, called *adaptation step* or *step size*, since it controls the amplitude of the corrections applied to the filter coefficients. A wrong choice of μ may cause the algorithm to diverge, i.e., it can lead the filter coefficients away from the minimum point, with modulus possibly approaching infinity [Haykin, 1996]. For this reason, it is not unusual to find a time-varying step size μ_n .

Since a recursive relation is established by Eq. (3.1), it is necessary to define an initial value for the weights at instant $n = 0$. When there is no prior information about the cost function, \mathbf{w}_0 is typically set equal to the null vector in supervised approaches [Haykin, 1996], while, in unsupervised tasks, the center spike initialization method is preferred, in which all the coefficients of \mathbf{w}_0 are set to be null, with exception of the central tap, set to unity [Ding et al., 1991; Foschini, 1985].

Based on this, the adaptation of the weights of the filter can be done accordingly to Alg. 3.1.

Algorithm 3.1 Steepest-Descent

1. Initialization of \mathbf{w}_0 and μ_0 ;
2. Using present guess of the solution, compute the gradient vector $\nabla J(\mathbf{w}_n)$;
3. Compute the next guess using

$$\mathbf{w}_{n+1} = \mathbf{w}_n - \mu_n \nabla_{\mathbf{w}} J(\mathbf{w}_n);$$

4. Update the step size μ_n , if necessary;
 5. Go back to step 2 and repeat the process.
-

The stability of the steepest-descent algorithm requires additional care, as unstable

behavior is possible due to the presence of feedback [Haykin, 1996; Ding et al., 1991]. The stability performance is determined by two factors: (i) the step size parameter μ , and (ii) the gradient vector $J(\mathbf{w}_n)$, as these two parameters entirely control the transfer function of the feedback loop [Haykin, 1996]. Depending on the cost function $J(\mathbf{w}_n)$, the condition for the stability can be studied by means of the natural modes of the algorithm [Widrow, 1971]. There are alternative approaches in which the step size adjustment is not strictly necessary, but, in turn, more complex computations are required. The Newton's method, for instance, demands the computation of the Hessian matrix, which could be unduly costly in certain cases [Haykin, 1998].

Gradient methods with update rule given by Eq. (3.1) can be classified as local search tools, since the gradient $\nabla J(\mathbf{w}_n)$ is a local operator, i.e., it is able to measure the growth profile at a given point of the surface cost, which reveals certain information about an infinitesimal neighborhood but not a clue about where the global optimum might be. Hence, these methods converge to local solutions. However, the gradient-based algorithms are a common choice for optimization due to their great simplicity. In addition to that, further simplification can be achieved by considering relaxations on the gradient $\nabla J(\mathbf{w}_n)$, as discussed in the following.

3.1.1 The Approximate Gradient

Ideally, exact measurements of the gradient vector $\nabla J(\mathbf{w}_n)$ allied to a suitable choice of the step size μ would certainly lead the steepest-descent algorithm to a minimum. However, in signal processing problems, exact measures of the gradient vector are not generally possible and it must be estimated from the available data. Very conveniently, in certain cases, it is possible to reduce the computational complexity by assuming further approximated versions of the gradient $\nabla J(\mathbf{w}_n)$.

Undoubtedly, these approaches may cause significant impact on the optimization performance, which can be associated with a lower convergence rate and/or with a slightly mismatch regarding the desired solution [Haykin, 1996; Shynk, 1989]. But, for certain applications, this impact is not a major issue. A remarkable example is the *stochastic gradient approach*, whose fundamental idea is to use instantaneous estimates in lieu of the mathematical expectation [Robbins and Monro, 1951; Haykin, 1996]. In that sense, the classical auto-correlation function for a given signal x_n would be approximated as

$$E[x_n x_n^*] \approx x_n x_n^*, \quad (3.2)$$

being $E[\cdot]$ the mathematical expectation operator. This estimate is unbiased in the sense that its expected value equals the true value of the mathematical expectation.

Algorithms derived from the stochastic approach, named *stochastic gradient algorithms*, may seem, at first sight, incapable of achieving good performance, since they

use instantaneous and, hence, imprecise estimates. However, since the algorithms operate in a recursive manner, they implicitly average the estimates during the course of adaptation [Haykin, 1996].

Examples of stochastic gradient algorithms are the Least-Mean-Square (LMS) [Widrow, 1971], the Constant Modulus Algorithm (CMA) [Godard, 1980], the Sato algorithm [Sato, 1975], among others.

The approximate gradient is also conveniently used when the computation of the gradient presents some difficulties, i.e., when the true gradient leads to complex expressions. Examples of this situation frequently arise in the adaptation of IIR filters, whose gradient depends on all the coefficients past values [Johnson Jr., 1984; Shynk, 1989]. In these cases, a slightly modified version of the gradient $\nabla J(\mathbf{w}_n)$ (for instance, a truncated version) is adopted. However, since a modified gradient is adopted, a small but tolerable deviation on the solutions may happen [Johnson Jr., 1984; Mendel, 1973].

3.2 Metaheuristics

Metaheuristics are search strategies with wide applicability to hard optimization problems, such as those that often arise in signal processing tasks. They are sometimes inspired by natural phenomena, which has been shown to provide efficient methodologies to explore the search space. They usually encompasses stochastic components to gain diversity on the search and they do not use the gradient or Hessian matrix of the objective function [Boussaïd et al., 2013]. Compared to iterative methods, the metaheuristics are not able to guarantee that a global solution will be found, but they are known to be more robust against local convergence and to be efficient in obtaining multiple solutions in a multimodal optimization task [Blum and Roli, 2003].

The advent of metaheuristics in the signal processing field can be attributed to a natural consequence of the more complex filtering criteria arising from the development of blind methods and of statistical decision and information-theoretic formulations [Attux et al., 2015; Chen et al., 1993; Principe, 2010], as well as the increasing adoption of nonlinear and recurrent filtering structures [Romano et al., 2010; Haykin, 1998]. The most widespread methods in signal processing are, historically, evolutionary algorithms [Chen and Wu, 1998], but particle swarm optimization has also received a significant deal of attention [Krusienski and Jenkins, 2004].

The success of a metaheuristic in a given optimization problem will basically depend on the balance between the exploration (diversification) and the exploitation (intensification). Exploration is intended to identify regions of the search space with high-quality solutions, while exploitation is meant to intensify the search in some promising areas of the accumulated search experience. The main differences among the existing metaheuristics concern how this balance is pursued [Boussaïd et al., 2013]. Particularly, in this work, we

are interested in the differential evolution (DE) algorithm [Storn and Price, 1997], whose global search strategy is coherent with the main aspects of the problems to be considered, as will be presented in the following.

3.2.1 Differential Evolution

Differential Evolution is an evolutionary search paradigm conceived to handle the optimization of multidimensional continuous-valued functions [Price et al., 2005]. The main feature of this technique is the fact that the candidate solutions are modified by mechanisms that exploit the information available in the current population, instead of using conventional operators based on random perturbations generated by specific distributions [Storn and Price, 1997]. Since it is not a gradient-based approach, the functions are not required to be differentiable.

The standard DE algorithm begins by randomly creating N_P parameter vectors $\mathbf{p}_i \in \mathbb{R}^{L \times 1}$, called individuals, being L the number of parameters in each vector. The objective is to find the parameter vector that maximizes (or minimizes) an objective function $f(\mathbf{p}) : \mathbb{R}^L \mapsto \mathbb{R}$, also called fitness function. At each iteration (or generation) g , a new mutated vector is generated for each individual according to the following expression:

$$\hat{\mathbf{p}}_i(g) = \mathbf{p}_j(g) + F(\mathbf{p}_k(g) - \mathbf{p}_l(g)), \quad (3.3)$$

where $j, k, l \in \{1, 2, \dots, N_P\}$ are randomly selected and mutually distinct indexes and F controls the size of the step that is taken in the direction given by $(\mathbf{p}_k(g) - \mathbf{p}_l(g))$.

Then, the elements of the mutated vector $\hat{\mathbf{p}}_i(g)$ are mixed with those of the original individual $\mathbf{p}_i(g)$ according to the following crossover rule:

$$\tilde{\mathbf{p}}_i^j(g) = \begin{cases} \hat{\mathbf{p}}_i^j(g) & \text{with probability } CR, \\ \mathbf{p}_i^j(g) & \text{with probability } (1 - CR), \end{cases} \quad (3.4)$$

where $j = 1, \dots, L$, and the parameter CR determines the rate at which the elements of the combined vector $\tilde{\mathbf{p}}_i(g)$ come from $\hat{\mathbf{p}}_i(g)$ or from $\mathbf{p}_i(g)$.

The last step involves the selection of the individuals that shall remain in the population to the next iteration. The procedure consists in comparing the combined vectors $\tilde{\mathbf{p}}_i(g)$ with the corresponding original individuals $\mathbf{p}_i(g)$, $i = 1, \dots, N_P$: if $f(\tilde{\mathbf{p}}_i(g))$ is better than $f(\mathbf{p}_i(g))$, then $\mathbf{p}_i(g + 1) = \tilde{\mathbf{p}}_i(g)$; otherwise, $\mathbf{p}_i(g + 1) = \mathbf{p}_i(g)$. These three steps – mutation, combination and selection – are repeated until a maximum number of iterations is reached. The pseudo-code presented in Alg. 3.2 summarizes the DE method for optimization.

In the problems to be encompassed in this work, we will constantly face multimodal objective functions, being required additional efforts to avoid local convergence during

Algorithm 3.2 Differential Evolution

Initialize all N_P individuals \mathbf{p}_i with random positions in the search-space;
while Maximum number of iterations is not reached **do**
for Each individual $\hat{\mathbf{p}}_i(g)$, $i \in N_P$ **do**
 Randomly pick three different individuals $\mathbf{p}_j(g)$, $\mathbf{p}_k(g)$, $\mathbf{p}_l(g)$, for $j, k, l \in \{1, 2, \dots, N_P\}$
 Generate new mutated vector:

$$\hat{\mathbf{p}}_i(g) = \mathbf{p}_j(g) + F(\mathbf{p}_k(g) - \mathbf{p}_l(g))$$

Combination of the original individual:

for Each $j \in \{1, \dots, L\}$ **do**

$$\tilde{\mathbf{p}}_i^j(g) = \begin{cases} \hat{\mathbf{p}}_i^j(g) & \text{with probability } CR, \\ \mathbf{p}_i^j(g) & \text{with probability } (1 - CR), \end{cases}$$

end for

Selection:

if $f(\tilde{\mathbf{p}}_i(g))$ is better than $f(\mathbf{p}_i(g))$ **then**

$$\mathbf{p}_i(g + 1) = \tilde{\mathbf{p}}_i(g)$$

else

$$\mathbf{p}_i(g + 1) = \mathbf{p}_i(g)$$

end if

end for

Pick the best individual of the population and present as best found candidate for solution until moment

end while

optimization. Indeed, instead of using stochastic (random) operators, the search mechanisms employed by the DE metaheuristic showed to be an efficient approach to extensively exploit the search space in local and global instances, which may significantly improve the success rate [Storn and Price, 1997].

3.3 Conclusion

There are several techniques that can be employed to perform optimization. However, in this work, there are two options that reveal themselves attractive when dealing with signal processing tasks: gradient-based optimization and metaheuristics. On the one hand, the gradient approach is a low cost and a canonical choice for optimization in equalization scenarios, mainly when the use of the approximate gradient is a reliable option. However, the simplicity comes at the cost of a potentially locally convergent method – since the gradient is a local operator – and the requirement that the objective function be continuous and differentiable. On the other hand, the metaheuristics tends to be more complex, but its use is justified depending on the nature of the optimization task, which may be significantly different from that found in more classical frameworks. Particularly, the DE metaheuristic is a preferred option here, since it encompasses the information available in the current population without only relying on random operators to explore the search space, which results in a very good compromise between local and global search capabilities. This feature shall be very useful in problems where the cost function is multimodal, which will be a constant issue in this work.

Chapter 4

Statistical and Adaptive Signal Processing Problems

The previous chapters provided a brief insight on the triad: filtering structure, adaptation criterion and optimization method, which, within the signal processing area, are fundamental elements to tackle a given problem. Particularly, in this work, we are mainly interested in two problems for which the information about the temporal structure of the signals shall be useful: the channel equalization and the Blind Source Separation (BSS) problems. In the following, we present the historical background on these two problems, where it will become evident the importance of establishing an important synergy among the triad.

4.1 Channel Equalization

The problem of channel equalization occupies a prominent place within the signal processing area, since it counts with applications in a diverse set of scenarios such as astronomy, biomedicine, speech, radar, sonar and seismic [Romano et al., 2010]. However, its definition has a particular character in the context of communication systems [Haykin, 2001]. In simple terms, in a communication system, the information flow between the parts is established through a transmission channel, which, depending on the environment it is inserted in, might cause distortions on the sent information and, consequently, impair the correct interpretation of the received message. In these cases, a filtering structure is usually adopted, here named *equalizer*, whose ideal objective is to mitigate the channel distorting effects [Haykin, 1996; Romano et al., 2010].

The block diagram that illustrates the communication system is presented in Fig. 4.1, where $H(z)$ is the channel transfer function, usually unknown, and $W(z)$ is the equalizer transfer function; the signals s_n , x_n and y_n are the transmitted, the received and the equalized signals, respectively. The signal s_n is commonly referred to as *source*. Note

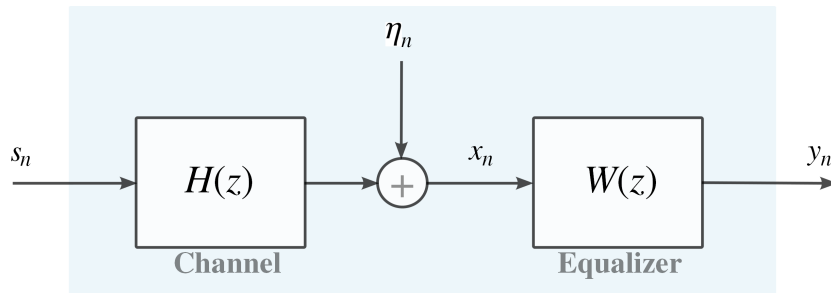


Figure 4.1: Block diagram of a communication system.

that there might also be the presence of noise, denoted by η_n , which could be the result of interference from other sources or even thermal noise. When limited to a finite bandwidth, the noise is usually modeled by a Gaussian distributed signal, but, in non-conventional environment, there might result different noise types, like the Laplacian or impulsive noise [Romano et al., 2010; Principe, 2010]. In that sense, it is expected from the equalizer to neutralize the dispersive effect caused by the channel – the well known “Intersymbol Interference” (ISI) – and, if possible, to perform noise attenuation. In other words, it is expected that the equalizer output y_n be as close as possible to the source s_n .

From the receiver standpoint, it can be admitted, ideally, that the equalizer output y_n be a time shifted and/or a scaled version of s_n , i.e.,

$$y_n = a s_{n-k}, \quad (4.1)$$

where a is a scale factor and k an arbitrary time delay. If the relation given by Eq. (4.1) is obeyed, then the equalizer has completely compensated the channel (removing the ISI) and the noise disturbances.

In the literature, an approach that is usually followed in theoretical formulations focuses on the relation between channel and equalizer, being the noise neglected for simplification purposes. In this case, a combined channel+equalizer impulse response is considered, $c_n = \sum_{i=-\infty}^{\infty} w_i^* h_{n-i}^*$, which is the convolution between the channel and the equalizer (assuming, hypothetically, an infinite length in both causal and non-causal parts). Mathematically, the output signal of the combined channel+equalizer system is

$$\begin{aligned} y_n &= \mathbf{w}^H \mathbf{x}_n = \sum_{i=-\infty}^{\infty} w_i^* x_{n-i} \\ &= \sum_{i=-\infty}^{\infty} w_i^* \left(\sum_{j=-\infty}^{\infty} h_j^* s_{n-i-j} \right), \end{aligned} \quad (4.2)$$

and, by adopting $j = l - i$, there results

$$\begin{aligned}
 y_n &= \sum_{i=-\infty}^{\infty} w_i^* \left(\sum_{l=-\infty}^{\infty} h_{l-i}^* s_{n-l} \right) \\
 &= \sum_{l=-\infty}^{\infty} \left(\sum_{i=-\infty}^{\infty} w_i^* h_{l-i}^* \right) s_{n-l} \\
 &= \sum_{l=-\infty}^{\infty} c_l s_{n-l} = \mathbf{c}^T \mathbf{s}_n.
 \end{aligned} \tag{4.3}$$

Hence, the output y_n can be directly expressed as a function of the source s_n .

In order to obtain the relation given by Eq. (4.1), the combined channel+equalizer system $\mathbf{c} = [c_{-\infty} \cdots c_{-1} c_0 c_1 \cdots c_{\infty}]^T$ must be a vector with a single non-null element equal to a , i.e.,

$$\mathbf{c} = \left[0 \cdots 0 \ a \ 0 \cdots 0 \right]^T. \tag{4.4}$$

This situation is referred to as the Zero-Forcing (ZF) condition [Haykin, 1996], whose name is related with the fact that \mathbf{c} is forced to be null for all considered delays but a single one. It is important to mention that the ZF condition may not be attainable, depending on the channel and equalizer models.

Although the combined channel+equalizer system represents an important theoretical indicative of the equalization degree, in practice, the unknown channel impulse response limits its use. In any case, the partial or complete channel equalization will only be possible if the equalizer structure and parameters are correctly adjusted, a result that can only be accomplished with a well chosen/defined triad: the filtering structure, the criterion and the optimization method. In channel equalization, the main approaches regarding the triad choice are divided into two classes: supervised and unsupervised.

4.2 Supervised Equalization

In supervised channel equalization, it is assumed that there is a finite sequence of the source that is available to be used as a reference signal d_n by the equalizer. When the sequence d_n is transmitted, there starts a training period for the receiver, which can use the sequence d_n known *a priori* to perform the equalizer adaptation.

In light of this, the supervised criteria aim at the exploitation of the statistical information concerning the reference signal d_n and other signals of interest, but the approaches might vary depending on the equalizer structure. In our study, FIR and IIR filters will play a central role and a special attention will be dedicated to them.

4.2.1 Finite Length Equalizers

When the equalizer can be modeled as a simple linear combiner, such as an FIR filter, the problem formulation can gain further mathematical simplicity, mainly from the quadratic perspective, whose elegant derivation is able to lead to a closed-form solution, also known as the Wiener solution. However, this SOS-based analysis can impose certain performance limitations when signals are non-Gaussian. In this case, a promising approach is the use of the ITL framework. Hence, in order to provide a more complete perspective of the problem, the SOS-based Wiener filtering paradigm and two supervised ITL-based approaches will be described in the following.

Wiener Filtering

Probably the key pillar in supervised equalization is the paradigmatic Wiener criterion [Haykin, 1996; Romano et al., 2010], whose origin dates back to the independent works of Kolmogorov and Wiener, in 1941 and 1942, respectively [Haykin, 1996].

Basically, the criterion is totally formulated from the notion of the Mean-Squared Error (MSE) between the reference signal d_n and the equalizer output y_n :

$$J_{MSE}(\mathbf{w}) = E[|e_n|^2] = E[|d_n - y_n|^2], \quad (4.5)$$

where $E[\cdot]$ is the expectation operator. The objective is, then, to minimize the MSE cost, so that, ideally, the error energy is as close as possible to zero.

Assuming that the source is a stationary discrete-time stochastic process, further simplification can be achieved with the analysis of the SOS. Indeed, in this case, the correlation matrix \mathbf{R}_X associated with signal x_n and the cross-correlation vector \mathbf{p}_{XD} between signals x_n and d_n are given by

$$\mathbf{R}_X = E[\mathbf{x}_n \mathbf{x}_n^H] = \begin{bmatrix} r_X(0) & r_X(1) & \cdots & r_X(N) \\ r_X(-1) & r_X(0) & \cdots & r_X(N-1) \\ \vdots & \vdots & \ddots & \vdots \\ r_X(-N) & r_X(-N+1) & \cdots & r_X(0) \end{bmatrix}, \quad (4.6)$$

and

$$\mathbf{p}_{XD} = E[\mathbf{x}_n d_n^*], \quad (4.7)$$

respectively, where $\mathbf{x}_n = [x_n \ x_{n-1} \ \cdots \ x_{n-N}]^T$ is the equalizer input vector and $r_X(k) = E[x_n x_{n-k}^*]$ is the autocorrelation function. Based on these entities, the MSE

cost can be expanded as:

$$\begin{aligned}
J_{MSE}(\mathbf{w}) &= E[|e_n|^2] = E[e_n e_n^*] \\
&= E[(d_n - \mathbf{w}^H \mathbf{x}_n)(d_n^* - \mathbf{x}_n^H \mathbf{w})] \\
&= E[d_n d_n^*] - \mathbf{w}^H E[\mathbf{x}_n d_n^*] - E[d_n \mathbf{x}_n^H] \mathbf{w} + \mathbf{w}^H E[\mathbf{x}_n \mathbf{x}_n^H] \mathbf{w} \\
&= \sigma_D^2 - \mathbf{p}_{XD}^H \mathbf{w} - \mathbf{w}^H \mathbf{p}_{XD} + \mathbf{w}^H \mathbf{R}_X \mathbf{w},
\end{aligned} \tag{4.8}$$

where σ_D^2 is the variance associated with the signal d_n . The Eq. (4.8) exposes the quadratic character of the MSE cost with respect to the FIR equalizer coefficients \mathbf{w} . Since \mathbf{R}_X is typically positive definite, the MSE cost forms a paraboloid with a single minimum point.

In order to reach the minimum cost value, a possible approach is to identify the condition that leads to the null derivative. In that sense, the differentiation of $J_{MSE}(\mathbf{w})$ with respect to \mathbf{w} results in:

$$\begin{aligned}
\nabla_{\mathbf{w}} J_{MSE}(\mathbf{w}) &= \frac{dJ_{MSE}(\mathbf{w})}{d\mathbf{w}} = \frac{d}{d\mathbf{w}} (\sigma_D^2 - \mathbf{p}_{XD}^H \mathbf{w} - \mathbf{w}^H \mathbf{p}_{XD} + \mathbf{w}^H \mathbf{R}_X \mathbf{w}) \\
&= -2\mathbf{p}_{XD} + 2\mathbf{R}_X \mathbf{w},
\end{aligned} \tag{4.9}$$

and, making Eq. (4.9) equal to zero (i.e., the null derivative), it yields

$$\mathbf{w}_o = \mathbf{R}_X^{-1} \mathbf{p}_{XD}, \tag{4.10}$$

where \mathbf{w}_o is the equalizer coefficient vector \mathbf{w} at its optimum value in the minimum mean-squared error sense. This vector is called Wiener solution.

The minimum MSE value can then be obtained by replacing Eq. (4.10) in Eq. (4.8):

$$\begin{aligned}
J_{MSE}(\mathbf{w}_o) &= \sigma_d^2 - \mathbf{p}_{XD}^H \mathbf{w}_o - \mathbf{w}_o^H \mathbf{p}_{XD} + \mathbf{w}_o^H \mathbf{R}_X \mathbf{w}_o \\
&= \sigma_d^2 - \mathbf{p}_{XD}^H \mathbf{R}_X^{-1} \mathbf{p}_{XD}.
\end{aligned} \tag{4.11}$$

It is important to remark that the Wiener solution (Eq. (4.10)) depends on the temporal delay k considered for the reference signal, which might be $d_n = s_{n-k}$. For each delay k , there might be a different Wiener solution, being necessary to perform a search for the delay k that leads to the best performance.

Gradient-Based Algorithms

As we have seen in Section 3.1, the gradient-based algorithms can be attractive due to their relative simplicity. From the large set of algorithms, we highlight the ones based on the deterministic gradient and the *Least-Mean-Square* (LMS) [Romano et al., 2010].

Deterministic Gradient Algorithm

Since the equalizer coefficients \mathbf{w} may change throughout time instants (or updates), we will henceforth call them \mathbf{w}_n , which is the vector of coefficients of the FIR equalizer at time instant n .

Following the gradient update rule given by Eq. (3.1) and using the gradient of the MSE cost shown in Eq. (4.9), the deterministic gradient algorithm will be defined by the updates

$$\mathbf{w}_{n+1} = \mathbf{w}_n - \mu(-2\mathbf{p}_{XD} + 2\mathbf{R}_X\mathbf{w}_n). \quad (4.12)$$

It is important to note that no matrix inversion is necessary in the process. However, the cross-correlation vector \mathbf{p}_{XD} and the correlation matrix \mathbf{R}_X still must be estimated.

LMS Algorithm

The LMS algorithm is an optimization method widely used in the linear channel equalization problem, mainly due to its robustness and simplicity. This method is based on the stochastic gradient approach (Section 3.1) proposed by Robbins and Monro [1951], whose main characteristic is the substitution of the mathematical expectation by instantaneous estimates.

For the MSE, the stochastic gradient approach of the cross-correlation vector \mathbf{p}_{XD} and the correlation matrix \mathbf{R}_X are

$$\begin{aligned} \mathbf{p}_{XD} &\longrightarrow \hat{\mathbf{p}}_{XD} = \mathbf{x}_n d_n^* \\ \mathbf{R}_X &\longrightarrow \hat{\mathbf{R}}_X = \mathbf{x}_n \mathbf{x}_n^H, \end{aligned} \quad (4.13)$$

which leads to the following approximate gradient:

$$\hat{\nabla} J_{MSE}(\mathbf{w}_n) = -2\mathbf{x}_n d_n^* + 2\mathbf{x}_n \mathbf{x}_n^H \mathbf{w}_n. \quad (4.14)$$

Hence, from Eq. (4.14) and the gradient update rule given by Eq. (3.1), the recursive relation of the LMS algorithm is

$$\mathbf{w}_{n+1} = \mathbf{w}_n + \mu(d_n^* - \mathbf{x}_n^H \mathbf{w}_n) \mathbf{x}_n, \quad (4.15)$$

where the multiplicative factor of 2 in Eq. (4.14) was not considered – since this only causes a scale change on the step size μ . The complex form of the LMS algorithm was originally proposed by Widrow et al. [1975] and is also called by the name *stochastic gradient-based algorithm*.

In 1996, Macchi [1996] performed a study on the convergence properties of the LMS algorithm and observed that, although the instantaneous estimates of \mathbf{p}_{XD} and \mathbf{R}_X present high variance, the recursive nature of the LMS algorithm performs, in a certain way, an

average estimate of \mathbf{p}_{XD} and \mathbf{R}_X throughout the iterative process, being the step size μ the major responsible for the algorithm convergence.

ITL Filtering

From a general perspective, the ITL methods applied to the supervised problem aim at the extraction of richer statistical characterization about the error signal $e_n = d_n - y_n$, which can be particularly convenient in non-Gaussian scenarios [Principe, 2010]. The most common methods are Rényi's entropy [Erdogmus and Principe, 2002a,b] and correntropy [Principe, 2010] (introduced in Section 2.3.1).

Regarding the Rényi's definition about entropy, its application in the supervised channel equalization problem is associated with the notion of uncertainty, in the sense that the distortion effect caused by the channel might contribute to the increase of the error uncertainty. Ideally, it is expected that the error signal e_n be a null sequence after a successful equalization, a circumstance in which the error entropy is null. However, if the error is not null, its entropy will tend to increase [Principe, 2010]. In light of this, Erdogmus and Principe [2002a] proposed the ITL criterion which aims at the minimization of the quadratic Rényi's entropy of the error, i.e.,

$$\min_{\mathbf{w}} H_2^R(E) = \min_{\mathbf{w}} -\log \left(\int f_E^2(v) dv \right), \quad (4.16)$$

where $f_E(v)$ is the PDF associated with the error. However, since the channel and noise are usually unknown in the equalization problem, the error PDF must be estimated, being a promising approach the Parzen window method with Gaussian kernel functions (see Section 2.3.1), which results in:

$$\hat{J}_{HR}(\mathbf{w}) = -\log \left(\frac{1}{N_e^2} \sum_{i=1}^{N_e} \sum_{j=1}^{N_e} G_{2\sigma^2}(e_j - e_i) \right), \quad (4.17)$$

where N_e is the number of considered error samples. For simplification purposes, the IP cost can also be used. Differently from the MSE cost, the cost \hat{J}_{HR} is no longer a paraboloid and, consequently, a closed-form solution is difficult to be obtained.

Other important supervised ITL criterion is that based on correntropy (Section 2.3.2). Since this entity can be seen as a similarity measure capable of extracting the HOS about the RVs, one can apply it to the equalization problem by maximizing the correntropy between the reference d_n and the equalizer output y_n signals, resulting in

$$\max_{\mathbf{w}} v_{D,Y} = \int_{\mathbb{R}^2} \kappa_{\sigma}(\mathbf{v}) f_{D,Y}(\mathbf{v}) d\mathbf{v}, \quad (4.18)$$

where $f_{D,Y}(\mathbf{v})$ is the joint PDF associated with the RVs D and Y . Again, using the

Gaussian function (Eq. (2.11)) as the kernel and the sample mean instead of the statistical expectation, there results:

$$\hat{J}_{cor}(\mathbf{w}) = \frac{1}{N_e} \sum_{i=1}^{N_e} G_{\sigma^2}(d_i - y_i) = \frac{1}{N_e} \sum_{i=1}^{N_e} G_{\sigma^2}(e_i). \quad (4.19)$$

In comparison with the quadratic Rényi's estimator, the correntropy-based cost $\hat{J}_{cor}(\mathbf{w})$ presents the advantages of requiring a lower computational cost (note that there is a single summation operator in Eq. (4.19)) and being less sensitive to variations on the kernel size σ . On the other hand, it can demand a larger number of samples N_e to provide a good estimate [Santamaría et al., 2006; Principe, 2010].

In situations where the channel is linear and the additive noise is Gaussian, both mentioned ITL criteria provide solutions that tend to be close to the MSE optimum [Principe, 2010; Boccato et al., 2016]. However, this is not the case when the source and/or noise are non-Gaussian distributed, a case in which the ITL algorithms tend to be more robust than that based on the MSE. Furthermore, the ITL-based approach gains special distinction from the classical MSE approach when nonlinear relationships emerge, such as those caused by the use of a multilayer perceptron neural network as an equalizer [Santamaría et al., 2002]. But we remind the reader that a linear structure might also lead to nonlinear relations, as occurs in IIR filters (Section 1.1.1), as we will see later.

From a general perspective, the computational burden associated with the costs can be reduced through the use of the adaptive algorithms – e.g., similarly to the LMS approach, where the estimation of the cross-correlation vector \mathbf{p}_{XD} and the correlation matrix \mathbf{R}_X are simplified, an adaptive algorithm can rely on a reduced number of samples for the ITL entities estimation.

Gradient-Based Algorithms

Regarding the ITL approaches, the gradient-based algorithms are also applied to channel equalization problems. Although local convergence is possible in this case (since the cost surface might be more complex than a paraboloid), the use of these methods in ITL is justified by its reduced computational cost [Santamaría et al., 2002; Principe, 2010].

For the quadratic Rényi's entropy estimator, Eq. (4.17), the gradient is given by [Santamaría et al., 2002]

$$\nabla_{\mathbf{w}_n} \hat{J}_{HR}(\mathbf{w}_n) \propto \frac{1}{2N_e^2 \sigma^2} \sum_{i=1}^{N_e} \sum_{j=1}^{N_e} G_{2\sigma^2}(e_{n-i} - e_{n-j}) (e_{n-i} - e_{n-j}) (\mathbf{x}_{n-i} - \mathbf{x}_{n-j}), \quad (4.20)$$

where the negative log was suppressed, since the null gradient point remains the same.

For the correntropy estimator, the gradient is [Principe, 2010]

$$\nabla_{\mathbf{w}_n} \hat{J}_{cor}(\mathbf{w}_n) = \frac{-1}{N_e \sigma^2} \sum_{i=1}^{N_e} G_{\sigma^2}(e_{n-i}) e_{n-i} \mathbf{x}_{n-i}. \quad (4.21)$$

The resulting algorithms are obtained by replacing Eqs. (4.20) and (4.21) in Eq. (3.1). Note that the stochastic approach is encompassed in the Rényi's entropy estimator via the Parzen window method, while, for the correntropy estimator, Eq. (4.19), there is a substitution of the mathematical expectation by sample estimation.

It is important to emphasize that, due to approximations on the gradient, the algorithms convergence may result in oscillations around the solution (the so-called *misadjustment* effect [Haykin, 1996]), which can be softened by the correct adjustment of the step size μ .

4.2.2 Infinite Length Equalizers

As presented in Section 1.1.1, the IIR structure is able to provide important features that may demand special care on the criterion definition, which contributed to the development of several approaches for this infinite length filter [Horvath Jr., 1976; Long et al., 1987; Regalia, 1994]. Among these approaches, we highlight the *equation-error* [Mendel, 1973] and the *output-error* [Johnson Jr., 1984] formulations, since they aim at simpler interactions with respect to criteria and/or optimization algorithms. Although the main efforts were aimed in the context of system identification, their application in channel equalization problems is straightforward. In the following, the two formulations – that are based on the MSE – will be presented in detail.

Equation-Error Formulation

The equation-error formulation is based on a simple but effective approach: in order to avoid the nonlinear relationship that emerges between the equalizer output y_n and the IIR coefficients, it is assumed that delayed versions of y_n , say y_{n-m} , already achieved equivalence with the reference signal d_{n-m} , being $m > 0$. Hence, the output of the IIR structure is modified to¹

$$y_{e,n} = \sum_{i=0}^{N_b} b_i x_{n-i} + \sum_{j=1}^{N_a} a_j d_{n-j}, \quad (4.22)$$

or, in a vector representation,

$$y_{e,n} = \boldsymbol{\theta}^T \boldsymbol{\phi}_{e,n}, \quad (4.23)$$

¹Very interestingly, the equation-error formulation can also be viewed as a Decision Feedback Equalizer (DFE) without error propagation.

where $\phi_{e,n} = [x_n \ x_{n-1} \ \dots \ x_{n-N_b} \ d_{n-1} \ \dots \ d_{n-N_a}]^T$ – the vector θ is as defined in Eq. (1.5). Note that Eq. (4.22) is very similar to Eq. (1.4), with exception that d_{n-m} is employed in lieu of y_{n-m} . As consequence, the feedback part in Eq. (4.22) is replaced by a feedforward linear combination of d_{n-m} .

As a supervised approach, a simple and efficient criterion for this formulation can be obtained by means of the minimization of the MSE between the reference signal d_n and the output signal $y_{e,n}$, i.e.,

$$J_{MSEE}(\theta) = E [|e_{e,n}|^2] = E [(d_n - y_{e,n})(d_n - y_{e,n})^*], \quad (4.24)$$

which is a unimodal cost in function of θ , i.e., the cost has a single minimum.

After optimization, which could be, for instance, via a gradient-based algorithm, the coefficients a_j , for $j = \{1, \dots, N_a\}$, are ‘copied’ to an all-pole filter in cascade with $B(z)$ [Shynk, 1989], as shown in Fig. 4.2. Although it seems to be a very convenient approach, the equation-error formulation may lead to biased solutions, depending how far is y_n from d_n . In fact, the presence of noise is a preponderant factor leading to biased solutions [Shynk, 1989], and, due to this, this approach is usually preferred in scenarios with high *Signal-to-Noise Ratio* (SNR).

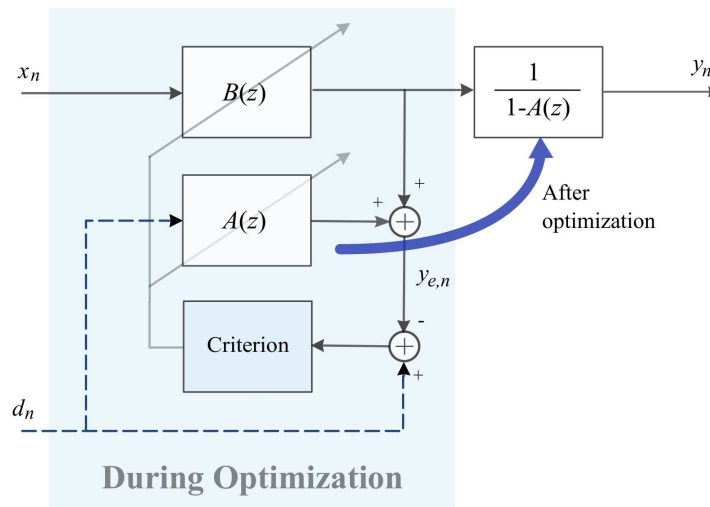


Figure 4.2: Equation-error formulation - Copy operation.

Since the equation-error formulation allows to approximate the IIR structure by two FIR filters, a closed-form solution similar to Eq. (4.10) can be obtained. However, a gradient-based algorithm is usually preferred in practical scenarios due to its lower computational complexity, such as the LMS-based algorithm [Widrow et al., 1976] described in the following.

LMS Algorithm

By changing the equalizer output y_n to the approximate $y_{e,n}$ (Eq. (4.22)), the equation-error formulation is able to reduce the relation between $\boldsymbol{\theta}$ and $y_{e,n}$ to a linear one, allowing the direct implementation of the LMS-based algorithm [Shynk, 1989; Haykin, 1996].

In this case, the gradient of the $J_{MSEE}(\boldsymbol{\theta})$ cost is given by

$$\begin{aligned}\nabla_{\boldsymbol{\theta}} J_{MSEE}(\boldsymbol{\theta}) &= -e_{e,n} \nabla_{\boldsymbol{\theta}} y_{e,n} \\ &= -e_{e,n} \boldsymbol{\phi}_{e,n},\end{aligned}\tag{4.25}$$

and, similarly to the FIR equalizer counterpart (Eq. (4.15)), the weights optimization will follow the update rule:

$$\begin{aligned}\boldsymbol{\theta}_{n+1} &= \boldsymbol{\theta}_n - \mu \nabla_{\boldsymbol{\theta}_n} J_{MSEE}(\boldsymbol{\theta}_n) \\ &= \boldsymbol{\theta}_n + \mu e_{e,n} \boldsymbol{\phi}_{e,n},\end{aligned}\tag{4.26}$$

where the initial coefficients $\boldsymbol{\theta}_0$ are generally set to be null.

Output-Error Formulation

In the output-error formulation, no assumptions are made on the IIR structure, but on the derivatives of the gradient-based methods. In this case, the relation between $\boldsymbol{\theta}$ and y_n (given by Eq. (1.4)) is, as already known, nonlinear.

As in the equation-error formulation, the MSE-based criterion is the common approach, whose cost is given by

$$J_{MSOE}(\boldsymbol{\theta}) = E [|e_{o,n}|^2] = E [(d_n - y_n)(d_n - y_n)^*].\tag{4.27}$$

Note that, in this case, there is no closed-form solution and the cost $J_{MSOE}(\boldsymbol{\theta})$ may significantly differ from the previous paraboloid of the equation-error [Johnson Jr., 1984].

The nonlinear relationship between $\boldsymbol{\theta}$ and y_n becomes evident through the gradient of $J_{MSOE}(\boldsymbol{\theta})$, which can be written as

$$\frac{d}{d\boldsymbol{\theta}} J_{MSOE}(\boldsymbol{\theta}_n) = -e_{o,n} \left(\frac{d}{d\boldsymbol{\theta}_n} y_n \right)\tag{4.28}$$

being

$$\frac{\partial}{\partial a_{j,n}} y_n = y_{n-j} + \sum_{k=1}^{N_a} a_{k,n} \frac{\partial y_{n-k}}{\partial a_{j,n}};\tag{4.29}$$

$$\frac{\partial}{\partial b_{i,n}} y_n = x_{n-i} + \sum_{k=1}^{N_a} a_{k,n} \frac{\partial y_{n-k}}{\partial b_{i,n}}.$$

The partial derivative on the right side of Eq. (4.29) is non-null and can be seen as a

direct result of the feedback part existent on the IIR structure: the past samples of y_n are dependent on the past values of the coefficients, which, in turn, are related to the present ones – $a_{j,n}$ and $b_{i,n}$ – due to the successive iterations of the gradient-based optimization approaches [Shynk, 1989]. Note that Eq. (4.29) is not easily computed, since the partial derivatives are taken with respect to the current values of the coefficients $a_{j,n}$ e $b_{i,n}$, being not recursive.

In order to simplify the gradient computation, some approximations are usually considered [Johnson Jr., 1984; Shynk, 1989], which result in different algorithms. In the present work, we consider two of them: the *Pseudolinear Regression* (PLR) [Feintuch, 1976] and the simplified *Recursive Prediction Error* (RPE) [Ljung and Söderström, 1983; Ljung, 1998].

PLR Algorithm

The PLR algorithm is based on a relaxation involving the IIR equalizer coefficients $\boldsymbol{\theta}$ and its output y_n . Basically, the gradient of the cost $J_{MSOE}(\boldsymbol{\theta}_n)$ is approximated to

$$\begin{aligned}\nabla_{\boldsymbol{\theta}} J_{MSOE}(\boldsymbol{\theta}) &= -e_{o,n} \nabla_{\boldsymbol{\theta}} y_n \\ &\approx -e_{o,n} \boldsymbol{\phi}_n,\end{aligned}\tag{4.30}$$

which is based on the supposition that y_n and $\boldsymbol{\theta}$ are linearly combined. Hence, the coefficients update rule becomes

$$\boldsymbol{\theta}_{n+1} = \boldsymbol{\theta}_n + \mu e_{o,n} \boldsymbol{\phi}_n.\tag{4.31}$$

This approach is very similar to the LMS algorithm, but it does not make use of the reference signal d_n to compose the vector $\boldsymbol{\phi}_n$, which should be as defined in Eq. (1.5).

Simplified RPE Algorithm

For the RPE algorithm, it is assumed a slow adaptation of the coefficients, so that $\boldsymbol{\theta}_n \approx \boldsymbol{\theta}_{n-1} \approx \dots \approx \boldsymbol{\theta}_{n-N_i}$, being N_i a given number of iterations [Johnson Jr., 1984]. As consequence, the derivative of Eq. (4.29) is approximated to

$$\begin{aligned}\frac{\partial}{\partial a_{j,n}} y_n &\approx y_{n-j} + \sum_{k=1}^{N_a} a_{k,n} \frac{\partial y_{n-k}}{\partial a_{j,n-k}}; \\ \frac{\partial}{\partial b_{i,n}} y_n &\approx x_{n-i} + \sum_{k=1}^{N_a} a_{k,n} \frac{\partial y_{n-k}}{\partial b_{i,n-k}},\end{aligned}\tag{4.32}$$

where $j = \{1, \dots, N_a\}$ and $i = \{0, \dots, N_b\}$. In this case, the derivatives are recursive, and can actually be seen as signals filtered by the all-pole filter $1/(1 - A(z))$. This is the main idea behind the standard RPE algorithm. However, each component of the gradient vector for $j = \{1, \dots, N_a\}$ and $i = \{0, \dots, N_b\}$ must be filtered by $1/(1 - A(z))$ individually.

In order to reduce the complexity, a simplified RPE approach can be achieved if assumed:

$$\begin{aligned} \frac{\partial y_n}{\partial a_{j,n}} &\approx \dot{y}_{n-j}; \\ \frac{\partial y_n}{\partial b_{i,n}} &\approx \dot{x}_{n-i}, \end{aligned} \quad (4.33)$$

for $j = \{1, \dots, N_a\}$ and $i = \{0, \dots, N_b\}$. Hence, each component of the gradient is simply a delayed version of \dot{y}_n or \dot{x}_n , which leads to [Johnson Jr., 1984; Shynk, 1989]

$$\begin{aligned} \dot{y}_n &\approx y_n + \sum_{k=1}^{N_a} a_{k,n} \dot{y}_{n-k}; \\ \dot{x}_n &\approx x_n + \sum_{k=1}^{N_a} a_{k,n} \dot{x}_{n-k}, \end{aligned} \quad (4.34)$$

which is, basically, the filtering of y_n and x_n by the all-pole filter $1/(1 - A(z))$, as illustrated in Fig. 4.3. The signals \dot{y}_n and \dot{x}_n are called simplified gradient components and, according

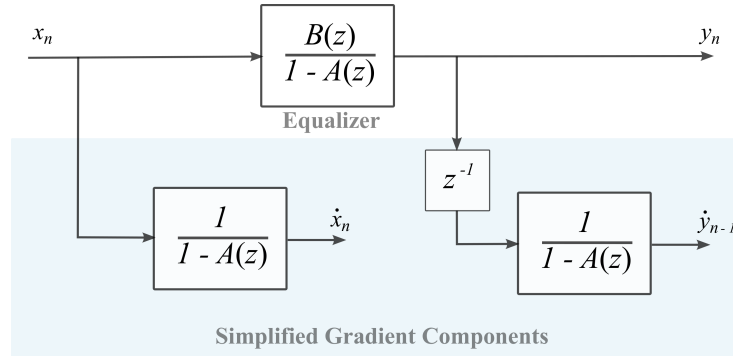


Figure 4.3: Output-error formulation - Simplified gradient components.

to Eq. (4.33), its delayed versions are necessary to compose the gradient vector. Thus, the approximate gradient becomes

$$\begin{aligned} \nabla_{\boldsymbol{\theta}} J_{MSOE}(\boldsymbol{\theta}) &= -e_{o,n} \nabla_{\boldsymbol{\theta}} y_n \\ &\approx -e_{o,n} \dot{\boldsymbol{\phi}}_n, \end{aligned} \quad (4.35)$$

being $\dot{\boldsymbol{\phi}}_n = [\dot{x}_n \ \dot{x}_{n-1} \ \dots \ \dot{x}_{n-N_b} \ \dot{y}_{n-1} \ \dots \ \dot{y}_{n-N_a}]^T$ the vector of the signals filtered by $1/(1 - A(z))$. Finally, the update rule for the simplified RPE algorithm can be computed

as

$$\boldsymbol{\theta}_{n+1} = \boldsymbol{\theta}_n + \mu e_{o,n} \dot{\boldsymbol{\phi}}_n, \quad (4.36)$$

which is very similar to the previous approach, except by the use of the simplified gradient components \dot{y}_n and \dot{x}_n instead of the signals y_n and x_n , respectively.

In this work, both PLR and RPE-based approaches will be studied, but from the perspective of the ITL framework. In fact, in the context of the system identification problem, some initial steps were taken considering the matching of distributions [Lai, 2002; Lai et al., 2003], but without relying on the use of these algorithms. A major discussion on this topic will be provided in Chapter 7.

4.3 Unsupervised Equalization

Under the supervised perspective, the need for the reference sequence d_n might drastically reduce the transmission rate in several practical applications. In fact, during the equalizer training process, there is no effective information transmission, since the reference sequence is already known by the receiver. This standpoint motivated the rise of new techniques able to perform channel equalization without relying on the reference signal d_n . To this class of problems, it is assigned the name *unsupervised* or *blind channel equalization*.

It is possible to state that the blind equalization problem was a frequent research topic during the decades of 70 to 90, which is a direct consequence of its wide horizon of applications, such as telecommunications, audio and speech processing, radar and sonar, biomedical signal/image processing and geophysics [Romano et al., 2010].

From a general perspective, a completely blind approach implies in a tremendous difficulty for reducing the ISI. However, a promising approach is to use, implicitly or explicitly, some general prior statistical information about the source signal. For instance, in prediction error filtering, it is assumed that the sources are statistically independent (or, at least, uncorrelated), or, in classical Bussgang and Godard techniques, it is assumed that the modulation scheme is known *a priori* [Haykin, 1996; Romano et al., 2010].

Although some of the pioneering works on this topic were based on some intuitive approaches, mainly involving specific modulations, like the Pulse Amplitude Modulation (PAM) or the Quadrature Amplitude Modulation (QAM) [Godfrey and Rocca, 1981; Bellini and Rocca, 1986], it was later theoretically verified that the HOS statistics were a requirement for solving the problem. This idea motivated the employment of ITL methods within this topic. Hence, next, we present a brief overview in blind equalization, starting from the main theoretical results, following by some selected elements of the classical techniques and ending with some ITL methods. Differently from the supervised approach, no distinction is made regarding the equalizer structure, but the standard adoption is of

FIR filters as equalizers.

4.3.1 The Theoretical Pillars in Blind Equalization

The works of Benveniste et al. [1980] and of Shalvi and Weinstein [1990] introduced the theorems responsible for establishing the theoretical conditions for blind equalization. These theorems were named after their authors: the Benveniste-Goursat-Ruget (BGR) and the Shalvi-Weinstein (SW) theorems.

The Benveniste-Goursat-Ruget Theorem

In simple terms, the BGR theorem [Benveniste et al., 1980; Romano et al., 2010] can be posed as

Theorem 1 (BGR Theorem). *Let the transmitted signal be composed of non-Gaussian i.i.d. samples and both channel $H(z)$ and equalizer $W(z)$ be linear time-invariant filters, in a noiseless scenario. Under these conditions, if the distribution of the source, $f_S(v)$, and of the equalizer output, $f_Y(v)$, are equal, then the channel will have been perfectly equalized.*

This theorem ensures that equalization can be obtained using only the statistical properties about the signals, however, it is required the knowledge of the source distribution. The limitation concerning Gaussian distributions results from the linear filtering process, in which Gaussian distributed signals remains Gaussian after filtering, and no further information besides the variance can be extracted [Romano et al., 2010].

The Shalvi-Weinstein Theorem

Ten years later, Shalvi and Weinstein [1990] were able to establish less stringent conditions for blind equalization under assumptions similar to those of the BGR theorem:

Theorem 2 (SW Theorem). *Let the transmitted signal be composed of non-Gaussian i.i.d. samples and both channel $H(z)$ and equalizer $W(z)$ be linear time-invariant filters, in a noiseless scenario. Under these conditions, if $E[|s_n|^2] = E[|y_n|^2]$ and a higher than second-order nonzero cumulant of s_n and y_n are equal, then the channel will have been perfectly equalized.*

In other words, the SW theorem states that equalization can be performed by using only the second-order statistics and the cumulants of the source and equalized signals [Romano et al., 2010]. This simplified conditions provided the theoretical basis to understand the performance of the classical blind algorithms, presented in the following.

4.3.2 Bussgang Techniques

The blind approaches known as Bussgang techniques have in common the prior knowledge of some statistics of the source and the implicit use of the HOS necessary to solve the problem. The higher complexity in comparison with the MSE cost contributes to the rise of certain local minima as well as other points, such as maxima and saddle points, which is a very rich and dynamical scenario.

The Bussgang techniques traditionally employ linear FIR filters as equalizers, a criterion with implicit HOS and an LMS-like algorithm for optimization. Although these three elements are involved in the derivation, in the literature, the approaches belonging to this class of techniques are usually referred by their algorithms names.

The Decision-Directed and The Sato Algorithms

The Decision-Directed (DD) algorithm makes use of a memoryless nonlinear decision-device, whose objective is to provide an estimate of the reference signal [Lucky, 1965]. Interestingly, the nonlinearity involved in the decision process is responsible for implicitly introducing the HOS necessary to solve the problem.

The DD criterion can be viewed as a modified MSE criterion, whose reference signal is substituted by an estimate based on the equalizer output signal y_n . Its cost function can be defined as

$$J_{DD}(\mathbf{w}) = E [|\text{dec}(y_n) - y_n|^2], \quad (4.37)$$

where $\text{dec}(\cdot)$ is the nonlinear decision function.

By using the stochastic approach to compute the gradient (similarly to the LMS algorithm), the resulting update rule of the DD algorithm becomes

$$\mathbf{w}_{n+1} = \mathbf{w}_n + \mu (\text{dec}^*(y_n) - \mathbf{x}_n^H \mathbf{w}_n) \mathbf{x}_n. \quad (4.38)$$

The information about the source is encompassed in the decision process. For instance, in case the transmitted signal is modulated according to the Binary Phase-Shift Keying (BPSK) scheme, the decision function can be defined as

$$\text{dec}(y_n) = \text{sgn}(y_n) = \begin{cases} +1, & \text{if } y_n \geq 0 \\ -1, & \text{if } y_n < 0 \end{cases}. \quad (4.39)$$

It is important to emphasize that the equalization performance is limited to the type of the chosen nonlinearity. The decision-device will only provide reliable estimates of the reference signal if the algorithm initialization already provides a satisfactory open-eye condition, i.e., a relatively good initialization. This justifies the usual application of the DD algorithm together with a supervised approach, e.g., the LMS algorithm. In this case, the LMS algorithm is used during the transmission of a header in the message,

which should lead the algorithm to an open-eye condition; after that, the transmission can be switched to the blind mode, and the DD algorithm will be able to complete the equalization process, converging, ideally, to the Wiener solution [Macchi and Eweda, 1984].

An extension of this work was accomplished by Sato [1975], having in mind multilevel modulation schemes, e.g., the M-ary baseband *Pulse Amplitude Modulation* (M-PAM). Basically, Sato [1975] proposed the use of the decision function:

$$dec(y_n) = \gamma \operatorname{sgn}(y_n), \quad (4.40)$$

where γ is a scale factor defined as:

$$\gamma = \frac{E[s_n^2]}{E[|s_n|]}. \quad (4.41)$$

This approach was able to achieve more robust performance than the DD algorithm, being able to operate in a complete blind fashion, i.e., even in closed-eye condition.

The convergence aspects for the DD algorithm are, to a great extent, also valid for the Sato algorithm. This similarity emerges, for instance, when the source is BPSK modulated and both algorithms are coincident. Thus, both are susceptible to local minima convergence – even in the case in which the equalizer is doubly infinite and the source is PAM modulated [Ding et al., 1993].

Godard Algorithm

The blind techniques proposed by Godard [1980] are based on a criterion which measures the dispersion of the equalized signal around a prior value, without making use of the phase information. This approach allows that even complex modulations – such as the Quadrature Amplitude Modulation (QAM) – be adopted. The cost function, also referred to as ‘ p -order dispersion’, is of the form

$$J_{\text{Godard}}(\mathbf{w}, p) = E[(|y_n|^p - R_p)^2], \quad (4.42)$$

where p is a positive integer and R_p is a predetermined constant value, given by

$$R_p = \frac{E[|s_n|^{2p}]}{E[|s_n|^p]}. \quad (4.43)$$

By computing the gradient and using the classical stochastic approximation, Godard obtained the following update rule for the homonym algorithm:

$$\mathbf{w}_{n+1} = \mathbf{w}_n - \mu y_n^* |y_n|^{p-2} (|y_n|^p - R_p) \mathbf{x}_n. \quad (4.44)$$

Particularly, the case $p = 2$ is of great practical interest due to its robustness and fast convergence [Godard, 1980]. Referred to as the *Constant Modulus* (CM) [Treichler and Agee, 1983] criterion, this case also presents local minima convergence, even on the combined channel+equalizer system domain [Ding et al., 1991]. However, the initialization strategy named *center-spike* contributed to the reduction of the local convergence rate [Foschini, 1985]. This same initialization method was investigated for the Shalvi-Weinstein criterion, which revealed connections between these two approaches [Foschini, 1985].

4.3.3 The Shalvi-Weinstein Algorithm

The SW criterion [Shalvi and Weinstein, 1990] is based on the Theorem 2 and uses, as crucial element, the quantity called *kurtosis*, which is able to extract HOS of the signals of interest. In that sense, the kurtosis of the equalizer output signal can be defined as

$$k_Y = E [|y_n|^4] - 2E^2 [|y_n|^2] - |E [y_n^2]|^2, \quad (4.45)$$

in which the use of the fourth-order statistics is evident.

Since the SW theorem also encompasses a variance constraint, a possible option for the SW criterion is to formulate it through a maximization problem subject to a constraint, i.e.:

$$\max_{\mathbf{w}} J_{SW}(\mathbf{w}) = \max_{\mathbf{w}} |k_Y|; \quad (4.46)$$

subject to

$$E [|y_n|^2] = E [|s_n|^2]. \quad (4.47)$$

As can be noted, it does not belong to the Bussgang techniques because it encompasses explicit use of the HOS and makes no assumption on the source distribution (except non-Gaussianity). The maximization of k_Y is related with the idea that, for *i.i.d.* sources, linear distortions caused by the channel result in a reduction of the kurtosis. In that sense, by maximizing k_Y , it is ideally expected that the channel effect be suppressed and k_Y reaches its maximum value, which is equal to k_S .

The stochastic gradient approach results in the following update rule to be performed in two steps:

$$\tilde{\mathbf{w}}_{n+1} = \mathbf{w}_n - \mu \text{sgn}(k_S) |y_n|^2 y_n \mathbf{x}_n, \quad (4.48)$$

in which k_S is the kurtosis associated with the source, and

$$\mathbf{w}_{n+1} = \frac{\tilde{\mathbf{w}}_{n+1}}{\|\tilde{\mathbf{w}}_{n+1}\|}, \quad (4.49)$$

which is related with the normalization constraint of Eq. (4.47); however, in order to

ensure a fixed variance at the equalizer output, the spectral prewhitening of the channel output is required [Shalvi and Weinstein, 1990].

The SW algorithm showed to be an interesting blind technique to encompass the HOS of the signals of interest. However, in a more recent trend, the increase of the computational capacity contributed to the adoption of criteria aligned with the idea of the BGR theorem, in which the probability distributions are encompassed in the formulation, as will be seen in the following.

4.3.4 ITL Criteria

The BGR and SW theorems make explicit the idea that, for a successful equalization in the blind context, the use of the HOS about the signals of interest is of fundamental importance. In that sense, the ITL-based methods [Principe, 2010] reveal themselves to be a very promising approach, since they seek an extensive extraction and utilization of the statistical information about the signals, including the HOS.

Basically, there are three main ITL approaches applied to the blind equalization problem, which are the Rényi's entropy, the quadratic divergence and the correntropy-based methods.

Rényi's Entropy

In parallel with the development of supervised ITL criteria [Santamaría et al., 2002], one of the first blind ITL approaches aimed at bringing together entropy and the p -order dispersion that engenders the Godard's family of cost functions [Godard, 1980]. However, in order to obtain simpler estimators for entropy, instead of Shannon's definition, the quadratic Rényi's entropy [Principe, 2010] (Eq. (2.19)) is considered, which results

$$J_{HRD}(\mathbf{w}) = H_2^R(Y^p - R_p) = H_2^R(Y^p), \quad (4.50)$$

where the RV Y^p is associated with the modulus signal $|y_n|^p$, $R_p = E[|s_n|^{2p}] / E[|s_n|^p]$ and $p \in \mathbb{Z}$. The last equality in Eq. (4.50) comes from the fact that the entropy does not depend on the mean of the RV. As in the supervised case, it is desired to minimize the $J_{HRD}(\mathbf{w})$ cost.

As usual within the ITL framework, the PDF associated with Y^p , $f_{Y^p}(v)$, is estimated according to the Parzen window method with Gaussian kernel functions (Section 2.3.1), resulting in

$$\hat{J}_{HRD}(\mathbf{w}) = \frac{1}{N_y^2} \sum_{i=0}^{N_y-1} \sum_{j=0}^{N_y-1} G_{2\sigma^2}(|y_{n-j}|^p - |y_{n-i}|^p), \quad (4.51)$$

where N_y is the number of samples of y_n .

Generally, for FIR equalizers, a stochastic gradient-based algorithm is used for optimization. Additionally, assuming $p = 2$, the gradient of Eq. (4.51) is

$$\nabla_{\mathbf{w}_n} \hat{J}_{HRD}(\mathbf{w}_n) \propto \frac{1}{2N_y^2\sigma^2} \sum_{i=0}^{N_y-1} \sum_{j=0}^{N_y-1} G_{2\sigma^2} (|y_{n-j}|^2 - |y_{n-i}|^2) (|y_{n-j}|^2 - |y_{n-i}|^2) \cdot (y_{n-i}\mathbf{x}_{n-i} - y_{n-j}\mathbf{x}_{n-j}), \quad (4.52)$$

where the negative log was suppressed [Santamaría et al., 2002]. The resulting algorithm is obtained by replacing Eq. (4.52) in the update rule given by Eq. (3.1).

Since this method makes use of the statistical information brought by only the filter output signal y_n , a constraint over the equalizer is necessary to avoid convergence towards the trivial solution, such as keeping one of the taps unitary [Santamaría et al., 2002].

The Quadratic Divergence Between Distributions

In consonance with the BGR theorem, the idea of matching the distributions associated with the equalizer output and with the source gains new insight when combined with the QD measure within the ITL framework (Section 2.3.2). In that sense, a possible cost function can be written as [Santamaría et al., 2002b; Lázaro et al., 2005]

$$\begin{aligned} J_{QD}(\mathbf{w}) &= \int (f_{Y^p}(v) - f_{S^p}(v))^2 dv \\ &= \int f_{Y^p}^2(v)dv + \int f_{S^p}^2(v)dv - 2 \int f_{Y^p}(v)f_{S^p}(v)dv, \end{aligned} \quad (4.53)$$

where $f_{Y^p}(v)$ and $f_{S^p}(v)$ are the PDFs associated with the RVs $Y^p = \{|y(n)|^p\}$ and $S^p = \{|s(n)|^p\}$, respectively. Note that this method considers the modulus of the symbols to the power p , similarly to the p -order dispersion [Godard, 1980]. Also, it is important to mention that the second term after the last equality of Eq. (4.53) is generally disregarded, since it is assumed that $f_{S^p}(v)$ is a target PDF and remains fixed during the filter adaptation process.

In communication problems, the PMF of the source $p_S(v)$ is assumed to be known. In the work of Lázaro et al. [2005], the convolution between the Gaussian kernel and the discrete distribution of the source $p_S(v)$ is considered to simplify the cost estimation. In this case, the distribution of the source is approximated to a PDF according to

$$\hat{f}_{S^p}(v) = \sum_{i \in \mathcal{A}} p_S(s_i) G_\sigma(v - |s_i|^p) \quad (4.54)$$

where \mathcal{A} is the alphabet of all possible occurrences of the RV S and s_i is the i -th symbol $\in \mathcal{A}$. Using the Parzen window method with Gaussian kernels for $f_{Y^p}(v)$, the QD cost

function can be estimated as

$$\begin{aligned} \hat{J}_{QD}(\mathbf{w}) &= \frac{1}{N_y^2} \sum_{i=0}^{N_y-1} \sum_{j=0}^{N_y-1} G_{2\sigma^2}(|y_{n-j}|^p - |y_{n-i}|^p) \\ &\quad - \frac{2}{N_y N_{\mathcal{A}}} \sum_{i \in \mathcal{A}} \sum_{j=0}^{N_y-1} G_{2\sigma^2}(|y_{n-j}|^p - |s_i|^p), \end{aligned} \quad (4.55)$$

where $N_{\mathcal{A}}$ is the number of elements in \mathcal{A} . Note that we have not considered the second term of Eq. (4.53) for obtaining Eq. (4.55).

Assuming $p = 2$, the gradient of Eq. (4.55) is

$$\begin{aligned} \nabla_{\mathbf{w}_n} \hat{J}_{QD}(\mathbf{w}_n) &= \frac{-1}{2N_y^2 \sigma^2} \sum_{i=0}^{N_y-1} \sum_{j=0}^{N_y-1} G_{2\sigma^2}(|y_{n-i}|^2 - |y_{n-j}|^2) (|y_{n-i}|^2 - |y_{n-j}|^2) \cdot \\ &\quad \cdot (y_{n-i} \mathbf{x}_{n-i} - y_{n-j} \mathbf{x}_{n-j}) \\ &\quad + \frac{2}{N_y N_{\mathcal{A}} \sigma^2} \sum_{i \in \mathcal{A}} \sum_{j=0}^{N_y-1} G_{2\sigma^2}(|y_{n-j}|^2 - |s_i|^2) (|y_{n-j}|^2 - |s_i|^2) y_{n-j} \mathbf{x}_{n-j}, \end{aligned} \quad (4.56)$$

which can be directly applied in Eq. (3.1) to obtain the gradient-based algorithm. In order to reduce computational complexity, one can consider $N_y = 1$, there vanishing the first term of Eq. (4.56) [Lázaro et al., 2005].

4.3.5 Correntropy

Finally, a correntropy-based criterion can also be used in the context of blind equalization, as proposed by Santamaría et al. [2006]. Very interestingly, the authors consider the case in which the sources are not necessarily *i.i.d.* and may present a temporal structure. In this case, correntropy can be used to extract the HOS and the temporal structure of the underlying signals to perform blind equalization, resulting in the following cost function:

$$J_{cor}(\mathbf{w}) = \sum_{m=1}^M (v_S(m) - v_Y(m))^2, \quad (4.57)$$

where $M \geq 1$ is the number of lags considered, $v_S(m) = v_{S_n, S_{n-m}}$ and $v_Y(m) = v_{Y_n, Y_{n-m}}$ are the (auto)correntropy of the source s_n and of the equalizer output y_n for delay m , respectively.

In context of communications, the correntropy of the source $v_S(m)$ is assumed to be known, and the correntropy associated with the equalizer output, $v_Y(m)$, is estimated via

the method shown in Section 2.3.2, resulting in

$$\hat{J}_{cor}(\mathbf{w}) = \sum_{m=1}^M \left(v_S(m) - \frac{1}{N_y} \sum_{i=0}^{N_y-1} G_{\sigma^2}(y_{n-i} - y_{n-m-i}) \right)^2. \quad (4.58)$$

Again, a gradient-based algorithm can be used for optimization, with

$$\nabla_{\mathbf{w}} \hat{J}_{cor} = \sum_{m=1}^M (v_S(m) - \hat{v}_Y(m)) \left(\frac{-1}{\sigma^2 N_y} \sum_{i=0}^{N_y-1} G_{\sigma^2}(y_{n-i} - y_{n-m-i}) \cdot (y_{n-i} - y_{n-m-i})(\mathbf{x}_{n-i} - \mathbf{x}_{n-m-i}) \right). \quad (4.59)$$

We highlight that, although correntropy was the subject of intense research in the last decade [Santamaría et al., 2006; Liu et al., 2006; Li et al., 2007; Gunduz and Principe, 2009; Principe, 2010], the study of the case in which the sources are non-*i.i.d.* is still incipient in the blind equalization context. In fact, as previously mentioned, this topic composes one of the main subjects to be investigated in this work.

4.4 Blind Source Separation

In many practical applications, it is of interest to retrieve a set of source signals from some samples (or observations) that actually are the mixtures of these sources. Since no prior knowledge about the source distributions is assumed, the problem is referred to as Blind Source Separation (BSS) [Comon and Jutten, 2010; Romano et al., 2010]. It counts with a diverse set of applications, in which we mention: audio signals [Makino et al., 2006], astronomical data [Jutten et al., 2007], brain images [Calhoun et al., 2001] and other medical applications [Comon and Jutten, 2010].

In general terms, the BSS problem can be formulated as: let $\mathbf{s}(n) = [s_1(n) \cdots s_N(n)]^T$ be a vector of N sources at time instant n (note that we have used a different notation, being the time index n used within parenthesis, as customary in the BSS formulation [Comon and Jutten, 2010; Romano et al., 2010]) and an unknown mixing function $\Phi(\cdot)$, such that

$$\mathbf{x}(n) = \Phi(\mathbf{s}(n)), \quad (4.60)$$

with $\mathbf{x}(n) = [x_1(n) \cdots x_M(n)]^T$ the observation vector with M mixtures. Using only a limited number of samples of $\mathbf{x}(n)$, it is desired to obtain an unmixing function $\Psi(\cdot)$, such that

$$\mathbf{y}(n) = \Psi(\mathbf{x}(n)) \quad (4.61)$$

be as close as possible to the sources $\mathbf{s}(n)$, up to scale and permutation factors [Comon and

Jutten, 2010]. Note that this problem is similar to that of equalization, if Multiple-Inputs Multiple-Outputs (MIMO) systems are considered.

Throughout three decades of existence, this issue was object of great attention from the academic community, where most of the initial efforts were aimed at the standard linear and instantaneous mixing model, with the assumption that the sources are mutually independent. The results contributed to a solid theoretical framework known as Independent Component Analysis (ICA) [Comon and Jutten, 2010], in which the MI (Section 2.3.2) plays a central role. However, in certain practical scenarios, the linear and instantaneous approach may not be adequate, being necessary the adoption of nonlinear models, in which we cite, for instance, the Linear-Quadratic (LQ) mixtures and the Post-Nonlinear (PNL) models [Deville and Duarte, 2015]. In that sense, we briefly present some aspects of both linear and nonlinear cases within the BSS problem.

4.4.1 The Linear Case

In the linear and instantaneous BSS problem, the mixtures can be modeled as

$$\mathbf{x}(n) = \mathbf{A}\mathbf{s}(n), \quad (4.62)$$

where \mathbf{A} is the $M \times N$ mixing matrix. Assuming that the mixing matrix \mathbf{A} is invertible, a linear separating structure can be employed, i.e.,

$$\mathbf{y}(n) = \mathbf{W}\mathbf{x}(n), \quad (4.63)$$

where \mathbf{W} is an $N \times M$ separating matrix. The challenge, however, is to obtain $\mathbf{W} = \mathbf{A}^{-1}$, up to scale and row permutations, based only on the observed samples $\mathbf{x}(n)$ and a minimal amount of information about the sources.

Particularly, we consider two hypotheses about the sources: in the first case, the sources are assumed to be statistically independent, and, in the second case, the sources are additionally assumed to be temporally colored.

MI-Based Criteria

The assumption of mutual independent sources can be mathematically expressed through the relation:

$$f_{S_1, \dots, S_N}(\mathbf{v}) = \prod_{i=1}^N f_{S_i}(v_i), \quad (4.64)$$

where $\mathbf{v} = [v_1, \dots, v_N]^T$, $f_{S_1, \dots, S_N}(\mathbf{v})$ is the joint PDF associated with the sources and $f_{S_i}(v_i)$ is the marginal distribution of the i -th source. Based on this assumption, Comon [1994] showed that it is possible to obtain the separating matrix \mathbf{W} in an unsupervised

fashion.

Very interestingly, the concept of MI can be used to quantify independence between random variables, leading to a promising separation criterion. Hence, based on Eq. (2.22), the MI among the outputs of the separating system is

$$\begin{aligned} I(Y_1; \dots; Y_N) &= \int_D f_{Y_1, \dots, Y_N}(\mathbf{v}) \log \left(\frac{f_{Y_1, \dots, Y_N}(\mathbf{v})}{\prod_{i=1}^N f_{Y_i}(v_i)} \right) d\mathbf{v} \\ &= \sum_{i=1}^N H^S(Y_i) - H^S(Y_1, \dots, Y_N), \end{aligned} \quad (4.65)$$

where the MI should be minimized and, for $I(Y_1; \dots; Y_N) = 0$, mutual independence is reached [Comon and Jutten, 2010].

For linear mixtures, it can be shown that [Comon and Jutten, 2010]

$$H^S(Y_1, \dots, Y_N) = H^S(X_1, \dots, X_M) + \log |\det(\mathbf{W})|. \quad (4.66)$$

Since the term $H^S(X_1, \dots, X_M)$ does not depend on \mathbf{W} , it can be disregarded in the minimization process. Thus, the resulting MI-based criterion is

$$\min_{\mathbf{W}} J_{MI}(\mathbf{W}) = \min_{\mathbf{W}} \sum_{i=1}^N H^S(Y_i) - \log |\det(\mathbf{W})|. \quad (4.67)$$

In this case, the sources are not allowed to be Gaussian distributed except for one of them, due to reasons similar to those presented in the BGR theorem [Hyvärinen et al., 2001].

The criterion given by Eq. (4.67) can be estimated following a diverse set of approaches [Hyvärinen et al., 2001; Comon and Jutten, 2010; Silva et al., 2016], even the kernel-based estimators presented in Section 2.2.1. However, it is evident that use of the HOS is an unavoidable requirement for performing BSS, except if more information about the sources can be used, such as the temporal structure.

Temporally Colored Sources

Besides the mutual independence assumption, the sources can also be considered temporally non-*i.i.d.*, which, fortunately, is far from being a prohibitive assumption, given its large occurrence in practical BSS problems [Hyvärinen et al., 2001]. In such cases, the information about the temporal structure of the underlying signals is most valuable, since only the SOS reveal to be sufficient for performing linear BSS – i.e., if the SOS exhibit sufficient diversity (non-coincident spectral densities), the HOS are no longer necessary. In addition, the temporal information also allows the separation of Gaussian sources, which are not separable using any of the classical approaches which ignore the temporal structures [Comon and Jutten, 2010].

Within the SOS-based framework, the time structure can be extracted via the autocorrelation (or autocovariance) functions. However, for a successful separation, it is required that the sources be wide sense stationary and that their power spectral densities be mutually distinct, i.e., that their correlation profile obeys

$$E[s_i(n)s_i(n-k)] \neq E[s_j(n)s_j(n-k)], \quad (4.68)$$

for $i \neq j$ and some delay $k \neq 0$ [Romano et al., 2010]. In fact, the mutual independence assumption guarantees that the sources be mutually uncorrelated and the autocorrelation matrix of the sources for delay k is always diagonal, i.e., for unitary variance sources,

$$\mathbf{R}_S(m) = E[\mathbf{s}(n)\mathbf{s}^T(n-k)] = \mathbf{I}_N, \quad (4.69)$$

where \mathbf{I}_N is an $N \times N$ identity matrix. Based on this, the information of the time-lagged correlation can be used instead of the HOS, so that

$$E[y_i(n)y_j(n-k)] = 0, \quad (4.70)$$

for $i \neq j$ and an arbitrary delay $k \geq 0$ [Hyvärinen et al., 2001]. This is equivalent to force the off-diagonal elements of $\mathbf{R}_Y(k)$ to be null:

$$\begin{aligned} \mathbf{R}_Y(k) &= E[\mathbf{y}(n)\mathbf{y}^T(n-k)] \\ &= \mathbf{W}\mathbf{A}\mathbf{R}_S(k)\mathbf{A}^T\mathbf{W}^T \\ &= \mathbf{W}\mathbf{A}\mathbf{I}_N\mathbf{A}^T\mathbf{W}^T. \end{aligned} \quad (4.71)$$

This idea composes the essence of the AMUSE algorithm [Tong et al., 1991], but it is necessary that the lagged correlation be different for all sources at time delay k .

An extension of this idea using d time lags leads to algorithms like SOBI [Belouchrani et al., 1997] and TDSEP [Ziehe and Müller, 1998]. Hence, the objective is to simultaneously diagonalize all the corresponding lagged covariance matrices, which leads to the cost

$$J_{SOBI}(\mathbf{W}) = \sum_{k=0}^d \text{off}(\mathbf{R}_Y(k)) = \sum_{k=0}^d \sum_{i \neq j} (E[y_i(n)y_j(n-k)])^2, \quad (4.72)$$

where $\text{off}(\cdot)$ is the sum of the squares of the off-diagonal elements of a given matrix and d the maximum number of delays. The separation can be achieved by minimizing Eq. (4.72).

It is important to remark that, although it is assumed that the sources are mutually independent, the mentioned algorithms only require that the sources be uncorrelated. However, in order to obtain good results, it is important that the sources power spectra be different from each other [Romano et al., 2010].

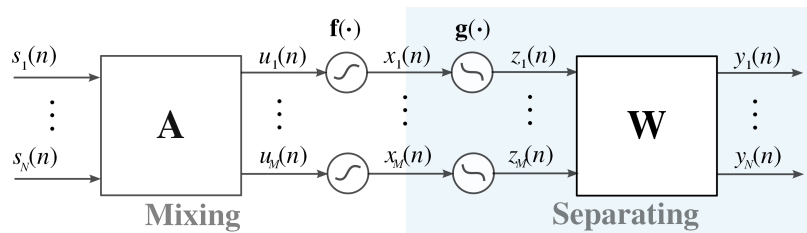


Figure 4.4: Mixing and separating systems in the PNL model.

4.4.2 The Nonlinear Case

Recently, there has been a considerable effort for extending the ICA framework to nonlinear mixing models, in view of its promising applications like smart chemical sensor arrays [Duarte et al., 2009] and hyperspectral imaging [Meganem et al., 2011]. However, from a general standpoint, mutual independence may not be sufficient for performing separation. Thus, the studies on this topic were focused on a constrained set of nonlinear models in which the ICA methods are still valid [Hosseini and Jutten, 2003], such as the Post-Nonlinear (PNL) models [Taleb and Jutten, 1999].

The Post-Nonlinear Mixtures

The PNL system comprises two stages of mixing: the linear and the nonlinear stages. As illustrated in Fig. 4.4, the mixtures can be written as

$$\mathbf{x}(n) = \mathbf{f}(\mathbf{A}\mathbf{s}(n)), \quad (4.73)$$

being $\mathbf{f}(\cdot)$ a set of M component-wise functions. As a counterpart of the mixing system, the separation system output is

$$\mathbf{y}(n) = \mathbf{W}\mathbf{g}(\mathbf{x}(n)), \quad (4.74)$$

where \mathbf{W} is an $N \times M$ matrix and $\mathbf{g}(\cdot)$ is a set of M component-wise functions, ideally the inverse of $\mathbf{f}(\cdot)$ [Comon and Jutten, 2010].

Basically, it is possible to classify the separation techniques for PNL mixtures into two main classes: the *joint* and the *two-stage* approaches [Deville and Duarte, 2015].

In the former, the main idea is to jointly adjust $\mathbf{g}(\cdot)$ and \mathbf{W} by minimizing a given statistical dependence measure; generally, the use of the ICA framework represents an efficient methodology for performing separation, but it will be possible if [Achard and Jutten, 2005]: (i) the mixing matrix \mathbf{A} is invertible and effectively mixes the sources (there are at least two nonzero elements in each row and column); (ii) $\mathbf{f}(\cdot)$ and $\mathbf{g}(\cdot)$ must be monotonic functions; (iii) at most one source is Gaussian, and (iv) the joint PDF of the sources is differentiable and its derivative is continuous on its support. Satisfied these

conditions, the MI criterion can be applied [Taleb and Jutten, 1999]:

$$\min_{\mathbf{W}} J_{MI}(\mathbf{W}) = \min_{\mathbf{W}} \sum_{i=1}^N H^S(Y_i) - \log |\det(\mathbf{W})| - E \left[\log \prod_{i=1}^N |g'_i(x_i(n))| \right], \quad (4.75)$$

where $g'_i(\cdot)$ is the derivative of the i -th separation function $g_i(\cdot)$. As in the linear case, the term $H^S(X_1, \dots, X_M)$ was disregarded. The gradient-based algorithm for this case is usually done through the use of the score functions [Taleb and Jutten, 1999], but issues like local convergence and constrained adaptation of the nonlinearities require special attention.

On the other hand, for the two-stage approach, the linear and the nonlinear mixing stages are addressed separately, i.e., two different but ‘simpler’ problems need to be solved: $\mathbf{g}(\cdot)$ is adapted so that the nonlinear part of the mixtures are completely suppressed and, then, \mathbf{W} is adjusted to solve the classic linear BSS problem. There are a number of methods for adapting $\mathbf{g}(\cdot)$ – the first stage –, as those based on some *a priori* information [Duarte et al., 2012], but the most common approach is that based on Gaussianization: from the perspective of the central limit theorem, the resultant RVs after the linear mixing stage will tend to be “more” Gaussian. Thus, the most intuitive idea for adapting $\mathbf{g}(\cdot)$ is to make its output $\mathbf{z}(n)$ Gaussian again [Ziehe et al., 2003]. This strategy reveals to be more effective when the number of sources N is large – according to the central limit theorem – or when the sources are Gaussian distributed. One can also include among these ideas the notion of the matching of probability distributions, which was one of the first methods in the PNL two stage approach [White, 1982]. In this case, the nonlinearity compensation is accomplished when the distributions associated with $\mathbf{u}(n)$ and with $\mathbf{z}(n)$ are matched – note, however, that the *a priori* knowledge of the distribution of $\mathbf{u}(n)$ is required. The second stage – i.e., the adaptation of the linear term \mathbf{W} – is usually solved with classical ICA methods, which encompass HOS [Comon and Jutten, 2010; Deville and Duarte, 2015]. However, when the sources are temporally colored, methods based on second-order statistics (SOS) can be applied, since they are known for its robustness and reliable simplicity. This idea is exploited in [Ziehe et al., 2003] by using a Gaussianization method in the first stage followed by a Temporal Decorrelation Separation (TDSEP) method [Comon and Jutten, 2010] in the second stage. In fact, this approach is interesting because it merges the simplicity of the second-order framework with simple source priors, for solving the complex nonlinear mixtures.

It is important to remark that, in both joint and two-stage approaches, the study of the PNL mixtures in light of the use of the temporal structure of the sources and the SOS is still incipient. In fact, an initial step in this direction was given by the Gaussianization method in the two-stage approach [Ziehe et al., 2003; Deville and Duarte, 2015], but a deeper investigation on the real necessity of the HOS in scenarios with colored sources is

lacking. In this work, we intend to follow a study on this line, as will be seen later.

4.5 Conclusion

In this chapter, a brief background on the channel equalization and the blind source separation problems was presented. The main purpose was to provide the reader with the main structures, criteria and optimization methods that are typically employed in each signal processing problem, since they form the basis for the subsequent chapters.

Regarding the channel equalization problem, the supervised and the blind approaches were considered. In the supervised branch, when the equalizer structure is an FIR filter, the classical approach is the MSE criterion and the LMS algorithm, but for scenarios encompassing non-Gaussian signals and/or recursive/nonlinear elements, the ITL criteria like those based on the Rényi's entropy and on the correntropy might be promising alternatives. When the filtering structure is a recursive IIR filter, the equation-error and the output-error formulations are reliable supervised approaches, which leads to interesting gradient-based algorithms: the (already mentioned) LMS, the PLR and the RPE. On the other side, for the unsupervised case, we showed that this branch is mainly supported by the BGR and the SW theorems, which establish the main theoretical and statistical conditions to ensure a successful blind equalization. These theorems also reveal the unavoidable necessity of the HOS to solve the problem. Based on this, there emerges a set of methods, such as the Bussgang techniques (the DD, the Sato and the Godard methods), which make use of nonlinear devices and/or implicit HOS of the source to perform equalization, the SW method, that explicitly uses a statistical moment higher than two, and, finally, the most recent trend, the ITL-based approaches (such as the QD and the blind versions of the Rényi's entropy and the correntropy criteria), which makes a more extensive use of the HOS. Usually, the equalizer structure is assumed to be an FIR filter adapted via a gradient-based algorithm, but this approach may vary, depending on the complexity of the scenario.

Concerning the BSS problem, a brief panorama was provided on the linear and nonlinear mixing/demixing systems. In the linear case, we saw that, under the assumption of mutual independence between sources, the MI can be used as a separation criterion, in which the use of the HOS are mandatory. Due to this, at most one of the sources can be Gaussian. If colored sources are considered, i.e., sources with temporal structure, the sole use of the SOS is sufficient for performing separation, unless the power spectra of the sources be coincident. For the nonlinear case, special attention is dedicated to the PNL model, in which the ICA framework is still valid under certain conditions. In a joint approach, the MI can be applied; however, due to the constrained optimization process and the possible local convergence of the MI-based algorithm, the two-stage approach showed to be a promising alternative: in the first stage, the nonlinear part is treated and,

in the second stage, the linear part. Even separating the problem in two relatively simpler instances, the HOS still show to be necessary, mainly in the nonlinear stage.

It is important to notice that this overview also reveals promising investigative lines to be followed. In the equalization problem, for instance, the study of the IIR structures is, in a certain sense, limited to the MSE-based approaches. Since there is a nonlinear relationship between the filter coefficients and the filter output, the use of the ITL-based criteria might be an interesting approach to be followed. In the blind equalization case, the exploitation of the temporal structure of the non-*i.i.d.* sources can be made by the correntropy, however, in view of some particularities of this ITL-based measure, this approach is still incipient and demands further efforts, including a theoretical analysis of the viability of this approach. For the nonlinear BSS problem, although some initial steps were taken towards the use of the temporal structures of the sources, it is still lacking a study able to encompass a more extensive use of the temporal information in this scenario.

Part II

Contributions

Chapter 5

Theoretical Conditions for Blind Equalization in the Context of a Temporally Structured Source

In the context of blind channel equalization, two celebrated theorems contributed to a deeper understanding of the problem and its statistical demands: the Benveniste-Goursat-Ruget (BGR) [Benveniste et al., 1980] and the Shalvi-Weinstein (SW) [Shalvi and Weinstein, 1990] theorems. They were responsible for bringing a solid theoretical justification to the performance reached by empirical methods, still not well understood up to that moment. Undoubtedly, the definition of the statistical requirements to solve the problem contributed to the development of more efficient methods [Shalvi and Weinstein, 1990, 1993; Regalia, 1999; Santamaría et al., 2002a,b].

The BGR and SW theorems are able to cover a wide range of practical scenarios that involve *i.i.d.* sources and linear channel/equalizers. However, outside this context, the classical theorems show to be insufficient. In that sense, there remains a gap associated with alternative scenarios, like the ones encompassing sources that present temporal or spatial statistical dependence. In fact, non-*i.i.d.* source scenarios have significant occurrence in real applications – such as audio-related scenarios, images/videos and channel coding in communications – and the statistical properties necessary in these cases can completely diverge from those of the classical approach [Neves et al., 2009]. In this thesis, they compose a special class of the problem and will be referred to as *colored blind channel equalization*.

In light of this, as one of the contributions of this work, we present in this chapter a detailed theoretical analysis on the required conditions for the extension of the BGR and SW theorems towards the adoption of non-*i.i.d.* sources (or temporally structured sources).

Whenever possible, the theoretical analysis to be performed will invoke certain math-

ematical results, like some elegant theorems found in the literature. However, due to the complexity involved on the mathematical computations, we will also rely on some empirical results. The option for this type of approach compromises the proposition of novel theorems, but, on the other hand, we are still able to hold the objective of establishing the required statistical conditions for the colored blind channel equalization problem.

The theoretical analysis to be performed makes a consistent use of the properties defined in the BGR and SW theorems. In that sense, we present a detailed explanation of the classical theorems before proceeding to the analysis of their extensions.

5.1 Recapitulation: The Classical Theorems for Channel Equalization

For the derivation of the classical BGR and SW theorems [Benveniste et al., 1980; Shalvi and Weinstein, 1990], concepts like the combined channel+equalizer impulse response and the ZF condition were crucial. For both, the systems that compose the communication block are assumed to be discrete-time linear structures, without additive noise, as Fig. 5.1 depicts. In this case, the combined channel+equalizer system is simply

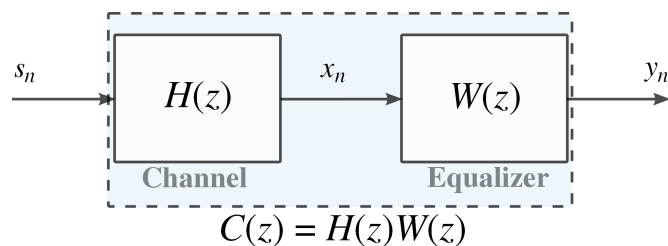


Figure 5.1: Block diagram of the communication system assumed in the classical theorem.

the concatenation of the channel $H(z)$ and the equalizer $W(z)$, whose coefficients can be obtained through the convolution between them, i.e.:

$$c_n = w_n * h_n = \sum_{i=-\infty}^{\infty} w_i^* h_{n-i}, \quad (5.1)$$

where h_n and w_n are the coefficients of the channel and the equalizer systems, respectively. Note that both channel and equalizer might assume infinite length for both causal and non-causal parts. In terms of the Z-transform, the convolution in the time-domain is simplified to a product

$$C(z) = W(z)H(z). \quad (5.2)$$

As shown in Eq. (4.3), the equalizer output y_n can be written as a function of c_n .

When the ZF condition is attained, the combined channel+equalizer impulse response

should be as defined by Eq. (4.4) or, in terms of the Z-transform, $C(z) = \alpha z^{-k}$, being α a scale factor. In the complex domain, it also admitted a phase shift redundancy θ , so that the ZF condition becomes $C(z) = e^{j\theta} z^{-k}$ [Shalvi and Weinstein, 1990].

It is also important to remark that the BGR theorem makes use of the probabilistic distribution associated with a RV. In that sense, the notation assumes that a signal y_n , for instance, is associated with the RV Y , which, in turn, has a probability distribution denoted by $f_Y(v)$. In addition to that, the theorems refer to a generic continuous or discrete distribution, however, whenever convenient, we make distinction about (continuous) PDFs and (discrete) PMFs.

If the notions of combined channel+equalizer system, ZF condition and probabilistic distribution are clear, we are able to present the BGR and SW theorems in detail.

5.1.1 The Benveniste-Goursat-Ruget Theorem

The relevance of the BGR theorem comes from its pioneering character in establishing the theoretical conditions for blind equalization [Romano et al., 2010]. However, to be satisfied, the theorem must fulfill the following assumptions [Benveniste et al., 1980]:

1. Channel, $H(z)$, and equalizer, $W(z)$, are (real valued) linear time-invariant filters, with finite energy;
2. the source distribution, $f_S(v)$, is symmetric, with finite variance, non-Gaussian and its sequence composed by (real valued) *i.i.d.* samples.

which are reasonable conditions in view of the channel equalization task.

In order to characterize the possible solutions for the equalizer, the authors use a lemma which describes the possible distributions for *i.i.d.* sequences that are not modified when filtered [Benveniste et al., 1980]:

Lemma 3 (Pólya Theorem). *Consider a sequence s_n of *i.i.d.* random variables with distribution $f_S(v)$, being $f_S(v)$ symmetric with finite variance. Assume that there is a sequence c_n (here, the combined channel+equalizer impulse response), with at least two nonzero terms, such that $\sum_{i=0}^{L_c-1} c_i^2 = 1$, and the distribution associated with $y_n = c_n * s_n$ is $f_Y(v) = f_S(v)$. Then $f_S(v)$ is a Gaussian distribution.*

The proof for Lemma 3 can be found in [Benveniste et al., 1978] and [Kakosyan et al., 1984]. Although not mentioned in the original work of Benveniste et al. [1980], we have found in the literature that Lemma 3 is equivalent to Pólya's theorem, written in 1923 [Kakosyan et al., 1984].

Lemma 3 establishes that, if c_n has more than one non-null tap and its energy is unitary, then the distributions matching $f_Y(v) = f_S(v)$ implies that the source is Gaussian distributed. Based on this, the BGR theorem can be expressed as:

Theorem 4 (BGR Theorem). *Consider an equalizer system, $W(z)$, such that the distribution of the random variable Y (associated with the signal y_n) is $f_Y(v) = f_S(v)$. Denote by $C(z) = H(z)W(z)$ the combined channel+equalizer system, and assume that the distribution $f_S(v)$ is non-Gaussian. Then $C(z) = \pm 1z^{-k}$, which is identity except for a possible delay k .*

Proof. Consider the combined channel+equalizer impulse response $c_n = w_n * h_n$. If $f_Y(v) = f_S(v)$, we have $E[y_n^2] = E[s_n^2]$, which gives, using the independence of s_n :

$$\begin{aligned} E[y_n^2] &= \sum_{i=0}^{L_c-1} \sum_{j=0}^{L_c-1} c_i c_j E[s_{n-i} s_{n-j}] \\ &= \sum_{i=0}^{L_c-1} c_i^2 E[s_n^2], \end{aligned} \tag{5.3}$$

being necessary that $\sum_{i=0}^{L_c-1} c_i^2 = 1$.

Hence, it remains to prove that $C(z) = \pm 1z^{-k}$. Lemma 3 applied to $C(z)$ gives the result. \square

In other words, the BGR theorem establishes by means of statistical properties (and without any knowledge about the channel impulse response) that, if the distribution associated with the equalizer output y_n is matched with the distribution of the source s_n , then equalization was successfully performed. However, Gaussian distributions are not allowed, since, as shown by Lemma 3, a linearly filtered Gaussian process remains Gaussian [Papoulis, 1991] and, in this case, distribution matching only implies in power normalization [Romano et al., 2010].

5.1.2 Shalvi-Weinstein Theorem

In some applications, the complete knowledge of the source distribution may be difficult to be obtained or even estimated. In that sense, in 1990, a decade after the BGR theorem proposition, Shalvi and Weinstein [1990] were able to demonstrate a novel theorem that stated the conditions for perfect equalization relying only on a few statistical moments of the involved signals.

The assumptions made by the SW theorem are equivalent to those of the BGR theorem, except that signals and systems now can belong to the complex domain.

The SW theorem requires the use of an entity named kurtosis, defined in Eq. (4.45). Very interestingly, the kurtosis is able to carry statistical information of the signals of interest up to the fourth-order, and is null for Gaussian distributions. This allowed Shalvi and Weinstein to conceive the homonym theorem:

Theorem 5 (Shavi-Weinstein Theorem). *If $E[|y_n|^2] = E[|s_n|^2]$ then*

1. $|k_Y| \leq |k_S|$,
2. $|k_Y| = |k_S|$ if and only if $C(z) = \pm e^{j\theta} z^{-k}$, in which θ is a phase shift and k a delay.

Proof. Consider the combined channel+equalizer impulse response $c_n = w_n * h_n$ and the *i.i.d.* source s_n . The second-order statistics and the kurtosis of y_n results

$$\begin{aligned} E[|y_n|^2] &= E[|s_n|^2] \left(\sum_l |c_l|^2 \right) \\ k_Y &= k_S \left(\sum_l |c_l|^4 \right). \end{aligned} \tag{5.4}$$

Let $\mathbf{c} = [c_0 \ c_1 \ \cdots \ c_{L_c}]^T$ be a vector of complex variables such that $\sum_i |c_i|^2 < N < \infty$. Then,

$$\sum_l |c_l|^4 \leq \left(\sum_l |c_l|^2 \right)^2, \tag{5.5}$$

where equality holds if and only if c_n has at most one nonzero component. Thus, if $\sum_l |c_l|^2 = 1$, then

1. $\sum_l |c_l|^4 \leq 1$;
2. $\sum_l |c_l|^4 = 1$ if and only if $C(z) = \pm e^{j\theta} z^{-k}$, in which θ is a phase shift and k a delay.

Hence, recalling Eq. (5.4), the proof follows immediately [Shalvi and Weinstein, 1990]. \square

Differently from the BGR theorem, which requires the matching of the distributions (i.e., all statistical moments), the SW theorem uses as a necessary and sufficient condition for equalization the matching of the second-order statistics, $E[|y_n|^2] = E[|s_n|^2]$, and of the kurtosis, $|k_Y| = |k_S|$, which are simpler to be obtained and/or estimated.

The theoretical advance provided by these two theorems was fundamental to the emergence of a wide range of methods and criteria for blind equalization. Even nowadays, these theorems serve as inspiration for new criteria, such as the kernel-based PDF matching approach [Lázaro et al., 2003a, 2005; Santamaría et al., 2002b].

Notwithstanding, it is not unusual to find practical scenarios in which the assumptions encompassed by the theorems are not matched. This is the case, for instance, when one must deal with sources that present a temporal structure, i.e., sources that are not *i.i.d.* In light of this, it would be interesting if the BGR and SW theorems could be extended to also include these cases. This is one of the main goals of the present thesis.

5.2 Extension of the Classical Theorems for Sources with Temporal Structure

Speech filtering, coding, medical and seismic analysis are some examples of scenarios that encompass sources with temporal or spatial structure. In all these cases, the source cannot be classified as *i.i.d.* and, hence, the BGR and SW theorems are not valid. In that sense, our objective is to analyze the conditions to extend the BGR and SW theorems so that they be able to encompass non-*i.i.d.* sources. For the sake of simplicity, we will henceforth refer to statistical dependence as ‘temporal structure’ – although the dependence may belong to other domains instead of temporal.

The temporal structure in the sources is usually seen as the inherent result of the system which generates the sources (for example, in speech signals, the sound waves are majorly produced by the vocal folds – or vocal cords –, without any intermediate filtering process). However, in our work, we assume that the non-*i.i.d.* source can be modeled by an *i.i.d.* signal filtered by a linear system called *Pre-Coder*, with transfer function $P(z)$, as illustrated by Fig. 5.2:

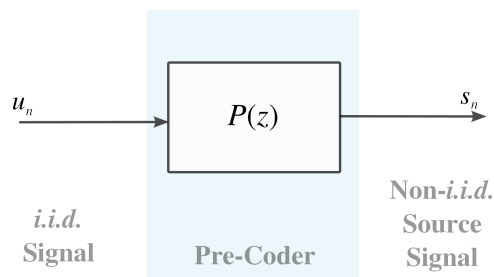


Figure 5.2: Non-*i.i.d.* source as the result of a filtering process over an *i.i.d.* signal.

where u_n is an *i.i.d.* signal and s_n the resulting non-*i.i.d.* (or colored) source. As one can note, the element responsible for imprinting the temporal structure on the signal is the pre-coder $P(z)$. In that sense, the ‘colored’ communication system can be described according to the following block diagram [Santamaría et al., 2006]:

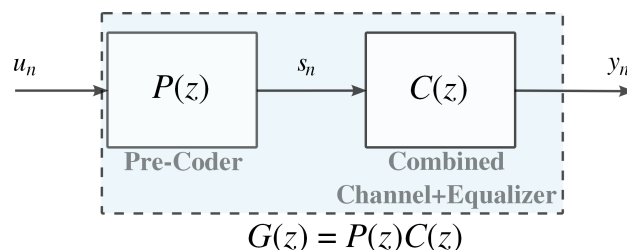


Figure 5.3: Source with temporal structure: Communication system block diagram.

Note that Fig. 5.3 shows the combined channel+equalizer system, $C(z) = H(z)W(z)$, and the combined pre-coder+channel+equalizer, $G(z) = P(z)C(z) = P(z)H(z)W(z)$, which shall be useful for our analysis.

In order to analyze the possible extensions of the BGR and SW theorems to encompass non-*i.i.d.* sources, the assumptions made on the pre-coder system will be crucial. In fact, as we intend to show, the extensions are not straightforward, but they can be achieved by resorting to theorems found in the literature and under certain relaxation in the set of possible solutions. As a result, we achieve two possible approaches in the context of the BGR theorem (considering univariate and multivariate distributions) and one approach in the context of the SW theorem. They will be described in the following.

5.2.1 Extension of the BGR Theorem - Univariate Distributions

We start with assumptions similar to the BGR theorem, but include the pre-coder system and the non-*i.i.d.* source s_n :

1. Pre-coder, $P(z)$, channel, $H(z)$, and equalizer, $W(z)$, are linear time-invariant filters, with finite energy;
2. the signal u_n is composed by *i.i.d.* samples and its associated distribution, $f_U(v)$, is symmetric, with finite statistical moments and non-Gaussian;
3. the source sequence s_n may present temporal dependence but its distribution, $f_S(v)$, is symmetric, with finite variance and non-Gaussian.

It is important to note that we assume the pre-coder system $P(z)$ to be a linear system, i.e., $\mathbf{p} = [p_0 \ p_1 \ \cdots \ p_{L_p}]^T$. Although this may imply in a significant constraint on the non-*i.i.d.* sources representativeness, its simplicity contributes with the mathematical tractability of the problem.

Using the combined pre-coder+channel+equalizer system $G(z)$, with impulse response g_n (in vector notation, $\mathbf{g} = [g_0 \ g_1 \ \cdots \ g_{L_g}]^T$), the idea of density matching can be directly extended to non-*i.i.d.* sources with the Marcinkiewicz's theorem, initially proposed in 1939 [Marcinkiewicz, 1939]. It can be stated as follows:

Theorem 6 (Marcinkiewicz Theorem). *Consider a finite or infinite sequence u_n of *i.i.d.* samples with distribution $f_U(v)$, symmetric and with finite statistical moments. Suppose that $s_n = p_n * u_n$ and $y_n = g_n * u_n$ exists and that their distributions are identical, $f_S(v) = f_Y(v)$, for all $v \in \mathbb{R}$. Under these hypothesis, either the elements of $\{|p_n|\}$ and $\{|g_n|\}$ only differ on the order, or $f_U(v)$ is a Gaussian distribution.*

The complete proof for this theorem can be found in [Marcinkiewicz, 1939].

Basically, this theorem states that if the distributions $f_S(v)$ and $f_Y(v)$ are matched, then either the pre-coder p_n and the combined pre-coder+channel+equalizer impulse response g_n are equal, up to a permutation in its coefficients (with sign ambiguity), or $f_U(v)$ is Gaussian (and nothing can be said about the system coefficients).

Hence, in the case in which $f_U(v)$ is non-Gaussian, the matching of $f_S(v)$ and $f_Y(v)$ implies that g_n is equal to p_n or a permuted version of $|p_n|$. This means that, for instance, if $\mathbf{p} = [p_0 \ p_1]^T$, then

$$\begin{aligned} \mathbf{g} &= [p_0 \ p_1]^T, \text{ or} \\ \mathbf{g} &= [-p_0 \ p_1]^T, \text{ or} \\ \mathbf{g} &= [p_1 \ p_0]^T, \text{ or} \\ \mathbf{g} &= [p_1 \ -p_0]^T, \text{ or} \\ \mathbf{g} &= [p_0 \ 0 \ -p_1]^T \end{aligned} \tag{5.6}$$

are examples of possible permutations of $|p_n|$. Recalling that $G(z) = P(z)C(z)$, when g_n is equal to $\pm p_n$, this means that one of the possible solutions is $C(z) = \pm 1$ (ZF condition). However, when g_n is a permuted version of $|p_n|$, the solution for $C(z)$ may not be the ZF condition and, in that sense, the Marcinkiewicz theorem does not provide a complete compliance with the blind equalization problem.

Notwithstanding, as we intend to show, if additional care is taken in the equalization process, it is possible to reduce all the possible permutations to the case in which $C(z) = \pm 1z^{-k}$. To clarify this point, we divide all possible permutations into two classes:

1. g_n is a time-shifted version of $\pm p_n$;
2. g_n is the result of a change in the order and/or in the sign of the coefficients of p_n , with exception of the cases defined by class 1.

In the class 1, since g_n is a time-shifted version of $\pm p_n$, it gives $G(z) = \pm P(z)z^{-k}$ and, since $G(z) = P(z)C(z)$, it is necessary that $C(z) = \pm 1z^{-k}$ (the ZF condition). Note that, in this case, the zeros (roots) of the polynomial $G(z)$ are the same of $P(z)$ plus null zeros (due to z^{-k}).

For the class 2, we assume that $P(z)$ is a monic and irreducible polynomial in function of z (i.e., the polynomial has the nonzero coefficient of highest degree equal to 1 and cannot be factored). In this case, $P(z)$ can be written as

$$\begin{aligned} P(z) &= (z - r_0)(z - r_1) \dots (z - r_{L_p-1}) \\ &= \prod_{i=0}^{L_p-1} (z - r_i) \\ &= 1z^{L_p} + p_{L_p-1}z^{L_p-1} + \dots + p_0z^0, \end{aligned} \tag{5.7}$$

where r_i , for $i = 0, \dots, L_p-1$, are the zeros (or roots) associated with $P(z)$, and p_i are its coefficients. The roots determine the polynomial, which will be unique [Bourbaki, 1972]. Note that a permutation of the roots r_i does not change the coefficients p_i , but a change on the coefficients p_i can completely change the roots r_i . This means that a permutation or a sign change in the coefficients of the pre-coder p_n yields zeros that are

different from those of $P(z)$. Now, if we recall that $G(z) = P(z)C(z)$, to $G(z)$ result in the correct zeros demanded for the permutation of p_n , then $C(z)$ will require an infinite number of coefficients (or an infinite impulse response). Indeed, from the assumptions made, $C(z)$ is only able to provide zeros (while the zeros of $P(z)$ are fixed). Hence, the only way to achieve the zeros of the permutation of p_n is that $C(z)$ cancels all the zeros of $P(z)$ (with an infinite number of zeros) and provide the new ones necessary for the permutation [Oppenheim et al., 1997].

Finally, from the standpoint of the Marcinkiewicz theorem, if we neglect the solutions of $C(z)$ which have an infinite number of zeros, then $C(z) = \pm 1z^{-k}$ is the only possible solution, i.e., the zero forcing condition is achieved.

In practical (linear) scenarios, this constraint over the set of solutions of $C(z)$ can be done according to the situation:

- Channel, $H(z)$, and equalizer, $W(z)$, only present zeros in their transfer functions (i.e., they can be modeled by FIR filters);
- Channel, $H(z)$, and/or equalizer, $W(z)$, present poles in their transfer functions (i.e., one or both the systems can be modeled by IIR filters).

In the first case, no action is demanded: since $H(z)$ and $W(z)$ are of finite length, the combined system $C(z) = H(z)W(z)$ will never be able to cancel the zeros of $P(z)$ – note, however, that the ZF condition is not attainable in this case. For the second situation, the poles of $H(z)$ and/or $W(z)$ must not match (or cancel) the zeros of $P(z)$, otherwise, a permutation on the coefficients of $P(z)$ might be achieved by $C(z)$. From the equalizer's point of view, the constraint on the solutions is possible to be made via the estimation of $C(z)$ or via the prior knowledge of $P(z)$. This point will be elucidated in Chapter 6.

Example

Consider that $P(z) = p_0 + p_1z^{-1} = 1 + 0.5z^{-1}$ or, alternatively, $\mathbf{p} = [p_0 \ p_1]^T = [1 \ 0.5]^T$. If no delayed version of $P(z)$ is considered, then, there are eight possible permutations of sign and values of the coefficients, as shown in Tab. 5.1.

Assuming that u_n is a binary $\{+1, -1\}$ *i.i.d.* sequence, the resulting distribution or PMF of the pre-coded sequence s_n , $p_S(v)$, will be as illustrated in Fig. 5.4. Interestingly, for all possible permutations $\hat{P}(z)$ of the pre-coder, the resulting PMF $p_S(v)$ will be identical to that of Fig. 5.4. In other words, the PMF $p_S(v)$ carries ambiguities on the linear system $P(z)$, being impossible to define which of the permutations $\hat{P}(z)$ generated $p_S(v)$.

According to the Marcinkiewicz theorem, g_n can be any permuted version of $|p_n|$, i.e., $G(z)$ can be any of the permutations $\hat{P}(z)$ in Tab. 5.1 (plus the delayed ones that we do not show). Since $G(z) = P(z)C(z)$, it is necessary that $C(z)$ assume the values indicated

Table 5.1: Permutations of $P(z)$ and required responses for the combined channel+equalizer system $C(z)$.

	Permutations of $P(z)$	$\hat{C}(z)$
1	$\hat{P}(z) = 1 + 0.5z^{-1}$	1
2	$\hat{P}(z) = -1 - 0.5z^{-1}$	-1
3	$\hat{P}(z) = 0.5 + 1z^{-1}$	$(0.5 + 1z^{-1})/P(z)$
4	$\hat{P}(z) = -0.5 - 1z^{-1}$	$(-0.5 - 1z^{-1})/P(z)$
5	$\hat{P}(z) = 1 - 0.5z^{-1}$	$(1 - 0.5z^{-1})/P(z)$
6	$\hat{P}(z) = -1 + 0.5z^{-1}$	$(-1 + 0.5z^{-1})/P(z)$
7	$\hat{P}(z) = 0.5 - 1z^{-1}$	$(0.5 - 1z^{-1})/P(z)$
8	$\hat{P}(z) = -0.5 + 1z^{-1}$	$(-0.5 + 1z^{-1})/P(z)$

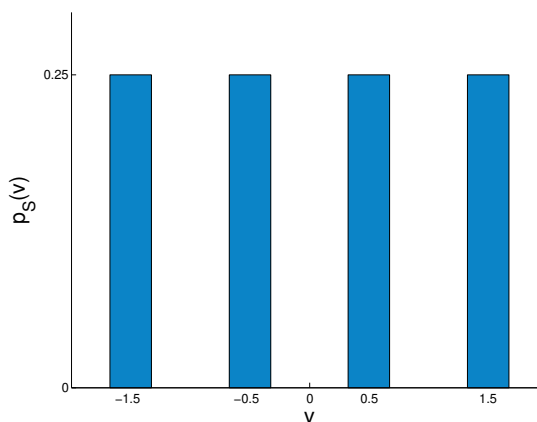


Figure 5.4: Distribution of $p_S(v)$ for pre-coder $P(z)$.

in Tab. 5.1 to achieve each possible permutation. Note that, except for $\hat{P}(z) = 1 + 0.5z^{-1}$ and $\hat{P}(z) = -1 - 0.5z^{-1}$, $C(z)$ must have an infinite impulse response.

If the delayed versions of $P(z)$ are also considered, the permutations $\hat{P}(z) = 1z^{-1} + 0.5z^{-2}$, $\hat{P}(z) = 1 + 0.5z^{-2}$ and $\hat{P}(z) = -0.5z^{-1} + 1z^{-2}$, for instance, will produce the distribution $p_S(v)$ depicted in Fig. 5.4 as well. However, analogously to the previous case, $C(z)$ will have a finite impulse response only when $\hat{P}(z) = \pm P(z)z^{-k}$ (i.e., $C(z) = \pm 1z^{-k}$).

Very interestingly, if it is assumed that $P(z) = 1$, the Marcinkiewicz theorem will reduce to the BGR theorem. Indeed, the only permutation possible in this case requires that $C(z) = \pm 1z^{-k}$, i.e., the ZF condition.

5.2.2 Extension of the BGR Theorem - Multivariate Distributions

An interesting possibility of extracting the temporal structure of the source in a more extensive manner is to consider multivariate distributions instead of the univariate ones. In fact, as we intend to show, the multivariate distributions are able to carry valuable

information about temporal statistical dependence. In light of this, we analyze in this section the BGR theorem extension regarding multivariate distributions.

We start by defining the notation used in the multivariate perspective. Assume that $\mathbf{s}_n = [s_n \ s_{n-1} \ \dots \ s_{n-M}]^T$ is a column vector with s_n and M delayed versions of it. The random vector $\underline{S} = \{S_n, S_{n-1}, \dots, S_{n-M}\}$ is associated with the samples vector \mathbf{s}_n , and its multivariate distribution is denoted by $f_{\underline{S}}(\mathbf{v})$.

The main motivation for this approach comes from the fact that, if the signal is non-*i.i.d.*, then

$$f_{\underline{S}}(\mathbf{v}) \neq \prod_{i=0}^M f_{S_{n-i}}(v_i), \quad (5.8)$$

being $\mathbf{v} = [v_0 \ v_1 \ \dots \ v_M]^T$. This means that the multivariate distribution cannot be obtained from its marginal distributions: the difference between $f_{\underline{S}}(\mathbf{v})$ and $\prod_{i=0}^M f_{S_{n-i}}(v_i)$ is exactly the temporal structure information (also, for stationary RVs $f_{S_{n-i}}(v_i)$ is identical for all delays i , hence the simplified notation $f_S(v)$ for univariate distributions). Indeed, from the perspective of information theory, the evaluation of the information content of multivariate distributions can significantly contribute to reduce the associated uncertainty. In terms of Shannon's joint entropy, this idea is expressed through the following property [Cover and Thomas, 1991]:

$$\begin{aligned} H^S(\underline{S}) &= \sum_{i=0}^M H^S(S_{n-i} | S_{n-i+1}, \dots, S_{n-0}) \\ &\leq \sum_{i=0}^M H^S(S_{n-i}), \end{aligned} \quad (5.9)$$

where M is the number of distinct considered delays. It is important to remark that the uncertainty reduction only occurs if there exists dependence between the variables. If the variables are independent, the adoption of multivariate distributions can result in unnecessary additional computational cost.

However, in parallel with the univariate case, the class of multivariate Gaussian distributions do not provide new statistical information in their HOS. On the other hand, the temporal information may still be extracted from the SOS. In view of this, we split our analysis into two cases: multivariate non-Gaussian distributions and multivariate Gaussian distributions.

Multivariate Non-Gaussian Distributions

The assumptions for this analysis are the following:

1. Pre-coder, $P(z)$, channel, $H(z)$, and equalizer, $W(z)$, are linear time-invariant filters, with finite energy;

2. the signal u_n is composed by *i.i.d.* samples and its associated distribution, $f_U(v)$, is symmetric, with finite statistical moments and non-Gaussian;
3. the source sequence s_n may present temporal dependence but its multivariate distribution, $f_{\underline{S}}(\mathbf{v})$, is (transpositional) symmetric, with finite variance and non-Gaussian.

With respect to the previous assumption in the univariate case, the main difference is that the distribution of s_n is assumed to be multivariate.

Very interestingly, in the context of channel equalization and stationary signals, the marginal densities of $f_{\underline{S}}(\mathbf{v})$ – i.e., $f_{S_{n-i}}(v_i)$, for $i = 0, \dots, M$ – are identical and, if it is considered the matching of the multivariate distributions $f_{\underline{S}}(\mathbf{v}) = f_{\underline{Y}}(\mathbf{v})$, then the matching of their marginal must also occur. Note, however, that the inverse may not hold, i.e., the matching of the marginal distributions does not imply in the matching of the multivariate distributions, as stated by Eq. (5.8).

Recalling the Marcinkiewicz theorem (Theorem 6), it is known that if $f_S(v)$ is non-Gaussian, then the matching of the marginal distributions $f_S(v) = f_Y(v)$ implies that g_n is equal to p_n or any permuted version of $|p_n|$. This permutation ambiguity is a consequence of the univariate distribution $f_S(v)$ being invariant to permutations of $|p_n|$. However, if we consider a multivariate distribution $f_{\underline{S}}(\mathbf{v})$, more information is taken into account and we are able to make the following assumption:

Assume that u_n is a non-Gaussian *i.i.d.* sequence and that the pre-coder $P(z)$ is of depth L_p , i.e., $P(z) = p_0 + p_1z^{-1} + \dots + p_{L_p}z^{-L_p}$. The non-*i.i.d.* source $s_n = p_n * u_n$ is associated with the random vector $\underline{S} = \{S_n, S_{n-1}, \dots, S_{n-M}\}$, with distribution $f_{\underline{S}}(\mathbf{v})$. If the dimension of the distribution $(M+1)$ is equal to or higher than the length of the pre-coder (L_p+1) , i.e., $M \geq L_p$, then only $P(z)z^{-k}$ or $-P(z)z^{-k}$ yields the same distribution $f_{\underline{S}}(\mathbf{v})$ – and no other permutation of $P(z)$.

The proof for this statement is difficult to be obtained, since its mathematical formulation is rather complex. However, its validity is appealing, as shown in the following example.

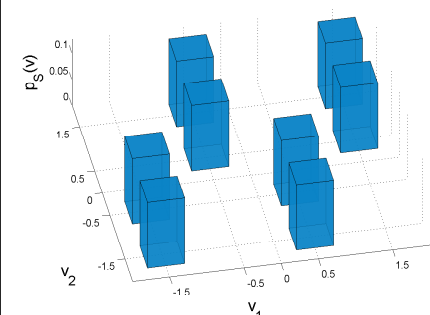
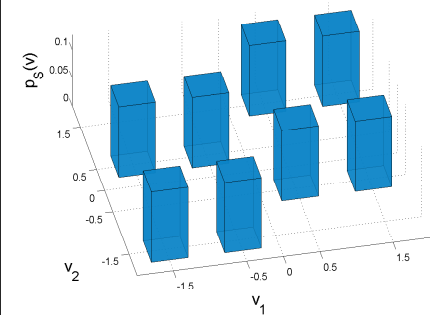
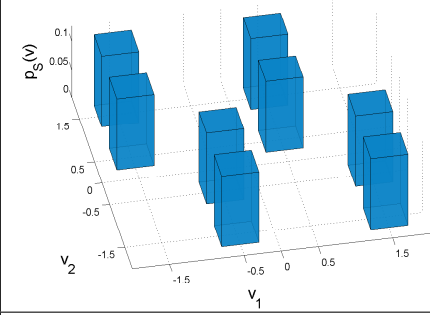
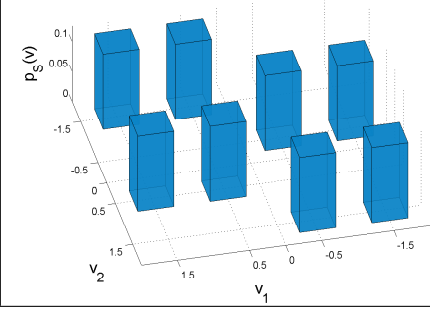
Example

Assume that u_n is an *i.i.d.* binary $\{+1, -1\}$ sequence and consider the pre-coder $P(z) = 1 + 0.5z^{-1}$. The permutations of sign and values of the coefficients of the pre-coder and the resulting multivariate distributions for s_n ($M = 1$) are as shown in Tab. 5.2.

Differently from the univariate case, the multivariate distributions are distinguishable among each other.

In addition, a simple time shift (z^{-k}) in any case of $\hat{P}(z)$ in Tab. 5.2 does not change the PMF $p_{\underline{S}}(\mathbf{v})$. However, permutations like $\hat{P}(z) = 1 + 0z^{-1} + 0.5z^{-2}$, $\hat{P}(z) = -1 + 0z^{-1} + 0.5z^{-2}$ and $\hat{P}(z) = -0.5 + 0z^{-1} + 1z^{-2}$, or even with higher order, result in the

Table 5.2: Permutations of $P(z)$ and associated multivariate distribution.

Permutations of $P(z)$		$p_{\underline{S}}(\mathbf{v})$
1	$\hat{P}(z) = 1 + 0.5z^{-1}$	
2	$\hat{P}(z) = -1 - 0.5z^{-1}$	
3	$\hat{P}(z) = 0.5 + 1z^{-1}$	
4	$\hat{P}(z) = -0.5 - 1z^{-1}$	
5	$\hat{P}(z) = 1 - 0.5z^{-1}$	
6	$\hat{P}(z) = -1 + 0.5z^{-1}$	
7	$\hat{P}(z) = 0.5 - 1z^{-1}$	
8	$\hat{P}(z) = -0.5 + 1z^{-1}$	

distribution $f_{\underline{S}}(\mathbf{v})$ showed in Fig. 5.5. In fact, in these cases, $L_p > M$ and the dimension of the multivariate distribution is insufficient to represent the temporal structure.

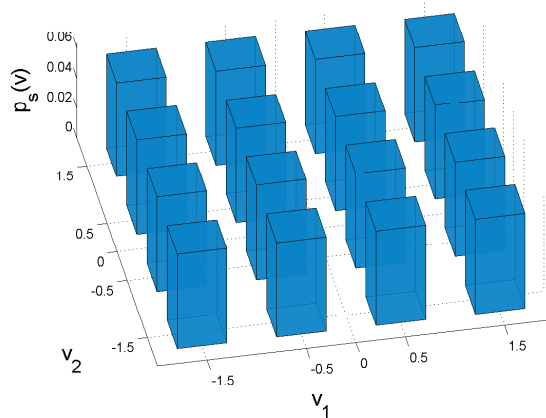


Figure 5.5: Source distribution for pre-coder with $L_c = 2$.

In view of this, the ambiguity caused by $f_{\underline{S}}(\mathbf{v})$ with respect to the pre-coder $P(z)$ is simply a sign factor or a time shift, i.e., $\pm P(z)z^{-k}$. Thus, in the context of the communication system, suppose that $s_n = p_n * u_n$ and $y_n = g_n * u_n$ exists, are non-Gaussian, and that their multivariate distributions are identical, i.e., $f_{\underline{S}}(\mathbf{v}) = f_{\underline{Y}}(\mathbf{v})$ for $M \geq L_p$. Under these hypotheses, it is necessary that $G(z) = P(z)C(z) = \pm P(z)z^{-k}$, implying in the single solution $C(z) = \pm 1z^{-k}$, which is the ZF condition.

This observations are very similar to BGR theorem, but the requirements for perfect equalization are now completely fulfilled by means of the knowledge of the source multivariate distribution. In that sense, this multivariate perspective is the most complete extension of the BGR theorem towards colored blind channel equalization.

Multivariate Gaussian Distributions

So far, we know that the use of multivariate distributions can be useful for reducing the ambiguities associated with the elements of the pre-coder. However, when the source distribution is Gaussian, the HOS information is not relevant and additional care is necessary.

The Gaussian distribution occupies a special place in engineering applications, due to its large occurrence in practical scenarios. Interestingly, it can be totally described by the statistics up to second-order:

$$f_{\underline{S}}(\mathbf{v}) = \frac{1}{\sqrt{(2\pi)^{M+1} \det(\underline{\Sigma}_{\underline{S}})}} \exp \left[\frac{-1}{2} (\mathbf{v} - \underline{\boldsymbol{\mu}}_{\underline{S}})^T \underline{\Sigma}_{\underline{S}}^{-1} (\mathbf{v} - \underline{\boldsymbol{\mu}}_{\underline{S}}) \right], \quad (5.10)$$

where $\underline{\boldsymbol{\mu}}_{\underline{S}} = [\mu_0 \dots \mu_M]^T$ is the column vector with the mean values and $\underline{\Sigma}_{\underline{S}}$ is the covariance matrix. Hence, the distribution can be totally characterized with the sole

knowledge of $\underline{\mu}_S$ and $\underline{\Sigma}_S$.

Starting from the assumption that $f_S(\mathbf{v})$ is Gaussian, we invoke the Cramér theorem [Cramér, 1936]¹,

Theorem 7 (Cramér Theorem). *If the distribution of two RVs is jointly Gaussian, then their marginal distributions are Gaussian as well.*

This means, under our assumption, that the marginals $f_{S_{n-i}}(v_i)$, for $i = 0, \dots, M$, are also Gaussian distributed.

From the Marcinkiewicz theorem (Theorem 6), the matching of marginals that are Gaussian implies in no further information about neither $P(z)$ nor $G(z)$. However, in the context of multivariate distributions, the matching of the distributions $f_S(\mathbf{v}) = f_Y(\mathbf{v})$ can be analyzed in the context of the Kullback-Leibler (KL) divergence [Cover and Thomas, 1991]. Thus, assuming that $f_S(\mathbf{v})$ and $f_Y(\mathbf{v})$ are multivariate Gaussian distributions, then the KL divergence between them can be defined as:

$$\begin{aligned} D_{KL}(Y||S) &= \int_D f_Y(\mathbf{v}) \log \left(\frac{f_Y(\mathbf{v})}{f_S(\mathbf{v})} \right) d\mathbf{v} \\ &= \frac{1}{2} \left(\log \frac{\det(\underline{\Sigma}_S)}{\det(\underline{\Sigma}_Y)} + \text{Tr}(\underline{\Sigma}_S^{-1} \underline{\Sigma}_Y) - (M+1) \right) = 0. \end{aligned} \quad (5.11)$$

where $D \in \mathbb{R}^{M+1}$ and $\text{Tr}(\cdot)$ denotes the trace, i.e., the sum of the elements on the main diagonal of a matrix. When $D_{KL}(Y||S) = 0$, the distributions are identical.

From the symmetry assumption, it implies that $\underline{\mu}_S = \underline{\mu}_Y = \mathbf{0}$. Hence, for Eq. (5.11) to be valid, it is sufficient that the covariance matrices be equal, i.e., $\underline{\Sigma}_Y = \underline{\Sigma}_S$. Based on this, we are able to perform an analysis on the conditions necessary for the covariances to match.

The covariance matrices associated with \underline{Y} and \underline{S} are

$$\underline{\Sigma}_Y = \begin{bmatrix} E[y_n^2] & E[y_n y_{n-1}] & \cdots & E[y_n y_{n-M}] \\ E[y_{n-1} y_n] & E[y_{n-1}^2] & \cdots & E[y_{n-1} y_{n-M}] \\ \vdots & & \ddots & \vdots \\ E[y_{n-M} y_n] & E[y_{n-M} y_{n-1}] & \cdots & E[y_{n-M}^2] \end{bmatrix} \quad (5.12)$$

$$\underline{\Sigma}_S = \begin{bmatrix} E[s_n^2] & E[s_n s_{n-1}] & \cdots & E[s_n s_{n-M}] \\ E[s_{n-1} s_n] & E[s_{n-1}^2] & \cdots & E[s_{n-1} s_{n-M}] \\ \vdots & & \ddots & \vdots \\ E[s_{n-M} s_n] & E[s_{n-M} s_{n-1}] & \cdots & E[s_{n-M}^2] \end{bmatrix}.$$

¹In the same work, Cramér [1936] also proposes his most celebrated theorem, which states that if the sum of two independent RV are Gaussian, then the summands must be Gaussian as well.

The equality $\underline{\Sigma}_Y = \underline{\Sigma}_S$ implies that each element

$$E[y_{n-i}y_{n-j}] = E[s_{n-i}s_{n-j}], \quad (5.13)$$

for $i, j = 0, \dots, M$ must be matched. Using Eq. (4.3), the elements of $\underline{\Sigma}_Y$ can be expanded as

$$E[y_{n-i}y_{n-j}] = \sum_{k=0}^{L_c-1} \sum_{l=0}^{L_c-1} c_k c_l E[s_{n-i-k}s_{n-j-l}]. \quad (5.14)$$

By combining, Eqs. (5.13) and (5.14), it results

$$E[y_{n-i}y_{n-j}] = \sum_{k=0}^{L_c-1} \sum_{l=0}^{L_c-1} c_k c_l E[s_{n-i-k}s_{n-j-l}] = E[s_{n-i}s_{n-j}], \quad (5.15)$$

which is a second-order polynomial in function of the combined channel+equalizer coefficients c_n . In that sense, the matching of covariance matrices $\underline{\Sigma}_Y = \underline{\Sigma}_S$ can be viewed as a system of quadratic equations. Notwithstanding, in order to achieve the desired solution for the system, it is necessary that the number of non-redundant equations be equal (determined case) or larger (overdetermined case) than the number of unknown variables.

Assuming that u_n is stationary and real-valued, then $E[y_{n-i}y_{n-j}] = E[y_{n-j}y_{n-i}]$ and $E[s_{n-i}s_{n-j}] = E[s_{n-j}s_{n-i}]$ (the correlation matrices are Toeplitz [Haykin, 1996]) and, thus, some quadratic equations are redundant. In this case, the quadratic equations system in the matching $\underline{\Sigma}_Y = \underline{\Sigma}_S$ is composed of, at most, $M + 1$ non-redundant equations.

If both the source s_n and the output signal y_n do not present a temporal structure for delay k , i.e., if $E[s_n s_{n-k}] = E[y_n y_{n-k}] = 0$, then, the matching results in equations of the type $0 = 0$, which do not contribute to solving the system. In fact, the number of valid equations will depend on the temporal structure of y_n , which will be of length $L_p + L_c + 1$. In other words, the pre-coder and the combined channel+equalizer systems are the responsible for introducing correlation in the time samples of y_n .

Since the analysis is held in the combined channel+equalizer domain, the number of equations necessary to solve the system only depends on the number of unknown variables for c_n , which is only $L_c + 1$ equations. If L_c is finite, then it is demanded that $M \geq L_c$. Otherwise, if L_c is infinite, then we also need $M = \infty$. Hence, if the number of equations is sufficient, then the solution for the system (and for the matching of covariance matrices) is the intersection point of the surfaces generated by each quadratic equation in the system.

Example

We consider the case in which u_n is an *i.i.d.* Gaussian distributed sequence, with zero mean and unit variance, and the pre-coder has transfer function $P(z) = 1 + 0.5z^{-1}$. For the combined channel+equalizer system $C(z)$, two possibilities are assumed: in the first one,

$L_c = 1$, i.e., $C(z) = c_0 + c_1z^{-1}$ and, in the second, $L_c = 2$, i.e., $C(z) = c_0 + c_1z^{-1} + c_2z^{-2}$. In the first case, we have two unknown variables, c_0 and c_1 , and, in the second, three unknown variables, c_0 , c_1 and c_2 .

We adopt $M = L_c$ and, for each case, we have the following covariance matrices $\underline{\Sigma}_S$:

$$\underline{\Sigma}_S = \begin{bmatrix} 1.25 & 0.5 \\ 0.5 & 1.25 \end{bmatrix}, \quad \underline{\Sigma}_S = \begin{bmatrix} 1.25 & 0.5 & 0 \\ 0.5 & 1.25 & 0.5 \\ 0 & 0.5 & 1.25 \end{bmatrix}, \quad (5.16)$$

for $M = 1$ and $M = 2$, respectively. Hence, the system of equations, in this case, will be

$$\begin{cases} E[y_{n-k}^2] = 1.25 \\ E[y_n y_{n-1}] = 0.5 \end{cases}, \quad \begin{cases} E[y_{n-k}^2] = 1.25 \\ E[y_n y_{n-1}] = 0.5 \\ E[y_n y_{n-2}] = 0 \end{cases}, \quad (5.17)$$

where each equation can be written in function of \mathbf{c} , as indicated by Eq. (5.14).

By varying the values of \mathbf{c} we are able to identify the cases in which each equation is valid, as plotted in Fig. 5.6. In the case $L_c = 1$ (Fig. 5.6(a)), since we have only two

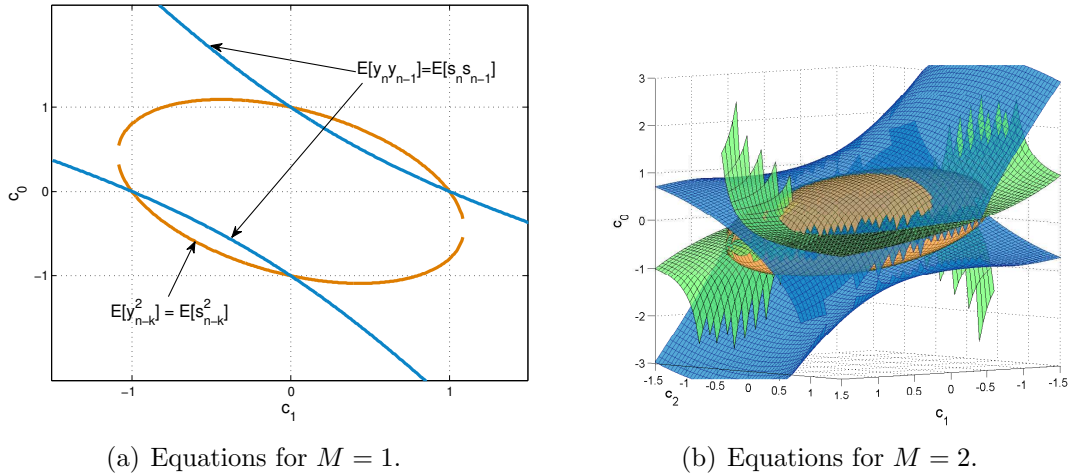


Figure 5.6: System of equations - Intersection.

unknown variables, it is possible to visualize the equations in the plane. There are four points where the curves intercept each other, which are $C(z) = \pm 1$ and $C(z) = \pm 1z^{-1}$, i.e., all the cases when the ZF condition is attained. In the case $L_c = 2$ (Fig. 5.6(b)), the equations constitute surfaces in the 3D-space, and the intersection among them occur in six points: $C(z) = \pm 1$, $C(z) = \pm 1z^{-1}$ and $C(z) = \pm 1z^{-2}$, i.e., all possible ZF solutions for $L_c = 2$.

In both cases, all equations of the system are satisfied in the intersection points, which are the points where the matching $\underline{\Sigma}_Y = \underline{\Sigma}_S$ is achieved.

In the overdetermined case, i.e., when the number of equations is larger than the number of unknowns ($M > L_c$), the equations in excess form redundant equations (by construction) and the system always have a valid solution. Thus once is satisfied $M \geq L_c$, the matching of the covariances $\underline{\Sigma}_Y = \underline{\Sigma}_S$ can always be performed. However, the covariance matrices carry ambiguity of sign and direct/inverse order of the coefficients of the involved systems, as we will see in the following example.

Example

We assume again that u_n is an *i.i.d.* Gaussian distributed sequence with pre-coder $P(z) = 1 + 0.5z^{-1}$. The permutations of sign and values of the coefficients of the pre-coder and the resulting covariance matrices $\underline{\Sigma}_S$ (for $M = 1$) are as shown in Tab. 5.3. Note

Table 5.3: Permutations of $P(z)$ and associated covariance matrices.

	Permutations of $P(z)$	$\underline{\Sigma}_S$
1	$\hat{P}(z) = 1 + 0.5z^{-1}$	$\underline{\Sigma}_S = \begin{bmatrix} 1.25 & 0.5 \\ 0.5 & 1.25 \end{bmatrix}$
2	$\hat{P}(z) = -1 - 0.5z^{-1}$	
3	$\hat{P}(z) = 0.5 + 1z^{-1}$	
4	$\hat{P}(z) = -0.5 - 1z^{-1}$	
5	$\hat{P}(z) = 1 - 0.5z^{-1}$	$\underline{\Sigma}_S = \begin{bmatrix} 1.25 & -0.5 \\ -0.5 & 1.25 \end{bmatrix}$
6	$\hat{P}(z) = -1 + 0.5z^{-1}$	
7	$\hat{P}(z) = 0.5 - 1z^{-1}$	
8	$\hat{P}(z) = -0.5 + 1z^{-1}$	

that the permutations 1 to 4 are associated with the same covariance matrix. Thus, it is not possible to distinguish among them only by $\underline{\Sigma}_S$. The same occurs for permutations 5 to 8.

In all cases, a time shift (z^{-k}) does not imply in changes on the covariance matrix $\underline{\Sigma}_S$. Permutations that increase the order of the polynomial, like $\hat{P}(z) = 1 + 0z^{-1} + 0.5z^{-2}$, $\hat{P}(z) = -1 + 0z^{-1} + 0.5z^{-2}$ or $\hat{P}(z) = -0.5 + 0z^{-1} + 1z^{-2}$, result in covariance matrices different from those exhibited in Tab. 5.3.

The ambiguity in the matching $\underline{\Sigma}_Y = \underline{\Sigma}_S$ will imply in the following solutions for $G(z)$: (i) $G(z) = \pm P(z)z^{-k}$ or (ii) $G(z) = \pm P(z^{-1})z^{-k}$. In the first case, since $G(z) = P(z)C(z)$, it is necessary that $C(z) = \pm 1z^{-k}$, and the ZF condition is attained. In the case (ii), $C(z)$ will require an infinite number of coefficients to invert the order of the coefficients of $P(z)$. Just like the analyzed case in Section 5.2.1, this case can be controlled by avoiding an infinite impulse response of $C(z)$.

5.2.3 Extension of the SW Theorem

An analogous analysis of the BGR theorem extension can be performed for the SW theorem. The assumptions are similar to the previous case, being the main difference that signals can belong either to the real or complex domains:

1. Pre-coder, $P(z)$, channel, $H(z)$, and equalizer, $W(z)$, are linear time-invariant filters, with finite energy;
2. the real/complex signal u_n is composed by *i.i.d.* samples and its associated distribution, $f_U(v)$, is symmetric, with finite statistical moments and non-Gaussian;
3. the real/complex source sequence s_n may present temporal dependence but its distribution, $f_S(v)$, is symmetric, with finite variance and non-Gaussian.

In the context of Fig. 5.3, we are able to analyze the second-order statistics and the kurtosis (Eq. (4.45)) of the involved signals. Starting with the second moment, analogously to Eq. (5.4), we have

$$E[|s_n|^2] = E[|u_n|^2] \left(\sum_i |p_i|^2 \right), \quad (5.18)$$

and

$$E[|y_n|^2] = E[|u_n|^2] \left(\sum_j |g_j|^2 \right), \quad (5.19)$$

for the source s_n and output y_n signals, respectively. For mathematical convenience, we assume that $\sum_i |p_i|^2 = 1$.

By matching the mentioned second-order statistics, i.e., $E[|y_n|^2] = E[|s_n|^2]$, it is necessary that the equivalence holds

$$\sum_j |g_j|^2 = \sum_i |p_i|^2 = 1. \quad (5.20)$$

Regarding the fourth-order statistics, the kurtosis of the signals s_n and y_n , based on Eq. (5.4), can be written as

$$k_S = k_U \left(\sum_i |p_i|^4 \right), \quad (5.21)$$

and

$$k_Y = k_U \left(\sum_j |g_j|^4 \right). \quad (5.22)$$

Now, supposing the matching of the kurtosis k_S and k_Y , it results

$$\sum_j |g_j|^4 = \sum_i |p_i|^4. \quad (5.23)$$

Similarly to the SW theorem, from Eq. (5.5), we can write

$$\begin{aligned} \sum_i |p_i|^4 &\leq \left(\sum_i |p_i|^2 \right)^2 \\ &\leq 1, \end{aligned} \quad (5.24)$$

and

$$\begin{aligned} \sum_j |g_j|^4 &\leq \left(\sum_j |g_j|^2 \right)^2 \\ &\leq 1, \end{aligned} \quad (5.25)$$

where equality holds if and only if p_n and g_n has one nonzero component of magnitude 1. This means that

$$\begin{aligned} |k_S| &\leq |k_U| \\ |k_Y| &\leq |k_U|, \end{aligned} \quad (5.26)$$

and, when equality is reached, the problem is reduced to the classical SW theorem.

However, for intermediate values $0 < |k_Y| < |k_U|$, the kurtosis k_Y can be associated with up to an infinite number of configurations of p_n and g_n . In that sense, Eqs. (5.20) and (5.23) can only provide a limited amount of information, being sufficient for equalization of a temporally structured source only if the number of unknown coefficients is equal to or lower than two – it will be a system of two equations and two unknown variables –, otherwise, there will be an infinite set of solutions.

Consequently, Eqs. (5.20) and (5.23) are not sufficient for equalization of temporally structured sources (only if the number of unknown coefficients is equal to or lower than two – otherwise, there will be an infinite set of solutions).

In view of this, it would be interesting if additional information about the temporal structure of the signals were also considered. Very interestingly, a temporal-based kurtosis measure was proposed in the context of the blind source separation problem [Hyvärinen et al., 2001]:

$$k_S(i,j) = E [|s_{n-i}|^2 |s_{n-j}|^2] - 2E^2 [s_{n-i} s_{n-j}^*] - |E [s_{n-i} s_{n-j}]|^2, \quad (5.27)$$

being called *cross-kurtosis*.

With the cross-kurtosis at hand, we are able to compose a set of equations (similarly to the approach followed in Section 5.2.2) to find the desired solution. Thus, our objective will be to match the second-order statistics and the cross-kurtosis of the source s_n with those of the output signal y_n , considering time delays from 0 to M .

Regarding the SOS, the cross-correlation for the source s_n and the output y_n signals

are, respectively,

$$E [s_{n-i} s_{n-j}^*] = \sum_{k=0}^{L_p} \sum_{l=0}^{L_p} p_k^* p_l E [u_{n-i-k} u_{n-j-l}^*], \quad (5.28)$$

and

$$E [y_{n-i} y_{n-j}^*] = \sum_{k=0}^{L_g} \sum_{l=0}^{L_g} g_k^* g_l E [u_{n-i-k} u_{n-j-l}^*], \quad (5.29)$$

for $i, j = \{0, \dots, M\}$. Due to the *i.i.d.* assumption for u_n , $E [u_{n-i-k} u_{n-j-l}^*] = E [|u_n|^2]$ when $i+k = j+l$, and $E [u_{n-i-k} u_{n-j-l}^*] = 0$ otherwise.

Similarly, for the cross-kurtosis, we have

$$k_S(i, j) = E [|s_{n-i}|^2 |s_{n-j}|^2] - 2E^2 [s_{n-i} s_{n-j}^*] - |E [s_{n-i} s_{n-j}^*]|^2, \quad (5.30)$$

and

$$k_Y(i, j) = E [|y_{n-i}|^2 |y_{n-j}|^2] - 2E^2 [y_{n-i} y_{n-j}^*] - |E [y_{n-i} y_{n-j}^*]|^2, \quad (5.31)$$

where the first term of $k_S(i, j)$ is

$$E [|s_{n-i}|^2 |s_{n-j}|^2] = \sum_k \sum_l \sum_m \sum_o p_k^* p_l p_m p_o^* E [u_{n-k-i} u_{n-l-i}^* u_{n-m-j}^* u_{n-o-j}], \quad (5.32)$$

being [Shalvi and Weinstein, 1990]

$$E [u_{n-k-i} u_{n-l-i}^* u_{n-m-j}^* u_{n-o-j}] = \begin{cases} E [|u_n|^4], & k+i = l+i = m+j = o+j \\ E^2 [|u_n|^2], & k+i = l+i \neq m+j = o+j, k+i = m+j \neq l+i = o+j \\ |E [u_n^2]|^2, & k+i = o+j \neq l+i = m+j \\ 0, & \text{otherwise.} \end{cases} \quad (5.33)$$

The second term of $k_S(i, j)$ is as Eq. (5.28) and, finally, the third term is

$$E [s_{n-i} s_{n-j}] = \sum_{k=0}^{L_p} \sum_{l=0}^{L_p} p_k^* p_l^* E [u_{n-i-k} u_{n-j-l}], \quad (5.34)$$

in which $E [u_{n-i-k} u_{n-j-l}] = E [u_n^2]$ when $i+k = j+l$, and $E [u_{n-i-k} u_{n-j-l}] = 0$ otherwise. The terms are very similar with respect to y_n , being in function of g_n instead of p_n .

If signals are stationary and, along with the systems, belong to the complex domain, the complex-valued covariance matrices are Hermitian (i.e., $\Sigma^H = \Sigma$) and there will be up to $2(M+1)$ non-redundant equations. For the cross-kurtosis, if the matrices \mathbf{K}_S and \mathbf{K}_Y are considered, whose elements of the i -th row and the j -th column are the cross-kurtosis $k_S(i, j)$ and $k_Y(i, j)$ elements, then the matrices will also be Hermitian, and there will be up to $2(M+1)$ non-redundant equations as well (note that the number of unknown

variables for c_n in the complex domain is $2(L_c+1)$). In that sense, it is necessary that $M \geq (L_c-1)/2$ to obtain valid solutions for \mathbf{c} . If all variables are in the real domain, the number of non-redundant equations are half the one of the complex case, i.e., $2(M+1)$ non-redundant equations, but there are only L_c+1 unknown coefficients, resulting in the same requirement of $M \geq (L_c-1)/2$.

The temporal structure will be responsible for generating valid equations to the system. Similarly to the case of the matching of covariance matrices, there could be used up to L_p+L_c+1 time delays. When the source is Gaussian, it is known that $k_S(0,0)$ and $k_Y(0,0)$ are null [Hyvärinen et al., 2001] and this equation is not valid. In this case, there is up to L_p+L_c valid equations in the system for the cross-kurtosis.

As one might note, the cross-kurtosis encompasses the use of the quadratic terms of p_n or g_n , which may generate permutation ambiguities of the involved systems. In fact, the cross-kurtosis is invariant to phase shift $e^{j\theta}$ (sign change for real-valued variables) and reverse ordering of the coefficients.

Example

Consider the real-valued *i.i.d.* sequence u_n with symbols $\{+1, -1\}$ and pre-coder $P(z) = 1 + 0.5z^{-1}$. Since the variables are on the real domain, it is assumed that the cross-kurtosis only depends on the delay m :

$$k_S(m) = E [|s_n|^2 |s_{n-m}|^2] - 2E^2 [s_n s_{n-m}^*] - |E [s_n s_{n-m}]|^2. \quad (5.35)$$

The permutations of sign and values of the coefficients of the pre-coder and the resulting cross-kurtosis (for $M = 3$) are as shown in Tab. 5.4. It is possible to note that the cross-

Table 5.4: Permutations of $P(z)$ and associated cross-kurtosis $k_S(m)$.

	Permutations of $P(z)$	$ k_S(m) $												
1	$\hat{P}(z) = 1 + 0.5z^{-1}$	<table border="1"> <caption>Data for Figure 5.4: k_S(m) vs m</caption> <thead> <tr> <th>m</th> <th> k_S(m) </th> </tr> </thead> <tbody> <tr> <td>0</td> <td>2.1</td> </tr> <tr> <td>1</td> <td>0.8</td> </tr> <tr> <td>2</td> <td>1.6</td> </tr> <tr> <td>3</td> <td>1.6</td> </tr> <tr> <td>4</td> <td>1.6</td> </tr> </tbody> </table>	m	k_S(m)	0	2.1	1	0.8	2	1.6	3	1.6	4	1.6
m	k_S(m)													
0	2.1													
1	0.8													
2	1.6													
3	1.6													
4	1.6													
2	$\hat{P}(z) = -1 - 0.5z^{-1}$													
3	$\hat{P}(z) = 0.5 + 1z^{-1}$													
4	$\hat{P}(z) = -0.5 - 1z^{-1}$													
5	$\hat{P}(z) = 1 - 0.5z^{-1}$													
6	$\hat{P}(z) = -1 + 0.5z^{-1}$													
7	$\hat{P}(z) = 0.5 - 1z^{-1}$													
8	$\hat{P}(z) = -0.5 + 1z^{-1}$													

kurtosis is invariant to all permutations in Tab. 5.4. A time shift (z^{-k}) does not imply in changes on the cross-kurtosis. Permutations that increase the order of the polynomial, like $\hat{P}(z) = 1 + 0z^{-1} + 0.5z^{-2}$, $\hat{P}(z) = -1 + 0z^{-1} + 0.5z^{-2}$ or $\hat{P}(z) = -0.5 + 0z^{-1} + 1z^{-2}$,

results in different measures for cross-kurtosis.

Tab. 5.4 also shows that the cross-kurtosis is constant for $m > L_p$. In fact, when there is no temporal structure the cross-kurtosis assumes a constant value different from zero.

If signals and systems were defined in the complex domain, then permutations with phase shift $e^{j\theta}$ – such as $\hat{P}(z) = 1e^{j\theta_0} + 0.5e^{j\theta_1}z^{-1}$ and $\hat{P}(z) = 0.5e^{j\theta_0} + 1e^{j\theta_1}z^{-1}$, being θ_0 and θ_1 arbitrary phase shifts – also results in the same cross-kurtosis of Tab. 5.4.

Gaussian signals can also be considered in the analysis. Assuming u_n an *i.i.d.* Gaussian distributed sequence with zero mean and unit variance, the resulting cross-kurtosis for the pre-coder $P(z) = 1 + 0.5z^{-1}$ and its permutations (in Tab. 5.4) is as illustrated in Fig. 5.7. Observe that, in this case, $k_S(0) = 0$, i.e., the kurtosis is null. Indeed, for

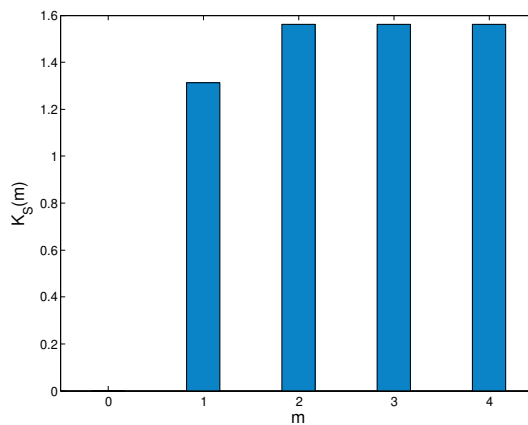


Figure 5.7: Cross-kurtosis for colored Gaussian Source.

Gaussian sources the kurtosis (or $k_S(0)$) will always be null.

Hence, the cross-kurtosis is able to identify the coefficients $|p_n|$, but with uncertainty about the phase shift and direct or inverse order of the coefficients. Recalling that the second-order statistics (covariance matrices) are also matched, the ambiguities can be reduced. In fact, if $E[s_{n-i}s_{n-j}^*] = E[y_{n-i}y_{n-j}^*]$ and if $k_S(i,j) = k_Y(i,j)$ are satisfied for $i,j = \{0, \dots, M\}$, with $M \geq (L_c - 1)/2$, then the possible solutions for $G(z)$ are: $G(z) = P(z)e^{j\theta}z^{-k}$ or $G(z) = P(z^{-1})e^{j\theta}z^{-k}$, being θ a phase shift. Since $G(z) = P(z)C(z)$, this implies, in the first case, that $C(z) = 1e^{j\theta}z^{-k}$, i.e., the ZF condition, and, in the second case, that $C(z)$ have an infinite impulse response.

Again, an additional care is necessary to avoid solutions for $C(z)$ with infinite impulse response that cancels the zeros of the pre-coder $P(z)$. This can be done in the same way of the preceding sections.

5.3 Summary of the Extensions

The theoretical analysis carried out so far revealed the required statistical conditions, based on the classical BGR and SW theorems, for solving the colored blind channel equalization problem. In rigorous terms, to ensure that the ZF condition be achieved, it is necessary to have a priori knowledge of the multivariate distribution of the temporally structured source, which must not be Gaussian. Indeed, this is the only case where the solutions for $C(z)$ have no permutations ambiguities.

In comparison with the classical approach, where the second- and fourth-order statistics are sufficient for equalization (SW theorem), the requirement of a priori knowledge of the source multivariate distribution exposes the complexity of the problem. Notwithstanding, we have also seen that, under certain constraints on the channel+equalizer system, the statistical conditions can be relaxed and even the second-order statistics can be sufficient for colored equalization.

In view of the several properties each extension carries, we present in Tab. 5.5 a summary with the possible ambiguous solutions for $C(z)$ and the number of delays required for each extension case, considering a generic FIR pre-coder $P(z)$.

It is also worth mentioning that, when $P(z) = 1$, the ambiguities for $C(z)$ are reduced to the ZF condition in all cases (however the source becomes *i.i.d.*).

In the following, we consider some test scenarios to verify the properties of Tab. 5.5 for each extension case.

5.4 Test Scenarios

In order to illustrate the properties of the extensions of the BGR and SW theorems towards temporally structured sources, we consider the following measures. In the context of the BGR theorem, we adopt the discrete Kullback-Leibler divergence, which can be defined as

$$D_{KL}(Y||S) = \sum_{\mathbf{v} \in \mathcal{S}} p_{\underline{Y}}(\mathbf{v}) \log \left(\frac{p_{\underline{Y}}(\mathbf{v})}{p_{\underline{S}}(\mathbf{v})} \right) \quad (5.36)$$

where $p_{\underline{Y}}(\mathbf{v})$ and $p_{\underline{S}}(\mathbf{v})$ are the multivariate PMFs associated with y_n and s_n , respectively, and \mathcal{S} is the set of all vector states associated with non-null probabilities; for the continuous case, we use the continuous version of Kullback-Leibler divergence, as defined in Eq. (5.11).

In the context of the SW theorem, for the use of second-order statistics, we consider the measure of the matching of covariances as

$$J_{cov} = \sum_{i,j=0}^M (E [y_{n-i}y_{n-j}^*] - E [s_{n-i}s_{n-j}^*])^2; \quad (5.37)$$

Table 5.5: Summary of the Extensions.

		$C(z)$ Ambiguities		Delays
		FIR $C(z)$	IIR $C(z)$	
BGR Theorem Extensions	Univariate Distributions	Non-Gauss. $\pm 1z^{-k}$ (ZF)	$\frac{\pm p_0 z^{-k_0} \pm p_1 z^{-k_1} \pm \dots \pm p_{L_p} z^{-k_{L_p}}}{P(z)}$	$M = 0$
		Gaussian ∞	∞	
BGR Theorem Extensions	Multivariate Distributions	Non-Gauss. $\pm 1z^{-k}$ (ZF)	–	$M \geq L_p$
		Gaussian $\pm 1z^{-k}$ (ZF)	$\frac{\pm P(z^{-1})z^{-k}}{P(z)}$	$M \geq L_c$
SW Theorem Extension	Cross-Kurtosis	Non-Gauss. $1e^{j\theta} z^{-k}$ (ZF)	$\frac{P(z^{-1})e^{j\theta} z^{-k}}{P(z)}$	$M \geq \frac{L_c - 1}{2}$
		Gaussian $1e^{j\theta} z^{-k}$ (ZF)	$\frac{P(z^{-1})e^{j\theta} z^{-k}}{P(z)}$	

and the matching of cross-kurtosis as

$$J_K = \sum_{i,j=0}^M (k_Y(i,j) - k_S(i,j))^2, \quad (5.38)$$

being $k_Y(i,j)$ and $k_S(i,j)$ as defined in Eq. (5.27). However, since the cross-kurtosis approach also depends on the matching of the covariances, the considered measure associated with the extension of the SW theorem was

$$J = J_{cov} + J_K. \quad (5.39)$$

Particularly, the matching of covariances, Eq. (5.37), is closely related to the matching of multivariate Gaussian distribution (BGR theorem extension), since, in this case, only the SOS are encompassed. In view of this, we also include this measure in the test scenarios.

For all considered measures, the matching conditions are satisfied when the above relations are null.

Each of these measures are able to verify the conditions established in our analysis when they reach their optimum values. They will be tested in two scenarios:

1. u_n is a real-valued *i.i.d.* sequence with symbols $\{+1, -1\}$, the pre-coder is $P(z) = 1 + 0.6z^{-1}$;
2. u_n is a real-valued *i.i.d.* Gaussian distributed sequence with zero mean and unit variance, the pre-coder is $P(z) = 1 + 0.6z^{-1}$;

Our objective will be to identify if, once attained the requirements regarding the analysis of the theorems extension, the solutions for the combined channel+equalizer system are the ZF condition and/or the possible permutations.

We consider two structures for the combined channel+equalizer system $C(z)$. In the first case, $C(z) = c_0 + c_1z^{-1}$, i.e., $C(z)$ has a finite impulse response. In the second case, $C(z)$ has infinite impulse response, but is implemented via an IIR structure of the form:

$$C(z) = \frac{c_0 + c_1z^{-1}}{P(z)} = \frac{c_0 + c_1z^{-1}}{1 + 0.6z^{-1}}. \quad (5.40)$$

Hence, in both cases, there are only two unknown variables c_0 and c_1 , which will be helpful for the solution visualization. The case in which the signals and systems belong to the complex domain will not be considered, since the number of unknown variables is higher and the visualization of the solutions would be compromised.

5.4.1 Scenario 1 - Non-Gaussian Source

In scenario 1, we start by analyzing the KL divergence, Eq. (5.36), for univariate ($M = 0$) and multivariate ($M = 1$) PMFs. From Tab. 5.5, we know that, for $C(z)$ with finite impulse response, $M = 0$ is sufficient to obtain the ZF condition. Thus, by performing a sweep for c_0 and c_1 from -1.5 to 1.5 in the FIR $C(z)$ system, we found the solutions displayed in Fig. 5.8.

There are 4 possible solutions for both cases: $\mathbf{c} = [1 \ 0]^T$, $\mathbf{c} = [-1 \ 0]^T$, $\mathbf{c} = [0 \ 1]^T$ and $\mathbf{c} = [0 \ -1]^T$, which can be represented by $C(z) = \pm 1z^{-k}$, for $k \in \{0, 1\}$, all the ZF solutions possible.

The procedure was repeated for the measures given by Eqs. (5.37) and (5.39) considering $M = 0$ and $M = 1$, being their surfaces contours plotted in Fig. 5.9.

For $M = 0$, the number of equations is insufficient to obtain the desired solutions for \mathbf{c} , as mentioned in Section 5.2.3. In the case of the covariance matching, Fig. 5.9(a), there is an infinite set of solutions for \mathbf{c} in the shape of an ellipse. On the other hand, for the cross-kurtosis and covariances matching, Fig. 5.9(c), the number of solutions is

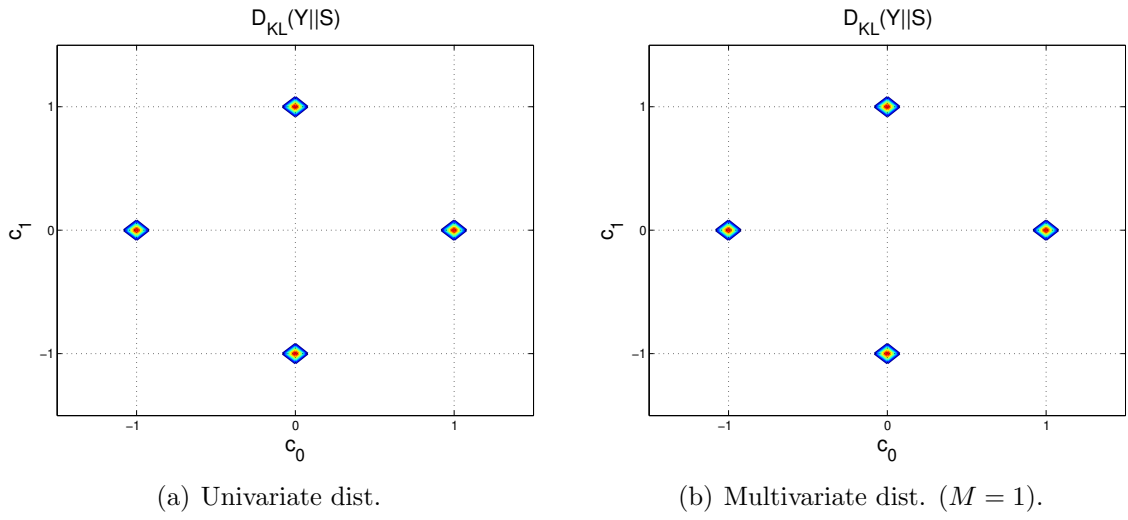


Figure 5.8: Scenario 1 - Solutions for FIR $C(z)$ - BGR theorem extensions.

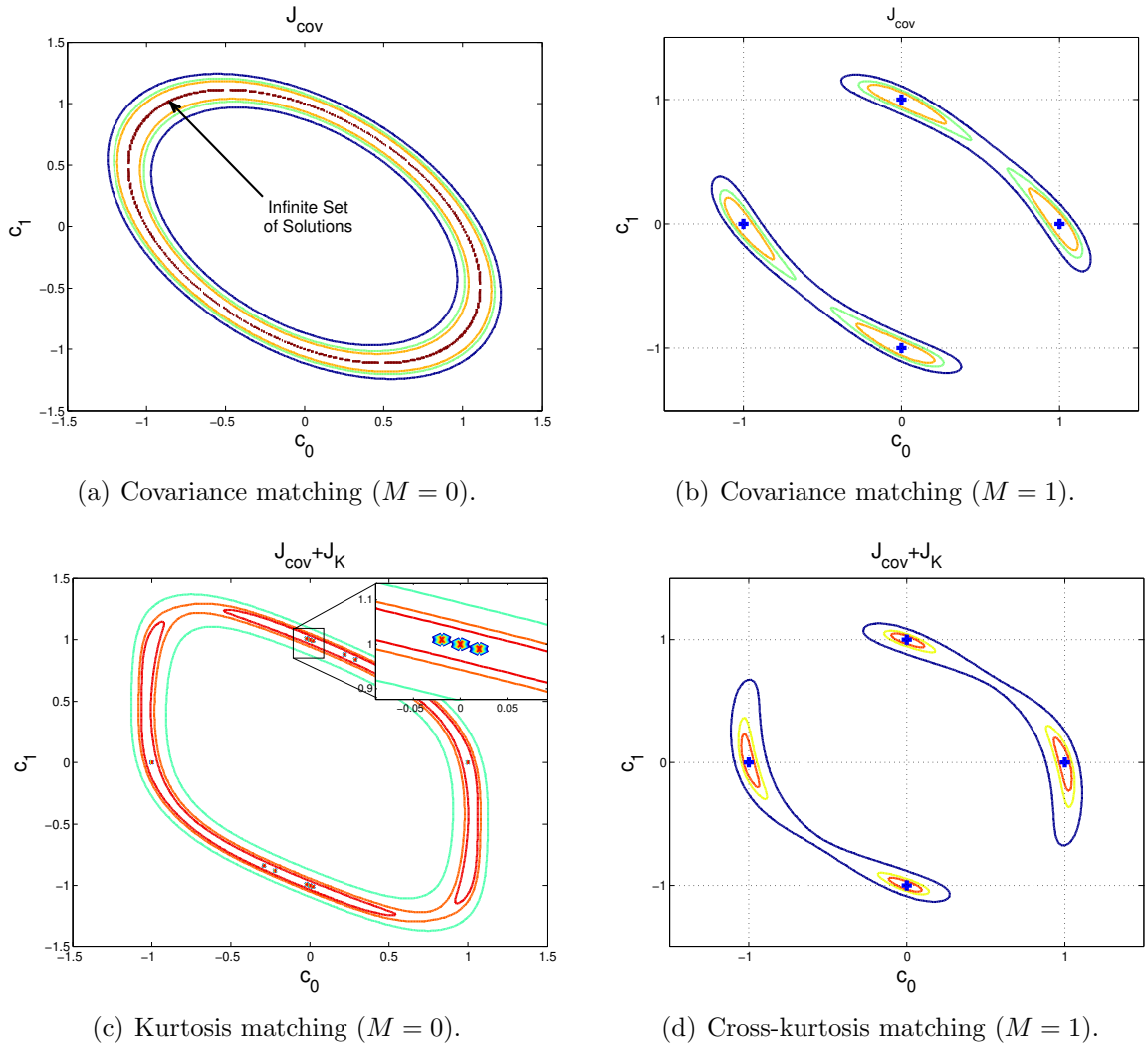


Figure 5.9: Scenario 1 - Contours for covariance and cross-kurtosis matching - Solutions for FIR $C(z)$.

reduced, but some of them do not satisfy the ZF condition. When the number of delays is increased to $M = 1$, the number of equations ($M + 1$) is equal to the number of unknown variables ($L_c + 1$) and it is possible to achieve the desired solutions. Indeed, as shown in Figs. 5.9(b) and 5.9(d), the only possible solutions are $C(z) = \pm 1z^{-k}$, for $k \in \{0, 1\}$.

For the combined channel+equalizer system with an infinite impulse response, we performed again the sweep for c_0 and c_1 from -1.5 to 1.5 . The resulting surface contours of the KL divergence for $M = 0$ and $M = 1$ are displayed in Fig. 5.10.

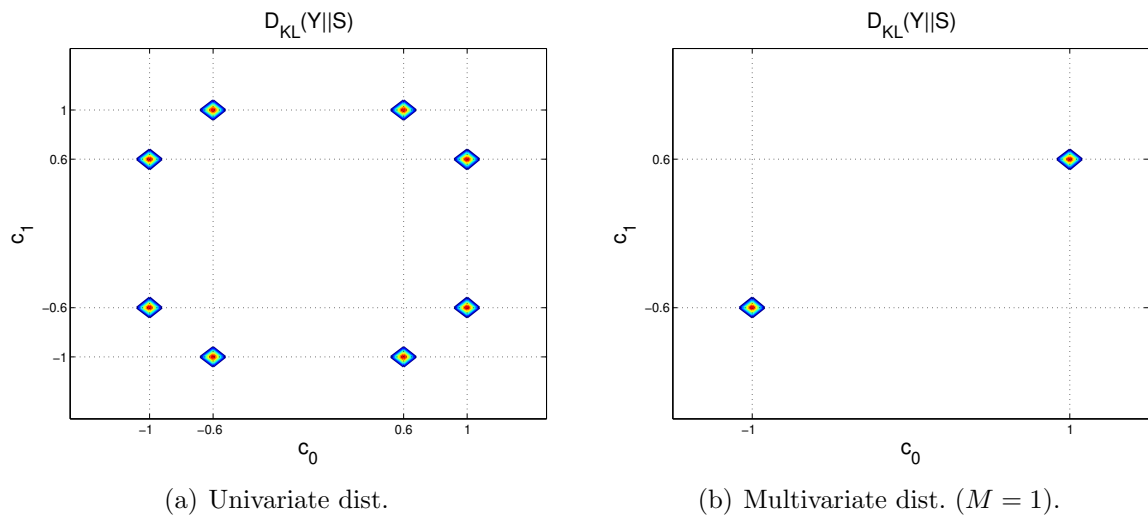


Figure 5.10: Scenario 1 - Solutions for IIR $C(z)$ - BGR theorem extensions.

According to Tab. 5.5, we know that for $M = 0$ the solutions for $C(z)$ are all possible permutations of the coefficients of $P(z)$. Indeed, as shown in Fig. 5.10(a), the solutions are $C(z) = 1 + 0.6z^{-1}/P(z)$, $C(z) = 1 - 0.6z^{-1}/P(z)$, $C(z) = -1 + 0.6z^{-1}/P(z)$, $C(z) = -1 - 0.6z^{-1}/P(z)$, $C(z) = 0.6 + 1z^{-1}/P(z)$, $C(z) = 0.6 - 1z^{-1}/P(z)$, $C(z) = -0.6 + 1z^{-1}/P(z)$ and $C(z) = -0.6 - 1z^{-1}/P(z)$. By increasing the number of delays, i.e., with $M = 1$, the only possible solutions are $C(z) = \pm 1$ (i.e., $C(z) = 1 + 0.6z^{-1}/P(z)$ and $C(z) = -1 - 0.6z^{-1}/P(z)$) and the ambiguous cases are solved.

Finally, for the covariance and the cross-kurtosis matching, the behavior of the combined channel+equalizer system with an infinite impulse response is as illustrated in Fig. 5.11, for $M = 0$ and $M = 1$.

According to Tab. 5.5, the possible solutions are $C(z) = \pm P(z^{-1})z^{-k}/P(z)$ if $M \geq L_c$. When $M = 0$, the set of possible solutions for $C(z)$ is infinite with respect to the covariance matching measure (Fig. 5.11(a)). When $M = 1$, it is possible to achieve the necessary conditions for solving the equations system, and the set of possible solutions are $C(z) = \pm P(z^{-1})z^{-k}/P(z)$ (more specifically, $C(z) = 0.6 + 1z^{-1}/P(z)$ and $C(z) = -0.6 - 1z^{-1}/P(z)$) and the ones associated with the ZF condition ($C(z) = 1 + 0.6z^{-1}/P(z)$ and $C(z) = -1 - 0.6z^{-1}/P(z)$), as shown in Fig. 5.11(b). With respect to the cross-kurtosis matching, when $M = 0$, it may lead to solutions other than

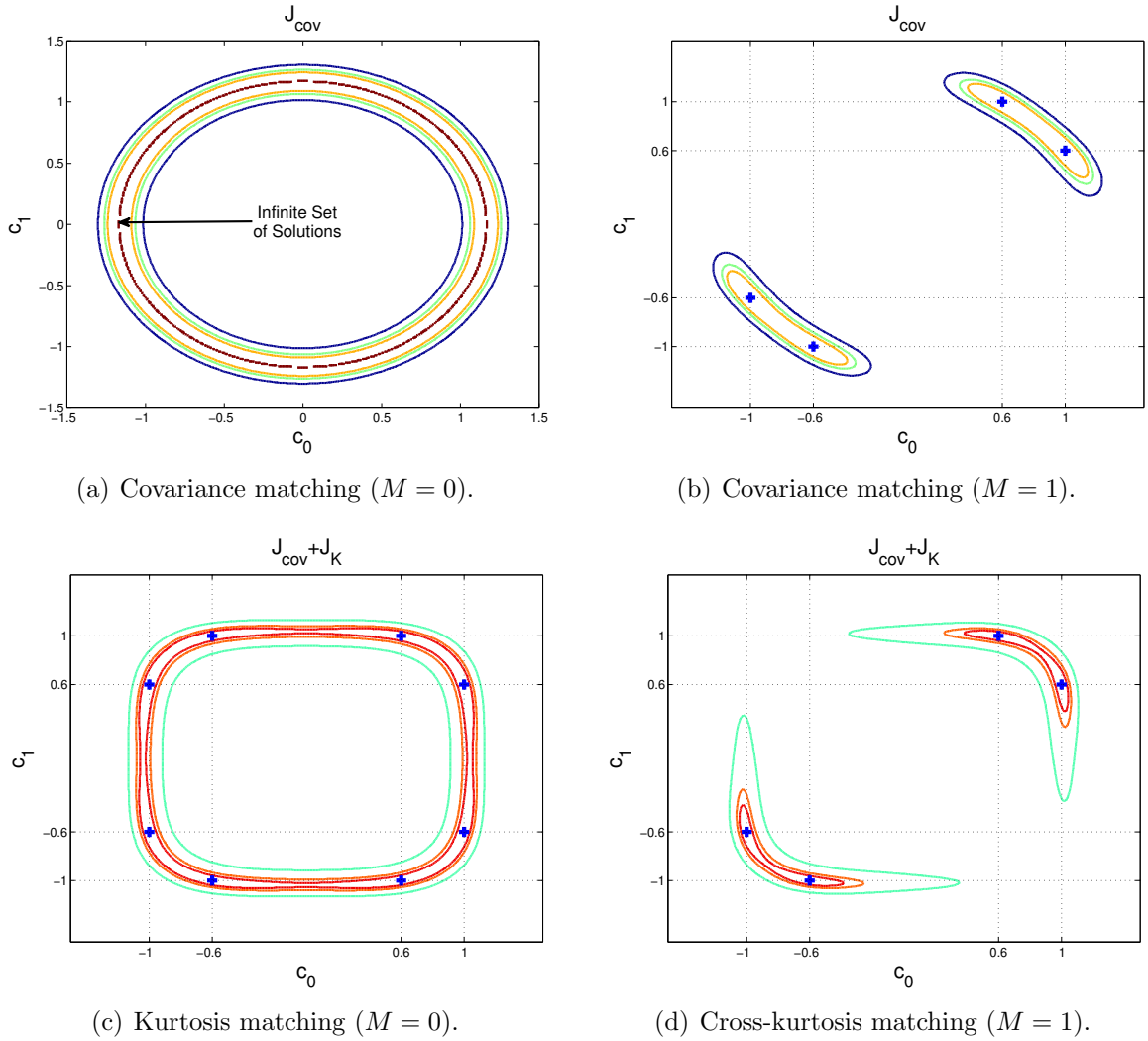


Figure 5.11: Scenario 1 - Contours for covariance and cross-kurtosis matching - Solutions for IIR $C(z)$.

the desired ones, as verified at the FIR $C(z)$ case. However, in this IIR $C(z)$ case, since a constrained model for $C(z)$ is adopted, the solutions found includes all possible permutations of the $P(z)$ coefficients, as indicated in Fig. 5.11(c). It is important to emphasize that, if the IIR $C(z)$ were not constrained, other solutions could also appear. By increasing M to unity, we achieve the necessary conditions for a valid solution and the solutions are $C(z) = \pm P(z^{-1})z^{-k}/P(z)$ and $C(z) = \pm 1z^{-k}$, as the covariance matching.

5.4.2 Scenario 2 - Colored Gaussian Source

When the source is a colored Gaussian, the HOS information becomes useless for equalization. For that reason, this distribution type form a special class of source. In the following, we present the analysis of the combined channel+equalizer system for the KL divergence (given by Eq. (5.11)), the covariance matching and cross-kurtosis matching for this scenario.

In the case the combined channel+equalizer system $C(z)$ has finite impulse response, we performed the grid search of the possible solutions for $C(z)$, by varying c_0 and c_1 from -1.5 to 1.5 . With respect to the KL divergence, the obtained solutions for $M = 0$ and $M = 1$ are as displayed in Fig. 5.12.

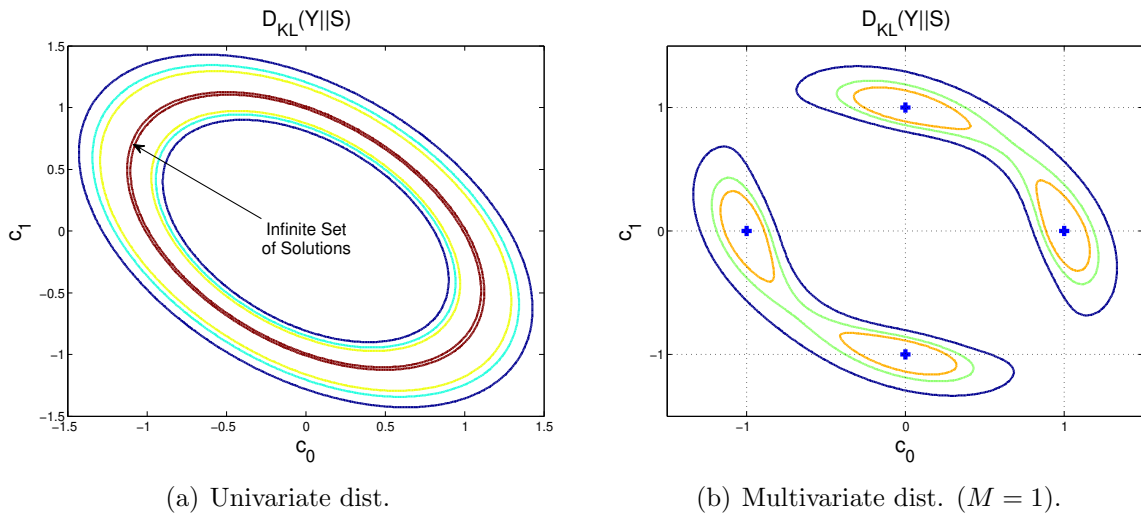


Figure 5.12: Scenario 2 - Solutions for FIR $C(z)$ - BGR theorem extensions.

Tab. 5.5 indicates that, for $M = 0$, the set of solutions for $C(z)$ is infinite. Indeed, the amount of statistical information in this case is insufficient for equalization and all the solutions that lie on the ellipse shown in Fig. 5.12(a) are possible. For $M = 1$, the multivariate distribution aggregates the temporal structure of the signal and, as shown in Fig. 5.12(b), the possible solutions are the ones associated with the ZF condition, i.e., $C(z) = \pm 1z^{-k}$, for $k \in \{0, 1\}$.

For the covariance and the cross-kurtosis matching, we have an interesting relation. When $M = 0$, the kurtosis is zero (see Fig. 5.7) and the measure given by Eq. (5.39) reduces to Eq. (5.37). In fact, as shown by Figs. 5.13(a) and 5.13(c), the surface contours are identical.

By increasing M to unity, the solutions for $C(z)$ becomes the ones that are in compliance with the ZF condition, for both covariance and cross-kurtosis matching. Actually, the number of equations achieved in the covariance matching is already sufficient to obtain valid solutions for \mathbf{c} and, hence, the cross-kurtosis matching, in this case, is redundant in terms of statistical information. It is also worth mentioning that, although the measures of the covariance matching and the KL divergence for Gaussian distributions assume different forms, they are equivalent in statistical terms. Indeed, note that Figs. 5.12(a) and 5.12(b) are very similar to 5.13(a) and 5.13(b), respectively.

For the IIR $C(z)$ case, the situation is analogous to the FIR $C(z)$ model. The surface contours of the KL divergence for $M = 0$ and $M = 1$ displayed at Fig. 5.14 reveal that an infinite set of solutions can be achieved when the number of delays considered

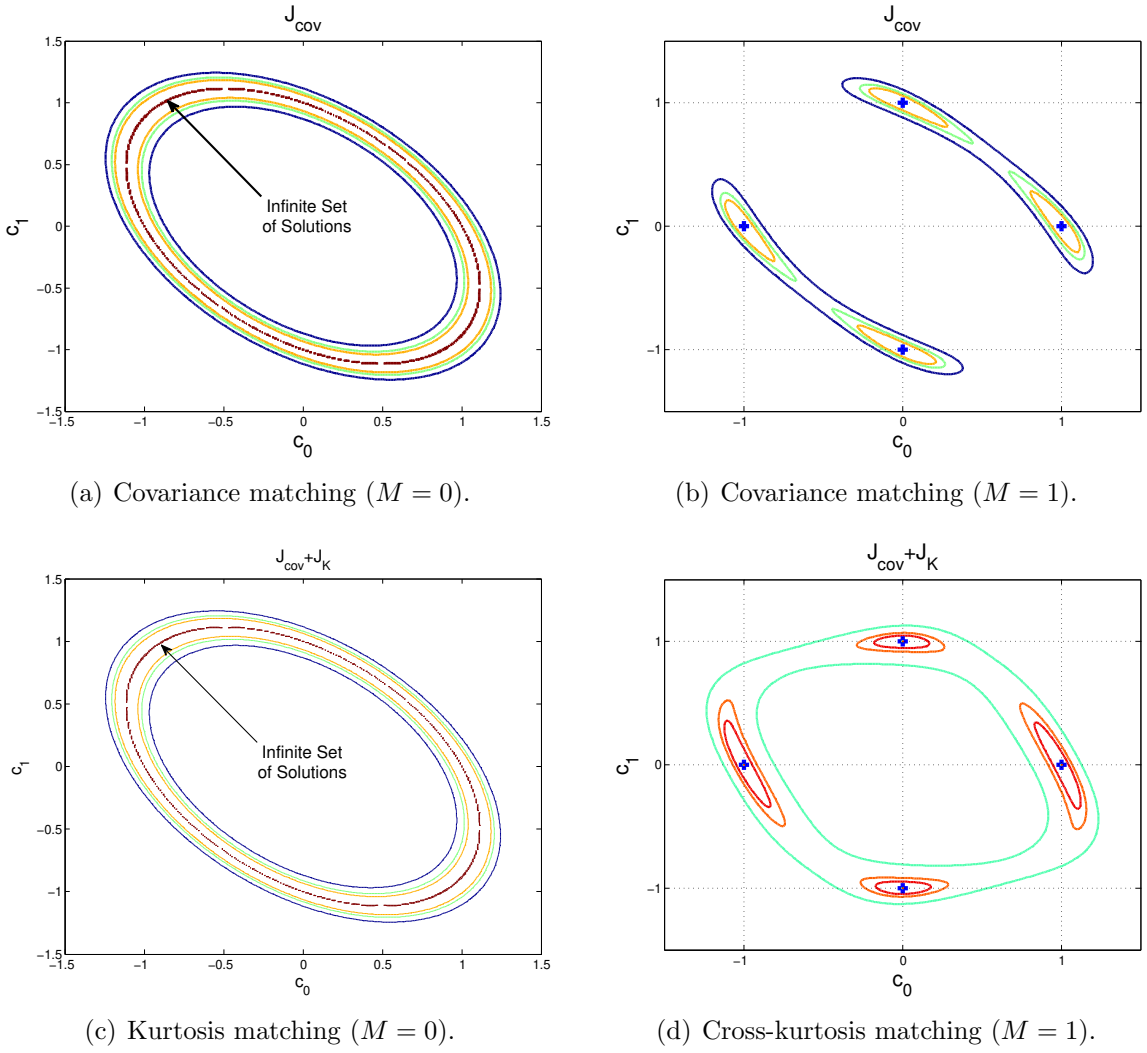


Figure 5.13: Scenario 2 - Contours for covariance and cross-kurtosis matching - Solutions for FIR $C(z)$.

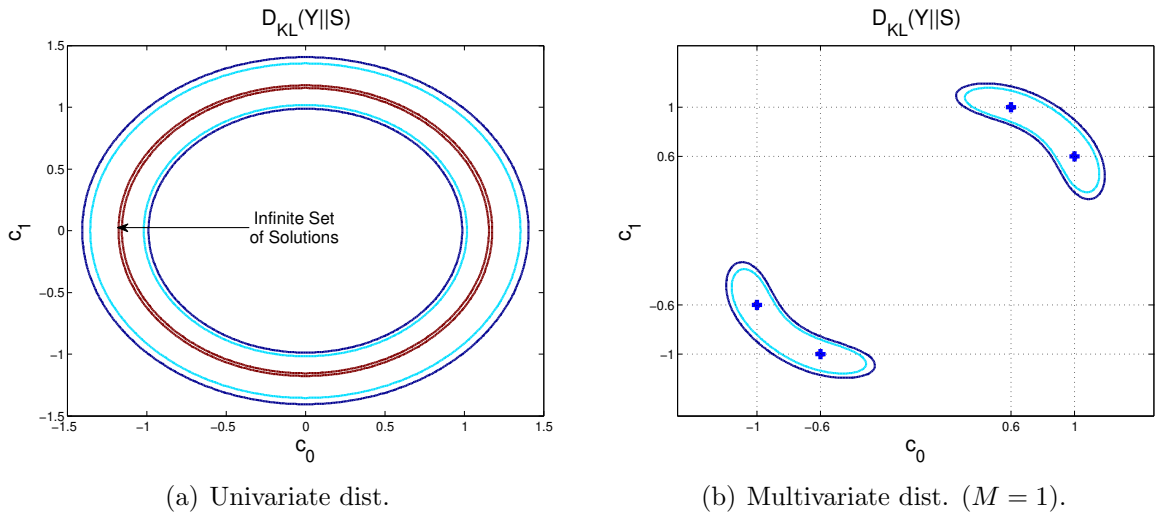


Figure 5.14: Scenario 2 - Solutions for IIR $C(z)$ - BGR theorem extensions.

is insufficient ($M = 0$), but, when $M \geq L_c$, the solutions that can be achieved are $C(z) = \pm P(z^{-1})z^{-k}/P(z)$ ($C(z) = 0.6 + 1z^{-1}/P(z)$ and $C(z) = -0.6 - 1z^{-1}/P(z)$) and the ZF condition ($C(z) = 1 + 0.6z^{-1}/P(z)$ and $C(z) = -1 - 0.6z^{-1}/P(z)$), as indicated in Tab. 5.5 and Fig. 5.14(b).

For the covariance matching, Figs. 5.15(a) and 5.15(b), the situation is identical to the KL divergence of Gaussian distributions, as occurred in the FIR $C(z)$ case.

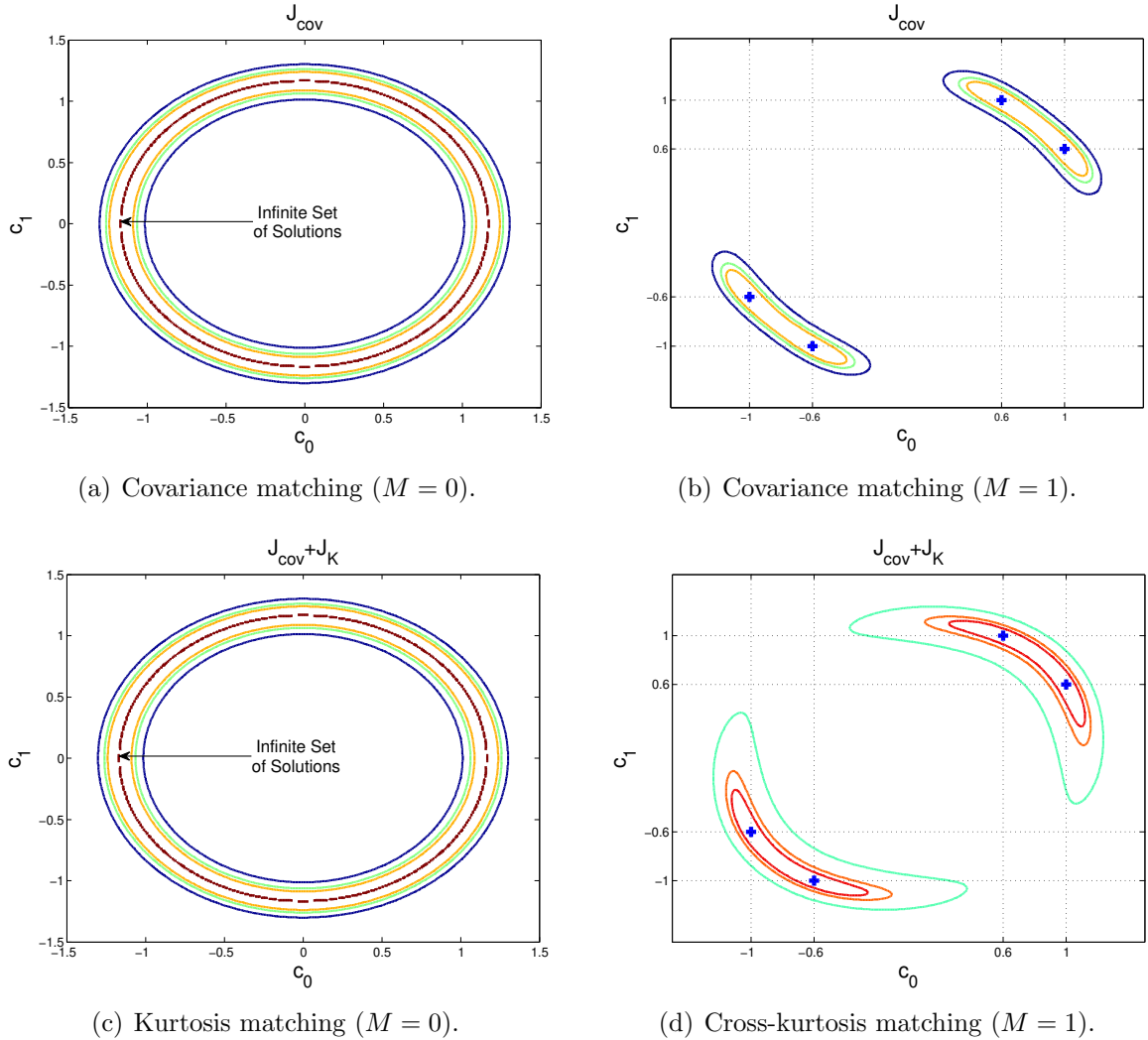


Figure 5.15: Scenario 2 - Contours for covariance and cross-kurtosis matching - Solutions for IIR $C(z)$.

Regarding the cross-kurtosis matching, the case in which $M = 0$ reduces to the covariance matching for Gaussian sources and Fig. 5.15(c) is identical to Fig. 5.15(a). For $M = 1$, the additional information used by the cross-kurtosis is, in a certain sense, redundant, since only the covariance information is sufficient for this case. Thus, the solutions for $C(z)$ shown in Fig. 5.15(d) are the same of that of Fig. 5.15(b), although the contours shape are different.

5.5 Conclusions

In light of the important theorems of Benveniste, Goursat and Rouget and Shalvi and Weinstein for blind channel equalization, we performed in this chapter a theoretical analysis of their extension towards temporally structured sources. The analysis encompassed univariate and multivariate distributions in the context of the BGR theorem and, regarding the SW theorem, the covariance function and the cross-kurtosis function for different time delays.

Due to the inherent mathematical complexity involving the addressed topics, we have not proposed new theorems for what can be called colored blind channel equalization. However, whenever possible, we invoked theoretical results from a deep prospection in the literature, like the theorems of Marcinkiewicz, Pólya and Cramér, which were crucial for the conducted analysis.

The analysis results showed that, differently from the SW theorem, the second- and the fourth-order statistics are not sufficient to ensure the zero forcing condition for colored blind channel equalization. However, more than the BGR theorem, it is required the complete knowledge of the multivariate (non-Gaussian) distribution of the source to guarantee the perfect equalization.

In addition, by imposing certain conditions on the combined channel+equalizer system, we also showed that the cross-kurtosis and even the second-order statistics (and Gaussian sources) considering different time delays can be sufficient to achieve the perfect equalization. However, additional care is necessary in order to avoid ambiguous solutions for the problem.

Similarly to the BGR and SW theorems, the analysis of the extension of these two theorems to colored blind equalization can contribute to the development of new methods and criteria. Furthermore, in view of the large computational resources available nowadays, even the estimation of multivariate densities can be performed in a considerably fast and reliable fashion. Thus, in the next chapter, we follow this idea and propose novel criteria and methods to be analyzed in real tasks of the colored blind channel equalization problem.

Chapter 6

Methods for Blind Channel Equalization in the Context of a Temporally Structured Source

Since the classical criteria for blind equalization, in general, implicitly assume statistical independence among samples, they tend to fail in scenarios where the source is temporally structured. Indeed, in these cases, it becomes necessary some kind of modification in the adopted methodology or, when possible, to perform a pre-processing step before transmission to mitigate the effects of dependence [LeBlanc et al., 1994; Axford et al., 1998; Neves et al., 2009]. Alternatively, based on the analysis of the previous chapter, it is possible to exploit the temporal structure of the source and use it to adapt the filter coefficients. This approach is particularly interesting because it allows the direct use of the temporal structure. In that sense, the employment of measures/entities capable of encompassing the statistical dependence present in the signals of interest is of great significance for solving the aforementioned problems.

Following this line of reasoning, in this chapter, we focus on the methods that can be used for solving the colored blind channel equalization problem. In fact, a initial step in that direction was made by Santamaría et al. [2006], where an entity based on the ITL framework – named correntropy – was used to extract the temporal dependence from data, as will be described in the following.

6.1 Background on Colored Blind Channel Equalization

In the problem of colored blind channel equalization, the temporal structure of the source is of crucial importance for performing the desired task. This temporal structure might be the result of inherent systems involved in the signal general process. However, for

its study, it is important to define a generative model. A reasonable hypothesis concerning this topic is that of assuming the source as the result of a filtering process over an *i.i.d.* signal (as assumed in Chapter 5). In this case, in the context of communications, a colored communication system can be outlined according to the block diagram illustrated in Fig. 6.1 [Santamaría et al., 2006], where u_n is an *i.i.d.* signal, s_n is the resulting non-*i.i.d.*

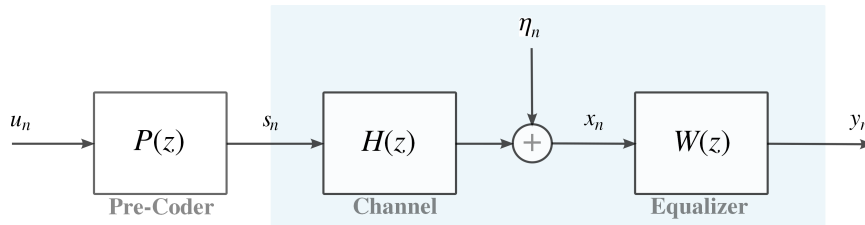


Figure 6.1: Block diagram of a communication system with non-*i.i.d.* source.

(or colored) source and $P(z)$ is the impulse response of the pre-coder system, responsible for introducing the temporal structure in the source; the other systems, $H(z)$ and $W(z)$, correspond, respectively, to the channel and the equalizer. Note that there could exist noise interference, as indicated by the signal η_n . In digital communications, it is usually assumed that the pre-coder $P(z)$ and the distribution of u_n are known.

In this scope, the metric known as correntropy [Santamaría et al., 2006] is the state-of-the-art approach within the ITL framework to perform colored channel equalization. In simple terms, correntropy is a bivariate function that brings together two important features: (i) it is capable of extracting information about the signal temporal structure and (ii) it makes effective use of higher-order statistics (HOS) by means of ITL kernel estimators [Santamaría et al., 2006; Fantinato et al., 2014]. The mathematical definition of correntropy can be found in Chapter 2. However, for convenience, we replicate its estimated version here:

$$\hat{v}_X(m) = \frac{1}{N_x} \sum_{i=1}^{N_x} G_{\sigma^2}(x_{n-i} - x_{n-m-i}), \quad (6.1)$$

where $G_{\sigma^2}(\cdot)$ is a univariate Gaussian kernel with kernel size σ and N_x is the window length (i.e., the number of pairs of entries x_{n-i} , x_{n-m-i}).

A simplified view of this similarity measure solely based on second-order statistics and able to consider time-correlation was proposed by our research group in [Fantinato et al., 2013]. Basically, the statistical dependence is extracted, in this case, through the use of the classical auto-correlation function – i.e., $r_X(m) = E[x_n x_{n-m}]$ – in a manner similar to the SOBI algorithm for BSS [Belouchrani et al., 1997].

Although correntropy, as an ITL entity, is potentially capable of providing, in comparison with the canonical second-order correlation, a richer characterization of temporal dependence, the extent of its effective relevance is a subject that deserves further inves-

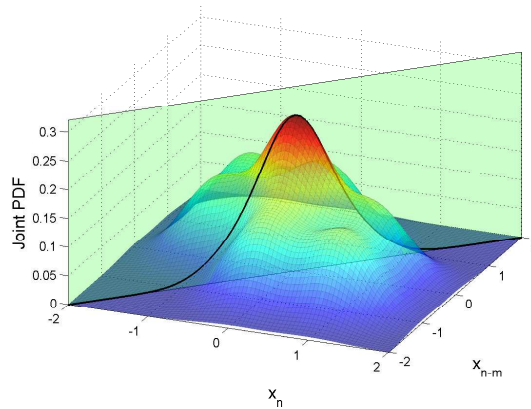


Figure 6.2: Integration of the joint PDF over the plane.

tigation. Indeed, as suggested in Chapter 5, there can be alternative strategies that can potentially extract more information from dependent sources.

6.1.1 Motivation for Further Investigation

Correntropy presents a number of interesting properties [Santamaría et al., 2006; Principe, 2010], however, its capability of extracting the temporal structure information may suffer from a certain type of limitation, as indicated by the three perspectives of correntropy presented in the following.

One possible interpretation of correntropy considers it as a similarity metric based on the joint distribution of the pair X_n and X_{n-m} [Principe, 2010]. However, not all statistical moments from this joint distribution are considered, which poses two main limitations: first, the considered statistical moments depend on the chosen kernel – in the case of a Gaussian kernel, all the even-order moments are considered –; second, the measure is sensitive to the sum of second and higher-order moments, which are weighted by terms inversely proportional to the kernel size σ [Principe, 2010]. In this sense, σ should be carefully determined so that the suitable statistical moments be favored with respect to less significant ones according to the problem at hand. For example, for values of $\sigma \geq 1$, correntropy tends to privilege the second-order moment (i.e., the classical correlation) [Principe, 2010; Fantinato et al., 2013, 2014].

The second aforementioned perspective of correntropy concerns the specific case in which $\sigma \rightarrow 0$, a situation where the higher-order moments become dominant. In such case, correntropy can be seen as the integral of the joint distribution over the plane in which $x_n = x_{n-m}$, as illustrated by Fig. 6.2. In practice, the adoption of significantly low values for σ is rare, but this shows that correntropy is subject to a “certain degree of partiality” regarding the statistical information provided by the joint distribution [Fantinato et al., 2014].

In addition, if it is considered that a pre-coder $P(z)$ was responsible for introducing the

time structure of the source, measuring only its correntropy is not enough for determining $P(z)$. In other words, correntropy can present representation ambiguity for $P(z)$, as illustrated in the following example.

Example

Assume that u_n is an *i.i.d.* binary $\{+1, -1\}$ sequence and consider the pre-coder $P(z) = 1 + 0.5z^{-1}$. The permutations of sign and values of the coefficients of the pre-coder and the resulting correntropy values for s_n , for m from 0 to 3, are as shown in Tab. 6.1. As can be noted, all permutations of the type $\hat{P}(z) = \pm P(z)z^{-k}$ or $\hat{P}(z) = \pm P(z^{-1})z^{-k}$, being k an arbitrary time delay, yields the same correntropy values (this situation is analogous to the covariance matching case seen in Chapter 5).

Table 6.1: Permutations of $P(z)$ and associated correntropy values for m from 0 to 3.

	Permutations of $P(z)$	$v_S(m)$
1	$\hat{P}(z) = 1 + 0.5z^{-1}$	
2	$\hat{P}(z) = -1 - 0.5z^{-1}$	
3	$\hat{P}(z) = 0.5 + 1z^{-1}$	
4	$\hat{P}(z) = -0.5 - 1z^{-1}$	
5	$\hat{P}(z) = 1 - 0.5z^{-1}$	
6	$\hat{P}(z) = -1 + 0.5z^{-1}$	
7	$\hat{P}(z) = 0.5 - 1z^{-1}$	
8	$\hat{P}(z) = -0.5 + 1z^{-1}$	

These perspectives, along with the analysis carried out in the previous chapter, form sufficient evidences that motivate us to proceed with the study on colored blind channel equalization beyond the use of the correntropy. In that sense, based on the extensions of the BGR and SW theorems, we will propose the use of alternative criteria, as described in next section.

6.2 Criteria for Colored Channel Equalization

Besides correntropy, we are going to make use of three more statistical entities that basically differ by the statistical moments they consider, which are: the correlation function (SOS), the cross-kurtosis function (second- and fourth-order statistics) and multivariate distributions (which encompass all statistical moments). Together, they will form fundamental ingredients to the proposition of the criteria to be studied.

Based on Chapter 5, we present in the following the criteria to be considered in the analysis, followed by some of their aspects related to estimation and optimization.

6.2.1 The Cost Functions

We consider five cost functions that are based on the matching of: correlation, cross-kurtosis, correntropies and multivariate densities. In the last case, two costs can be proposed, depending on the nature of the analyzed RVs – i.e., if they are discretely or continuously distributed.

Correlation Retrieval

From the simpler to the most complex, we start with the correlation-based cost function introduced in [Fantinato et al., 2013], which uses exclusively SOS. The cost named *Correlation Retrieval* (CR) aims at the matching of the correlation profile for $M + 1$ distinct delays:

$$J_{CR}(\mathbf{w}) = \sum_{m=0}^M |r_Y(m) - r_S(m)|^q, \quad (6.2)$$

where $r_S(m) = E[s_n s_{n-m}^*]$ and $r_Y(m) = E[y_n y_{n-m}^*]$ are the auto-correlation functions for delay m associated with the source s_n and the output signal y_n , respectively; M is the maximum arbitrary delay and q is a non-null positive value (usually assumed to be equal to 2). It is important to emphasize that we are assuming the signals to be stationary and, thus, the statistical properties are invariant to signal time shifts.

The objective is to minimize the CR cost, so that when $J_{CR} = 0$ the correlation profile of y_n is matched with that of the source s_n .

Estimation

The estimation of the CR cost is completely related to the estimation of the correlation function. However, since the pre-coder $P(z)$ and the distribution of u_n are assumed to be known in communications scenarios, the correlation profile of the source s_n can be analytically computed, i.e., its correlation values can be exactly obtained without the

need of estimation tools. Indeed, s_{n-m} can be written as

$$s_{n-m} = \begin{bmatrix} p_0^* & p_1^* & \cdots & p_{L_p}^* \end{bmatrix} \begin{bmatrix} u_{n-m} \\ u_{n-m-1} \\ \vdots \\ u_{n-m-L_p} \end{bmatrix} = \mathbf{p}^H \mathbf{u}_{n-m}, \quad (6.3)$$

so that

$$\begin{aligned} r_S(m) &= E[s_n s_{n-m}^*] = E[\mathbf{p}^H \mathbf{u}_n \mathbf{u}_{n-m}^H \mathbf{p}] \\ &= \mathbf{p}^H E[\mathbf{u}_n \mathbf{u}_{n-m}^H] \mathbf{p}, \end{aligned} \quad (6.4)$$

where the matrix $E[\mathbf{u}_n \mathbf{u}_{n-m}^H]$ will be, for $m = 0$, an identity matrix scaled by the variance of u_n , i.e., $E[\mathbf{u}_n \mathbf{u}_{n-m}^H] = \sigma_U^2 \mathbf{I}$ (since u_n is *i.i.d.*); for $m \neq 0$, $E[\mathbf{u}_n \mathbf{u}_{n-m}^H]$ will have its m -th diagonal equal to σ_U^2 and the other elements null.

On the other hand, the auto-correlation function for y_n may be difficult to be analytically computed, since the channel $H(z)$ and the noise η_n are considered unknown. However, it can be estimated from samples through the following relation:

$$\hat{r}_Y(m) = \frac{1}{N_y} \sum_{i=0}^{N_y-1} y_{n-i} y_{n-m-i}^*, \quad (6.5)$$

where N_y is the number of pairs $\{y_n, y_{n-m}\}$ used in the estimation.

Alternatively, the correlation function $r_Y(m)$ can be estimated in function of the correlation matrix of x_n . Similarly to Eq. (6.4), we are able to write:

$$\begin{aligned} r_Y(m) &= E[y_n y_{n-m}^*] = E[\mathbf{w}^H \mathbf{x}_n \mathbf{x}_{n-m}^H \mathbf{w}] \\ &= \mathbf{w}^H E[\mathbf{x}_n \mathbf{x}_{n-m}^H] \mathbf{w} = \mathbf{w}^H R_{X_n X_{n-m}} \mathbf{w}. \end{aligned} \quad (6.6)$$

Hence, once $\hat{R}_{X_n X_{n-m}}$ is estimated, $\hat{r}_Y(m)$ is a direct function of the filter weights \mathbf{w} . This approach tends to be computationally more efficient when the correlation profile of y_n must be evaluated several times – e.g., in optimization metaheuristics.

Finally, the estimated CR cost becomes

$$\hat{J}_{CR}(\mathbf{w}) = \sum_{m=0}^M |\hat{r}_Y(m) - r_S(m)|^q, \quad (6.7)$$

being $r_S(m)$ obtained according to Eq. (6.4) and $\hat{r}_Y(m)$ according to Eq. (6.5) or Eq. (6.6).

Matching of the Cross-Kurtosis

Based on the SW theorem extension (Section 5.2.3, in Chapter 5), it might also be interesting to use the information present on the fourth-order statistics via the cross-

kurtosis, whose definition is repeated here for convenience:

$$k_S(m) = E [|s_n|^2 |s_{n-m}|^2] - 2E^2 [s_n s_{n-m}^*] - |E [s_n s_{n-m}]|^2. \quad (6.8)$$

Considered as a nonlinear correlation function in the ICA theory, the cross-kurtosis might be particularly useful in nonlinear scenarios [Hyvärinen et al., 2001]. However, in this work, we are focused on the linear equalization problem.

Similarly to the matching of correlations, the matching of the cross-kurtosis can be outlined by means of the divergence measure:

$$J_{kurt}(\mathbf{w}) = \sum_{m=0}^M |k_Y(m) - k_S(m)|^q, \quad (6.9)$$

where $k_S(\cdot)$ and $k_Y(\cdot)$ are the cross-kurtoses associated with the source s_n and with the output signal y_n , respectively, and q is a non-null positive value. However, in accordance with the SW theorem extension, the SOS must also be encompassed, which results in

$$J_{MCK}(\mathbf{w}) = \sum_{m=0}^M |k_Y(m) - k_S(m)|^q + |r_Y(m) - r_S(m)|^q. \quad (6.10)$$

We refer to this cost simply by MCK (Matching of Cross-Kurtosis).

Estimation

In the context of communication channels, we assume that the cross-kurtosis of the source is known at the receiver. It can be analytically computed according to the following relations. For the first term of Eq. (6.8), we have

$$E [u_{n-k-i} u_{n-l-i}^* u_{n-m-j}^* u_{n-o-j}] = \begin{cases} E [|u_n|^4], & k+i = l+i = m+j = o+j \\ E^2 [|u_n|^2], & k+i = l+i \neq m+j = o+j, k+i = m+j \neq l+i = o+j \\ |E [u_n^2]|^2, & k+i = o+j \neq l+i = m+j \\ 0, & \text{otherwise.} \end{cases} \quad (6.11)$$

For the second term, it is basically the correlation function given by Eq. (6.4) to the power of 2 and scaled by -2 ; and, at last, the third term can be computed as

$$E [s_n s_{n-m}] = \mathbf{p}^H E [\mathbf{u}_n \mathbf{u}_{n-m}^T] \mathbf{p}^*, \quad (6.12)$$

in which the modulus of the result must be taken to the power of 2 and scaled by -1 . If the signals are treated in the real domain, Eqs. (6.4) and (6.12) are equivalent.

For the cross-kurtosis of the output signal y_n , we consider the sample mean estimation:

$$\hat{k}_Y(m) = \frac{1}{N_y} \sum_{i=0}^{N_y-1} |y_{n-i}|^2 |y_{n-m-i}|^2 - 2\hat{r}_Y^2(m) - \left| \frac{1}{N_y} \sum_{i=0}^{N_y-1} y_{n-i} y_{n-m-i} \right|^2. \quad (6.13)$$

The resulting estimated MCK cost becomes

$$\hat{J}_{MCK}(\mathbf{w}) = \sum_{m=0}^M \left| \hat{k}_Y(m) - k_S(m) \right|^q + \left| \hat{r}_Y(m) - r_S(m) \right|^q, \quad (6.14)$$

being $k_S(m)$ obtained by relations (6.11), (6.4) and (6.12); $\hat{k}_Y(m)$ obtained by Eq. (6.13); $r_S(m)$ by Eq. (6.4) and, finally, $\hat{r}_Y(m)$ by Eq. (6.5) (or Eq. (6.6)).

Matching of Correntropies

The pioneering work of Santamaría et al. [2006] introduced the idea of the matching between the correntropies of the source and of the equalized signal, since this ITL similarity measure could retain great portion of the statistical information. Mathematically, the correntropy-based criterion is the minimization of the following cost:

$$J_{cor}(\mathbf{w}) = \sum_{m=1}^M (v_S(m) - v_Y(m))^2. \quad (6.15)$$

where $v_S(m)$ and $v_Y(m)$ are the correntropy of the source s_n and of the equalizer output y_n , respectively.

Estimation

When the source is discrete, the correntropy can be analytically computed from a PMF associated with a filtered signal in the following manner. Consider the filter $P'(z) = P(z)(1 - 1z^{-m})$ and the filtered signal:

$$s'_n = \mathbf{p}'^H \mathbf{u}_n. \quad (6.16)$$

If the PMF associated with s'_n is

$$p_{S'}(v) = \sum_{i \in \mathcal{A}_{S'}} P(v = a_{S'}(i)) \delta(v - a_{S'}(i)), \quad (6.17)$$

where $\mathcal{A}_{S'}$ is the alphabet of all possible occurrences of S' , $a_{S'}(i)$ is the i -th symbol $\in \mathcal{A}_{S'}$ and $P(v = a_{S'}(i))$ is the probability of $v = a_{S'}(i)$; then, the correntropy can be calculated

as

$$v_S(m) = \sum_{i \in \mathcal{A}_{S'}} p_{S'}(a_{S'}(i)) G_{\sigma^2}(a_{S'}(i)). \quad (6.18)$$

When the source s_n is continuous, it might be a hard task to analytically compute the correntropy of S : it demands the computation of the continuous distribution of S' – the PDF $f_{S'}(v)$ – followed by the evaluation of the integral

$$v_S(m) = \int f_{S'}(v) G_{\sigma^2}(v) dv, \quad (6.19)$$

which is not always straightforward. When u_n is Gaussian distributed and the pre-coder $P(z)$ is linear, this integral can be easily computed through the property given by Eq.(2.12) – this property is valid when the kernel is a Gaussian-like function. For other cases, the estimation of the correntropy from a set of representative samples – i.e., via Eq. (6.1) – is usually preferred. Thus, the estimated values $\hat{v}_S(m)$, for $m = 1, \dots, M$, are stored and used in the receiver (we assume that the PDF of the source remains fixed, i.e., the source is assumed to be stationary).

The correntropy of the output signal y_n , $v_Y(m)$, is estimated via Eq. (6.1). Hence, the cost of the matching of correntropies can be estimated as

$$\hat{J}_{cor}(\mathbf{w}) = \sum_{m=1}^M \left(v_S(m) - \frac{1}{N_y} \sum_{i=0}^{N_y-1} G_{\sigma^2}(y_{n-i} - y_{n-m-i}) \right)^2, \quad (6.20)$$

where $v_S(m)$ can be analytically computed (via Eq. (6.18) or (6.19), depending on the nature of the source).

Matching of Multivariate Densities

So far, we have seen that the correlation, the cross-kurtosis and the correntropy measures are able to evaluate, from different perspectives, the similarity between a pair of RVs (with different time lags m). However, a broader range for this similarity measure can be attained if multivariate distributions are considered, as suggested in the analysis performed in Chapter 5. Indeed, the multivariate distributions are able to jointly evaluate RVs encompassing M different time delays.

Following this line of reasoning, it is desirable to measure how matched (or how similar) are two multivariate densities. Based on the works of Principe [2010] and Lázaro et al. [2005], a possibility for quantifying the similarity between two distributions can be the Quadratic Divergence (QD) measure. Assuming multivariate distributions, the resulting

multivariate QD, or simply MQD, can be expressed as

$$\begin{aligned} J_{MQD}(\mathbf{w}) &= \int_D (f_{\underline{Y}}(\mathbf{v}) - f_{\underline{S}}(\mathbf{v}))^2 d\mathbf{v} \\ &= \int_D f_{\underline{Y}}^2(\mathbf{v}) d\mathbf{v} + \int_D f_{\underline{S}}^2(\mathbf{v}) d\mathbf{v} - 2 \int_D f_{\underline{Y}}(\mathbf{v}) f_{\underline{S}}(\mathbf{v}) d\mathbf{v} \end{aligned} \quad (6.21)$$

where $\underline{Y} = \{Y_n, Y_{n-1}, \dots, Y_{n-M}\}$, $\underline{S} = \{S_n, S_{n-1}, \dots, S_{n-M}\}$, M is the number of distinct considered delays, $D \subseteq \mathbb{R}^{M+1}$. Note that, unlike correntropy, the MQD considers two stochastic process \underline{Y} and \underline{S} , whose number of delays M can be arbitrary [Fantinato et al., 2014]. It is important to remark that the joint distributions must be strictly stationary, i.e., a time shift does not provoke modifications on the joint distribution (similarly to correntropy). Although the concept of the quadratic divergence between distributions has been previously proposed, we highlight that taking into account multivariate distributions is an innovative contribution of our research.

Apparently, the possibility of using all statistical information of the multivariate distributions in the similarity measure given by Eq. (6.21) may seem computationally costly. However, the estimation of the joint PDFs can be performed with relative simplicity through the framework defined by kernel density estimation, which will be discussed in the following.

Estimation

The canonical strategy in ITL for density estimation is the use of the Parzen window method [Parzen, 1962], a kernel-based approach, which is aimed at the estimation of continuous densities (or PDFs). Although other methods like those based on order statistics [Pham, 2000; Even, 2003], on the k -nearest-neighborhood [Kraskov et al., 2004] and on histograms [Steuer et al., 2002] could also be employed, the Parzen window method is preferred here due to its simple extensibility to the multivariate case and, along with the use of Gaussian kernels, its leading to important simplifying properties, as will be shown.

Regardless of the source type, since it is assumed that the noise η_n is continuously distributed (but unknown), it is expected that the distribution associated with y_n , $f_{\underline{Y}}(\mathbf{v})$, be continuous as well and the Parzen window method can be applied with no further issues. In this case, the joint PDF of $f_{\underline{Y}}(\mathbf{v})$ can be estimated as:

$$\hat{f}_{\underline{Y}}(\mathbf{v}) = \frac{1}{N_y} \sum_{i=0}^{N_y-1} G_{\Sigma}(\mathbf{v} - \mathbf{y}_{n-i}), \quad (6.22)$$

where $G_{\Sigma}(\cdot)$ is the multivariate symmetric Gaussian kernel given by

$$G_{\Sigma}(\mathbf{v} - \mathbf{y}_{n-i}) = \frac{1}{\sqrt{\det(2\pi\Sigma)}} \exp \left[\frac{-1}{2} (\mathbf{v} - \mathbf{y}_{n-i})^T \Sigma^{-1} (\mathbf{v} - \mathbf{y}_{n-i}) \right], \quad (6.23)$$

with $\mathbf{y}_{n-i} = [y_{n-i} \ y_{n-i-1} \ \dots \ y_{n-i-M}]^T$, $\Sigma = \sigma^2 \mathbf{I}$, where \mathbf{I} is the identity matrix of dimension $M+1$.

Regarding the source, it may occur that its distribution be of a discrete nature. In fact, in general communication systems, the signal to be transmitted belongs to a pre-defined finite set of symbols, as in the BPSK and QAM schemes. When this is the case, for time-dependent sources, all the information about temporal dependence is contained in the joint PMF. Consider a generic PMF for \underline{S} described as:

$$p_{\underline{S}}(\mathbf{v}) = \sum_{i \in \mathcal{A}_{\underline{S}}} P(\mathbf{v} = \mathbf{a}_{\underline{S}}(i)) \delta(\mathbf{v} - \mathbf{a}_{\underline{S}}(i)), \quad (6.24)$$

where $\mathcal{A}_{\underline{S}}$ is the alphabet of all possible occurrences of \underline{S} , $\mathbf{a}_{\underline{S}}(i)$ is the i -th symbol $\in \mathcal{A}_{\underline{S}}$ and $P(\mathbf{v} = \mathbf{a}_{\underline{S}}(i))$ is the probability of $\mathbf{v} = \mathbf{a}_{\underline{S}}(i)$. Then, the MQD cost becomes

$$\begin{aligned} J_{MQD-D}(\mathbf{w}) &= \int_D (f_{\underline{Y}}(\mathbf{v}) - p_{\underline{S}}(\mathbf{v}))^2 d\mathbf{v} \\ &= \int_D f_{\underline{Y}}^2(\mathbf{v}) d\mathbf{v} + \int_D p_{\underline{S}}^2(\mathbf{v}) d\mathbf{v} - 2 \int_D f_{\underline{Y}}(\mathbf{v}) p_{\underline{S}}(\mathbf{v}) d\mathbf{v}, \end{aligned} \quad (6.25)$$

where there emerges an important remark: the second term of the last equality depends solely on the probabilities of the sources, being independent of the parametric model underlying the set of observable variables \mathbf{y}_i , and can be neglected. Actually, the integration of this term may diverge, making the similarity measure lose its properties. By neglecting it, the measure will not be a distance anymore, however, since this term is constant (the PMF $p_{\underline{S}}(\mathbf{v})$ is assumed to be stationary), there is no impact on the optimization process.

Using (6.24) and (6.22) instead of $p_{\underline{S}}(\mathbf{v})$ and $f_{\underline{Y}}(\mathbf{v})$ in Eq. (6.25), respectively, the estimation for the matching between a PDF and a PMF becomes:

$$\begin{aligned} \hat{J}_{MQD-D}(\mathbf{w}) &= \frac{1}{N_y^2} \sum_{i=0}^{N_y-1} \sum_{j=0}^{N_y-1} G_{2\Sigma}(\mathbf{y}_{n-i} - \mathbf{y}_{n-j}) + \int_D p_{\underline{S}}^2(\mathbf{v}) d\mathbf{v} \\ &\quad - \frac{2}{N_y} \sum_{i \in \mathcal{A}_{\underline{S}}} \left[p_{\underline{S}}(\mathbf{a}_{\underline{S}}(i)) \left(\sum_{j=0}^{N_y-1} G_{\Sigma}(\mathbf{a}_{\underline{S}}(i) - \mathbf{y}_{n-j}) \right) \right] \end{aligned} \quad (6.26)$$

where the first term after the last equality was obtained through the following relation:

$$\int_D G_{\Sigma}(\mathbf{v} - \mathbf{y}_{n-i}) G_{\Sigma}(\mathbf{v} - \mathbf{y}_{n-j}) d\mathbf{v} = G_{2\Sigma}(\mathbf{y}_{n-i} - \mathbf{y}_{n-j}), \quad (6.27)$$

which is a property valid for Gaussian kernels. Other kernels can be employed, although the resultant integration may not be simple. Remark that the term relative to the square of $p_{\underline{S}}(\mathbf{v})$ is not considered. This measure is called MQD-D, since it aims at discrete distributions.

When the source is continuously distributed, the situation is similar to correntropy: the use of the analytical PDF may lead to difficult integral computations (unless it is Gaussian distributed). Thus, it is usually preferred to adopt the Parzen window method for $f_{\underline{S}}(\mathbf{v})$ in the same way as Eq. (6.22). In this case, the estimation of the MQD cost becomes:

$$\begin{aligned} \hat{J}_{MQD-C} = & \frac{1}{N_y^2} \sum_{i=0}^{N_y-1} \sum_{j=0}^{N_y-1} G_{2\Sigma}(\mathbf{y}_{n-i} - \mathbf{y}_{n-j}) + \frac{1}{N_s^2} \sum_{i=0}^{N_s-1} \sum_{j=0}^{N_s-1} G_{2\Sigma}(\mathbf{s}_{n-i} - \mathbf{s}_{n-j}) \\ & - \frac{2}{N_y N_s} \sum_{i=0}^{N_y-1} \sum_{j=0}^{N_s-1} G_{2\Sigma}(\mathbf{y}_{n-i} - \mathbf{s}_{n-j}), \end{aligned} \quad (6.28)$$

where $\mathbf{y}_{n-i} = [y_{n-i} \ y_{n-i-1} \ \dots \ y_{n-i-M}]^T$, $\mathbf{s}_{n-i} = [s_{n-i} \ s_{n-i-1} \ \dots \ s_{n-i-M}]^T$; N_y and N_s are the window length (or the number of vector samples) for \underline{Y} and \underline{S} , respectively. Since this approach is based on the assumption that both RVs \underline{Y} and \underline{S} are associated with continuous distributions, we refer to the cost given by Eq. (6.28) as MQD-C. Generally, one of the PDFs is considered as a fixed target PDF. Thus, if we assume that $f_{\underline{S}}(\mathbf{v})$ remains unchanged, the second term in Eq. (6.28) can be disregarded in optimization problems.

Notwithstanding, this approach requires the receiver to store (or generate) a representative set of samples of s_n , which can be an attractive option if the number of samples to be stored is relatively small; otherwise, besides the necessity of a large memory, we will face the increase of the computational burden. In view of this, a promising alternative is to store the source PDF by means of a weighted Gaussian combination (with the aid of a RBF structure¹ – see Section 1.1.2), which is able to drastically reduce the memory usage, but demands an offline pre-processing step, as described in the following.

First, from a representative set of samples s_n , the PDF $f_{\underline{S}}(\mathbf{v})$ can be estimated in specific points $\boldsymbol{\nu}_i$ – for example, in a regular grid or in a certain region of interest – according to the relation

$$\hat{f}_{\underline{S}}(\boldsymbol{\nu}_i) = \frac{1}{N_s} \sum_{j=0}^{N_s-1} G_{\Sigma}(\boldsymbol{\nu}_i - \mathbf{s}_{n-j}), \quad (6.29)$$

for each of the specific points $\boldsymbol{\nu}_i$. Next, an RBF-based method with multivariate Gaussian kernels can be employed to approximate $\hat{f}_{\underline{S}}(\boldsymbol{\nu}_i)$. Once the RBF is trained, the combination

¹It is important to remark that this idea is related with the Gaussian Mixture Model [Yu et al., 2012]

of the activation functions (i.e., Gaussian kernels) can be viewed as $\hat{f}_{\underline{S}}(\mathbf{v}_i)$ itself. At the end of the process, the estimated PDF of the source can be mathematically expressed as

$$\hat{f}_{\underline{S}}(\mathbf{v}) = \sum_{j=k}^{N_a} c_k G_{\Sigma}(\mathbf{v} - \boldsymbol{\mu}_k), \quad (6.30)$$

being $\boldsymbol{\mu}_k$ the mean vector, c_k the weights of each Gaussian kernel and N_a the number of activation functions. A customary RBF approach is to first obtain the mean vectors $\boldsymbol{\mu}_k$ and variance Σ in a unsupervised way (e.g., using the k -means method [Haykin, 1998]) and, then, solve a linear combination problem for the weights c_k . In that sense, a reduced number N_a of activation functions can be employed, being necessary to store only the means $\boldsymbol{\mu}_k$ and the weights c_k of each Gaussian (the variances can be assumed to be constant). Finally, the MQD-C cost becomes

$$\begin{aligned} \hat{J}_{MQD-C} = & \frac{1}{N_y^2} \sum_{i=0}^{N_y-1} \sum_{j=0}^{N_y-1} G_{2\Sigma}(\mathbf{y}_{n-i} - \mathbf{y}_{n-j}) + \frac{1}{N_a^2} \sum_{i=1}^{N_a} \sum_{j=1}^{N_a} G_{2\Sigma}(\boldsymbol{\mu}_i - \boldsymbol{\mu}_j) \\ & - \frac{2}{N_y N_a} \sum_{i=0}^{N_y-1} \sum_{k=1}^{N_a} c_k G_{2\Sigma}(\mathbf{y}_{n-i} - \boldsymbol{\mu}_k), \end{aligned} \quad (6.31)$$

which is simpler and computationally more efficient.

6.2.2 Gradient-Based Optimization

All considered costs are differentiable, allowing the adoption of the stochastic gradient method for optimization, as described in Section 3.1. In fact, this is the preferred option in the ITL field [Santamaría et al., 2006; Principe, 2010], given the simplicity of the resulting algorithms. In the following, we present the gradient of each considered cost.

Correlation Retrieval

The analytical gradient of Eq. (6.2), assuming $q = 2$, can be written as

$$\nabla_{\mathbf{w}} J_{CR} = 2 \sum_{m=0}^M (r_Y(m) - r_S(m)) E [y_n^* \mathbf{x}_{n-m} + y_{n-m}^* \mathbf{x}_n]. \quad (6.32)$$

However, the entities $r_Y(m)$ and $E[y_n^* \mathbf{x}_{n-m} + y_{n-m}^* \mathbf{x}_n]$ must be estimated in practical applications and, depending on the adopted method, there could result different algorithms.

In classical SOS-based algorithms (like the LMS algorithm), the stochastic gradient approach is usually adopted. In [Fantinato et al., 2013], a semi-batch (sliding window)

approach is assumed in order to obtain a more precise derivative estimation:

$$\nabla_{\mathbf{w}} \hat{J}_{CR} = 2 \sum_{m=0}^M (\hat{r}_Y(m) - r_S(m)) \left(\frac{1}{N_y} \sum_{i=0}^{N_y-1} y_{n-i}^* \mathbf{x}_{n-m-i} + y_{n-m-i}^* \mathbf{x}_{n-i} \right), \quad (6.33)$$

being N_y the number of pairs $\{y_n, y_{n-m}\}$. This same approach will be considered in this work.

Matching of the Cross-Kurtosis

The Cross-Kurtosis-based cost (Eq. (6.10)) has the gradient:

$$\begin{aligned} \nabla_{\mathbf{w}} J_{MCK} &= 2 \sum_{m=0}^M (k_Y(m) - k_S(m)) 2E [|y_n|^2 y_{n-m}^* \mathbf{x}_{n-m} + y_n^* \mathbf{x}_n |y_{n-m}|^2] \\ &\quad - 2E [y_n y_{n-m}^*] E [y_n^* \mathbf{x}_{n-m} + \mathbf{x}_n y_{n-m}^*] \\ &\quad - E [y_n y_{n-m}] E [y_n \mathbf{x}_{n-m} + \mathbf{x}_n y_{n-m}]. \end{aligned} \quad (6.34)$$

Similarly to the CR cost, the main issue is how to estimate the expectations. In the work of Shalvi and Weinstein [1990], a mixture of empirical average and stochastic approximation is considered. However, in this work, we will consider the semi-batch approach, which results in

$$\begin{aligned} \nabla_{\mathbf{w}} \hat{J}_{MCK} &= 2 \sum_{m=0}^M (\hat{k}_Y(m) - k_S(m)) \left(\frac{2}{N_y} \sum_{i=0}^{N_y} |y_{n-i}|^2 y_{n-m-i}^* \mathbf{x}_{n-m-i} + y_{n-i}^* \mathbf{x}_{n-i} |y_{n-m-i}|^2 \right) \\ &\quad - \left(\frac{2}{N_y} \sum_{i=0}^{N_y} y_{n-i} y_{n-m-i}^* \right) \left(\frac{1}{N_y} \sum_{i=0}^{N_y} y_{n-i}^* \mathbf{x}_{n-m-i} + \mathbf{x}_{n-i} y_{n-m-i}^* \right) \\ &\quad - \left(\frac{1}{N_y} \sum_{i=0}^{N_y} y_{n-i} y_{n-m-i} \right) \left(\frac{1}{N_y} \sum_{i=0}^{N_y} y_{n-i} \mathbf{x}_{n-m-i} + \mathbf{x}_{n-i} y_{n-m-i} \right). \end{aligned} \quad (6.35)$$

When $N_y = 1$, the resulting algorithm reduces to the standard stochastic-gradient approach.

Matching of Correntropies

The gradient of the correntropy-based cost given by Eq. (6.15) can be computed as

$$\nabla_{\mathbf{w}} \hat{J}_{cor} = \frac{-1}{\sigma^2} \sum_{m=1}^M (v_S(m) - \hat{v}_Y(m)) E [G_{\sigma^2}(y_n - y_{n-m})(y_n - y_{n-m})(\mathbf{x}_n - \mathbf{x}_{n-m})], \quad (6.36)$$

considering, again, Gaussian kernel functions.

As in the work of Santamaría et al. [2006], a semi-batch approach is considered for

estimating the expectation:

$$\nabla_{\mathbf{w}} \hat{J}_{cor} = \sum_{m=1}^M (v_S(m) - \hat{v}_Y(m)) \left(\frac{-1}{\sigma^2 N_y} \sum_{i=1}^{N_y-1} G_{\sigma^2} (y_{n-i} - y_{n-m-i}) \cdot (y_{n-i} - y_{n-m-i})(\mathbf{x}_{n-i} - \mathbf{x}_{n-m-i}) \right), \quad (6.37)$$

which will be the same approach adopted in this work.

Matching of Multivariate Distributions

The considered matching of multivariate distributions can present two costs, depending on the nature of source: the J_{MQD-D} (Eq. (6.25)) and J_{MQD-C} (Eq. (6.21)). Since the cost function involves the distribution of the signals, a general gradient is not straightforward. Hence, we derive the gradients of the estimated costs (Eqs. (6.26) and (6.28)).

For the estimated MQD-D cost, \hat{J}_{MQD-D} , the gradient is

$$\begin{aligned} \nabla_{\mathbf{w}} \hat{J}_{MQD-D} &= \frac{-1}{2N_y^2} \sum_{i=0}^{N_y-1} \sum_{j=0}^{N_y-1} G_{2\Sigma} (\mathbf{y}_{n-i} - \mathbf{y}_{n-j}) ((\mathbf{X}_{n-i} - \mathbf{X}_{n-j})^T \Sigma^{-1} (\mathbf{y}_{n-i} - \mathbf{y}_{n-j})) \\ &\quad + \frac{2}{N_y} \sum_{i \in \mathcal{A}_S} \left[p_S(\mathbf{a}_S(i)) \left(\sum_{j=0}^{N_y-1} G_{\Sigma} (\mathbf{a}_S(i) - \mathbf{y}_{n-j}) \mathbf{X}_{n-j}^T \Sigma^{-1} (\mathbf{a}_S(i) - \mathbf{y}_{n-i}) \right) \right], \end{aligned} \quad (6.38)$$

where

$$\mathbf{X}_{n-i} = [\mathbf{x}_{n-i} \ \mathbf{x}_{n-i-1} \ \cdots \ \mathbf{x}_{n-i-M}] = \begin{bmatrix} x_{n-i} & x_{n-i-1} & \cdots & x_{n-i-M} \\ x_{n-i-1} & x_{n-i-2} & \cdots & x_{n-i-M-1} \\ \vdots & \vdots & \vdots & \vdots \\ x_{n-i-L_w} & x_{n-i-1-L_w} & \cdots & x_{n-i-M-L_w} \end{bmatrix} \quad (6.39)$$

and $\mathbf{y}_{n-i} = \mathbf{X}_{n-i}^T \mathbf{w}$.

The gradient of the continuous counterpart can be written as

$$\begin{aligned} \nabla_{\mathbf{w}} \hat{J}_{MQD-C} &= \frac{-1}{2N_y^2} \sum_{i=0}^{N_y-1} \sum_{j=0}^{N_y-1} G_{2\Sigma} (\mathbf{y}_{n-i} - \mathbf{y}_{n-j}) (\mathbf{X}_{n-i} - \mathbf{X}_{n-j})^T \Sigma^{-1} (\mathbf{y}_{n-i} - \mathbf{y}_{n-j}) \\ &\quad + \frac{1}{N_y N_s} \sum_{i=0}^{N_s-1} \sum_{j=0}^{N_y-1} G_{2\Sigma} (\mathbf{s}_{n-i} - \mathbf{y}_{n-j}) \mathbf{X}_{n-j}^T \Sigma^{-1} (\mathbf{s}_{n-i} - \mathbf{y}_{n-j}). \end{aligned} \quad (6.40)$$

Note that, in both cases, the second term of Eqs. (6.26) and (6.28) disappears, since the distribution of the source is independent of the equalizer coefficients \mathbf{w} .

When the source distribution is approximated by an RBF network, Eq. (6.31), the

derived gradient is

$$\begin{aligned} \nabla_{\mathbf{w}} \hat{J}_{MQD-C} &= \frac{-1}{2N_y^2} \sum_{i=0}^{N_y-1} \sum_{j=0}^{N_y-1} G_{2\Sigma}(\mathbf{y}_{n-i} - \mathbf{y}_{n-j}) (\mathbf{X}_{n-i} - \mathbf{X}_{n-j})^T \Sigma^{-1} (\mathbf{y}_{n-i} - \mathbf{y}_{n-j}) \\ &\quad + \frac{1}{N_y N_a} \sum_{k=1}^{N_a} \sum_{j=0}^{N_y-1} c_k G_{2\Sigma}(\mathbf{y}_{n-i} - \boldsymbol{\mu}_k) \mathbf{X}_{n-i}^T \Sigma^{-1} (\mathbf{y}_{n-i}). \end{aligned} \quad (6.41)$$

As can be noted, all gradient functions are estimated using a sliding sample window. The reason for this choice is to seek a fair and coherent comparison with the kernel-based methods.

The performance of the gradient-based methods will be evaluated in Section 6.6, where they will also be compared with an evolutionary algorithm for optimization.

6.3 Estimation Issues

Once we have formed a representative set of criteria for the colored blind channel equalization problem, some natural questions may arise, like “how many samples are necessary to achieve a reliable estimation of the costs?”, “what is the optimal kernel size to be used in the correntropy- and multivariate density-based criteria?” or still “how intense is the effect of the *curse of dimensionality* [Scott, 1992] in the multivariate densities?”. Undoubtedly, a generic answer for these questions is not easy to be found, since it will depend on the type of distributions underlying the set of observable variables and on the noise.

In that sense, we perform a few analyses on these questions having as background the colored blind channel equalization problem.

6.3.1 The Number of Samples vs. Dimensionality

In order to evaluate the effect of the number of samples and the number of delays over the estimated costs, we have selected two representative scenarios that are able to illustrate the key behavior of each criteria. In the first scenario, the source is associated with a discrete distribution (or a PMF) and, in the second scenario, the source is associated with a continuous density (or a PDF).

First Scenario: Discrete Colored Source

Consider a binary $\{+1, -1\}$ *i.i.d.* signal u_n which is pre-coded by the linear pre-coder

$$P(z) = 1 + 0.5z^{-1} - 0.3z^{-2} + 0.1z^{-3} + 0.15z^{-4}. \quad (6.42)$$

Hence, the resulting pre-coded signal s_n has a temporal structure of order $L_p = 4$. The PMFs associated with u_n and s_n can be seen in Fig. 6.3.

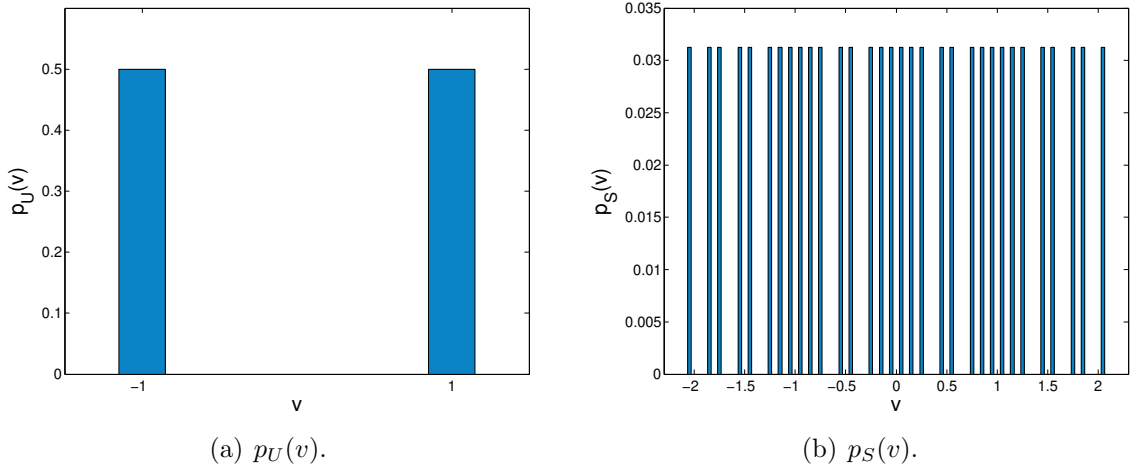


Figure 6.3: Scenario 1 - PMF of the *i.i.d.* and pre-coded signal.

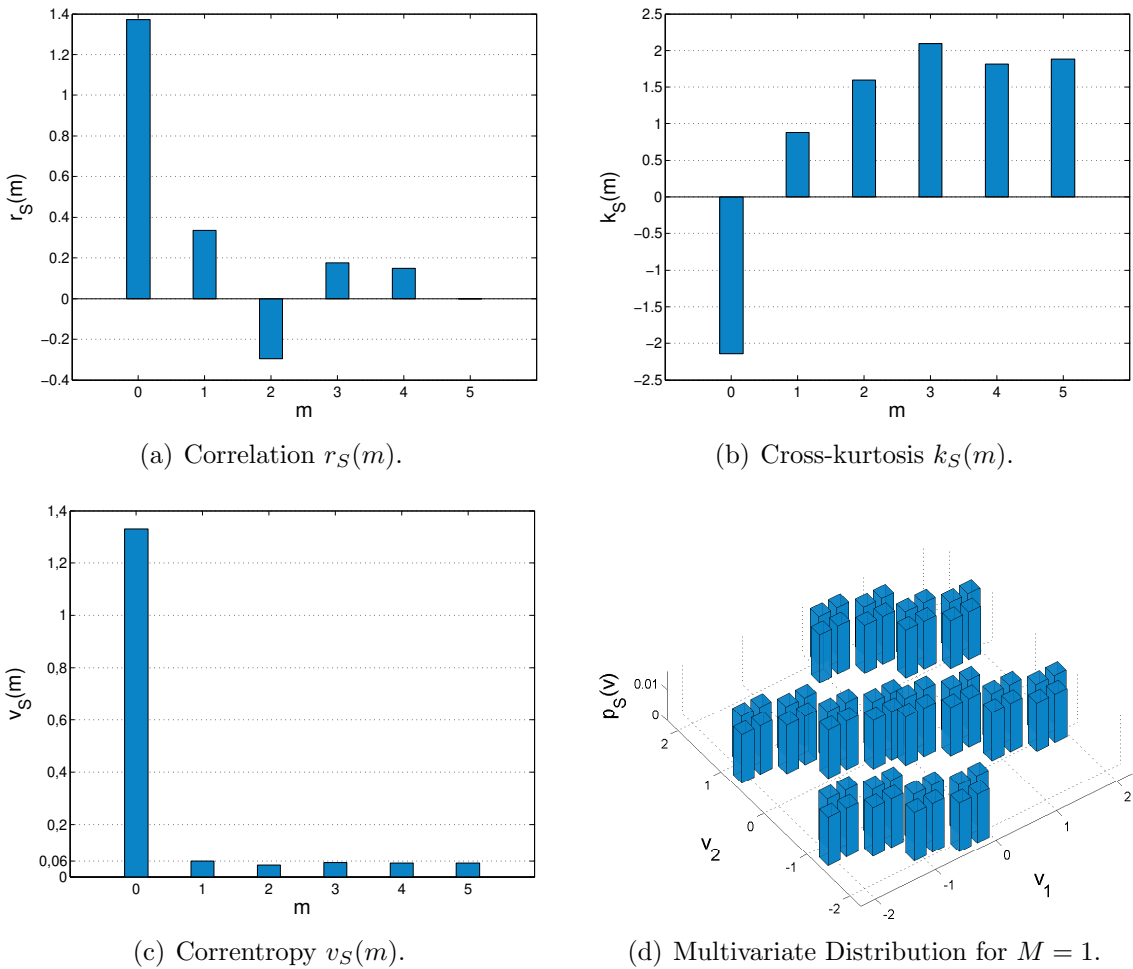


Figure 6.4: Scenario 1 - Analytical instances associated with the source s_n .

Since the PMF of u_n and the pre-coder $P(z)$ are known, we are able to analytically

compute the correlation, the cross-kurtosis, the correntropy and the PMF associated with s_n . Fig. 6.4 shows these values for $M = 5$ (except for the multivariate PMF, in which, for the sake of visualization, the $M = 1$ case was plotted). For correntropy, the chosen kernel size was $\sigma = 0.3$.

Assuming that there is a set of samples of s_n available, we wish to estimate the correlation, cross-kurtosis, correntropy and the multivariate distribution according to Eqs. (6.5), (6.13), (6.1) and (6.22), respectively. However, to establish a relation between the number of samples and the number of considered delays, it is assumed that N_s can have the values $\{30, 60, 100, 200, 300, 400, 500, 600, 700\}$ and M the values $\{0, 1, 2, 3, 4, 5\}$.

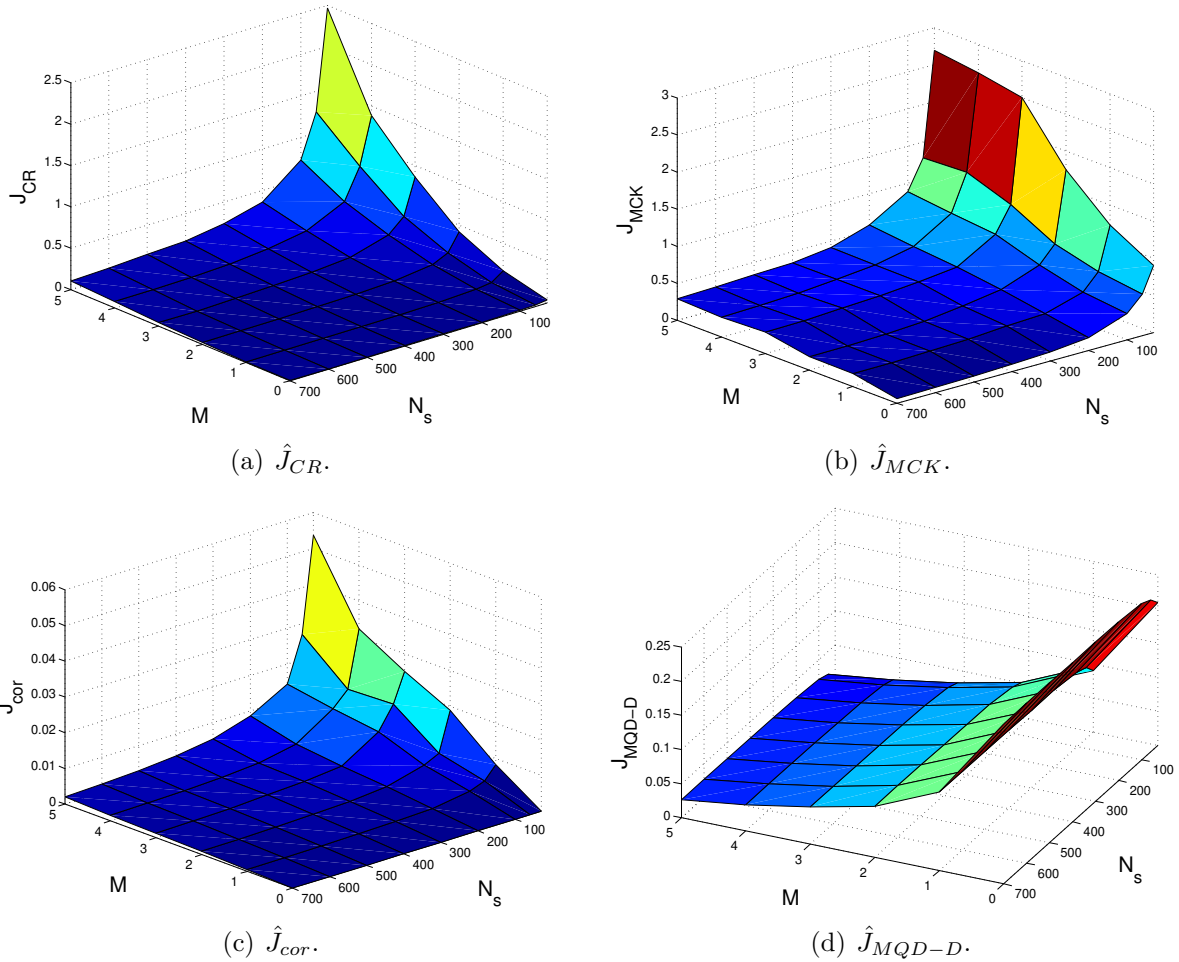


Figure 6.5: Scenario 1 - Cost values: $N_s \times M$.

Having obtained the estimates, it is possible to measure how close they were to their analytical values using the costs presented in Section 6.2.1 (it suffices to replace the estimated entities associated with the RV Y by the estimates associated with the RV S). In other words, we apply the costs \hat{J}_{CR} , \hat{J}_{MCK} , \hat{J}_{cor} and \hat{J}_{MQD-D} to measure the distance between the estimates and the analytical values; the costs will be null when the estimates match the analytical values. For 100 independent experiments, the average measured costs for the values of N_s and M are displayed in Fig. 6.5 (it was assumed the kernel size

$\sigma = 0.3$ for correntropy and $\Sigma = \sigma^2 \mathbf{I} = 0.09 \mathbf{I}$ for the multivariate density estimation).

It is possible to note that \hat{J}_{CR} , \hat{J}_{MCK} and \hat{J}_{cor} present similar cost shapes. For the \hat{J}_{CR} cost, Fig. 6.5(a), the quality of the estimates decreases – i.e., the cost increases – exponentially by reducing the number of samples and/or increasing the number of delays M . For \hat{J}_{MCK} and \hat{J}_{cor} , by decreasing the number of samples, the quality of the estimates decreases (the costs are higher) exponentially; by increasing the number of delays M , the quality of the estimates tends to decrease logarithmically. The costs \hat{J}_{CR} and \hat{J}_{MCK} seem to present higher sensibility for large M and small N_s . Also, \hat{J}_{cor} presented the lower cost values if compared with \hat{J}_{CR} and \hat{J}_{MCK} ; however, the reason for this comes from small correntropy values (see Fig. 6.4(c) – $v_s(0)$ must not be taken into account, since it is not considered on the cost). On the other hand, for the \hat{J}_{MQD-D} cost, we have not considered its second term (as expressed by Eq. (6.25)), hence, it cannot be seen as a distance measure. However, the general behavior of the cost is still preserved (the lower the cost, the higher the quality of the estimation). In that sense, we are able to note that the increase of the number of delays M can improve the estimation (the \hat{J}_{MQD-D} cost attains lower values) and, along the N_s axis, for $N_s \geq 100$, \hat{J}_{MQD-D} is practically constant. This suggests that, in contrast with the “curse of dimensionality”, the number of samples may not be an issue for estimating multivariate PDFs. It is also important to mention that a wrong choice of the kernel size Σ may contribute to the increase of the residual errors in the estimation (i.e., a kernel size misadjustment). However, the analysis of the kernel size will be done in Section 6.3.2.

Now, we repeat the same procedure but consider noisy samples of s_n , i.e., we assume

$$s_n = \mathbf{p}^T \mathbf{u}_n + \eta_n, \quad (6.43)$$

being η_n an Additive White Gaussian Noise (AWGN), with resultant Signal-to-Noise Ratio (SNR) level of 5 dB, a considerably high noise energy level in terms of equalization. Fig. 6.6 shows the histogram of the noisy samples of s_n .

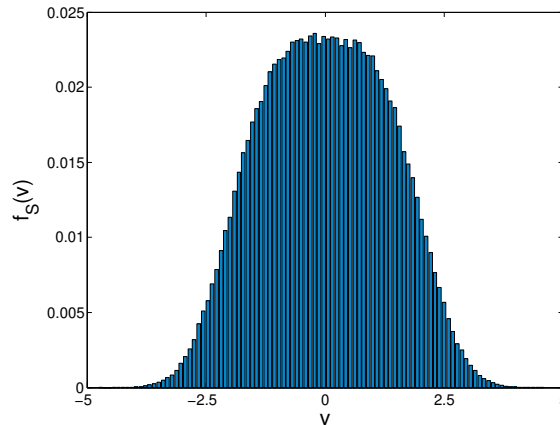


Figure 6.6: Histogram of the noisy samples of s_n .

The average costs for 100 independent experiments are displayed at Fig. 6.7. As it is possible to note, the \hat{J}_{CR} and the \hat{J}_{MCK} costs showed a considerable increase in the estimation error in comparison with the noiseless case (mainly the \hat{J}_{MCK} cost), being small values of M preferred in order to increase the estimation accuracy. For the kernel-based costs \hat{J}_{cor} and \hat{J}_{MQD-D} , their cost values remained practically the same of the noiseless case, revealing more robustness against noise. Indeed, this is a very attractive feature of kernel-based methods [Principe, 2010].

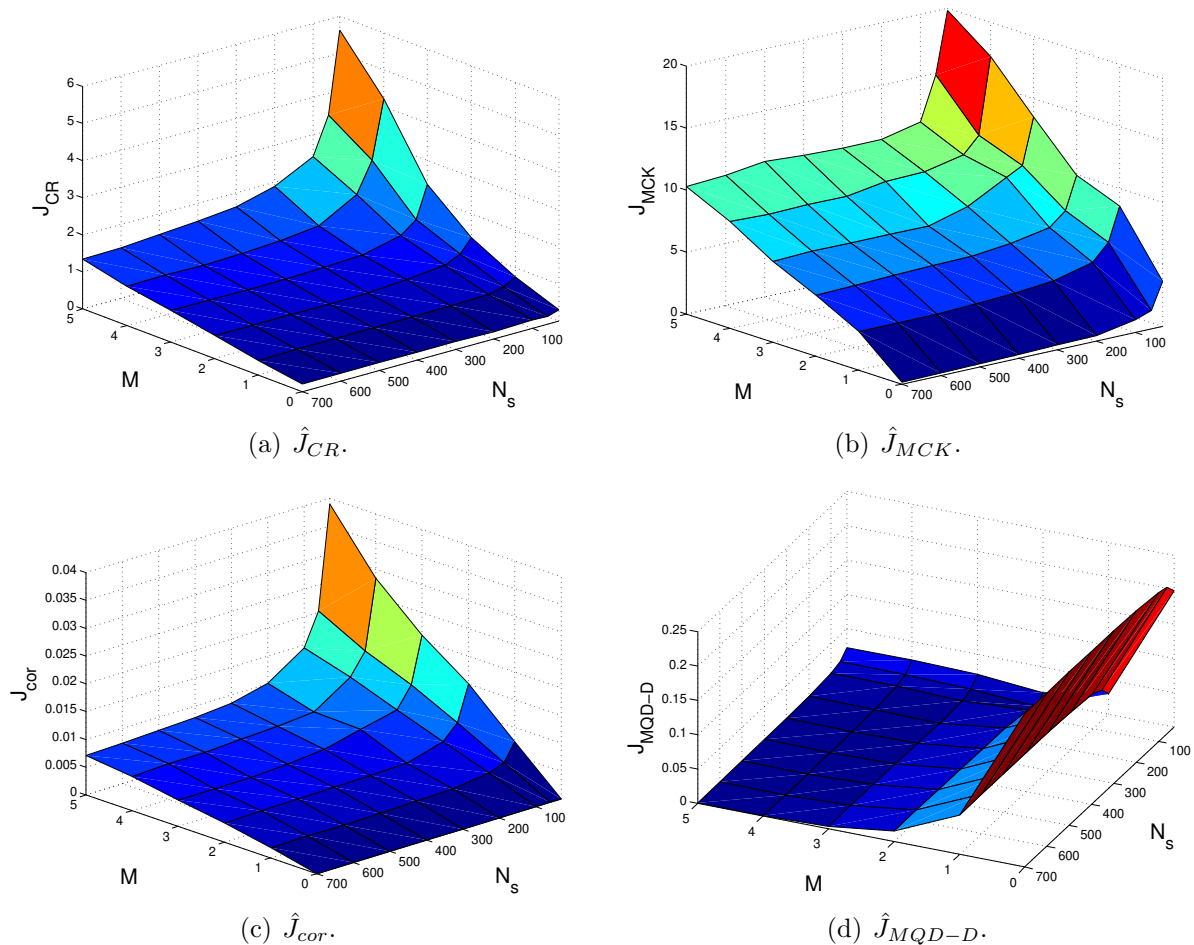


Figure 6.7: Scenario 1 - Cost values: $N_s \times M$ for noisy samples (SNR 5 dB).

Second Scenario: Colored Gaussian Source

Consider an *i.i.d.* Gaussian distributed signal u_n with zero mean and unit variance ($\sigma_U^2 = 1$) that is pre-coded by the same previous system $P(z)$, defined in Eq. (6.42). The histograms of the PDFs ($M = 0$) associated with u_n and s_n can be seen in Fig. 6.8.

The analytical computation of the correlation, the cross-kurtosis, the correntropy and the multivariate PDF associated with s_n is possible because the PDF of u_n and the pre-coder $P(z)$ are known. The correlation is analytically obtained via Eq. (6.4), while the cross-kurtosis via the group of Eqs. (6.11), (6.4) and (6.12). For correntropy, the analytical

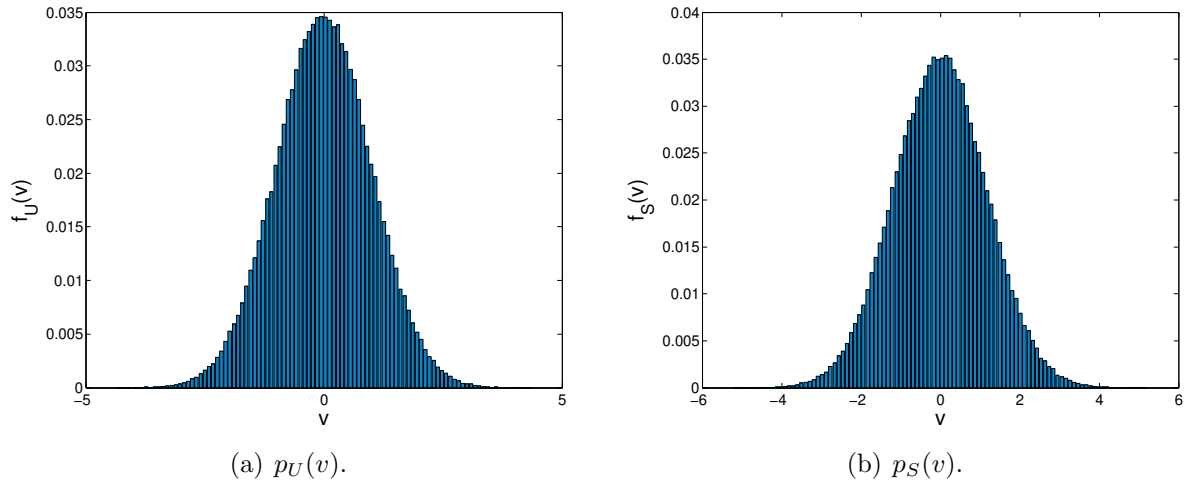


Figure 6.8: Scenario 2 - Histograms of the PDFs of the *i.i.d.* and pre-coded signal.

values can be computed according to Eq. (6.19), whose calculus is straightforward, since the source and the kernel function are both Gaussian. Basically, since u_n is Gaussian distributed, it is known that a linear combination of u_n will be Gaussian as well. More specifically, the PDF of s'_n (defined in Eq. (6.16)), $f_{S'}(v)$, will be

$$f_{S'}(v) = \frac{1}{\sqrt{2\pi\sigma_{S'}^2}} \exp\left(\frac{-1}{2\sigma_{S'}^2}v^2\right) = G_{\sigma_{S'}^2}(v), \quad (6.44)$$

being

$$\sigma_{S'}^2 = E[s_n'^2] = \mathbf{p}'^T E[\mathbf{u}_n \mathbf{u}_n^T] \mathbf{p}' = \mathbf{p}'^T \mathbf{p}', \quad (6.45)$$

where \mathbf{p}' is the modified pre-coder with transfer function $P'(z) = P(z)(1 - 1z^{-m})$. Hence, applying (6.44) in (6.19), there results

$$\begin{aligned} v_S(m) &= \int f_{S'}(v) G_{\sigma^2}(v) dv \\ &= \int G_{\sigma_{S'}^2}(v) G_{\sigma^2}(v) dv = G_{\sigma_{S'}^2 + \sigma^2}(0), \end{aligned} \quad (6.46)$$

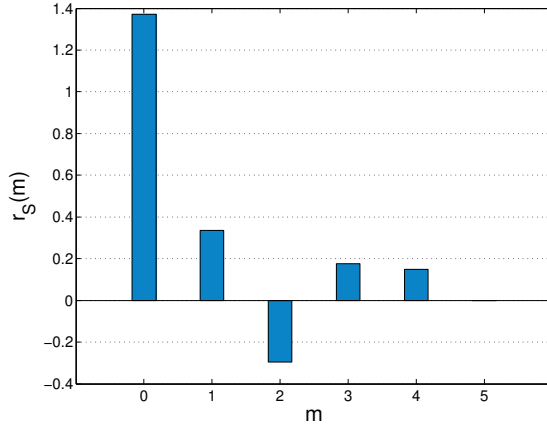
where the relation given by Eq.(2.12) was used. Note that $\sigma_{S'}^2$ may change in function of the considered delay m . Finally, for the multivariate PDF associated with s_n , we also know that it will be a multivariate Gaussian distribution of the type:

$$f_{\underline{S}}(\mathbf{v}) = G_{\underline{\Sigma}_S}(\mathbf{v}), \quad (6.47)$$

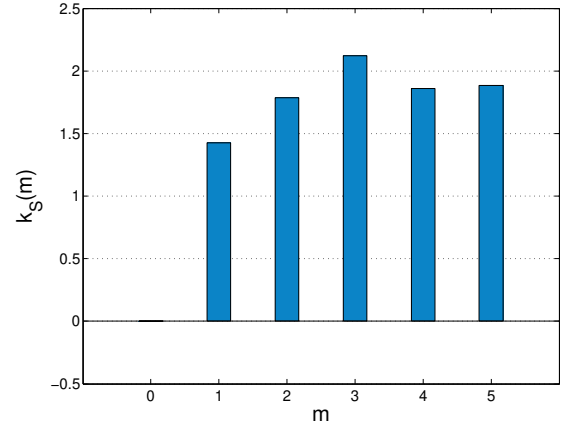
where $\underline{\Sigma}_S$ is the covariance matrix of s_n as defined in Eq. (5.12), which can also be analytically obtained.

Fig. 6.9 shows the analytical values obtained for $M = 5$ (for correntropy, the chosen kernel size was $\sigma = 0.3$, and, for the multivariate PDF, the $M = 1$ case is plotted for the

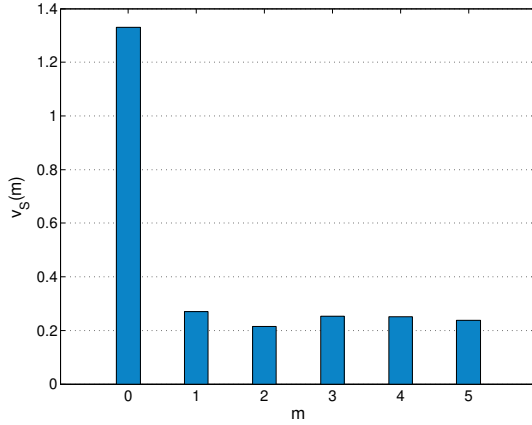
sake of visualization).



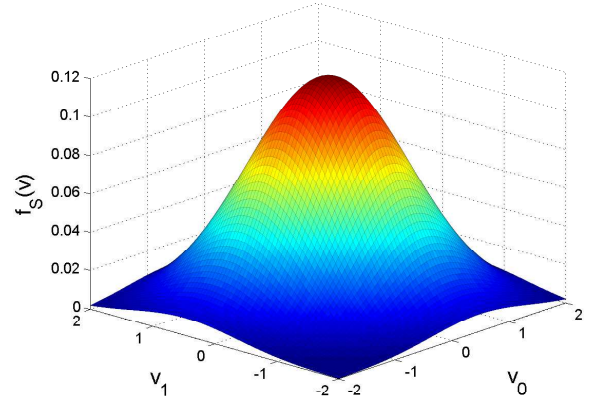
(a) Correlation $r_S(m)$.



(b) Cross-kurtosis $k_S(m)$.



(c) Correntropy $v_S(m)$.



(d) Multivariate Distribution for $M = 1$.

Figure 6.9: Scenario 2 - Analytical instances associated with the source s_n .

Similarly to the first scenario, we apply the costs \hat{J}_{CR} , \hat{J}_{MCK} and \hat{J}_{cor} to measure the distance between the estimates and the analytical values. For the MQD-C cost, we use a slightly modified version:

$$\hat{J}_{MQD-C} = \frac{1}{N_y^2} \sum_{i=1}^{N_y} \sum_{j=1}^{N_y} G_{2\Sigma}(\mathbf{y}_i - \mathbf{y}_j) + G_{2\Sigma_{\underline{s}}}(\mathbf{0}) - \frac{2}{N_y} \sum_{i=1}^{N_y} G_{\Sigma+\Sigma_{\underline{s}}}(\mathbf{y}_i), \quad (6.48)$$

since the source PDF is a multivariate Gaussian distribution.

Very interestingly, this scenario allows the use of the Silverman's rule [Silverman, 1986] for the kernel size adjustment, which allows the achievement of the optimum kernel size value – in a squared error sense – when the estimated distribution is Gaussian. Mathematically, Silverman's optimum kernel size can be computed as

$$\sigma_o^2 = \sigma_S^2 \left(\frac{4}{(N_s(2(M+1) + 1))} \right)^{2/(M+5)}, \quad (6.49)$$

where σ_S^2 is the variance of s_n . Hence, we adopt $\sigma^2 = \sigma_o^2$ and $\Sigma = \sigma_o^2 \mathbf{I}$ as kernel sizes for the \hat{J}_{cor} and the \hat{J}_{MQD-C} costs, respectively. However, since σ_o^2 depends on N_s and M , this value has to be updated for each considered value of N_s and M .

For 100 independent experiments, the mean costs values are as exhibited in Fig. 6.10 for $N_s = \{30, 60, 100, 200, 300, 400, 500, 600, 700\}$ and $M = \{0, 1, 2, 3, 4, 5\}$. Compared with the discrete case in Fig. 6.5, it is possible to note that the \hat{J}_{CR} presents a similar behavior, while \hat{J}_{MCK} revealed poorer estimates when N_s is small, i.e., the cost is higher for $N_s \leq 100$. For the kernel-based costs \hat{J}_{cor} and \hat{J}_{MQD-C} , the optimum kernel size σ_o^2 contributed to reduce the estimation error. For correntropy, the general tendencies were kept, i.e., by decreasing the number of samples, the quality of the estimates reduces exponentially and, by increasing the number of delays M , the quality of the estimates tends to reduce logarithmically. However, the cost values are lower than that of Fig. 6.5(c). For the \hat{J}_{MQD-C} cost, Fig. 6.10(d), it is now clear that, by increasing N_s or – counter intuitively – by increasing M , the estimates becomes more accurate (and \hat{J}_{MQD-C} attains lower values). Also, it is possible to note that reducing N_s or M the quality of the estimation deteriorates exponentially.

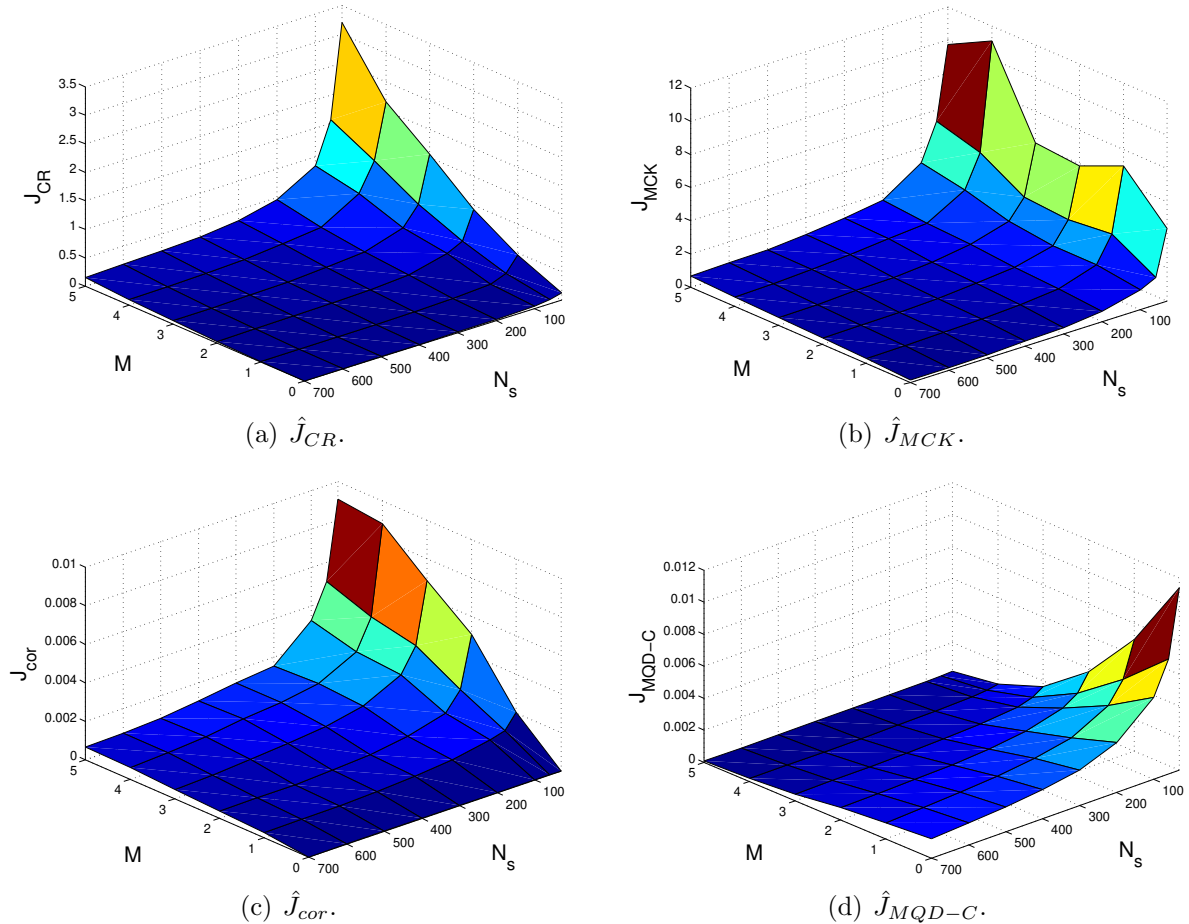


Figure 6.10: Scenario 2 - Cost values: $N_s \times M$.

Following the same line of the previous scenario, we also consider noisy samples ac-

according to the model given by Eq. (6.43). Again, an additive white Gaussian noise with resulting SNR level of 5 dB is considered. The surfaces of the focused costs are displayed in Fig. 6.11. Similarly to the discrete case, the \hat{J}_{CR} and the \hat{J}_{MCK} costs registered higher discrepancies between the estimated entities and their analytical values (mainly the \hat{J}_{MCK} cost). For correntropy and the multivariate PDF, Figs. 6.11(c) and 6.11(d), a slight differ-

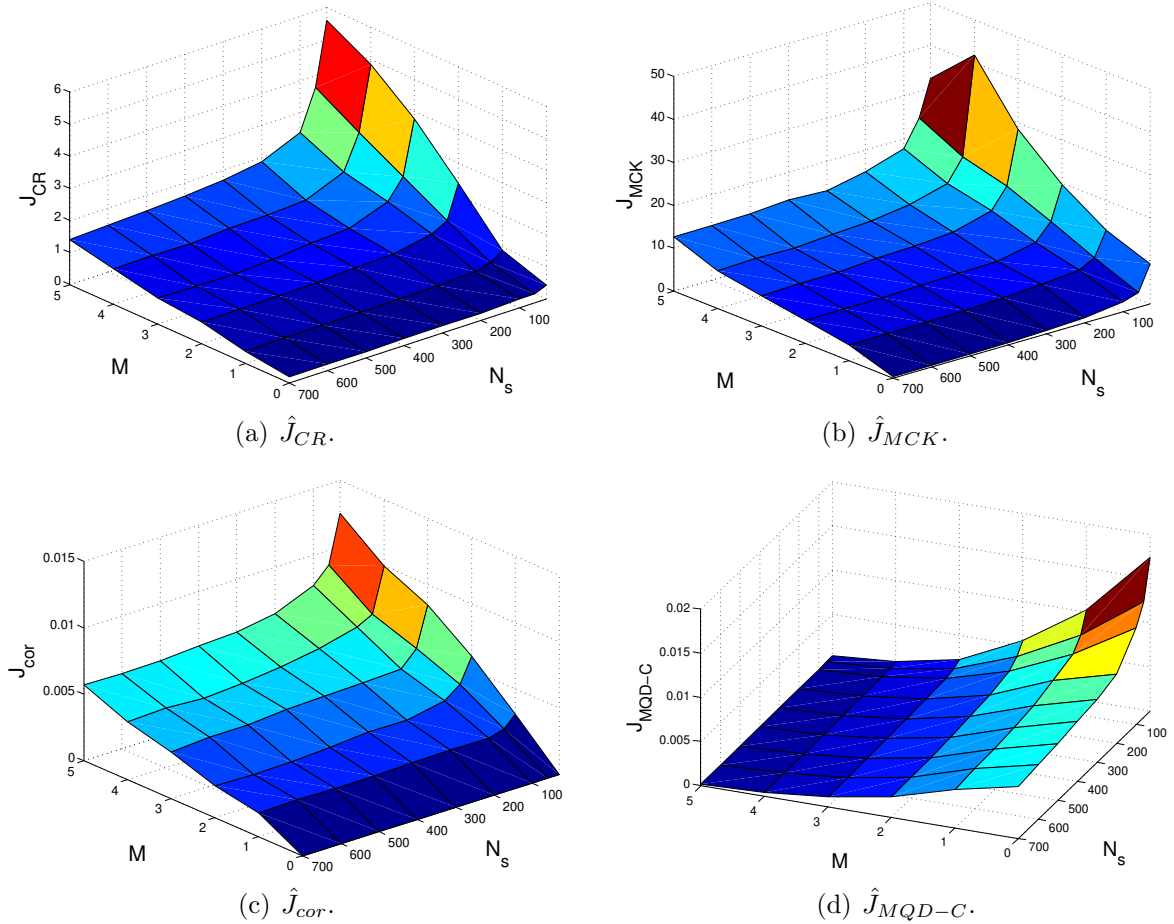


Figure 6.11: Scenario 2 - Cost values: $N_s \times M$ for noisy samples (SNR 5 dB).

ence in the costs was observed. However, the \hat{J}_{cor} cost exhibited a noticeable change when the number of delays M is increased, following a linear-like tendency of growth (hence, linearly reducing the estimation quality).

In a general perspective, we observed that, by increasing the number of samples, the estimates tend to become close to their correspondent analytical values, and, for \hat{J}_{CR} , \hat{J}_{MCK} and \hat{J}_{cor} , by increasing the number of delays, there may be a reduction on the estimation quality. However, in contrast with the “curse of dimensionality”, the MQD cost – in its discrete and continuous versions – revealed that, by increasing the number of delays M , there is no need of increasing the number of samples to improve the estimation quality. On the contrary, a relatively small number of samples ($N_s \approx 100$) can provide more information when a multivariate PDF is considered, improving the estimation quality. When the samples are corrupted by noise, the kernel-based estimators

showed great robustness. Undoubtedly, this result is associated with a correct choice of the kernel size, as we will see in the following.

6.3.2 The Kernel Size

As occurs in the majority of the ITL-based framework, the correntropy-based and the multivariate distribution-based criteria involve the adjustment of the kernel size parameter σ , which is sometimes associated with a smoothing factor over the estimates (as discussed in Chapter 2). From the literature, it is known that the correct choice of σ will depend on the type of the distribution, on the number of samples used in the estimation and on the dimension of the data. In order to illustrate these properties of σ , we recall the two scenarios considered in Section 6.3.1.

First Scenario: Discrete Colored Source

Our objective now is to measure the quality of the estimation of correntropy and the multivariate distribution by varying the parameters σ^2 , N_s and M . For this, we consider again the binary $\{+1, -1\}$ *i.i.d.* signal u_n which is pre-coded by the system given by Eq. (6.42) and the analytical instances illustrated in Fig. 6.4. We choose σ to vary along the values $\{0.1 : 0.1 : 2, 4\}$ (where $0.1 : 0.1 : 2$ are the values from 0.1 to 2 in steps of 0.1), N_s to have the values $\{30, 60, 100, 200, 300, 400, 500, 600, 700\}$, and M , $\{0, 1, 2, 3, 4, 5\}$. However, for the sake of visualization, we analyze separately $\sigma \times N_s$ and $\sigma \times M$, using, in the first case, a fixed value for M and, in the second case, a fixed value for N_s . The fixed values were chosen to be $M = 2$ and $N_s = 200$, since they are intermediate values of the considered range.

Similarly to the previous analysis, we performed 100 independent experiments considering noiseless and noisy samples (SNR of 5 dB), whose mean cost functions \hat{J}_{cor} and \hat{J}_{MQD-D} are displayed in Figs. 6.12 and 6.14 for the $\sigma \times N_s$ case. For correntropy, Fig. 6.12(a), it is possible to note that small values of σ can lead to a lower quality estimation (and, consequently, higher costs). However, by increasing the number of samples, the quality tends to improve exponentially. When there is noise, Fig. 6.12(c), the sensibility of the estimated correntropy increases for small values of σ . Hence, in this case, higher values of σ are also preferred. For the multivariate distribution, Fig. 6.12(b), the view is displayed from bottom to top, and, contrarily to correntropy, it is possible to see that small values of σ reduce the cost \hat{J}_{MQD-D} (hence, increase the quality of the estimation). Indeed, when σ tends to 0, the estimated PDF will tend to a PMF, which is the target of the cost; however, since the second term of Eq. (6.25) is neglected in \hat{J}_{MQD-D} , the perfect match between distributions will happen when $\hat{J}_{MQD-D} = -\infty$. If the number of samples is increased, it contributes to the quality of the estimation, particularly with lower values of σ . With the presence of noise, Fig. 6.12(d), \hat{J}_{MQD-D} indicates that small

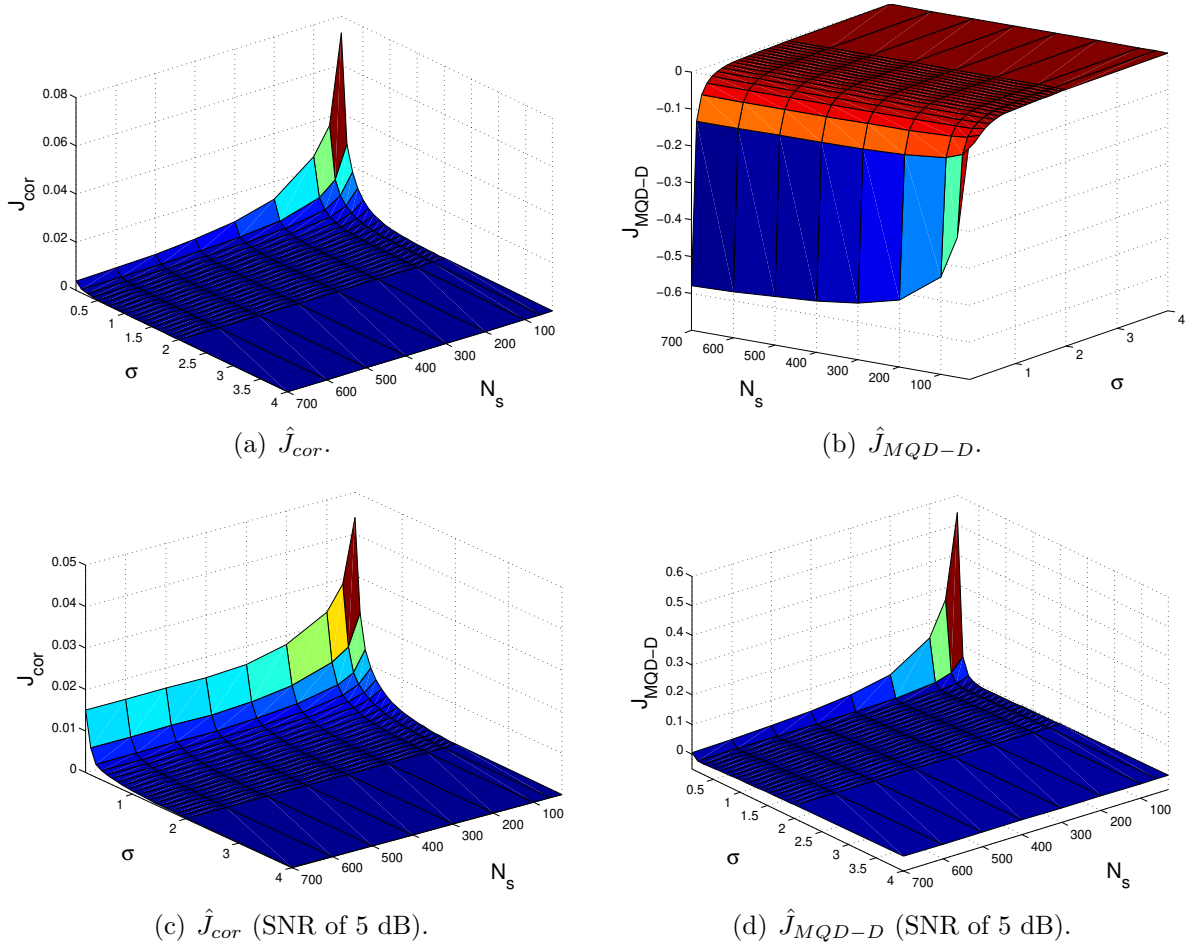


Figure 6.12: Scenario 1 - Cost values: $\sigma \times N_s$ and $M = 2$, with and without noise.

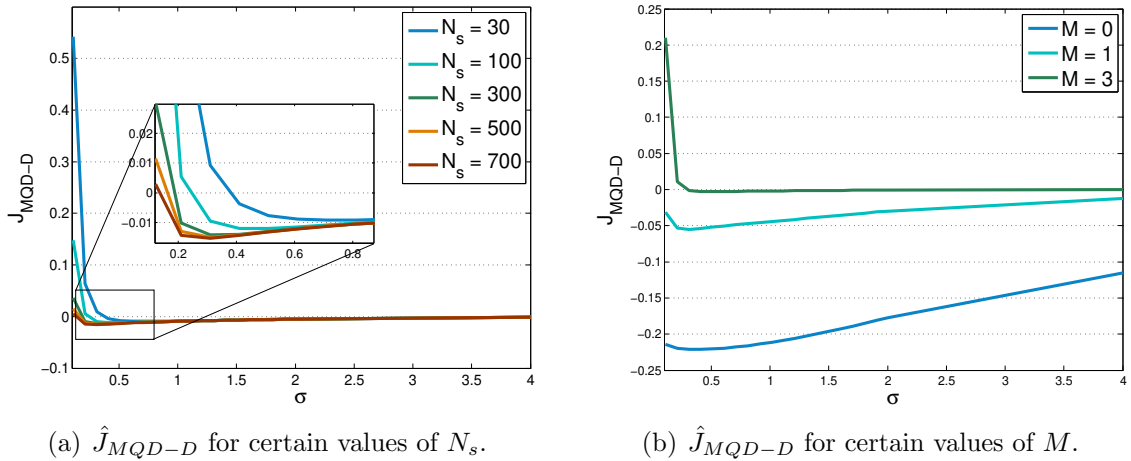


Figure 6.13: Scenario 1 - \hat{J}_{MQD-D} in function of σ (SNR of 5 dB).

values of σ can reduce the estimation quality. On the other hand, if σ is excessively increased, \hat{J}_{MQD-D} tends to 0. Interestingly, in the vicinity of $\sigma \approx 0.3$, \hat{J}_{MQD-D} attains its lowest value in this noisy case. The visualization of the minimum cost becomes clearer in Fig. 6.13(a), where it is possible to note that the optimum value of σ

number of samples.

For the $\sigma \times M$ case, Fig. 6.14 illustrates the mean cost values. For correntropy, the larger the number of delays M , the larger must be σ to obtain higher quality estimates – but $\sigma > 1$ seems to be sufficient for noiseless samples (Fig. 6.14(a)). When there is noise, Fig. 6.14(c), the quality of the estimates is reduced and, in this case, it is recommended that σ be greater than 2. It is important to recall that, for large values of σ , correntropy tends to emphasize the SOS [Principe, 2010]. Fig. 6.14(b) exhibits the \hat{J}_{MQD-D} cost – the

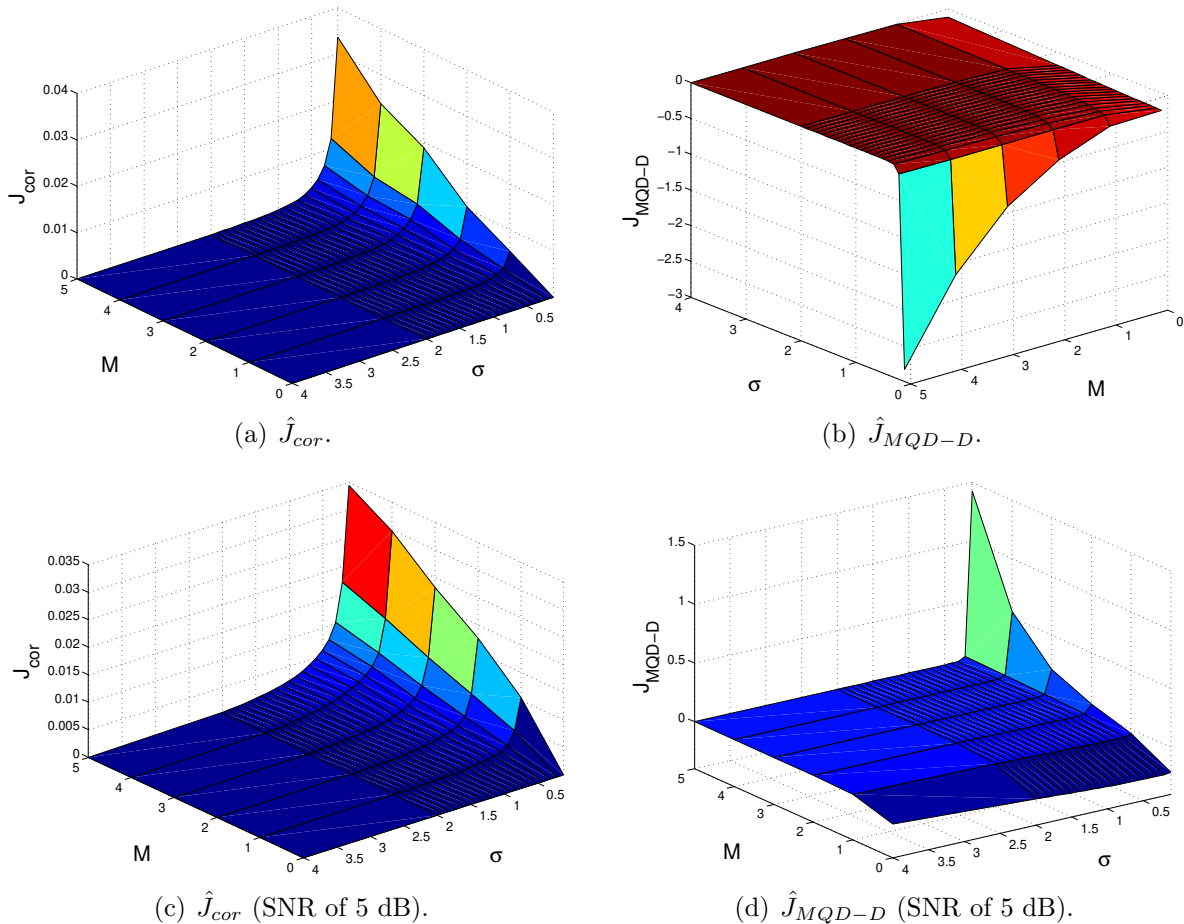


Figure 6.14: Scenario 1 - Cost values: $\sigma \times M$ and $N_s = 200$, with and without noise.

noiseless case – with a view from bottom to top, where a behavior similar to the $\sigma \times N_s$ case is observed, i.e., low values of σ ($\sigma < 0.2$) increase the estimation quality and, hence, the \hat{J}_{MQD-D} cost is reduced. In addition, by increasing the number of delays M , the better becomes the estimate when σ is small. However, when σ increases ($\sigma > 0.7$), the number of delays M causes no effect over \hat{J}_{MQD-D} , except for $M = 0$, in which \hat{J}_{MQD-D} attains slightly lower values (but we remind the reader that the multidimensional case is of great importance, since it can provide additional statistical information). By adding noise, Fig. 6.14(d), the \hat{J}_{MQD-D} cost accuses a reduction in the estimation quality when σ is small ($\sigma < 0.2$), similarly to the $\sigma \times N_s$ case. This becomes clearer in Fig. 6.13(b), where it is also possible to note that \hat{J}_{MQD-D} presents higher sensitivity to variations of

σ (for $\sigma > 0.2$) when M is small. Nonetheless, it is possible to achieve better estimates (lower costs of \hat{J}_{MQD-D}) for a small M .

Second Scenario: Colored Gaussian Source

Regarding the continuous distributions, we repeat our kernel size analysis for the previous case in which u_n is an *i.i.d.* Gaussian distributed signal. Following the former analysis procedure, we display in Fig. 6.15 the $\sigma \times N_s$ case. The optimum kernel size values obtained by the Silverman's rule (Eq. (6.49)) are also illustrated in Fig. 6.15. As one can

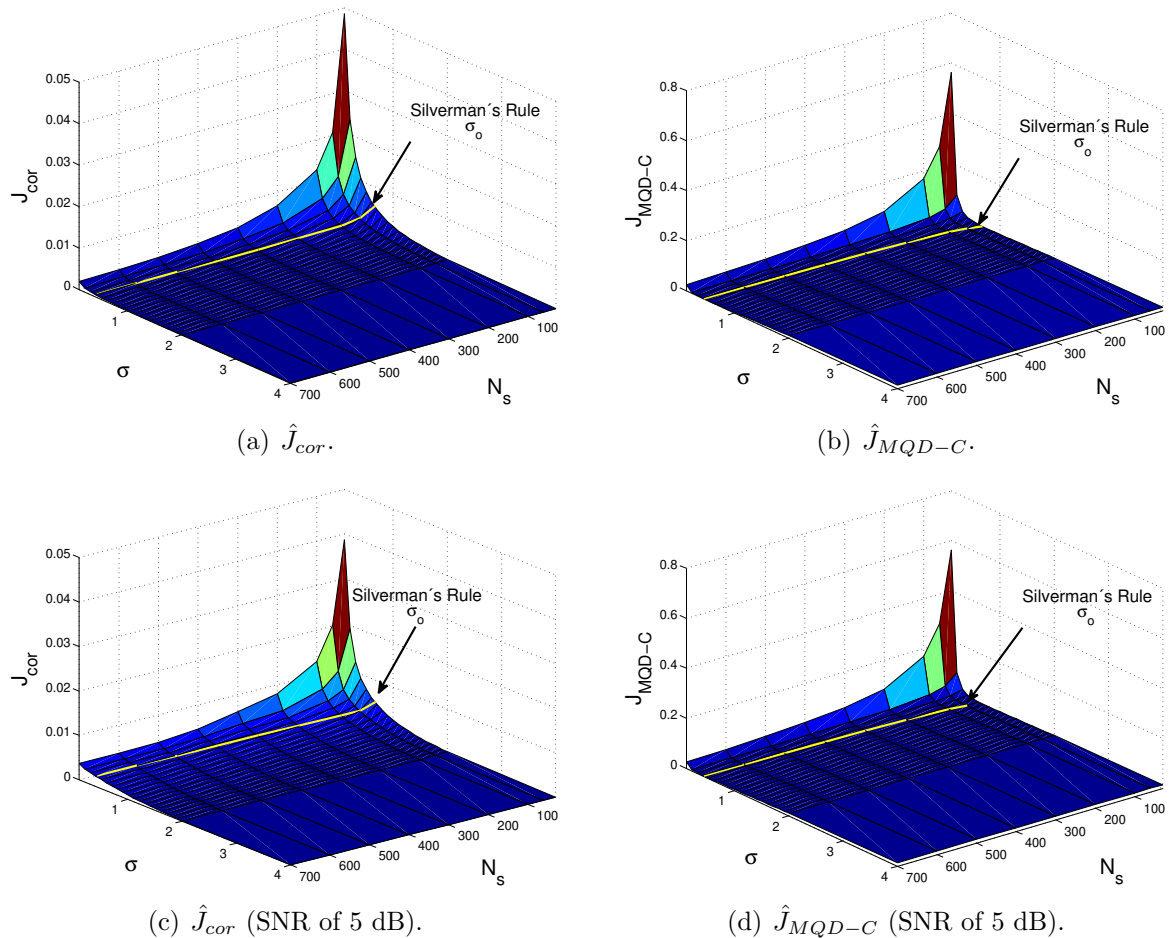


Figure 6.15: Scenario 2 - Cost values: $\sigma \times N_s$ and $M = 2$, with and without noise.

note, the noiseless case for correntropy, Fig. 6.15(a), is very similar to the discrete case, Fig. 6.12(a). However, the impact of the noise, Fig. 6.15(c), is less pronounced in this case. Again, a larger σ ($\sigma > 2$) is preferred in order to increase the estimation quality. It is also worth mentioning that the values provided by the Silverman's rule are not very suitable for correntropy, since the \hat{J}_{cor} cost registers certain degree of estimation error along the values of σ_o . For the \hat{J}_{MQD-C} cost, Figs. 6.15(b) and 6.15(d) – with and without noise, respectively – are similar to the noisy case for discrete source (Fig. 6.12(d)). Moreover, the optimum σ values lie within the range $0.3 < \sigma < 0.7$, depending on the number of

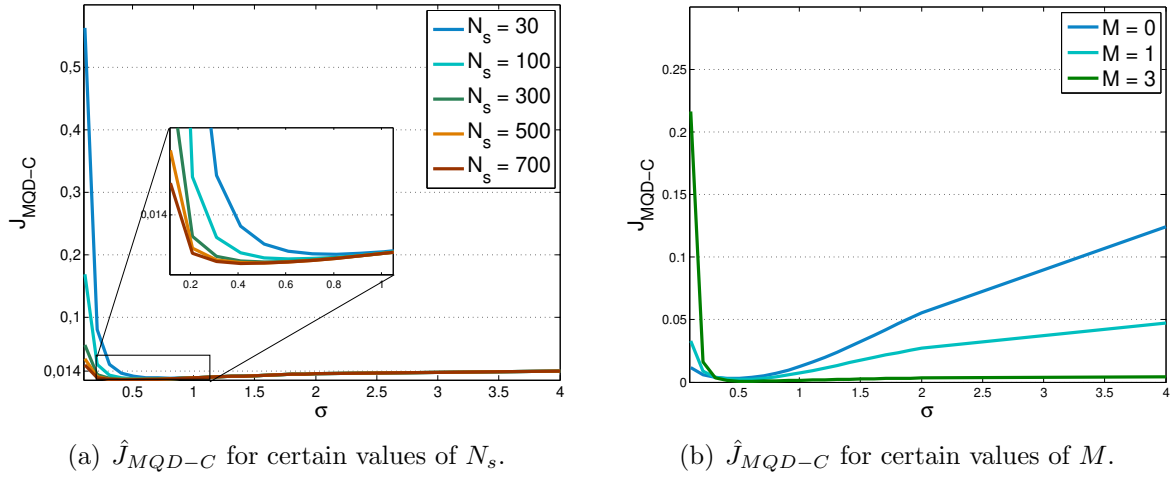


Figure 6.16: Scenario 2 - \hat{J}_{MQD-C} in function of σ .

samples, as shown in Fig. 6.16(a). More specifically, the optimum σ values are exactly the ones provided by the Silverman's rule, being perfectly suitable for the \hat{J}_{MQD-C} cost when the source is Gaussian.

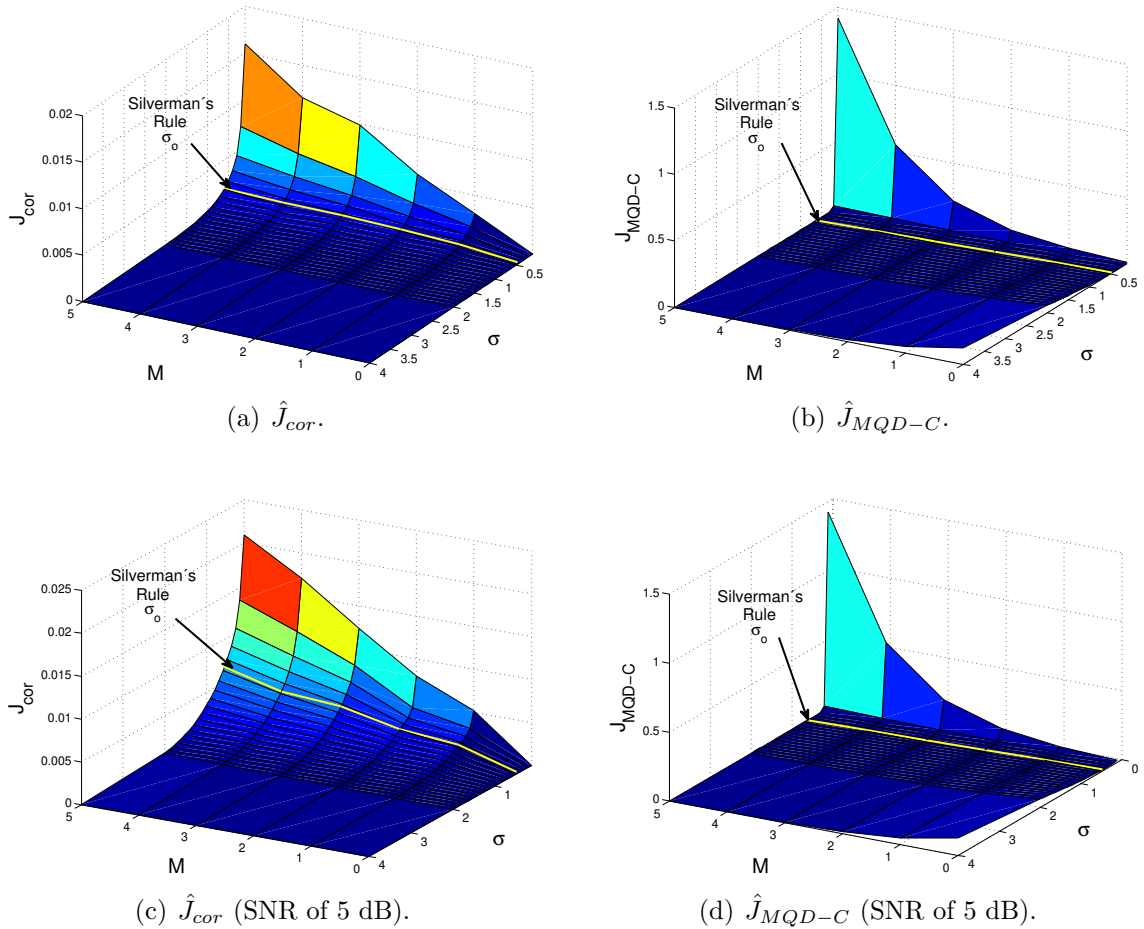


Figure 6.17: Scenario 2 - Cost values: $\sigma \times M$ and $N_s = 200$, with and without noise.

Fig. 6.17 shows the $\sigma \times M$ plots, for \hat{J}_{cor} and \hat{J}_{MQD-C} with and without noise (as well as the kernel sizes obtained by the Silverman's rule). The correntropy-based cost, Figs. 6.17(a) and 6.17(c), presented again a behavior similar to that of the discrete case, with lower values of the \hat{J}_{cor} cost for $\sigma > 2$ (far from the σ_o given by the Silverman's rule). The \hat{J}_{MQD-C} cost is practically indifferent to the presence of noise and Fig. 6.17(b) is very similar to Fig. 6.17(d). Again, low values of σ ($\sigma < 0.2$) cause a loss in the estimation quality and, differently from the discrete case (Figs. 6.12(b) and 6.14(d)), $M = 0$ does not lead to a reduction on the MQD cost: on the contrary, for a larger σ , the \hat{J}_{MQD-C} cost tends to increase (i.e., reducing the estimation quality). For $M \geq 3$, the effect of the kernel size becomes less prominent, except for considerably small values of σ ($\sigma < 0.2$), as can be clearly seen in Fig. 6.16(b). In addition, Fig. 6.16(b) also shows that the minimum value of \hat{J}_{MQD-C} (the optimum value for σ) is practically invariant to changes on the number of delays M . Indeed, the σ_o provided by the Silverman's rule forms a straight line in Fig. 6.17(b).

Finally, to conclude this section, we have that the increase on the number of delays M may require adjustments on the number of samples N_s and/or on the kernel size σ . More specifically, the correlation, the cross-kurtosis and the correntropy estimation showed to be more sensitive to the increase of M , requiring a larger number of samples to keep the quality of estimations. Notwithstanding, contrarily to the "curse of dimensionality", the use of multivariate densities estimated via kernel functions revealed to be an attractive option, since it does not require a large number of samples with the increase of M . This is a very interesting property that shall be useful when exploring the temporal structure of data, as we will see in the next section.

6.4 Methodology - Optimization and Performance

In order to properly compare the considered criteria, we will use two methods for the filter coefficient adaptation: gradient-based algorithms and metaheuristics; and, to assess the quality of the found solutions, we will make use of two performance measures.

In terms of the filter adaptation, traditionally, the gradient method is employed along with ITL criteria due to its lower computational cost. As mentioned in Section 3.1, this optimization method involves the adjustment of the step size μ , whose value must establish a fair comparison among the algorithms. In order to do so, the adjustment of μ will be done so that the filter coefficient mean displacement (in terms of the Euclidean distance) between iterations be equivalent. With the intention of being as fair as possible, this displacement was measured only after convergence of all algorithms, i.e.:

$$disp_w = \frac{1}{N_{it} - N_{conv} + 1} \sum_{i=N_{conv}}^{N_{it}} \|\mathbf{w}_{i+1} - \mathbf{w}_i\|, \quad (6.50)$$

where N_{it} is the maximum number of iterations and N_{conv} is the number of iterations required for convergence. The coefficient initialization will be made following the center-spike method, in which the taps are all null, except for the center tap, whose value is 1.

Notwithstanding, the unavoidable existence of local optima in the blind equalization problem can possibly lead the gradient-based algorithms to converge to suboptimal solutions, depending on the parameter initialization. With this in mind, the metaheuristics show more robustness against local convergence, but are computationally more costly, depending on the size of the search space, which grows as a function of the number of free coefficients in the equalizer. The evolutionary algorithm to be employed in the simulations will be the Differential Evolution (DE) [Storn and Price, 1997], a metaheuristic whose population adaptation operators strictly use the information available in the current solution candidates, instead of the classical random perturbations (for more information, see Chapter 3).

For performance evaluation in practical blind equalization problems, measures regarding the equalized samples, like the eye-diagram or the constellation analysis in PAM/QAM modulation schemes [Proakis and Manolakis, 1996] are usually considered. However, in our case, to exhibit a detailed profile of the criteria performance, we will count on two ISI-based metrics, which are representative measures of how much ISI remains in the equalization process. Usually, the quadratic ISI (QISI) measure is employed [Lázaro et al., 2003a,b; Santamaría et al., 2006], defined as

$$QISI_{dB} = 10 \log_{10} \frac{\left(\sum_{i=0}^{M_c} |c_i|^2 \right) - \max_j |c_j|^2}{\max_j |c_j|^2}, \quad (6.51)$$

where $\mathbf{c} = [c_0 \ c_1 \ \dots \ c_{L_c}]^T$ is the combined channel + equalizer impulse response, with length L_c+1 ; but a promising ISI measure capable of considering the HOS involved in the process is the entropy-based ISI (HISI) [Attux et al., 2015; Nose-Filho et al., 2013], defined as

$$HISI_{dB} = 10 \log_{10} \left(- \sum_{i=0}^{M_c} \alpha |c_i| \log_2 (\alpha |c_i|) \right), \quad (6.52)$$

where $\alpha = 1 / \sum_i |c_i|$. This alternative metric aims to measure the uncertainty about the channel by means of the Shannon's entropy, which can be more congruent to the analysis of non-Gaussian scenarios, as it encompasses the use of all the statistical moments, while the conventional ISI measure is a second-order statistically biased metric [Nose-Filho et al., 2013].

Example

The classical QISI reflects the preference for SOS-based approaches, given their relative

mathematical simplicity and the existence of a closed-form solution (in the MSE sense – see Chapter 4). However, in the works [Attux et al., 2015; Nose-Filho et al., 2013], it is shown that, depending on the distribution of the source, the QISI may not express the equalization optimality for non-ZF solutions, making HISI an interesting alternative measure.

In fact, when a ZF solution is attainable, i.e., the channel can be perfectly equalized, both QISI and HISI provide coherent measures. To illustrate this, we consider the following channel+equalizer with impulse response:

$$C(z) = \alpha + (1 - \alpha)z^{-1}, \quad (6.53)$$

with α varying from 0 to 1. The measured values for QISI and HISI are shown in Fig. 6.18(a), where it is possible to note that the optimal (minimal) values for both QISI and HISI happen at $\alpha = 0$ and $\alpha = 1$, the ZF solutions. However, for intermediate α values, the HISI measure weights the ISI effect differently from the QISI measure.

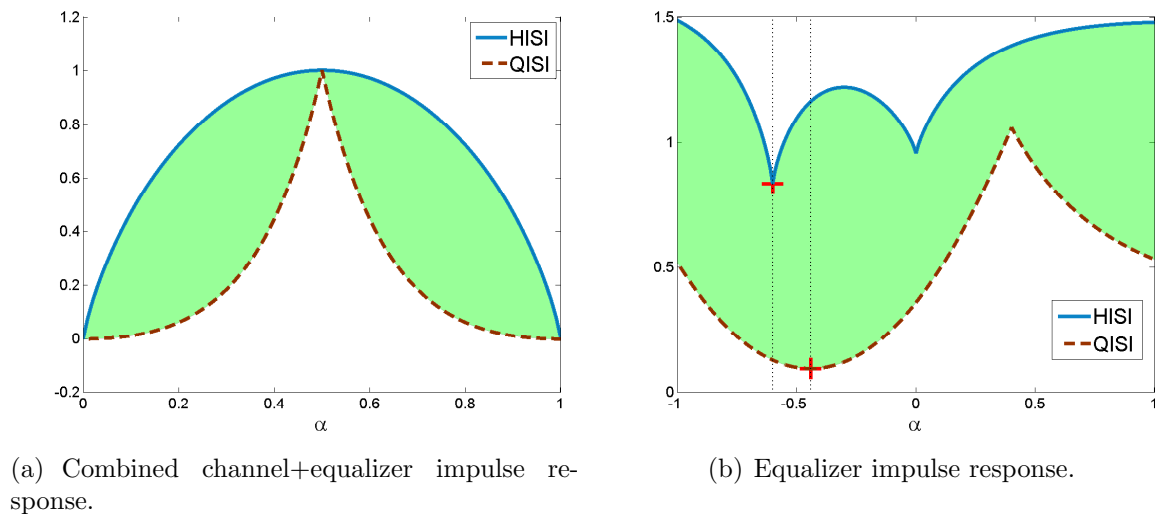


Figure 6.18: Measured values for QISI and HISI.

When the ZF solutions are not attainable (e.g., when both channel and equalizer are FIR filters), the difference between HISI and QISI becomes sharper. We use as example the following scenario. The channel is modeled according to a linear FIR filter with impulse response $H(z) = 1 + 0.6z^{-1}$ and the equalizer as

$$W(z) = 1 + \alpha z^{-1}. \quad (6.54)$$

In this case, by varying α from -1 to $+1$, we obtain the measures of QISI and HISI presented in Fig. 6.18(b). Now, the optimum value for QISI is different from that of HISI (denoted by red crosses in the figure). If it is considered that the source is a BPSK-

modulated signal, the performance of the each optimum in terms of the QISI and the HISI can be evaluated considering the classical eye diagram, as shown in Fig. 6.19. It is clear

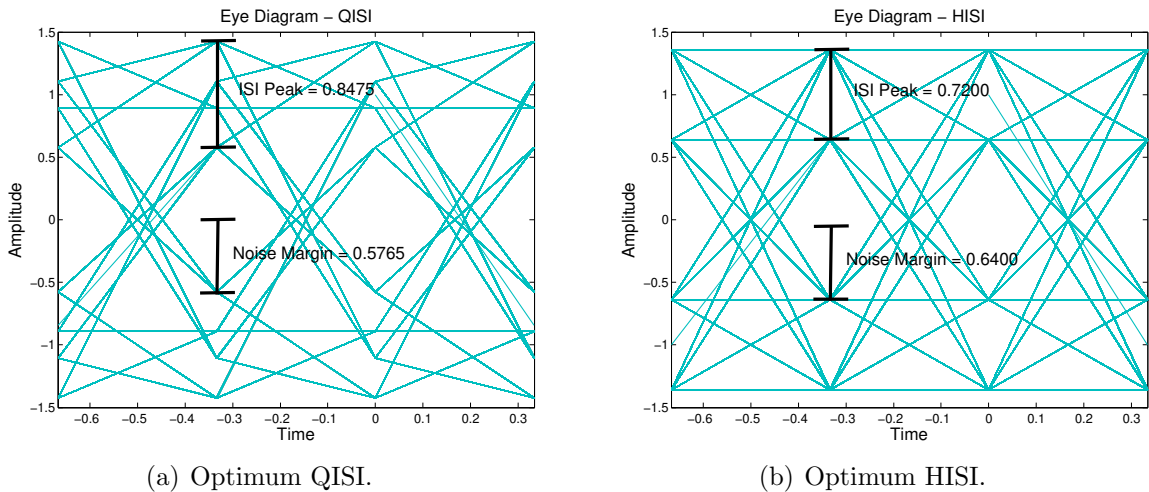


Figure 6.19: Eye diagram for the optimal cases of QISI and of HISI.

that both of them lead to an open-eyed solution for $W(z)$, but, the ISI peak measured in the optimum QISI case (0.8475) is higher than in the HISI case (0.7200) and the noise margin is narrower in the QISI case (0.5765 for QISI and 0.6400 for HISI). This indicates that, for this case, the HISI measure can be more adequate as a performance measure than the QISI.

Indeed, in the work of Nose-Filho et al. [2013], it is shown that the HISI can be an interesting performance measure when the source is not Gaussian, e.g., sparse and uniform sources. For the Gaussian case, the classical QISI suffices. In view of this, we will make use of both measures to obtain a more complete analysis of the criteria performance, always considering the scenario at hand.

The analysis will be firstly addressed in terms of the cost surfaces (simpler scenarios), followed by more complex adaptation scenarios within the colored blind channel equalization problem.

6.5 Cost Surfaces

In this first analysis, our intention is to study the behavior of these criteria surfaces as a function of the parameters \mathbf{w} of a linear FIR equalizer. For the sake of visualization of the cost functions, the equalizers \mathbf{w} will have only two adjustable coefficients, w_0 and w_1 , i.e.,

$$W(z) = w_0 + w_1 z^{-1}. \quad (6.55)$$

Hence, by varying the values of w_0 and w_1 , it is possible to evaluate the cost functions of interest and, consequently, their shape. In addition to that, to better compare the costs, we will use overlapping contours of the cost surfaces. The optimal solutions of each criterion will be obtained with the aid of the DE metaheuristic (see Chapter 3), whose parameters were set to $N_P = 100$, $F = 0.5$, $CR = 0.9$ and 100 iterations for all cases.

The cost surfaces will be analyzed in three different scenarios: one of them involving a discrete source and the other two involving continuous distributed sources, as will be described in the following.

6.5.1 Cost Surfaces - Scenario 1

In the first scenario, we consider that u_n is a BPSK modulated signal with symbols $\{-1, +1\}$ that are pre-coded by $P(z) = 1 - 0.5z^{-1} + 0.3z^{-2}$. The transmission channel can be modeled by the transfer function $H(z) = 1 + 0.6z^{-1}$, and there is AWGN, with an SNR equal to 27 dB. We will consider the $M = 1$ and $M = 2$ cases.

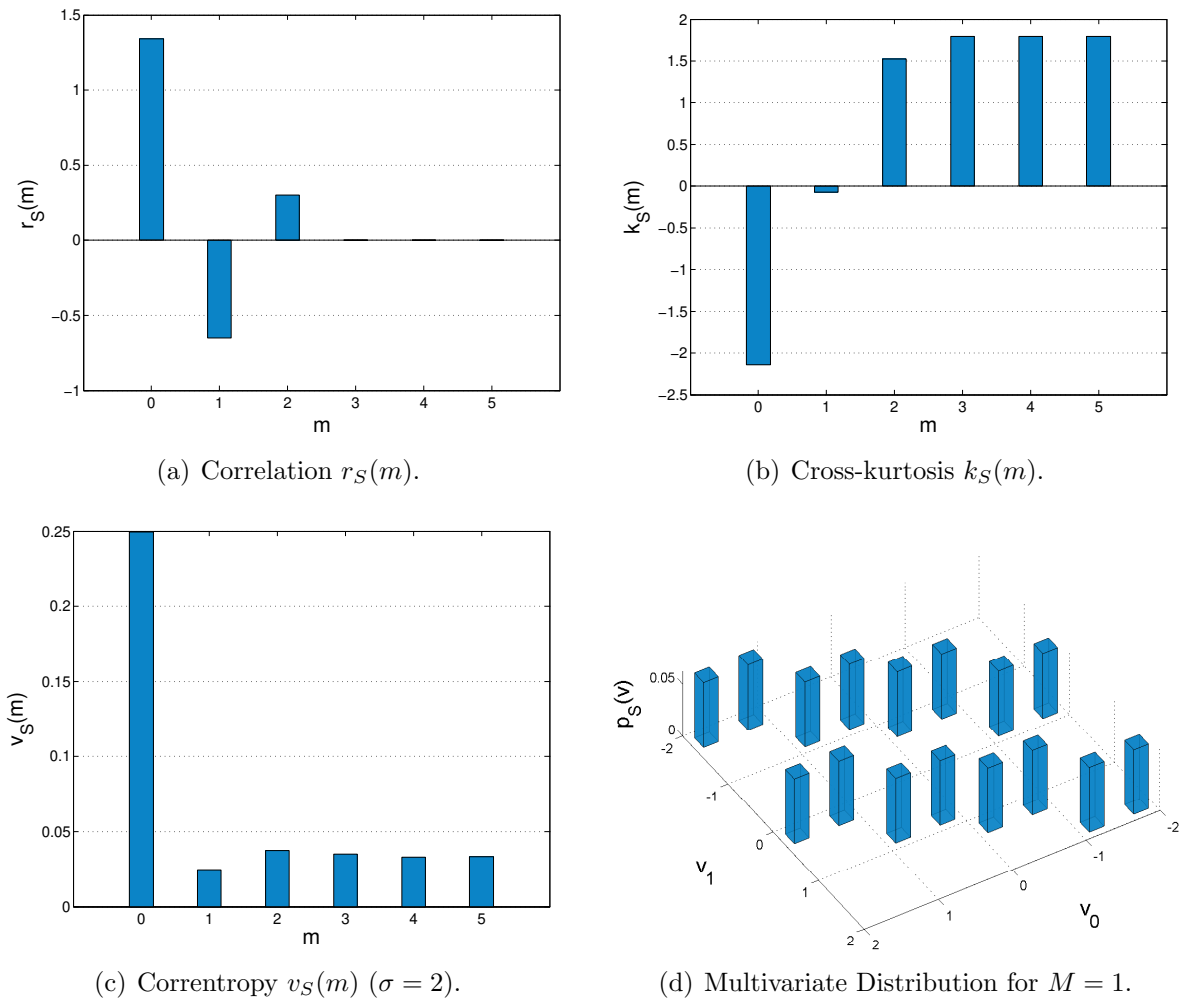


Figure 6.20: Cost Surface - Scenario 1: Analytical instances associated with the source

s_n .

Since we suppose that the pre-coder $P(z)$ and the source distribution are known, it is possible to obtain the analytical values of the correlation, cross-kurtosis and correntropy profiles of the source, as well as its joint PMF, as illustrated in Fig. 6.20.

The parameters σ and N_y were chosen to remain fixed, being their values adjusted according to the previous section, with $\sigma = 2$ for the correntropy-based cost, $\sigma = 0.4$ for the MQD-D cost (using $M = 1$ as reference), and $N_y = 200$ for all the considered costs.

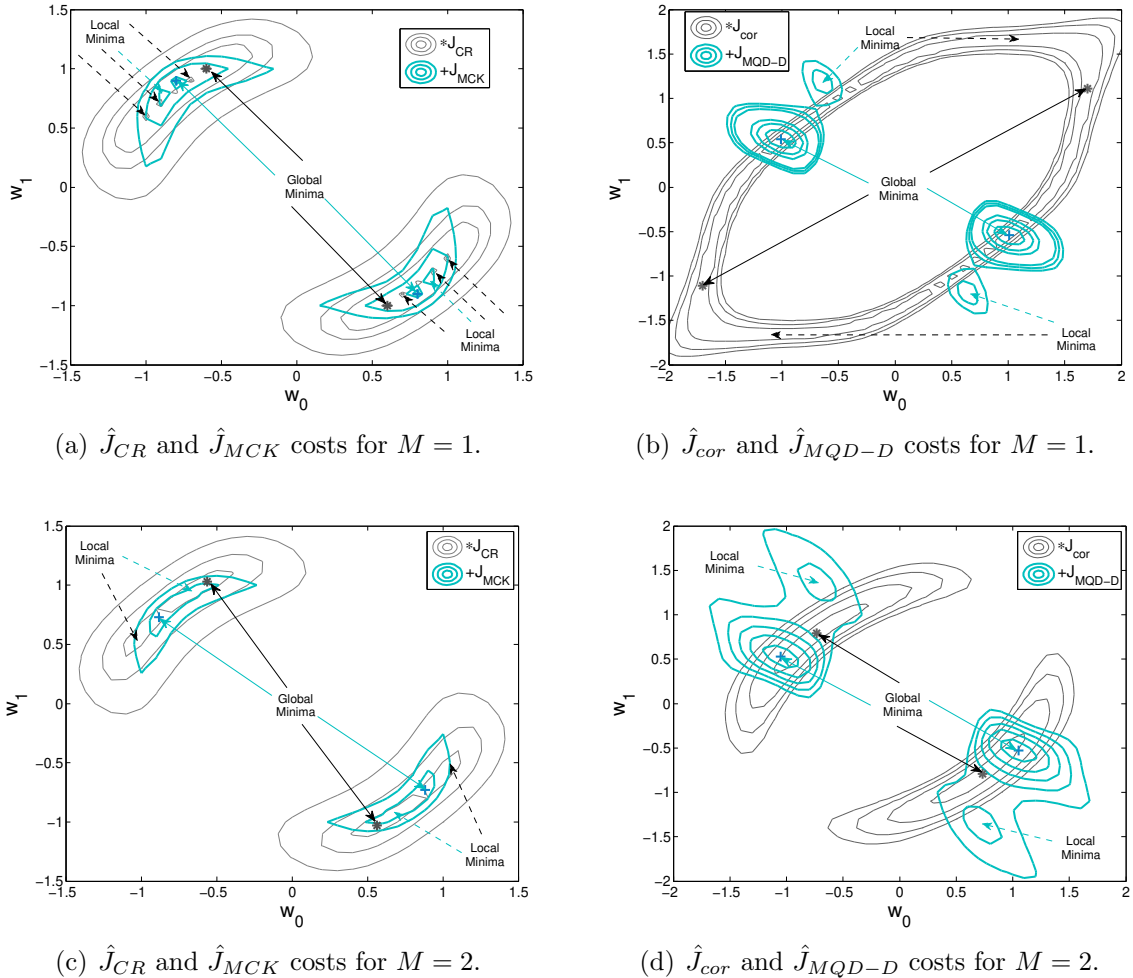


Figure 6.21: Cost Surface - Scenario 1: Surface contours for $M = 1$ and $M = 2$.

By varying the values of the coefficients of \mathbf{w} and by considering a set of 200 samples of s_n , it is possible to obtain the surface contours of the \hat{J}_{CR} , \hat{J}_{MCK} , \hat{J}_{cor} and \hat{J}_{MQD-D} costs for $M = 1$, as illustrated by Figs. 6.21(a) and 6.21(b), and for $M = 2$, in Figs. 6.21(c) and 6.21(d). Due to their blind character, it is possible to see that all criteria surfaces present axial symmetry and that there are multiple minima. Interestingly, the shapes of the surfaces are very distinct from each other and their minima are not coincident. This gives support to the idea that the exploited information is not equivalent. For the $M = 1$ case (Figs. 6.21(a) and 6.21(b)), the \hat{J}_{CR} cost presented several local minima, which can be an inconvenient issue for using local search operators, such as gradient-based methods.

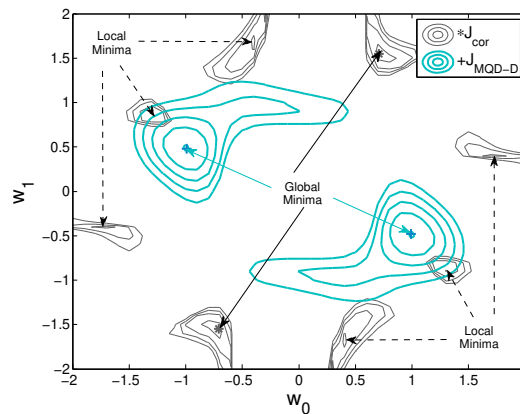


Figure 6.22: Cost Surface - Scenario 1: \hat{J}_{cor} and \hat{J}_{MQD-D} costs for $M = 2$ and $\sigma = 0.3$.

The \hat{J}_{MCK} cost presented a shape somehow similar to \hat{J}_{CR} , but with a reduced number of local minima and non-coincident global minima (indeed, the MCK cost is able to extract more statistical information than the CR cost). In Fig. 6.21(b), \hat{J}_{cor} presented an ellipse-like region where its global and local solutions can be found, while \hat{J}_{MQD-D} presented a completely different behavior, where it is possible to identify very distinct global and local minima.

By changing M to 2 (Figs. 6.21(c) and 6.21(d)), the cost contours tended to become more similar among each other. The \hat{J}_{CR} cost reduced the number of local minima, but the solutions are again not coincident with those of MCK (in fact, although a larger M is able to increase the amount of statistical information encompassed by the CR cost, the MCK cost is able to additionally encompass the fourth-order statistics). In Fig. 6.21(d), the MQD-D cost presented small variations on its cost shape and on the minima position, which means that, for the $M = 1$ case, the MQD-D cost already encompassed significant amount of statistical information. In contrast, the correntropy-based cost \hat{J}_{cor} significantly changed its surface shape and minima position and, interestingly, no longer presented local minima, which is an important property of the kernel size σ . It is important to emphasize that the correct choice of the kernel size σ can immensely contribute for smoothing the cost and reducing the number of local minima (i.e., taking into account the estimation issues presented in Section 6.3). Indeed, this property can also be exploited in the MQD-D cost if a higher value for σ is assumed, say $\sigma = 0.7$, as illustrated in Fig. 6.22 – note that the local minima of the MQD-D cost vanish. Contrarily, a sufficient low value of the kernel size may cause the reappearance of the local minima. Fig. 6.22 also depicts the correntropy-based cost with $\sigma = 0.3$, where it is possible to note several local minima. In general terms, for the MQD, σ is directly related to the PDF estimation, but, for correntropy, σ will be more closely associated with the weighting of the statistical moments. The value of σ , in both cases, is also related to a smoothing parameter: a small σ tends to create spurious minima, while a large σ , although reducing the effect of local minima, tends to

disturb the optimal solution [Lázaro et al., 2005].

In all cases, the global and local optima were found with the aid of the DE meta-heuristic, being the global solutions indicated by a plus ‘+’ or an asterisk ‘*’ sign.

Although the focus of this first analysis lies on the surface cost, it is also pertinent to evaluate the performance of the global minima and to identify their relation with the cost behavior. In that sense, the performance in terms of HISI and QISI of the global solutions for each criterion were evaluated in 10 independent experiments, whose mean values are shown in Tab. 6.2. For $M = 1$, it is possible to note a tendency of

Table 6.2: Solutions performance measures for the scenario 1.

		CR	MCK	cor	MQD-D
$M = 1$	HISI [dB]	1.6113	1.5898	0.9219	0.1919
	QISI [dB]	-1.8459	-2.4306	-4.1151	-9.8130
$M = 2$	HISI [dB]	1.2073	1.1669	0.6352	-0.3823
	QISI [dB]	-1.8714	-4.2261	-5.3767	-8.7600

a reduction of the HISI/QISI values when a ‘larger amount’ of statistical information is considered: the MQD-D criterion exhibits the best performance, being followed by the correntropy-based, the MCK and the CR cost. The CR and the MCK performance present similar performance measures, but it is important to remember that these costs are more vulnerable to estimation errors when the number of samples are considerably low (as explained in Section 6.3). In terms of QISI, the MQD-D criterion also performs better in comparison with the other three criteria, however, since the source is far from a Gaussian distribution, the HISI measure tends to be more suitable in this scenario. When $M = 2$, the criteria are able to extract more information and, as shown in Tab. 6.2, their performance is improved in terms of HISI. In terms of QISI, the increment of M caused the CR, the MCK and the correntropy-based criteria to experience an improvement in the performance, differently from the MQD-D criterion, which experiences a slight reduction. Even though, the MQD-D performance is still the best in terms of QISI as well – it is important to emphasize that the HISI is the preferred measure in this scenario, where the MQD-D criteria revealed a huge increase on its performance with $M = 2$.

6.5.2 Cost Surfaces - Scenario 2

We continue the cost surface analysis, but consider now a continuously distributed source. It is assumed that s_n is a colored Gaussian distributed signal, result of the pre-coding of u_n , an *i.i.d.* Gaussian distributed signal, by $P(z) = 1 - 0.5z^{-1} + 0.3z^{-2}$, the same previous pre-coder. The channel is also kept the same, i.e., $H(z) = 1+0.6z^{-1}$, and there is AWGN with an SNR equal to 27 dB.

The analytical values of the source statistics are shown in Fig. 6.23. For the matching of multivariate PDFs, we consider the cost given by Eq. (6.48).

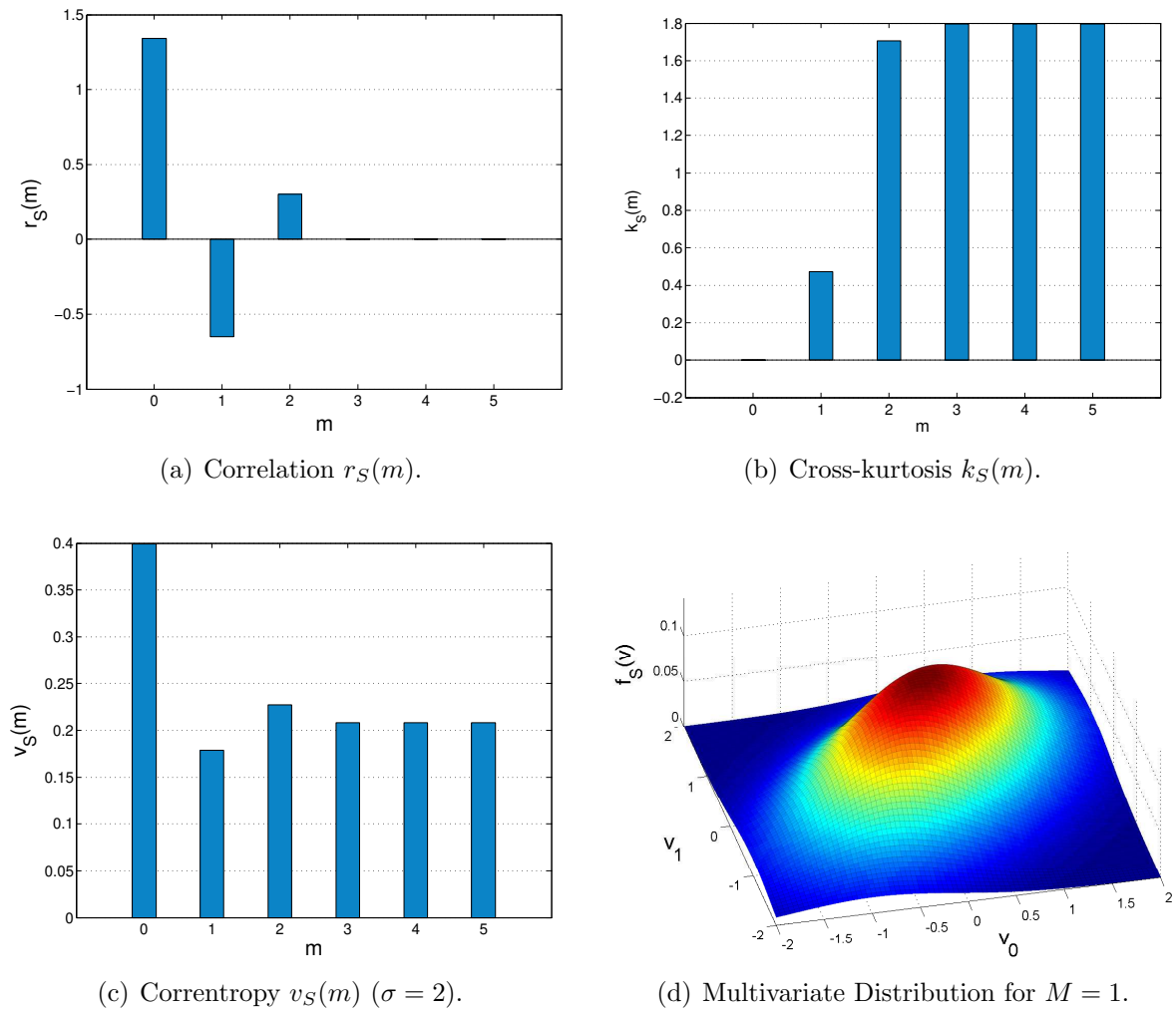


Figure 6.23: Cost Surface - Scenario 2: Analytical instances associated with the source s_n .

For the same criteria parameters of the previous scenario, the contours of \hat{J}_{CR} , \hat{J}_{MCK} , \hat{J}_{cor} and \hat{J}_{MQD-C} for the $M = 1$ and $M = 2$ cases are displayed in Fig. 6.24. For the $M = 1$ case, it is possible to note from Fig. 6.24(a) that the CR cost is very similar to the discrete case (Fig. 6.21(a)), while MCK is slightly different, with only global minima and close to the global CR solutions. This is due to the fact that, for the delay $m = 0$, the cross-kurtosis (or simply kurtosis) is null when the signal is Gaussian distributed (check Fig. 6.23(b)) and the second-order statistics term becomes stronger. The correntropy-based cost as well as the MQD-C cost present smoother surfaces in comparison with the discrete case (Fig. 6.21(b)). The correntropy-based cost, for example, shows a clearer ellipse-shape region where its solutions can be found; while the MQD-C cost presents only global minima. These effects are similar to that of increasing the kernel size σ ; however, in this case, the smoothing effect is caused by the continuous source [Boccatto et al., 2016]. When the considered number of delays is increased to $M = 2$, the CR and the MCK costs keep their general shapes, as shown in Fig. 6.24(c), but the number of local minima for

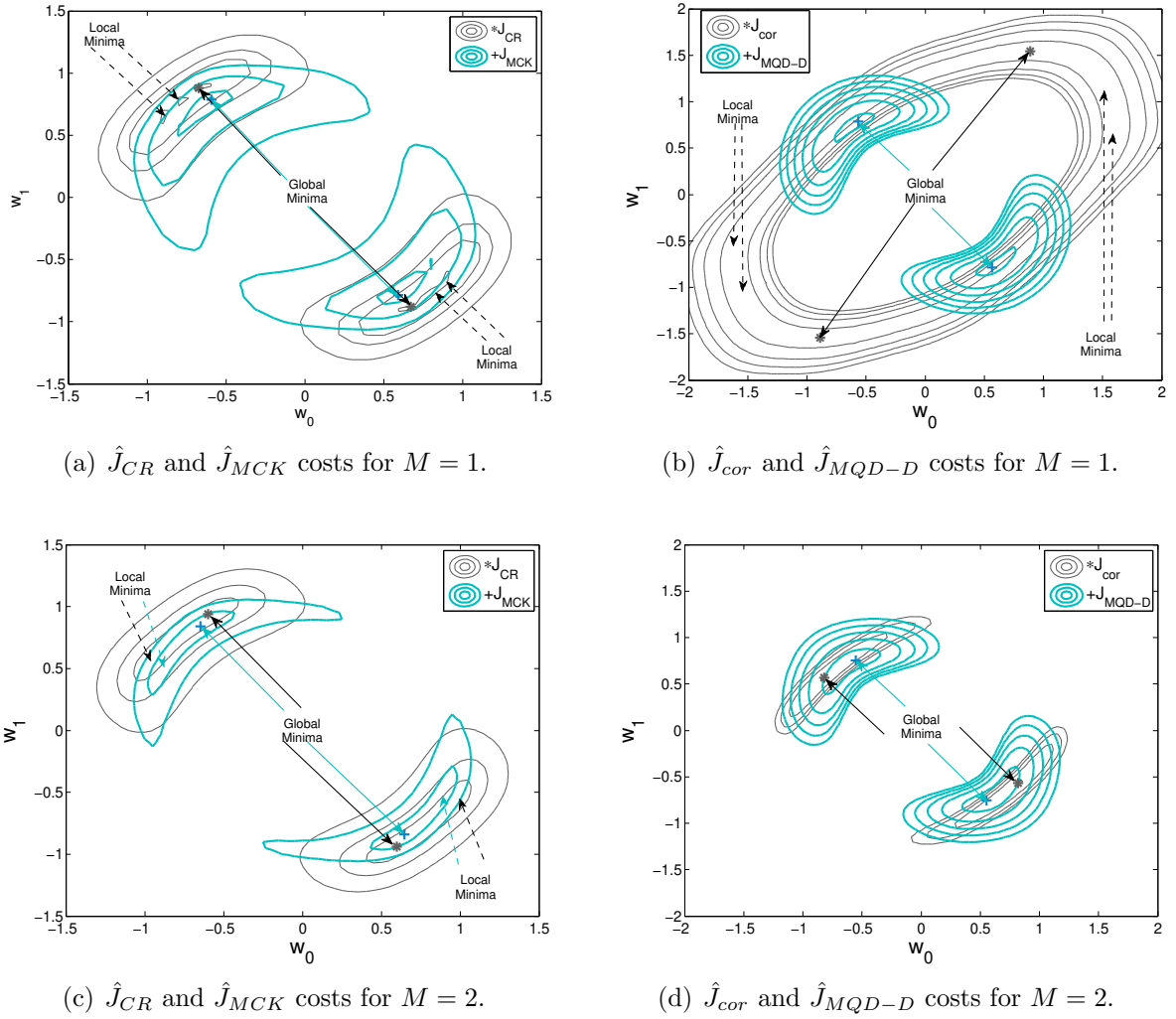


Figure 6.24: Cost Surface - Scenario 2: Surface contours for $M = 1$ and $M = 2$.

the CR criterion decreases and the MCK cost becomes less smoother, due to the increase on the number of fourth order statistical terms. For the MQD-C cost, changing M to 2 has not caused a major impact and the contours are basically the same as in the $M = 1$ case, as shown in Fig. 6.24(d). The correntropy, on the other hand, reduces the number of minima, leaving only the global ones – an effect similar to that verified for the discrete case.

For each case, a search for the global solutions was performed using the DE meta-heuristic. In 10 independent experiments, the HISI and QISI performances were evaluated, being their mean values displayed at Tab. 6.3. In general aspects, it is possible to note that the performance achieved by the criteria in terms of HISI and QISI were lower in comparison with the discrete case (Tab. 6.2), which could be a direct reflex of the limited statistics present on the Gaussian source (the scenarios involving other source distributions will be considered later). However, the MQD-C cost is still able to achieve the best HISI/QISI performance, being followed by correntropy – it is important to re-

Table 6.3: Solutions performance measures for scenario 2.

		CR	MCK	cor	MQD-C
$M = 1$	HISI [dB]	1.6044	1.5405	1.0839	0.5332
	QISI [dB]	-2.3677	-1.7517	-3.7352	-4.8128
$M = 2$	HISI [dB]	1.4905	1.4525	1.8105	1.1753
	QISI [dB]	-0.6298	-2.2061	-3.8591	-4.9520

mark that the QISI is more suitable in this scenario, given that the source is Gaussian. For $M = 1$, the MCK criterion performs slightly poorer than the CR in terms of QISI, but, for $M = 2$, the performance of the CR becomes more degraded. We recall that these two costs may present higher estimation errors for continuous sources and small number of samples, as discussed in Section 6.3, which might explain the CR behavior when M is increased. The correntropy and the MQD-C performance is practically kept the same by changing M , which suggests that, for this scenario (i.e., with a Gaussian source, a short length FIR channel and filter), $M = 1$ is sufficient for them.

6.5.3 Cost Surfaces - Scenario 3

In the last scenario of the cost surface analysis, we consider that the source statistics are estimated from a limited set of samples instead of relying on their analytical values. Situations like this commonly arise for continuous sources, whose analytical computation might be complex.

We assume that u_n is an *i.i.d.* signal associated with a continuous Laplace distribution, mathematically defined by:

$$f_U(v) = \frac{1}{2b} \exp\left(\frac{-|v - \mu|}{b}\right), \quad (6.56)$$

where $\mu = 0$ and $b = 2$ were chosen. The considered pre-coder has as transfer function $P(z) = 1 + 1.5z^{-1}$ and the channel is kept the same, $H(z) = 1 + 0.6z^{-1}$. Fig. 6.25(a) illustrates the histogram of the source s_n .

Although the distribution of u_n , $f_U(v)$, and the pre-coder $P(z)$ are assumed to be known, we will not obtain the analytical statistics of the source; contrarily, we will use this information to generate a set of samples to be used as reference signal s_n at the receiver. Note, however, that these samples will be different from the actually transmitted source (since it is an unsupervised scenario). As an example, we exhibit in Fig. 6.25(b) the estimated distribution $f_S(v)$ using a set of $N_s = 200$ samples, where two important issues must be noted: (i) the estimation might be poor and (ii) the estimated PDF is asymmetric. This might lead to important implications concerning the cost surfaces.

Using a given set of $N_s = 200$ samples of s_n , randomly generated (from the knowledge of $f_U(v)$ and $P(z)$), we have estimated the source statistics for M varying from 0 to 5, as

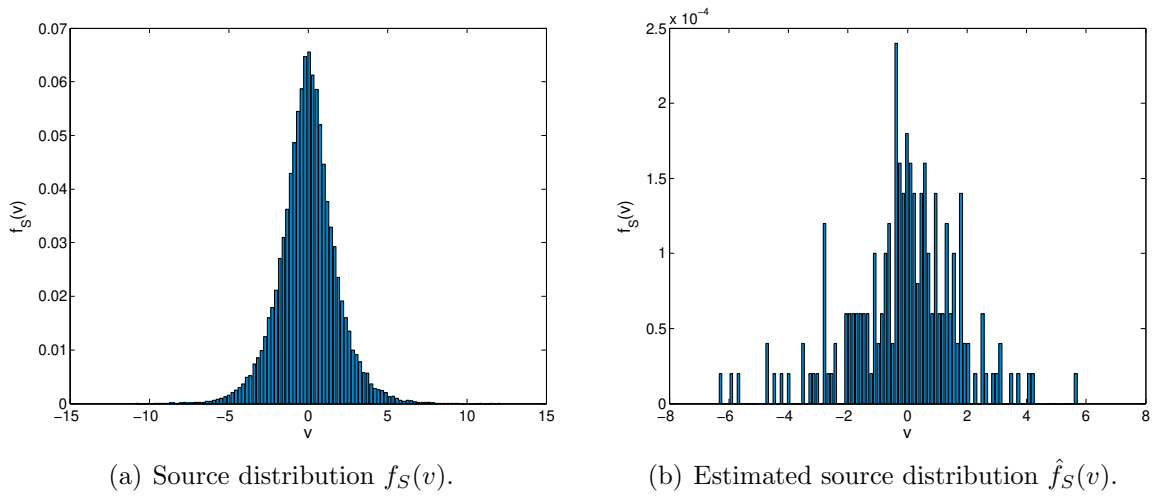


Figure 6.25: Costs Surfaces - Scenario 3: Source distribution and its estimation from samples.

shown in Fig. 6.26.

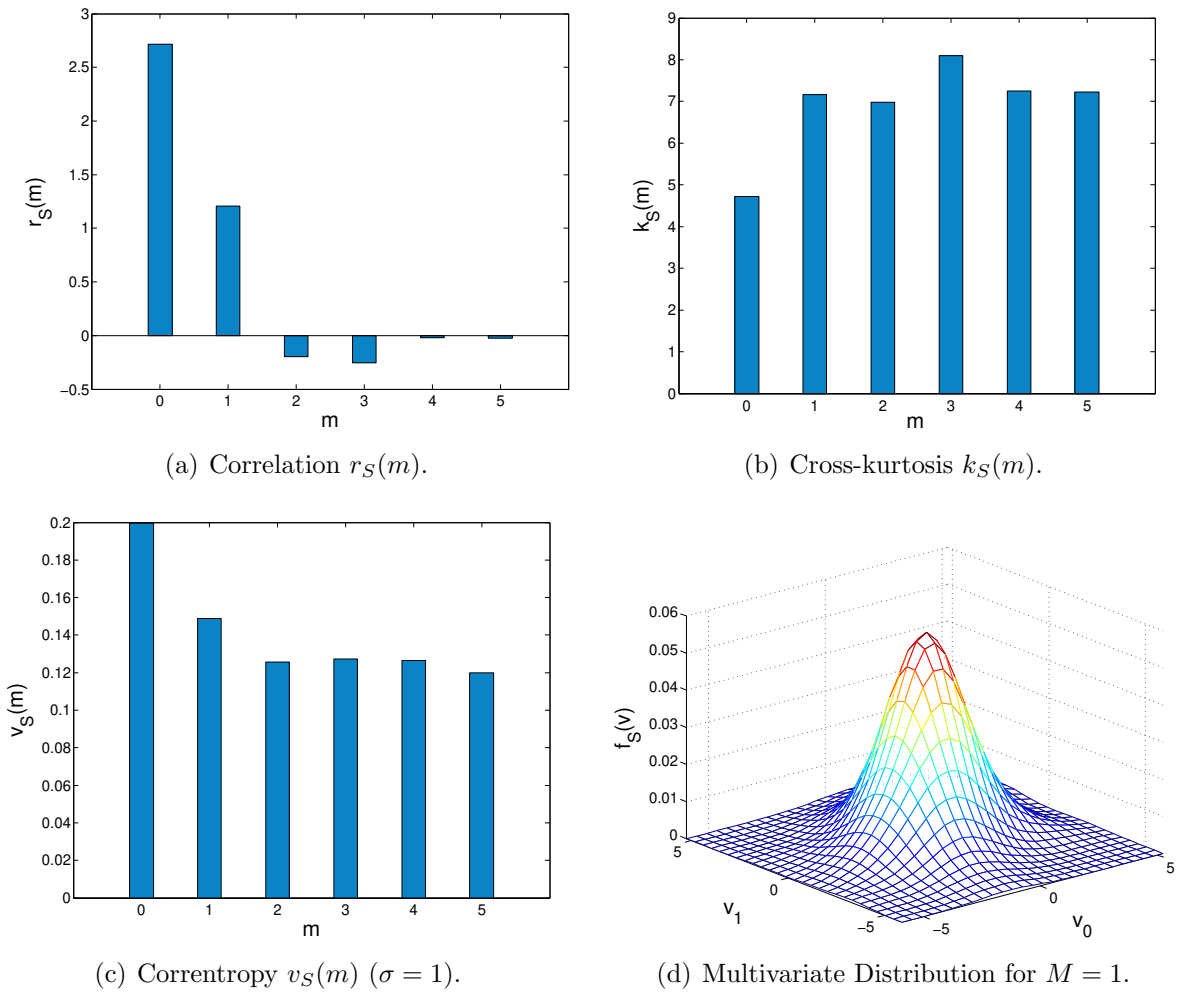


Figure 6.26: Cost Surfaces - Scenario 3: Estimation of the source statistics.

The same generated set will be used as reference samples s_n for the CR, the MCK, the correntropy-based and the MQD-C costs. We adopted $N_y = 200$ for all costs and the cases $M = 1$ and $M = 2$. For the correntropy-based and the MQD-C cost, the kernel sizes were chosen to be $\sigma_{cor} = 2$ and $\sigma_{MQD} = 0.5$, respectively. By varying the coefficients w_0 and w_1 from -2 to $+2$, we obtained the surface costs presented in Fig. 6.27. In comparison

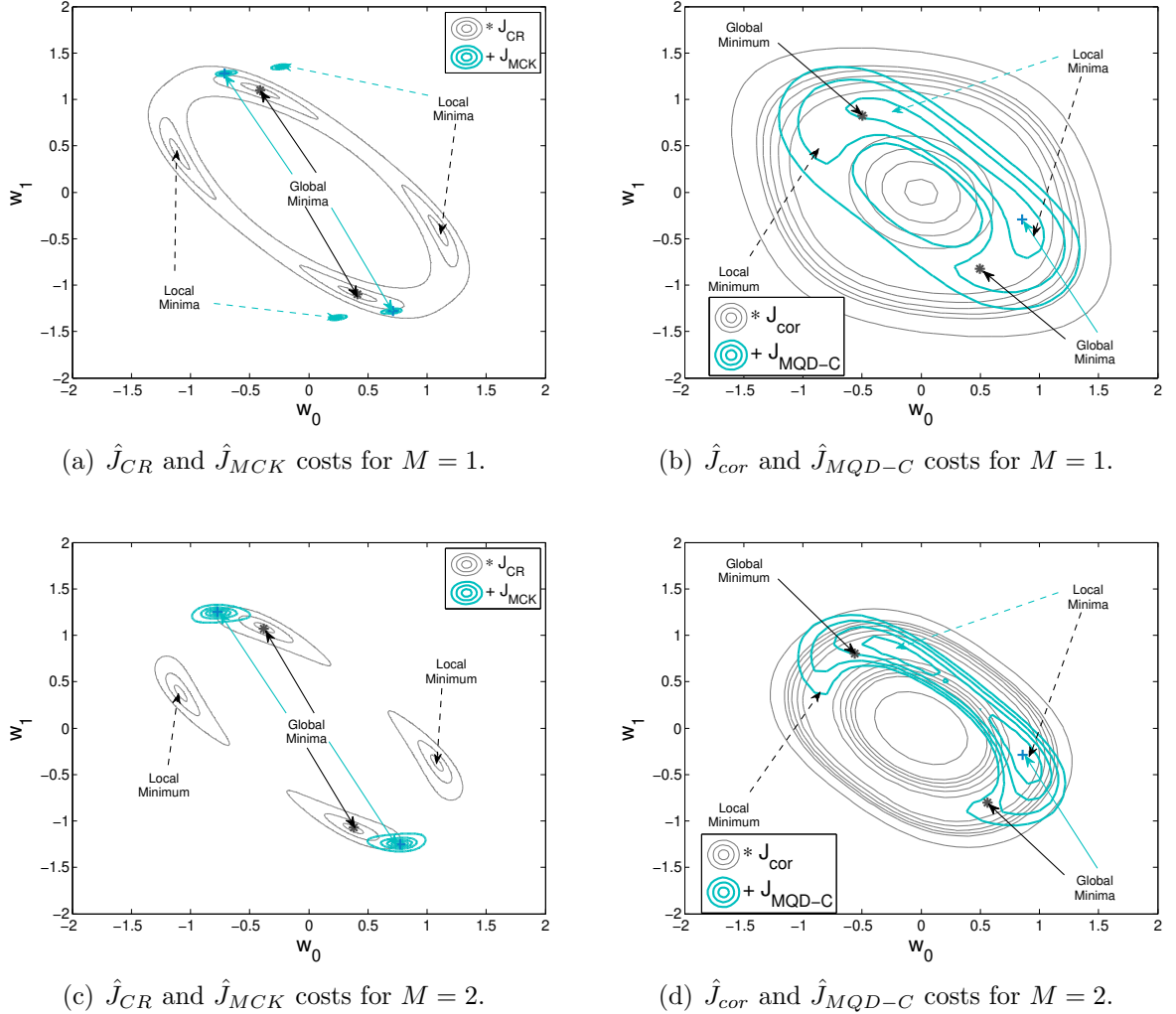


Figure 6.27: Cost Surface - Scenario 3: Surface contours for $M = 1$ and $M = 2$.

with the analytical Gaussian case, it is possible to note that the MQD-C cost is no longer symmetric with respect to the $w_0 = w_1$ axis, which is a direct consequence of the PDF $f_S(v)$ being asymmetric, and, due to this, there is a single global minimum for the MQD-C criterion. A similar effect was observed for the MCK cost when $M = 2$, where the asymmetry contributed to the local minima disappearance; however, for $M = 1$ the SOS is still strong and contributes to the presence of the local minima, as can be observed for the CR cost. The correntropy-based cost, just like the CR cost, kept the symmetry as well as the global and local minima.

In terms of performance, 30 experiments were carried out independently, where the

performances of the solutions found by the DE for each criteria were evaluated by the HISI and the QISI measure, whose mean values are displayed in Tab. 6.4. In comparison with

Table 6.4: Solutions performance measures for scenario 3.

		CR	MCK	cor	MQD-C
$M = 1$	HISI [dB]	1.6625	1.5726	1.2602	1.1325
	QISI [dB]	-0.6753	-1.5509	-2.3023	-2.8540
$M = 2$	HISI [dB]	1.2376	1.3773	1.6193	0.9639
	QISI [dB]	-3.2980	-1.8003	-2.5121	-3.3662

the previous scenario results in Tab. 6.3 (which is a valid comparison since the channel is the same), when $M = 1$, all criteria performances were worst in terms of both HISI and QISI. This reveals that all of them might suffer from estimation issues involving both the sources and the filter output, contributing to decrease the performance. By increasing M to 2, the performance is improved for all criteria in terms of the QISI, which can be considered more suitable in this scenario. Note, again that the MQD-C criterion performs better than the other criteria, which gives support to the idea presented in Section 6.3.1 that the MQD cost can present more reliable estimates from a reduced number of samples.

Finally, having these three scenarios in mind, it is possible to affirm that all criteria might present (undesired) local minima in scenarios where the ZF solution cannot be attained, an aspect that must be considered when adopting the optimization method. Moreover, it can be noted that, in general, by increasing the number of delays M , the HISI or the QISI performance associated with the criteria global solutions can be improved. In all cases, the MQD criterion was able to employ a larger amount of statistical information, leading to a better performance in comparison with the other criteria. However, a more detailed analysis will be carried out in the following section.

6.6 Performance Analysis

In order to properly evaluate the performance of the criteria, we consider from now on more complex scenarios involving larger pre-coders, channels and equalizers. The analysis will consider the cases in which: (i) the equalizer is not able to completely invert neither the pre-coder nor the channel; (ii) the equalizer is able to completely invert both the pre-coder and the channel; and (iii) the equalizer is able to completely invert channel but not the pre-coder. These pre-coder/channel/equalizer configurations will be distributed in scenarios encompassing discrete and continuous sources. For discrete sources, the source statistics will be analytically obtained, while, for continuous sources, they will be estimated from samples.

6.6.1 Discrete Source - Scenario 1

Starting with a discrete source, assume a binary *i.i.d.* signal u_n which is pre-coded by

$$P(z) = 1 + 2.1z^{-1} - 0.9z^{-2} + 0.4z^{-3} - 0.7z^{-4}, \quad (6.57)$$

i.e., a linear pre-coder of order $L_p = 4$. The pre-coder output s_n , is then transmitted through the channel with transfer function

$$H(z) = 0.76 - 0.25z^{-1} + 0.44z^{-2} - 0.02z^{-3}, \quad (6.58)$$

and there is the presence of AWGN with resulting SNR level of 20 dB. The equalizer is chosen to be a 5-tap FIR filter. Hence, again, there is no possibility of complete inversion of the channel, but we hope that the ISI can be at least partially mitigated.

Just like the previous cases, the distribution of u_n and the pre-coder $P(z)$ are assumed to be known, which allows us to analytically compute the correlation, the cross-kurtosis, the correntropy and the multivariate PMF of the source s_n . These values will be used as the target values for the considered criteria.

In a first step, the adaptation of the filter coefficients will be done with the aid of the DE metaheuristic with parameters: population size $N_P = 300$, adaptation step $F = 0.5$, crossover constant $CR = 0.9$ and maximum number of iterations 300, values that were chosen based on empirical tests that confirmed a wide exploration of the search space and a relatively high global convergence rate. For the criteria, $N_y = 200$ and M varying from 0 to 5 were considered. For the correntropy-based and the MQD-D costs, the kernel size σ was chosen based on the analysis of Section 6.3, being $\sigma_{cor} = 2$ for correntropy and $\sigma_{MQD} = 0.8$ for the multivariate PDF estimation (we used the reference value of σ for $M = 3$ in Fig. 6.14(b), since it is an intermediate value of M).

The objective will be that of evaluating the performance of the four studied criteria as a function of the number of delays M . For 25 independent trials, the equalizer was trained according to each criterion, and the solution found by the DE was evaluated in terms of the HISI and QISI performance measures. The mean values for each number of delays M are displayed in Fig. 6.28. In general lines, the HISI and the QISI measures revealed similar behavior, in a way that the analysis of only one of them is sufficient to obtain the evident conclusions: the MQD-D and the correntropy-based costs presented the best performances and, by increasing the number of delays, the performance is improved, but tends to a limit value. This suggests that there is a sufficient number of delays able to encompass the necessary information to perform equalization. Indeed, it is possible to note that, for $M = 4$, the criteria achieve lower values of HISI/QISI and, increasing M to 5, either the performance is just slightly improved or it remains the same. Hence, for this scenario, $M = 4$ can be a convenient choice, which is in accordance with the results shown in Chapter 5.

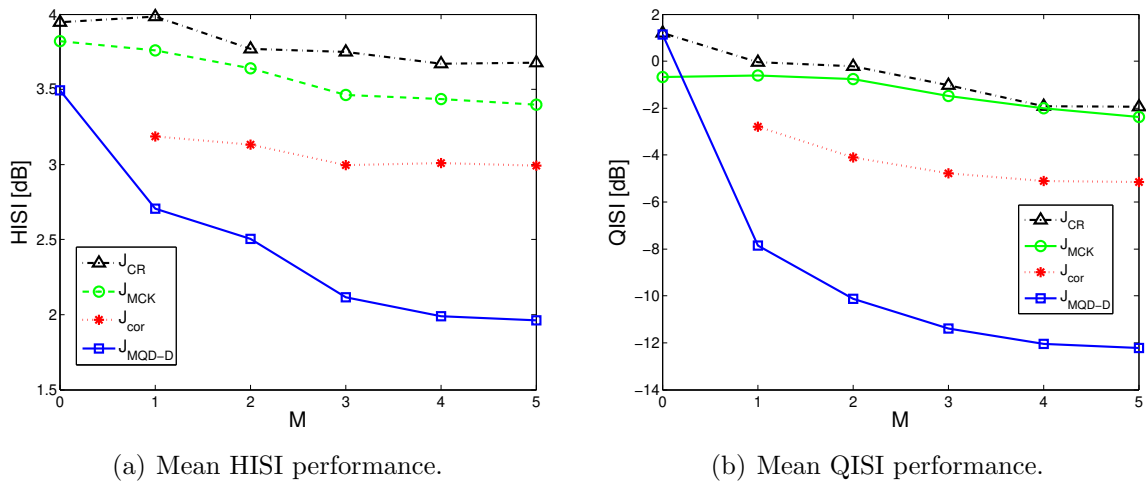


Figure 6.28: Discrete Sources - Scenario 1 - Mean HISI/QISI performance for the best solution found by the DE.

It is also clear that the MQD-D criterion can attain lower values of HISI/QISI while the correntropy-based criterion suffers certain type of limitation. This is a strong evidence that the multivariate distributions are able to encompass more statistical information. On the other hand, the CR and MCK criteria achieve HISI/QISI performance measures poorer than correntropy. Although their performance is also improved with M , the statistics considered by them limit their performance.

Algorithms Performance

As a classical procedure in channel equalization, it is also convenient to evaluate the gradient-based algorithm performance. In that sense, we consider the algorithms described in Section 6.2.2 with $N_y = 5$ and two cases for M : $M = 1$ and $M = 2$. The kernel sizes were the same adopted in the previous scenario, i.e., $\sigma_{cor} = 2$ and $\sigma_{MQD} = 0.5$.

Here, the objective of the analysis will be that of evaluating the convergence speed and the convergence to global optima. The performance measure used here will be only the QISI metric (Eq. (6.51)), since the HISI, in this case, provides the same conclusions as those of QISI – as in the previous metaheuristic optimization analysis.

For $M = 1$, the step sizes were chosen to be $\mu_{CR} = 3e-6$, $\mu_{cor} = 0.2$ and $\mu_{MQD} = 0.1$, with associated mean displacement of $1.5e-3$ ($N_{it} = 20000$ and $N_{conv} = 10000$); for $M = 2$, the step sizes were adjusted to $\mu_{CR} = 2e-6$, $\mu_{cor} = 0.08$ and $\mu_{MQD} = 0.3$, with mean displacement of $1.8e-3$ ($N_{it} = 20000$ and $N_{conv} = 15000$); the only exception was the MCK algorithm, whose step size adjustment faced instability issues, requiring a small step size of $\mu_{MCK} = 2e-10$ and $\mu_{MCK} = 1e-10$, for the $M = 1$ and $M = 2$ cases, respectively, being the mean displacement equal to $1e-6$ in both cases. The coefficient initialization was made following the center spike method, i.e., $\mathbf{w} = [0 \ 0 \ 1 \ 0 \ 0]^T$.

After running 50 independent experiments, the QISI performance along iterations was

computed, the mean values of which are displayed in Fig. 6.29. When $M = 1$, the CR,

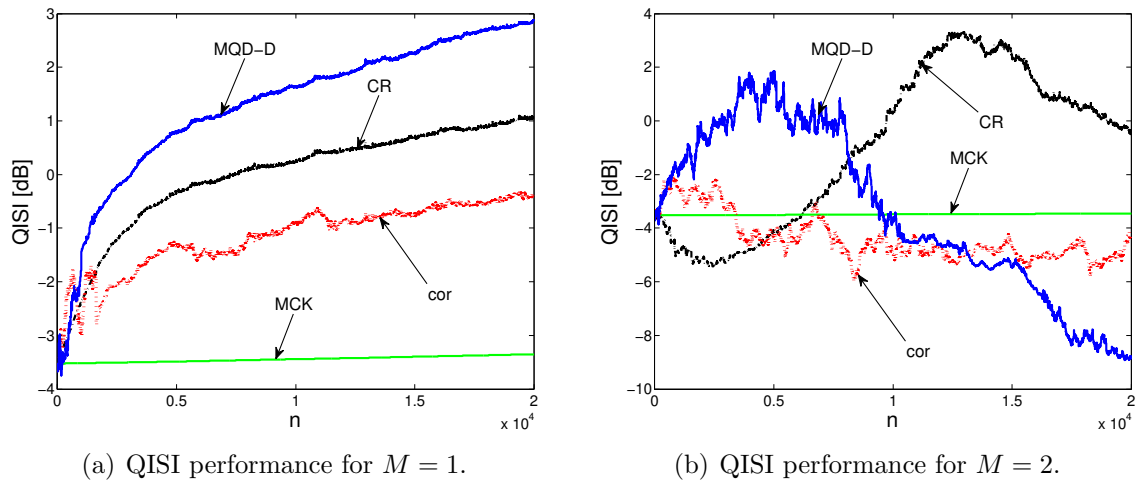
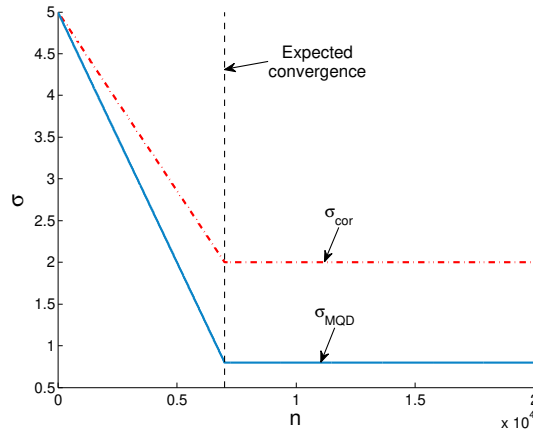
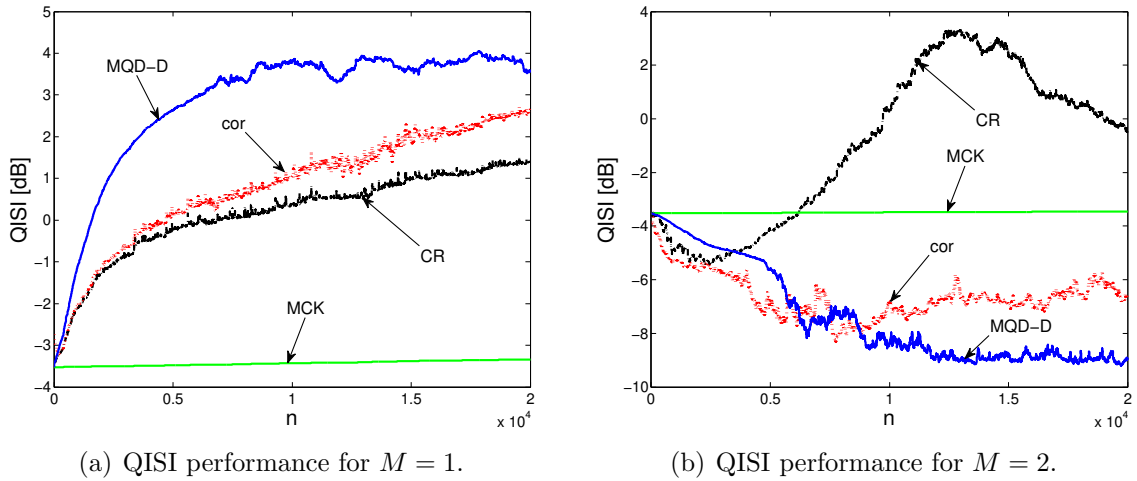


Figure 6.29: Discrete Sources - Scenario 1 - Algorithms QISI performance for $M = 1$ and $M = 2$.

the correntropy-based and the MQD-D algorithms converge to local minima, since the attained QISI level after convergence was higher than that found by the DE metaheuristic (Fig. 6.28(b)). By increasing M to 2, the correntropy-based and the MQD-D algorithms are able to achieve lower values of QISI, which are similar to the performance obtained by the DE, strongly suggesting that they converged to the global minima. Recalling that increasing M causes a smoothing effect on the correntropy and the MQD-D costs surfaces, this result is in consonance with the idea that larger values of M are able to reduce the number of local minima. On the other hand, the MCK algorithm faces stability issues, as it encompasses terms to the power up to four, which might result in an unstable behavior.

Very interestingly, the correntropy-based and the MQD-D algorithms are able to use an adaptive kernel size σ to aid their convergence. For instance, a large σ value can be assumed at the initial iterations, so that its smoothing properties reduces the local convergence rate. After that, the σ value can be gradually reduced until the desired kernel size value is achieved (this procedure is sometimes called *kernel annealing* [Principe, 2010]). Based on this, we adopted adaptive values for σ varying accordingly to Fig. 6.30. In other words, the kernel size is linearly reduced from an arbitrary large value to the desired value in N_{conv} iterations; after this stage, its value is kept constant for the algorithm final convergence. Using this approach, the QISI performance of the algorithms are presented in Fig. 6.31. It is clear that the convergence of the correntropy-based and the MQD-D algorithms becomes smoother and even faster, achieving convergence in $N_{conv} = 12000$ iterations. Note, however, that this approach does not avoid local convergence in the $M = 1$ case (it might improve the global convergence in certain cases, but the result will depend on the coefficient initialization).

Figure 6.30: Adaptive kernel size σ .(a) QISI performance for $M = 1$.(b) QISI performance for $M = 2$.Figure 6.31: Discrete Sources - Scenario 1 - Algorithms QISI performance for varying σ and for $M = 1$ and $M = 2$.

Robustness Against Noise - ISI x SNR Curves

In order to evaluate the criteria robustness against noise in a more extensive manner, we resort to the analysis of the ISI x SNR curve, encompassing Gaussian and impulsive noise. We consider again the same scenario of Section 6.6.1, the only difference being that now the noise signal η_n shall have its energy varied to ensure a given SNR level.

When the noise is Gaussian, its energy can be simply controlled by the variance σ_η^2 ; however, when the noise is impulsive, a more complex control is demanded, given the higher complexity of its PDF:

$$f_\eta(v) = \epsilon G_{\sigma_1^2}(v) + (1 - \epsilon) G_{\sigma_2^2}(v), \quad (6.59)$$

being $\sigma_1 \gg \sigma_2$ usually adopted, and a small value for ϵ . In our simulations, we considered $\epsilon = 0.1$ and a constant rate $\sigma_1^2/\sigma_2^2 = 15$. With this fixed relation, the values of σ_1 and σ_2 were adjusted to obtain the desired SNR level. The chosen parameters were similar to

those of the previous case, i.e., $N_y = 200$, $\sigma_{cor} = 2$ for correntropy, $\sigma_{MQD} = 0.8$ for the MQD-D cost and M varying from 0 to 5.

Again, we used the DE metaheuristic to search for the optimal solution in 25 independent experiments, whose parameters were $N_P = 300$, $F = 0.5$, $CR = 0.9$ and maximum number of iterations of 300. The mean QISI values as a function of the SNR level are displayed in Fig. 6.32 for the Gaussian and the impulsive noise cases. As expected, the best

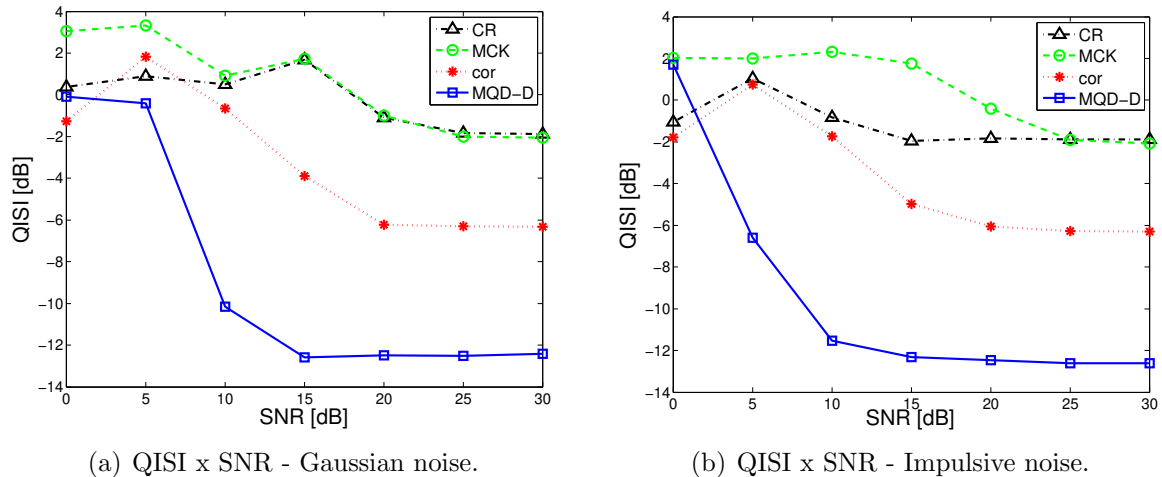


Figure 6.32: QISI x SNR - Gaussian and impulsive noise ($M = 4$).

QISI performance is achieved for higher SNR levels, but, it is possible to note that the MQD-D criterion can be more robust, since it still presents a relatively good performance (≈ -10 dB) for an SNR of 10 dB, while the other criteria require an SNR of 15 dB or more. For the impulsive noise, Fig. 6.32(b), the criteria seem to be more robust. The MQD-D criterion, for instance, achieved a reasonable QISI performance (≈ -6.5 dB) with an SNR level of 5 dB. The exception lies on the MCK criterion, whose terms involving the fourth power show to be more sensitive to the spikes present on the impulsive behavior of the noise (mainly for low SNR values). We emphasize that, in both noise types, the MQD-D criterion provided greater robustness against noise, a direct result of the more precise estimation of the multivariate PDFs via the kernel methods, as observed in Section 6.3.2.

6.6.2 Discrete Sources - Scenario 2 - IIR Filtering

The previous scenario considered the case in which neither the channel nor the pre-coder can be inverted, since the equalizer, as well as the channel and pre-coder, were FIR systems. Now, we consider the case in which the equalizer is an IIR filter long enough to invert both channel and pre-coder. Recalling Chapter 5, this case may lead to ambiguous solutions for the proposed criteria, which are not suitable for blind colored channel equalization. Since these recursive structures establish non-linear relations between the filter coefficients and the filter output, the gradient-based algorithms will not be considered

here, being left for future work.

Again, an *i.i.d.* BPSK modulated signal u_n is generated, being pre-coded by the system with transfer function $P(z) = 1+0.5z^{-1}$. The resulting signal s_n is transmitted through the channel $H(z) = 1+0.6z^{-1}$ and there is AWGN interference with SNR level of 25 dB. The adopted IIR equalizer has as transfer function

$$W(z) = \frac{b_0 + b_1z^{-1}}{1 + a_1z^{-1} + a_2z^{-2} + a_3z^{-3}}, \quad (6.60)$$

whose coefficients b_0, b_1, a_1, a_2 and a_3 will be adapted using the DE metaheuristic with parameters $N_P = 300, F = 0.5, CR = 0.9$ and maximum number of iterations 300. Remark that the IIR equalizer is able to assume the form $W(z) = \hat{P}(z)/(H(z)P(z))$, being $\hat{P}(z)$ a permuted version of $P(z)$, which is a plausible solution for the CR, the MCK and the correntropy-based criteria.

For all criteria we adopt $N_y = 200$ and M varying from 0 to 5. The kernel sizes were the same of the previous scenarios, i.e., $\sigma_{cor} = 2$ for correntropy and $\sigma_{MQD-D} = 0.8$ for the MQD-D criterion.

We performed 30 independent experiments whose solutions found by the DE metaheuristic were evaluated in terms of HISI and QISI. The average performance is as displayed at Fig. 6.33. Although all criteria are able to achieve the ZF condition, it turns

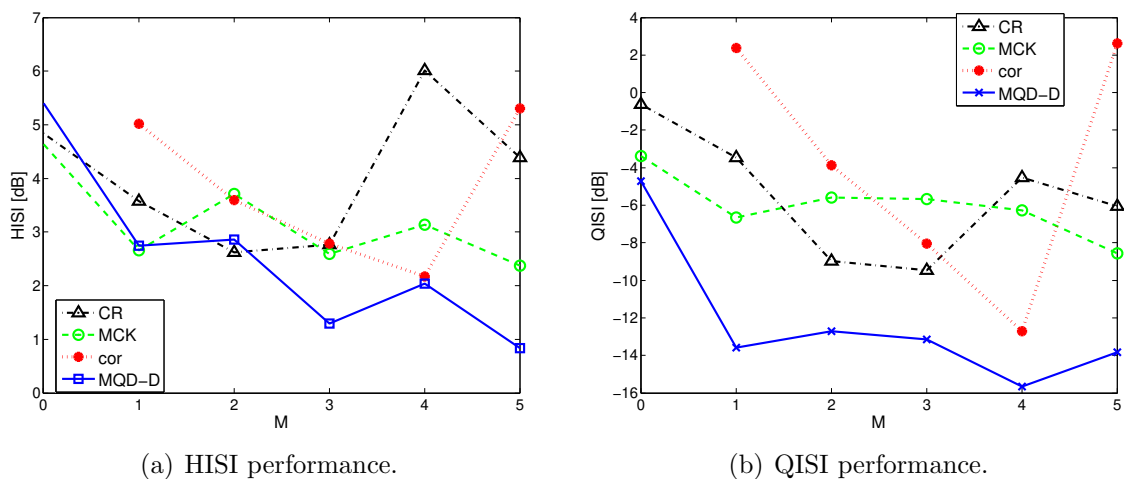


Figure 6.33: Discrete Sources - Scenario 2 - IIR equalizer.

out that the MQD-D attains lower values of HISI/QISI. In fact, the CR, the MCK and the correntropy-based criteria are also capable of converging to the ZF solution, but the average performance is reduced since they might also converge to solutions of the type $W(z) = \hat{P}(z)/(H(z)P(z))$, which are not adequate for colored blind channel equalization and are usually associated with lower HISI/QISI values. Fig. 6.33 also shows that the number of delays M must be larger than or equal to 1 – as stated in Chapter 5 – in order that the algorithms achieve a good solution. It is possible to note that by increasing M ,

the performance can be improved, since more temporal information can be encompassed up to a limit.

6.6.3 Continuous Source - Scenario 1

In this scenario, we assume that u_n is an *i.i.d.* signal associated with a continuous Laplace distribution, as defined in Eq. (6.56). Then, u_n is pre-coded by $P(z) = 1 + 0.5z^{-1}$, the resulting source s_n being transmitted by the minimum-phase channel $H(z) = 1 + 0.6z^{-1}$, with AWGN of an SNR level of 20 dB. The histogram of the source s_n is as shown in Fig. 6.25(a), which is very similar to a Gaussian distribution (due to the Gaussianizing effect on the pre-coding step). In this case, the QISI metric provides a more suitable performance measure and, for this reason, we will omit the HISI results. The equalizer is assumed to be a 4-tap FIR filter.

Here, we assume that the source statistics must be estimated instead of using their analytical values. We consider that a set of reference samples can be generated at the receiver by assuming that the distribution of u_n , $f_U(v)$, and the pre-coder $P(z)$ are known. Undoubtedly, the generated set of reference samples will differ from the transmitted source (similar to scenario 3 in Section 6.5), but they may provide valuable statistics. In that sense, we randomly generate a set of $N_s = 200$ samples with the same distribution of $f_U(v)$ and filter it with the known pre-coder transfer function $P(z)$; the resulting signal is used to yield reference samples s_n for the CR, the MCK, the correntropy-based and the MQD-C criteria. It is also assumed that there are a limited number of samples at the equalizer output, i.e., with $N_y = 200$ for all criteria.

For comparison purposes, we also consider the case in which a larger number of samples can be used, i.e., $N_s = 2000$. However, in order to avoid the computational burden, the source statistics are estimated once and stored for the use on the receiver. More specifically, the correlation, the cross-kurtosis and the correntropy profile of the source (for the number of delays M considered) are estimated according to Eqs. (6.5), (6.13) and (6.1), respectively. Regarding the MQD-C criterion, the multivariate source PDF estimated from samples was stored via the RBF approach described in Section 6.2.1, where 30 centers (using the k -means [Haykin, 1998]) and weights of Gaussian kernels were used. For the equalizer, we kept $N_y = 200$ for all criteria.

The kernel sizes were adjusted to $\sigma_{cor} = 2$ and $\sigma_{MQD} = 0.5$ for the correntropy-based and the MQD-C costs, respectively; the number of delays M were assumed to vary from 0 to 5. To perform the search for the minima, we used the DE metaheuristic with parameters $N_P = 200$, $F = 0.5$, $CR = 0.9$ and maximum number of iterations 200. In 25 independent experiments, the mean QISI performance for the cases with $N_s = 200$ and $N_s = 2000$ are as displayed in Fig. 6.34. It is possible to note that all criteria suffer with the source statistics estimation errors, since the QISI levels are higher in Fig. 6.34(a) than

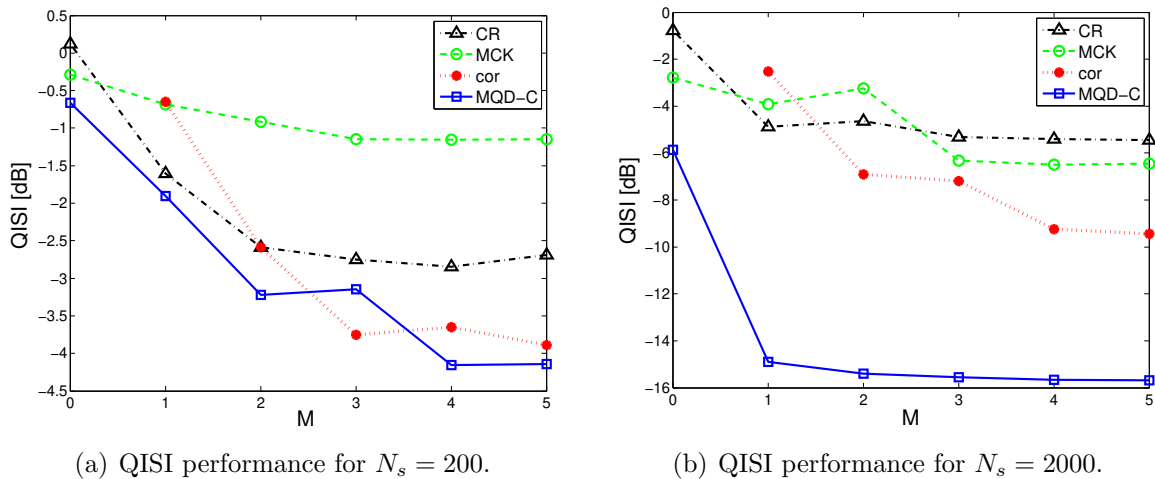


Figure 6.34: Continuous Sources - Scenario 1: Laplacian source.

in Fig. 6.34(b). Hence, it is strongly recommended to obtain reliable sources statistics as they can provide considerable improvement in the performance. Individually, the performances of the criteria were similar to those of the discrete case (Fig. 6.28), i.e., again, the multivariate PDF-based approach performed better than the others, being followed by the correntropy-based, MCK and CR criteria (Fig. 6.34(b)). In addition, it is possible to observe that increasing M can improve the performance, but $M = 1$ is sufficient for equalization (since $L_p = 1$, as discussed in Chapter 5).

Algorithm Performance

Similarly to the discrete counterpart, we also consider the gradient-based algorithms to search for the criteria solutions. The scenario is the same of the previous case. The source statistics were estimated with $N_s = 2000$ samples.

The criteria parameters are $N_y = 5$ and two cases for M ($M = 1$ and $M = 2$). The step sizes μ were adjusted using the equal mean displacement measure given by Eq. 6.50. For $M = 1$, the step sizes were chosen to be: $\mu_{CR} = 3e-6$, $\mu_{cor} = 0.2$ and $\mu_{MQD} = 0.008$, with associated mean displacement of $1e-3$; for $M = 2$, the step sizes: $\mu_{CR} = 2e-5$, $\mu_{cor} = 0.08$ and $\mu_{MQD} = 0.08$, with mean displacement of $disp_w = 1.2e-3$. Again, we opened an exception for the MCK algorithm due to instability issues, whose step sizes were chosen to be $\mu_{MCK} = 2e-10$ (mean displacement of $disp_w = 7e-6$) and $\mu_{MCK} = 1e-10$ (mean displacement of $disp_w = 3e-6$), for $M = 1$ and $M = 2$, respectively. The coefficient initialization was based on the center-spike method, however, since there is no center tap, it was considered that $\mathbf{w} = [0 \ 1 \ 0 \ 0]^T$. The adopted kernel sizes were $\sigma_{cor} = 2$ and $\sigma_{MQD} = 0.5$, for correntropy-based and the MQD-C algorithms, respectively.

For 50 Monte-Carlo simulations, the mean QISI performance along iterations for $M = 1$ and $M = 2$ is as displayed in Fig. 6.35. When $M = 1$, all the algorithms converged to local minima, with exception of the correntropy-based algorithm, which converged to

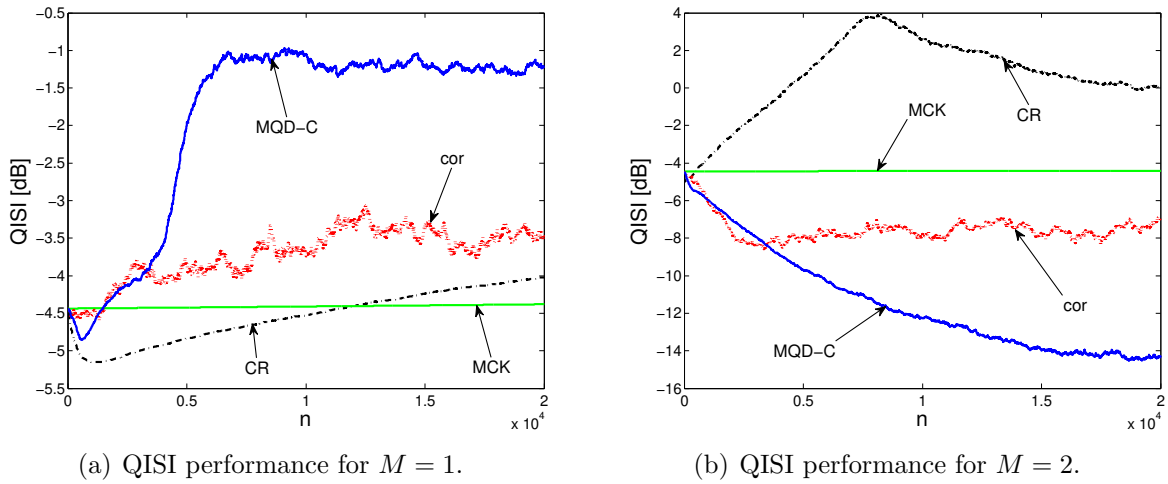


Figure 6.35: Continuous Sources - Scenario 1: Algorithms QISI performance for $M = 1$ and $M = 2$.

a QISI level similar to that found by the DE metaheuristic, as shown in Fig. 6.34(b). By increasing M to 2, the correntropy-based and the MQD-D algorithms are able to achieve lower values of QISI, similarly to the DE performance. Again, the increment in the number of delays M contributed for the performance improvement, but the CR algorithm still converges to a local minimum. The MCK algorithm suffers from instability issues and must keep an extremely small step size, which compromises its performance.

Similarly to the discrete case, it is also possible to adopt a varying kernel size. However,

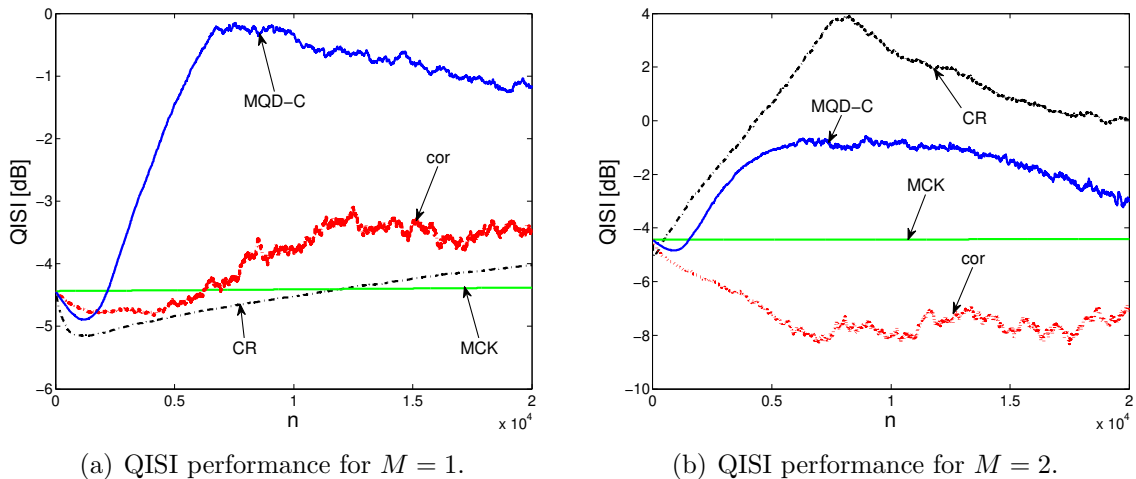


Figure 6.36: Continuous Sources: Algorithms QISI performance for varying σ and for $M = 1$ and $M = 2$.

as mentioned in the cost surface analysis, the continuous case already presents smoother costs and, by using large kernel sizes σ , the surfaces can become oversmoothed. Indeed, by applying the variable σ in the correntropy-based and the MQD-C algorithms, the mean QISI performance is as illustrated in Fig. 6.36 and, as can be noted, the large kernel sizes

only delayed the convergence of the algorithms, with a more severe effect on the MQD-C algorithm.

IIR Filtering

For the same Laplacian source signal, pre-coder $P(z) = 1 + 0.5z^{-1}$, minimum-phase channel $H(z) = 1 + 0.6z^{-1}$ and AWGN noise of 20 dB, we consider now the use of an IIR equalizer with transfer function given by Eq. 6.60. As in the discrete case, this IIR equalizer is able to obtain solutions like $W(z) = \hat{P}(z)/(H(z)P(z))$, which inverts both channel and pre-coder, and generate a permuted version of the pre-coder. Indeed, we know that this might lead to undesired solutions for the CR, MCK and correntropy-based criteria, however, as we are dealing with estimated source statistics, the costs and the solutions present some changes, as discussed in Section 6.5, scenario 3.

The criteria parameters are adjusted to $N_y = 200$ and with kernel sizes $\sigma_{cor} = 2$ and $\sigma_{MQD} = 0.5$, for the correntropy-based and the MQD-C costs, respectively. The number of delays M will vary from 0 to 5 and the source statistic will be estimated from $N_s = 2000$ samples, as in the previous section. After 30 Monte-Carlo runs, the mean QISI performance is obtained, being its values illustrated in Fig. 6.37. The results

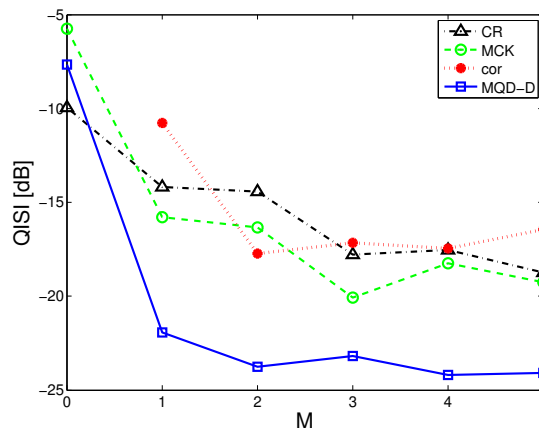


Figure 6.37: Laplacian Source: IIR equalizer.

are somewhat similar to those of the discrete case, Fig. 6.33(b), where the use of the multivariate distributions are able to extract more information and to solve ambiguities, resulting in the best performance. Although it is known that the asymmetry on the source statistics can reduce the number of minima, as depicted in Fig. 6.27, the ambiguities are not solved and the CR, the MCK and the correntropy-based approaches still converge to undesired solutions, reducing their performance.

6.6.4 Continuous Source - Scenario 2: Image Processing

In the second continuous source scenario, we consider the case in which a 100×100 -pixel image has been column-wise distorted by a linear system with transfer function

$H(z) = 0.2258 + 0.5161z^{-1} + 0.6452z^{-2} + 0.5161z^{-3}$ [Lázaro et al., 2005] and there is AWGN with resulting SNR of 20 dB. The original image and the distorted one are presented in Fig. 6.38(a) and Fig. 6.38(b).

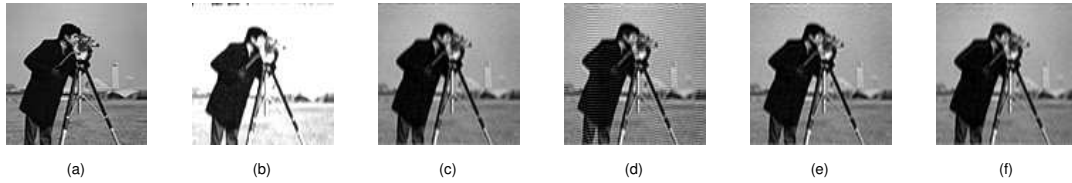


Figure 6.38: Image processing: (a) original; (b) received; recovered by (c) the CR, (d) the MCK, (e) the correntropy-based and (f) the MQD-C approach.

We assume that the original image was available to obtain estimates of the correlation, the cross-kurtosis, the correntropy and the joint PDF – via the Parzen window method, Eq. (6.29) –; however, after that, the samples were no longer available for the image recovery process. Since there is no prior knowledge of the dependence between samples, we empirically choose $M = 3$, as it should be able to allow a significant use of information about statistical dependence. The kernel size σ was considered to be 0.5 for the MQD-C – and the joint PDF estimation – and 2 for the correntropy. The joint PDF estimated from the original samples was stored by means of 30 centers and weights, obtained through an RBF with Gaussian kernels as activation functions, as described in Section 6.2.1. The correlation, cross-kurtosis and correntropy values of the source for $M = 3$ delays were recorded as well.

For illustration purposes, we exhibit in Fig. 6.39 the estimated source statistics. From the correlation, cross-kurtosis and correntropy, it seems that the temporal structure of the image signal is very long (at least for 5 delays), which corresponds to a long pre-coder $P(z)$.

Now, the distorted image will be filtered by an IIR linear equalizer

$$W(z) = \frac{b_0 + b_1z^{-1}}{1 + a_1z^{-1} + a_2z^{-2} + a_3z^{-3}}, \quad (6.61)$$

whose coefficients b_0 , b_1 , a_1 , a_2 , a_3 and a_4 are free parameters. Note that, in this case, the channel can be completely equalized, but the temporal structure of the image is long enough to avoid ambiguities on the solutions.

Since we have the original source statistics estimates, we can employ the CR, the MCK, the correntropy-based and the MQD-C criteria to recover the image quality from its distorted version. However, in order to reduce the computational cost, the equalizer will have access of only two randomly chosen columns of the Fig. 6.38(b) (equivalent to 200 pixel samples) for estimating the costs. By employing the DE metaheuristic for optimization, we can recover the images shown in Figs. 6.38(c) to (f). We can see that all criteria were able to recover the image with a considerably good quality, except for

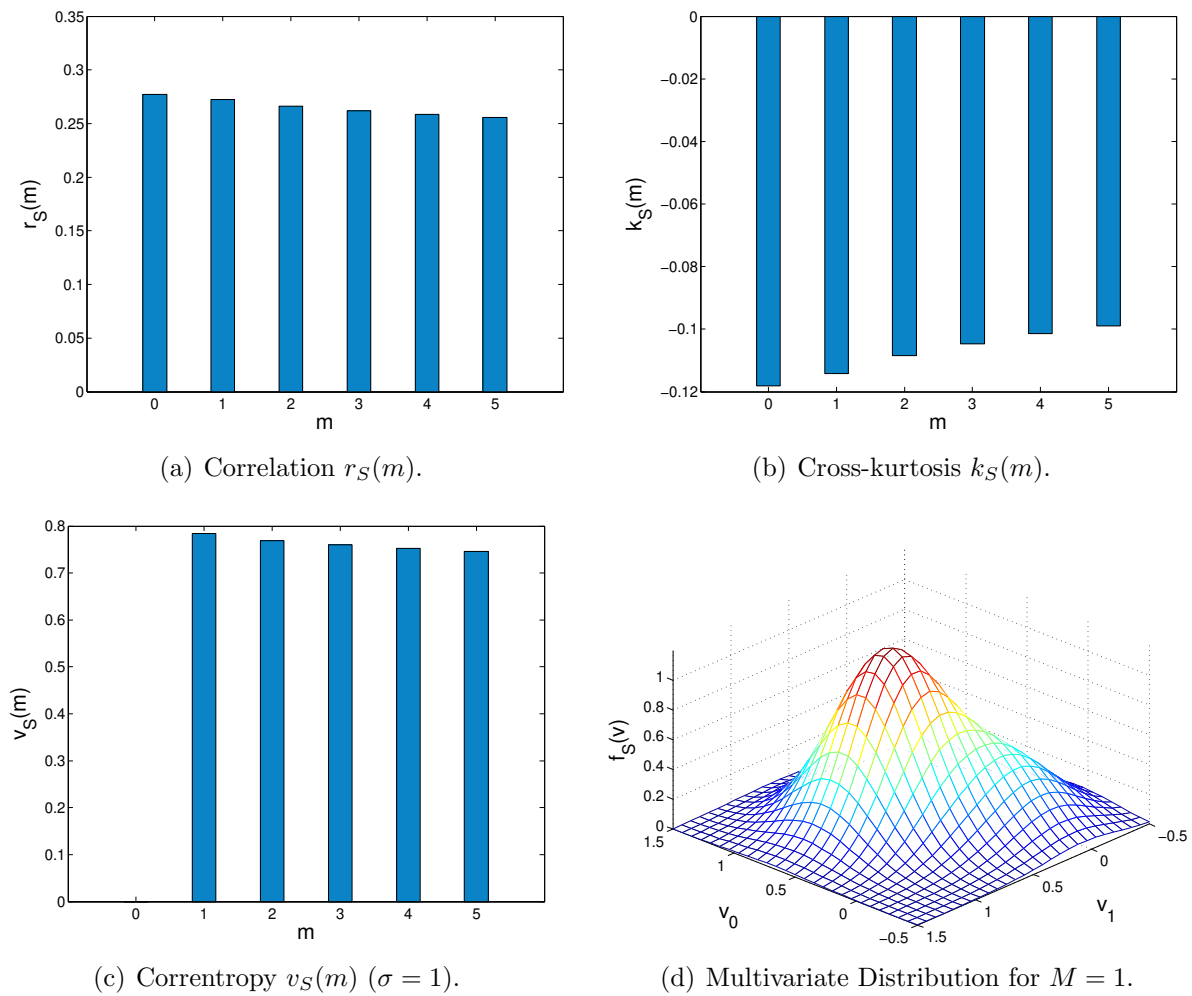


Figure 6.39: Image processing: Estimation of the source statistics.

the presence of noise, which was partially mitigated. The resulting MSE (after sign and variance correction) for each criteria solution found by the DE is as exhibited in Tab. 6.5. The CR, the correntropy-based and the MQD-C criteria presented similar results, while

Table 6.5: Image Processing - MSE values for the CR, MCK, cor and MQD-C criteria.

		CR	MCK	cor	MQD-D
$M = 3$	MSE	0.0316	0.0340	0.0328	0.0323

the MCK performed poorly. Indeed, it is possible to see in Fig. 6.38(d) that there are some residual noise errors, probably due to a poor estimation of the cross-kurtosis.

In fact, in this scenario, all criteria are equally likely to achieve the ZF solution, since there are no pre-coder ambiguities to deal with, given the excessively long temporal structure of the source. This might demand a large number of delays M to extract the dependence found in data. However, as can be noted, the choice of $M = 3$ can be a reasonable trade-off between performance and computational complexity in these cases.

6.7 Conclusions

The extension of the BGR and the SW theorems towards the colored blind equalization problem, studied in the previous chapter, provided us with sufficient elements to conceive criteria compliant with the necessary conditions for equalization. In that sense, we performed in this chapter the investigation of three criteria underlying the study of the theorems: *(i)* the correlation retrieval (CR), already proposed by our research group in [Fantinato et al., 2013]; *(ii)* the matching of the cross-kurtosis (MCK), a novelty in the equalization problem; and *(iii)* the matching of multivariate distributions (MQD), an original proposal that combines the multivariate kernel density estimators and the notion of quadratic divergence. The main concern was the investigation of these criteria as well as the correntropy matching approach, the state-of-the-art in colored blind equalization.

The criteria were presented encompassing aspects like the analytical calculus of the costs and their estimation, as well as their gradient calculus for the application in gradient-based methods for optimization. It is important to emphasize that the described method for analytical computation of the correntropy is also a contribution of this work (in the literature, the correntropy is analytically analyzed in terms of its Taylor series expansion [Principe, 2010; Yang et al., 2011]). Next, some statistical estimation issues like number of samples, number of delays and noise disturbances were analyzed, encompassing all considered criteria. For the correntropy and the multivariate distribution estimation, the analysis of the kernel size was also considered, in which its adjustment must be done considering the scenario (discrete or continuous data samples), number of samples and number of delays. In general terms, the correlation (CR), the cross-kurtosis (MCK) and the correntropy revealed certain estimation quality reduction when the number of delays is increased, requiring a larger number of samples to counterbalance the number of delays. For the multivariate density estimation, very interestingly, the so-called “curse of dimensionality” proved to be untrue when the estimation is done via multivariate kernel density estimators, in which a given number of samples, say 100 samples, is sufficient to obtain reliable estimates of 3, 4 or 5-dimension distributions. Particularly, this is a very attractive feature of the multivariate distributions, since their computational cost can be drastically reduced if the number of samples is small.

The surface costs were also analyzed in discrete and continuous scenarios, from the analytical and estimated source statistics perspective, being assumed FIR models for channels and equalizers. In all cases, all the costs presented local minima, which may not be suitable in terms of equalization. Hence, the optimization method must be chosen taking this information into account. Generally, by increasing the number of delays, all the costs tend to become smoother and the global minima tend to provide better solutions in terms of ISI reduction. When the source statistics are estimated, the MCK and the MQD costs might reduce the number of minima, or even become asymmetric, as occurs with

the MQD cost. Finally, for the correntropy-based and the MQD costs, the kernel size can also be adjusted to control the smoothness of their surface, but the minima position may change, potentially causing a reduction on the quality of the solution. Hence, a suitable value for the kernel size must be picked in order to obtain the desired performance.

A more detailed analysis of the criteria performance was considered in some communications scenarios involving colored sources. In this study three possible configurations of the pre-coder/channel/equalizer deserve to be outlined: (i) the equalizer is not able to completely invert neither the pre-coder nor the channel; (ii) the equalizer is able to completely invert both the pre-coder and the channel; and (iii) the equalizer is able to completely invert the channel but not the pre-coder. In the first configuration, we analyzed the case in which both channel and equalizer were modeled by FIR filters (and also the pre-coder) and, by searching the solutions via the DE metaheuristic, we could observe that the performance reducing the ISI is somehow proportional to the amount of statistics encompassed in the criteria, i.e., the CR criterion, which only considers the SOS, performed poorer; the MCK criterion, which, besides the SOS, also encompasses the fourth order statistics, performed better than the CR criteria, being surpassed by the correntropy-based criterion, which, since Gaussian kernels were considered, was able to encompass all the even statistical moments; but the best performance was achieved by the MQD cost, which, by using the distributions information, makes use of all statistical moments. Furthermore, by increasing the number of delays, the performances of the criteria were also improved, but tended to a limit value. However, a good performance can be attained only if the number of delays considered is larger than the pre-coder length (as discussed in Chapter 5). It is important to emphasize that these general results were obtained in both discrete and continuous scenarios. The gradient-based algorithms were also considered as optimization tools, where the increase of the number of delays aided the convergence to global solutions, but we emphasize that local converge might still happen and should be a major concern when using this optimization approach. For the configuration (ii), the channel could be completely equalized, but also the pre-coder. In this case, the CR, the MCK and the correntropy-based criteria presented reduced performance in the ISI removal in comparison with the MQD criterion, since they may converge to ambiguous solutions of the pre-coder, as mentioned in Chapter 5. At last, for configuration (iii), an image processing scenario is considered, whose temporal structure of the data is considerably long and cannot be inverted, only the channel. In this case, the ambiguities of pre-coder no longer exist and the criteria becomes equally likely to obtain the desired solution. Indeed, the obtained performances of all criteria are very close in this case.

In summary, the MQD criteria (in its continuous or discrete version) showed their wide potential in extracting the data temporal structure information, outperforming correntropy, the state-of-the-art in the context of colored blind equalization, and the other considered criteria, CR and MCK. Indeed, from the present analysis, it is clear that,

among the considered criteria, the MQD seems to be the most suitable, since it carries no ambiguity for the pre-coder and also is able to obtain more reliable estimates from a reasonably small amount of samples, even when the considered number of delays is relatively high.

Finally, this theoretical analysis on the criteria for colored blind channel equalization shows that it is possible to apply the direct processing of colored signals, which, as mentioned, can open a wide horizon of potential applications, such as image, video and audio processing as well as the use of coding schemes in symbolic level, which might considerably improve the performance in communications scenarios, given the vaster exploration of the redundancy present in data.

Chapter 7

Adaptive IIR Equalization Based on Information Theoretic Learning

IIR filters were object of intensive study along the decades of 1970 to 1990 [Horvath Jr., 1976; Johnson Jr., 1984; Goodwin and Sin, 1984; Treichler, 1985; Long et al., 1987; Regalia, 1994], counting with applications in a diverse set of problems, such as system identification, adaptive control, linear prediction, channel equalization and echo cancellation. After the year 2000, some efforts regarding the IIR filters were aimed at the use of metaheuristics/evolutionary algorithms for adaptation, which have shown to be a more robust technique than that based on the gradient methods [Chen, 2000; Krusienski and Jenkins, 2004; Chen and Luk, 2010]. Notwithstanding, there remains a gap concerning novel criteria for training these structures, which motivates us to study this problem using the concepts and methods from ITL [Principe, 2010], as well as their extension to encompass the temporal information more efficiently.

Within the scope of IIR filtering, it is of particular interest the inherent nonlinear relationship that arises between the coefficients of the IIR filter and its output y_n . On the one hand, this feature allows a significant flexibility of the structure, but, on the other hand, it may lead to some difficulties in terms of the mathematical manipulation. In view of this, there are two formulations that are able to aid the adaptation of the IIR filters, which are based on different approximations of an error signal e_n : these formulations are termed equation-error and output-error (presented in Section 4.2.2 of Chapter 4). Their importance is directly related to the gradient-based algorithms they engender, which are the *Least-Mean-Square* (LMS) – for the equation-error formulation –, the *Pseudolinear Regression* (PLR) and the *Recursive Prediction Error* (RPE) – both for the output-error formulation. Given their importance in IIR signal processing tasks, we will adopt these two formulations for the ITL methods, whose objective is to extract the statistical information about the underlying signal in a more extensive manner. This will be the main objective of this chapter.

Before presenting the proposed ITL criteria to be studied in this chapter, we discuss the main features considered in the equalization problem when using an IIR equalizer. In the sequence, the proposed ITL criteria will be adapted based on the LMS, PLR and RPE approaches to be used as gradient-based algorithms. Finally, the performance of the resulting algorithms will be evaluated, from which we will be able to outline the main conclusions of this study.

7.1 Supervised Equalization Using IIR Equalizers

In this chapter, we consider the problem of channel equalization from a supervised standpoint. Additionally, the equalizer is assumed to be an IIR filter. Fig. 7.1 shows

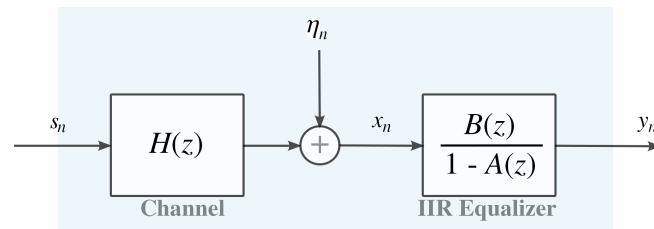


Figure 7.1: Block diagram of a communication system with an IIR equalizer.

the block diagram of the assumed communication system, where s_n is the source to be transmitted through the channel $H(z)$; $B(z)$ and $A(z)$ are the transfer functions of the feedforward and feedback parts of the IIR equalizer, respectively; and the presence of noise is assumed, denoted by the signal η_n . In the supervised approach, it is considered that a reference signal d_n is available at the receiver (equalizer), with d_n being a sequence obtained from a portion of s_n .

As discussed in Section 1.1.1, IIR filters are interesting processing tools, as they ally the simplicity of the linear structures and the capability of completely compensating other linear systems (when the filter length is sufficient). The IIR filter output y_n is as given by Eq. (1.4) and, to concisely represent the filter coefficients, we use the following relation:

$$\Theta(z) = \frac{B(z)}{1 - A(z)}. \quad (7.1)$$

This notation allows us to express the IIR filter output accordingly to Eq. 1.5, which we repeat here for convenience:

$$y_n = \boldsymbol{\theta}^T \boldsymbol{\phi}_n, \quad (7.2)$$

being $\boldsymbol{\theta} = [b_0 \ b_1 \ \dots \ b_{L_b} \ a_1 \ \dots \ a_{L_a}]^T$ and $\boldsymbol{\phi}_n = [x_n \ x_{n-1} \ \dots \ x_{n-L_b} \ y_{n-1} \ \dots \ y_{n-L_a}]^T$. This expression will be of utmost importance for the derivation of the gradient-based algorithms.

Since the equation- and output-error formulations are based on an error signal e_n ,

the time structure of the source is not of great relevance for this analysis – i.e., the subtraction operation in the error signal, $e_n = d_n - y_n$, in a certain sense, neutralizes the source temporal structure. However, the time structure that is ‘imprinted’ by the channel and by the equalizer remains valuable statistical information to be considered. Hence, our efforts will also be aimed at using multivariate densities, similarly to the preceding chapter.

In a simple way, the equation- and output-error formulations make different assumptions about the IIR filter output signal y_n . As presented in Section 4.2.2, the equation-error formulation assumes that the IIR feedback part is replaced by an FIR filtering of the reference signal d_n . Mathematically, this simply implies modifying the input vector ϕ_n in Eq. (7.2) to $\phi_{e,n} = [x_n \ x_{n-1} \ \dots \ x_{n-L_b} \ d_{n-1} \ \dots \ d_{n-L_a}]^T$, whose output will be denoted by $y_{e,n}$. In this case, the error signal will be

$$e_{e,n} = d_n - y_{e,n}. \quad (7.3)$$

On the other hand, the output-error formulation strictly follows the canonical relation given by Eq. (7.2), i.e., no further assumptions are made on the IIR structure. Thus, the error signal becomes

$$e_{o,n} = d_n - y_n. \quad (7.4)$$

Based on these two forms of error signals, we are able to extract their statistical content using the ITL framework, as presented in the following.

7.2 ITL Criteria for Adaptive IIR Filtering

ITL criteria are known for their capability of extracting the statistical information underlying the signals of interest in a relatively complete fashion. In the context of channel equalization, the use of Rényi’s entropy and correntropy-based criteria already showed to be promising approaches, particularly in scenarios involving non-linear structures (e.g., ANN and RBF-like structures) and non-Gaussian noise [Principe, 2010]. Thus, in view of the non-linear relationship that arises in IIR filtering (as seen in Section 4.2.2), the use of ITL methods deserve attention as an attractive alternative to the classical criteria for IIR filters. Previous efforts in this topic involved the (univariate) quadratic Rényi’s entropy [Lai, 2006] and the (univariate) matching of distributions [Lai, 2002; Lai et al., 2003], both in the system identification problem.

The proposals encompassing ITL criteria generally follow a univariate approach, which is a computationally convenient choice, counting with positive results in a number of applications. However, in accordance with the research line followed in this thesis, it will be convenient to adopt multivariate versions of the ITL criteria, since they are able to extract the temporal structure contained in the signals, the main focus of this work.

The set of ITL criteria to be considered in our study encompasses: (i) Shannon's entropy, whose estimator is based on the Parzen window method [Parzen, 1962], (ii) the already mentioned Rényi's entropy, (iii) the correntropy and, finally, (iv) the multivariate quadratic divergence (MQD, presented in Chapter 6). It is important to mention that the use of these ITL criteria in the channel equalization problem as well as their multivariate extension is a contribution of our work. These criteria will be presented in the following, where we assume a generic error signal e_n that can be replaced by $e_{e,n}$ or $e_{o,n}$, defined in Eqs. (7.3) and (7.4), respectively.

7.2.1 Multivariate Shannon's Entropy

The work of Shannon [1948] introduced the entity called entropy, which was essential to the development of Information Theory [Cover and Thomas, 1991]. Proportionally to the broadness of Shannon's work, this entity found a wide horizon of applications in several problems, among which we highlight the pattern recognition task [Duda et al., 2012], where, for the first time, Shannon's entropy was estimated using the kernel methods [Silva et al., 2005]. Here, we will consider the same method for estimating Shannon's entropy, however, we will apply it to the channel equalization problem.

Our aim using Shannon's entropy will be that of measuring the uncertainty about an error signal e_n . However, in our multivariate approach, we consider the error vector

$$\mathbf{e}_n = [e_n \ e_{n-1} \ \dots \ e_{n-M}]^T \quad (7.5)$$

of length $M+1$, which is associated with the RV $\underline{E} = \{E_n \ E_{n-1} \ \dots \ E_{n-M}\}$. Basically, this vector is the composition of the error signal e_n at time instant n and M of its delayed versions. Mathematically, the multivariate Shannon's differential entropy can be defined as

$$\begin{aligned} H^S(\underline{E}) &= - \int_D f_{\underline{E}}(\mathbf{v}) \log(f_{\underline{E}}(\mathbf{v})) \, d\mathbf{v} \\ &= -E[\log(f_{\underline{E}}(\mathbf{v}))], \end{aligned} \quad (7.6)$$

being $f_{\underline{E}}(\mathbf{v})$ the multivariate PDF of the RV \underline{E} (assumed to be of a continuous distribution – which requires the use of the differential entropy instead of its discrete version), and $D \subseteq \mathbb{R}^{M+1}$.

However, the analytical use of this instance is sometimes intangible in practical scenarios, being preferable the use of estimated versions of entropy. Hence, similarly to the work of Silva et al. [2005], we use a sample mean instead of the expectation operator in Eq. (7.6), i.e.:

$$\hat{H}^S(\underline{E}) = \frac{-1}{N_e} \sum_{i=0}^{N_e-1} -\log(f_{\underline{E}}(\mathbf{e}_i)) \quad (7.7)$$

and the Parzen window method for PDF estimation with multivariate kernels. Accord-

ing to this method, the multivariate PDF can be mathematically estimated through the following relationship:

$$\hat{f}_{\underline{E}}(\mathbf{v}) = \frac{1}{N_e} \sum_{j=0}^{N_e-1} G_{\Sigma}(\mathbf{v} - \mathbf{e}_j), \quad (7.8)$$

which, by replacing Eq. (7.8) in (7.7), results in

$$\hat{J}_{HS}(\boldsymbol{\theta}) = -\frac{1}{N_e} \sum_{i=1}^{N_e} \log \left(\frac{1}{N_e} \sum_{j=1}^{N_e} G_{2\Sigma}(\mathbf{e}_i - \mathbf{e}_j) \right), \quad (7.9)$$

where N_e is the number of error vectors e_n and $G_{\Sigma}(\cdot)$ is the multivariate symmetric Gaussian kernel given by

$$G_{\Sigma}(\mathbf{v} - \mathbf{e}_i) = \frac{1}{\sqrt{\det(2\pi\Sigma)}} \exp \left[\frac{-1}{2} (\mathbf{v} - \mathbf{e}_i)^T \Sigma^{-1} (\mathbf{v} - \mathbf{e}_i) \right], \quad (7.10)$$

with $\Sigma = \sigma^2 \mathbf{I}$, being σ the kernel size. In the $M = 0$ case, the estimated Shannon's entropy – Eq. (7.9) – is reduced to the univariate case proposed by Silva et al. [2005].

For equalization purposes, the estimated Shannon's entropy is a cost function that must be minimized. The main idea is that, by minimizing the entropy, the error reduces its uncertainty: ideally, the error distribution associated with the lowest uncertainty (or entropy) is a (multivariate) Dirac delta function. Preferably, it is desired that the spike be at the origin – i.e., $f_{\underline{E}}(\mathbf{v}) = \delta(\mathbf{v})$; however, when $f_{\underline{E}}(\mathbf{v}) = \delta(\mathbf{v} - \boldsymbol{\mu})$ for $\boldsymbol{\mu} \neq \mathbf{0}$ is likely to happen, additional care must be employed, e.g., by applying a constraint to the equalizer.

7.2.2 Multivariate Rényi's Entropy

In the problem of channel equalization, the most iconic ITL measure is undoubtedly Rényi's entropy, which was the pioneering approach allying the entities from Information Theory and PDF estimation via the Parzen window method [Erdogmus and Principe, 2002a; Principe, 2010].

Interestingly, Rényi's entropy establishes certain relationships with Shannon's entropy and, consequently, with the notion of uncertainty [Principe, 2010]. Besides that, Rényi's entropy for $\alpha = 2$ presents the advantage of leading to simple relations when kernel density estimators are used.

The multivariate Rényi's entropy of order α can be defined as

$$H^R(\underline{E}) = \frac{1}{1 - \alpha} \log \int_D f_{\underline{E}}^{\alpha}(\mathbf{v}) d\mathbf{v}, \quad (7.11)$$

where α is a constant, such that $\alpha \neq 1$ and $\alpha \geq 0$ [Principe, 2010]. By assuming, as usual, that $\alpha = 2$ and that the multivariate PDF of \underline{E} can be estimated via the Parzen window

method with Gaussian kernels, Eq. (7.8), Rényi's entropy can be estimated as

$$\hat{J}_{HR}(\boldsymbol{\theta}) = -\log \left(\frac{1}{N_e^2} \sum_{i=1}^{N_e} \sum_{j=1}^{N_e} G_{2\boldsymbol{\Sigma}}(\mathbf{e}_i - \mathbf{e}_j) \right) = -\log \hat{V}_2(\underline{E}), \quad (7.12)$$

where $\hat{V}_2(\underline{E})$ will be called the multivariate quadratic information potential (MIP) estimator.

Just like Shannon's entropy, we wish to reduce the uncertainty about the RV \underline{E} . Hence, the objective will be that of minimizing the cost function $\hat{J}_{HR}(\boldsymbol{\theta})$ given by Eq. (7.12). Since the logarithm is a monotonic function, it can be disregarded in optimization tasks and, alternatively, the MIP estimator can be maximized.

7.2.3 Multivariate Correntropy

In the literature, the correntropy is a simpler ITL measure able to encompass the HOS of the signals of interest. It can also be seen as a biased estimator of the information potential [Santamaría et al., 2006; Principe, 2010] and, for this reason, we also consider this criterion in our analysis.

In the previous chapter, the correntropy-based cost was able to encompass the signals time structure by means of a squared error expression (see Eq. (6.15) in Chapter 6). However, when an error signal e_n is involved, the temporal structure can be exploited by other means. In that sense, we propose the use of a multivariate version of correntropy, which can be defined as:

$$\begin{aligned} v_{\underline{E}} &= \int_D G_{\boldsymbol{\Sigma}}(\mathbf{v}) f_{\underline{E}}(\mathbf{v}) d\mathbf{v} \\ &= E[G_{\boldsymbol{\Sigma}}(\mathbf{v})], \end{aligned} \quad (7.13)$$

where a multivariate Gaussian kernel $G_{\boldsymbol{\Sigma}}(\cdot)$ was adopted.

Now, if we assume a sample mean estimator for the expectation operator, the multivariate correntropy becomes:

$$\hat{J}_{cor}(\boldsymbol{\theta}) = \frac{1}{N_e} \sum_{i=1}^{N_e} G_{\boldsymbol{\Sigma}}(\mathbf{e}_i). \quad (7.14)$$

Curiously, if the Parzen window method is considered for the PDF $f_{\underline{E}}(\mathbf{v})$ in Eq. (7.13), the resulting equation is equal to Eq. (7.14), except for the kernel size, which would be $2\boldsymbol{\Sigma} = 2\sigma^2\mathbf{I}$. However, since the kernel size is a free parameter, this scale factor is negligible.

Since the kernel functions present their peak value at the origin and the objective is to make the error signal e_n null, an intuitive equalization criterion will be that of maximizing the error correntropy cost $\hat{J}_{cor}(\boldsymbol{\theta})$ given by Eq. (7.14). Note that, differently

from Shannon's and Rényi's entropy, the case in which $f_{\underline{E}}(\mathbf{v}) = \delta(\mathbf{v} - \boldsymbol{\mu})$ for $\boldsymbol{\mu} \neq \mathbf{0}$ cannot be a global optimum for correntropy.

7.2.4 Matching of Multivariate Distributions

Motivated by the results obtained in the previous chapter, as well as by the efforts of Lai [2002], we also consider the MQD cost as criterion to be investigated in the IIR filtering problem.

Since we wish the error to be an impulse at the origin, i.e., that $f_{\underline{E}}(\mathbf{v}) = \delta(\mathbf{v})$, we may pose the problem as the matching between the densities $f_{\underline{E}}(\mathbf{v})$ and $p_{\underline{0}}(\mathbf{v}) = \delta(\mathbf{v})$. Recalling the MQD-D cost presented in Eq. (6.25), we are able to define an analogous cost function:

$$\begin{aligned} J_{MQD}(\boldsymbol{\theta}) &= \int_D (f_{\underline{E}}(\mathbf{v}) - p_{\underline{0}}(\mathbf{v}))^2 d\mathbf{v} \\ &= \int_D f_{\underline{E}}^2(\mathbf{v}) d\mathbf{v} + \int_D p_{\underline{0}}^2(\mathbf{v}) d\mathbf{v} - 2 \int_D f_{\underline{E}}(\mathbf{v}) p_{\underline{0}}(\mathbf{v}) d\mathbf{v}, \end{aligned} \quad (7.15)$$

in which, using $p_{\underline{0}}(\mathbf{v}) = \delta(\mathbf{v})$ and the Parzen window method for PDF estimation, Eq. (7.8), results in

$$\hat{J}_{MQD}(\boldsymbol{\theta}) = \frac{1}{N_e^2} \sum_{i=1}^{N_e} \sum_{j=1}^{N_e} G_{2\Sigma}(\mathbf{e}_i - \mathbf{e}_j) + \int_D p_{\underline{0}}^2(\mathbf{v}) d\mathbf{v} - \frac{2}{N_e} \sum_{j=1}^N G_{\Sigma}(\mathbf{e}_j), \quad (7.16)$$

where, again, the second term can be disregarded in optimization problems, as it does not depend on the IIR equalizer parameters. Note that the first term is basically the Rényi's entropy estimator for $\alpha = 2$ and the last term can be seen as a penalizing term that avoids solutions of the type $f_{\underline{E}}(\mathbf{v}) = \delta(\mathbf{v} - \boldsymbol{\mu})$ for $\boldsymbol{\mu} \neq \mathbf{0}$, just like correntropy. In that sense, the MQD cost can be seen as a linear combination of the Rényi's entropy and correntropy cost.

From a general perspective, all the considered ITL criteria makes use of a generic error signal, which allows their direct application as equalization criteria in the output- and equation-error formulations. To simplify the use of the adopted acronyms, Shannon's entropy-, Rényi's entropy, correntropy and multivariate distribution-based criteria will be referred to as HSEE, HREE, corEE and MQDEE, respectively, for the equation-error formulation; and as HSOE, HROE, corOE and MQDOE, respectively, for the output-error formulation.

Having defined the criteria, the next step is to derive the gradient-based algorithms according to the LMS, PLR and RPE approaches, as described in the following.

7.3 Novel ITL Algorithms for Adaptive IIR Filters

In the context of the equation-error formulation, an LMS-like algorithm usually is employed for training the IIR structure, while, in the output-error formulation, the PLR or the (simplified) RPE are the preferred options [Shynk, 1989], as presented in Section 4.2.2. Then, our intention is to employ the ITL criteria according to these approaches.

Basically, all algorithms make use of the gradient-based update rule given by

$$\theta_{n+1} = \theta_n - \mu \nabla_{\theta} J(\theta), \quad (7.17)$$

being the difference among them the gradient $\nabla_{\theta} J(\theta)$ of each approach. In the following, we present the gradient of each ITL cost function using the generic error signal, and later we specify the error terms according to the LMS, PLR and RPE approaches.

7.3.1 Gradient of ITL Criteria

Starting with the $\hat{J}_{HS}(\boldsymbol{\theta})$ cost, its gradient with respect to $\boldsymbol{\theta}$ can be computed as

$$\nabla_{\theta} \hat{J}_{HS}(\boldsymbol{\theta}) = \frac{1}{2N_e^2} \sum_{i=1}^{N_e} \frac{\sum_{j=1}^{N_e} G_{2\Sigma}(\mathbf{e}_i - \mathbf{e}_j) (\mathbf{e}_i - \mathbf{e}_j)^T \boldsymbol{\Sigma}^{-1} \nabla_{\theta} (\mathbf{e}_i - \mathbf{e}_j)}{\frac{1}{N_e} \sum_{k=1}^{N_e} G_{2\Sigma}(\mathbf{e}_i - \mathbf{e}_k)}; \quad (7.18)$$

being $\nabla_{\theta} (\mathbf{e}_i - \mathbf{e}_j)$ the gradient of the error signal difference, which will vary according to the approach, as we will see later.

Similarly, for the Rényi's entropy-based cost, the gradient is proportional to

$$\nabla_{\theta} \hat{J}_{HR}(\boldsymbol{\theta}) \propto \frac{1}{2N_e^2} \sum_{i=1}^{N_e} \sum_{j=1}^{N_e} G_{2\Sigma}(\mathbf{e}_i - \mathbf{e}_j) (\mathbf{e}_i - \mathbf{e}_j)^T \boldsymbol{\Sigma}^{-1} \nabla_{\theta} (\mathbf{e}_i - \mathbf{e}_j), \quad (7.19)$$

where it was assumed $\alpha = 2$. Note that the logarithmic function was disregarded – hence, the proportional symbol is used – without causing any impact in the criteria solution. Eq. (7.19) basically represents the gradient of the MIP estimator, but the sign must be changed if a maximization process is to be carried.

Continuing with the derivation, the gradient of correntropy-based cost can be expressed as

$$\nabla_{\theta} \hat{J}_{cor}(\boldsymbol{\theta}) = \frac{-1}{N_e} \sum_{i=1}^{N_e} G_{\Sigma}(\mathbf{e}_i) \mathbf{e}_i^T \boldsymbol{\Sigma}^{-1} \nabla_{\theta} \mathbf{e}_i; \quad (7.20)$$

and, finally, for the MQD cost,

$$\begin{aligned}\nabla_{\theta}\hat{J}_{MQD} &= \frac{1}{2N_e^2} \sum_{i=1}^{N_e} \sum_{j=1}^{N_e} G_{2\Sigma}(\mathbf{e}_i - \mathbf{e}_j) (\mathbf{e}_i - \mathbf{e}_j)^T \Sigma^{-1} \nabla_{\theta}(\mathbf{e}_i - \mathbf{e}_j) \\ &\quad + \frac{2}{N_e} \sum_{j=1}^{N_e} G_{\Sigma}(\mathbf{e}_j) \mathbf{e}_j^T \Sigma^{-1} \nabla_{\theta} \mathbf{e}_j.\end{aligned}\tag{7.21}$$

Note that the term $\nabla_{\theta}(\mathbf{e}_i - \mathbf{e}_j)$ is common to the gradients of Shannon's and Rényi's entropy, as well as the MQD. In addition to that, $\nabla_{\theta} \mathbf{e}_i$ can be identified in the gradient of the correntropy and MQD cost. In fact, the LMS-, LPS- and RPE-based algorithms will differ only in these terms, which will be described in the following.

7.3.2 LMS-Based Algorithms - Equation-Error Formulation

Based on the equation-error formulation, the generic error signal e_n becomes the signal $e_{e,n}$ defined in Eq. (7.3). Thus, the term $\nabla_{\theta}(\mathbf{e}_i - \mathbf{e}_j)$ becomes $\nabla_{\theta}(\mathbf{e}_{e,i} - \mathbf{e}_{e,j})$, which can be computed as

$$\nabla_{\theta}(\mathbf{e}_{e,i} - \mathbf{e}_{e,j}) = (\Phi_{e,j} - \Phi_{e,i}).\tag{7.22}$$

The term $\nabla_{\theta} \mathbf{e}_i$ becomes $\nabla_{\theta} \mathbf{e}_{e,i}$ and results

$$\nabla_{\theta} \mathbf{e}_{e,i} = -\Phi_{e,i},\tag{7.23}$$

being,

$$\Phi_{e,n} = \begin{bmatrix} x_n & x_{n-1} & \cdots & x_{n-M} \\ x_{n-1} & x_{n-2} & \cdots & x_{n-M-1} \\ \vdots & \vdots & \vdots & \vdots \\ x_{n-N_b} & x_{n-N_b-1} & \cdots & x_{n-M-N_b} \\ d_{n-1} & d_{n-2} & \cdots & d_{n-M-1} \\ \vdots & \vdots & \vdots & \vdots \\ d_{n-N_a} & d_{n-N_a-1} & \cdots & d_{n-M-1-N_a} \end{bmatrix}.\tag{7.24}$$

The substitution of these relations in the previously presented gradients yields the set of LMS-based algorithms to be analyzed.

7.3.3 PLR-Based Algorithms - Output-Error Formulation

In the output-error formulation, the PLR approach considers a linear approximation of the gradient, as described in Eq. (4.30). In this case, the term $\nabla_{\theta}(\mathbf{e}_i - \mathbf{e}_j)$ used in the gradients becomes $\nabla_{\theta}(\mathbf{e}_{o,i} - \mathbf{e}_{o,j})$ and results

$$\nabla_{\theta}(\mathbf{e}_{o,i} - \mathbf{e}_{o,j}) = (\Phi_j - \Phi_i);\tag{7.25}$$

and for the term $\nabla_{\theta}\mathbf{e}_i$:

$$\nabla_{\theta}\mathbf{e}_{o,i} = -\mathbf{\Phi}_i, \quad (7.26)$$

being

$$\mathbf{\Phi}_n = \begin{bmatrix} x_n & x_{n-1} & \cdots & x_{n-M} \\ x_{n-1} & x_{n-2} & \cdots & x_{n-M-1} \\ \vdots & \vdots & \vdots & \vdots \\ x_{n-N_b} & x_{n-N_b-1} & \cdots & x_{n-M-N_b} \\ y_{n-1} & y_{n-2} & \cdots & y_{n-M-1} \\ \vdots & \vdots & \vdots & \vdots \\ y_{n-N_a} & y_{n-N_a-1} & \cdots & y_{n-M-1-N_a} \end{bmatrix}. \quad (7.27)$$

To obtain the PLR-based algorithms, it is enough to replace these relations in the gradients presented in Section 7.3.1.

7.3.4 RPE-Based Algorithm - Output-Error Formulation

Finally, for the simplified RPE-based algorithm, an approximated gradient is derived from the assumption that the filter coefficients vary slowly along the time, i.e., $\boldsymbol{\theta}_n \approx \boldsymbol{\theta}_{n-1} \approx \dots \approx \boldsymbol{\theta}_{n-N_i}$ [Johnson Jr., 1984] – for more details, see Section 4.2.2.

In this case, the term $\nabla_{\theta}(\mathbf{e}_i - \mathbf{e}_j)$ can be expressed as

$$\nabla_{\theta}(\mathbf{e}_{o,i} - \mathbf{e}_{o,j}) = (\dot{\mathbf{\Phi}}_j - \dot{\mathbf{\Phi}}_i) \quad (7.28)$$

and the term $\nabla_{\theta}\mathbf{e}_i$ as

$$\nabla_{\theta}\mathbf{e}_{o,i} = -\dot{\mathbf{\Phi}}_i \quad (7.29)$$

where,

$$\dot{\mathbf{\Phi}}_n = \begin{bmatrix} \dot{x}_n & \dot{x}_{n-1} & \cdots & \dot{x}_{n-M} \\ \dot{x}_{n-1} & \dot{x}_{n-2} & \cdots & \dot{x}_{n-M-1} \\ \vdots & \vdots & \vdots & \vdots \\ \dot{x}_{n-N_b} & \dot{x}_{n-N_b-1} & \cdots & \dot{x}_{n-M-N_b} \\ \dot{y}_{n-1} & \dot{y}_{n-2} & \cdots & \dot{y}_{n-M-1} \\ \vdots & \vdots & \vdots & \vdots \\ \dot{y}_{n-N_a} & \dot{y}_{n-N_a-1} & \cdots & \dot{y}_{n-M-1-N_a} \end{bmatrix}. \quad (7.30)$$

The signals \dot{x}_n and \dot{y}_n are obtained according to Eqs. (4.34), respectively. Hence, by replacing of $\nabla_{\theta}(\mathbf{e}_{o,i} - \mathbf{e}_{o,j})$ and/or $\nabla_{\theta}\mathbf{e}_{o,i}$ in the gradients presented in Section 7.3.1, we arrive, straightforwardly, at the desired RPE-based algorithms.

It is important to mention that, in all the cases above, it is necessary that $N_e > M + \max\{N_a, N_b\}$, being $\max\{\cdot, \cdot\}$ the element with the largest value; otherwise, there will not be enough samples for estimation. Moreover, for the MQD-based and the Shannon's

and Rényi's entropy-based costs, N_e needs to be necessarily greater than or equal to 2, so that there can be at least one comparison between error samples.

In view of their higher potential when extracting the statistical information of the underlying signals as well as the use of the inherent kernel features, we expect to identify an improvement on the ITL-based algorithms performance in comparison with the classical mean-squared approaches. In that sense, we present in the following the performance analysis according to the two formulations: the equation- and the output-error.

7.4 Performance Analysis - Equation-Error Formulation

The equation-error formulation is a supervised approach in which the use of the MSEE criterion has already shown to be an attractive method in identification problems [Johnson Jr., 1984; Treichler, 1985; Regalia, 1994]. However, the MSEE weakness is its high sensitivity to the presence of noise, which may contribute to the rise of biased solutions [Shynk, 1989]. In that sense, we analyze in this section the performance of the proposed ITL algorithms in comparison with the classical MSEE approach, paying especial attention to their robustness against noise.

The analysis will firstly encompass the observation of the cost surfaces in a simple scenario, being followed by the performance analysis itself of the LMS-based algorithms in more complex scenarios. The cost surface analysis demands a simple scenario for the sake of visualization of the surfaces, with an IIR equalizer with only two free coefficients. To evaluate the performance of the solutions found by the algorithms, we will use the QISI measure, defined as

$$QISI_{dB} = 10 \log_{10} \frac{\left(\sum_{i=0}^{M_c} |c_i|^2 \right) - \max_j |c_j|^2}{\max_j |c_j|^2}, \quad (7.31)$$

where $\mathbf{c} = [c_0 \ c_1 \ \dots \ c_{L_c}]^T$ is the combined channel + equalizer impulse response. Since the QISI assumes an FIR model for c_n , the combined channel+equalizer IIR system (with poles and zeros) will be approximated by a sufficiently large FIR system of length $L_c = 300$ (a system only with zeros) [Oppenheim et al., 1997].

With the objective of establishing a fair step size μ for all algorithms, they will be adjusted to reach the equivalence of the coefficients mean displacement (or mean Euclidean distance) between iterations after convergence. Mathematically, the displacement is measured by

$$disp_{\theta} = \frac{1}{N_{it} - N_{conv} + 1} \sum_{i=N_{conv}}^{N_{it}} \|\boldsymbol{\theta}_{i+1} - \boldsymbol{\theta}_i\|, \quad (7.32)$$

where N_{it} is the maximum number of iterations and N_{conv} is the number of iterations required for convergence.

Besides the step size μ , the ITL algorithms also depend on the window length N_e , the kernel size σ and the number of delays M . The window length N_e will be equal for all algorithms (including the MSEE-LMS algorithm, whose coefficients update will be done using the mean gradient using N_e error samples), while the kernel size σ and the number of delays M will be varied in each case. Note that neither the σ nor the M parameters are encompassed in the MSEE-LMS algorithm.

7.4.1 Equation-Error Formulation - Scenario 1

Assuming that s_n is an *i.i.d.* BPSK modulated signal, we consider the scenario where the channel has as transfer function

$$H(z) = \frac{1 + 0.6z^{-1}}{1 - 0.5z^{-1}}, \quad (7.33)$$

and there is AWGN with SNR level of 10 dB. The IIR equalizer presents the following structure:

$$\Theta(z) = \frac{b_0}{1 - a_1z^{-1}}, \quad (7.34)$$

where b_0 and a_1 are two free parameters. Note that the equalizer structure is insufficient to lead to a ZF condition.

The ITL Costs Surfaces

Firstly, we wish to observe the criteria surface shape. In order to do so, we considered $N_e = 200$ for all criteria and varied b_0 and a_1 from -2 to 2 . For comparison purposes, we display in Fig. 7.2 the contours of the MSEE cost, for the noiseless and noisy case. It is possible to note that, for both cases, the surface is a paraboloid with a single optimum. However, with the presence of noise, Fig. 7.2(b), there is a clear shift or bias in the solution [Shynk, 1989]. In that sense, we hope that the proposed criteria be more robust against the noise bias.

To observe the surface of the ITL criteria, we first consider the kernel size of $\sigma = 3$, in which the resulting contours for the HSEE, HREE, corEE and MQDEE are as illustrated in Fig. 7.3. It is possible to note that the shape of the costs are similar to that of the MSEE, i.e., they also form a paraboloid, with exception to the MQDEE cost, whose surface is more flat and with contours in the shape of an “irregular ellipse”. Fig. 7.3 also shows that the ITL criteria optimum points also suffers the bias effect, since their solution does not match that of the MSEE in the noiseless case. However, the bias effect intensity may vary, as we will see later.

By reducing the kernel size to $\sigma = 0.7$, it is possible to note, as displayed at Fig. 7.4,

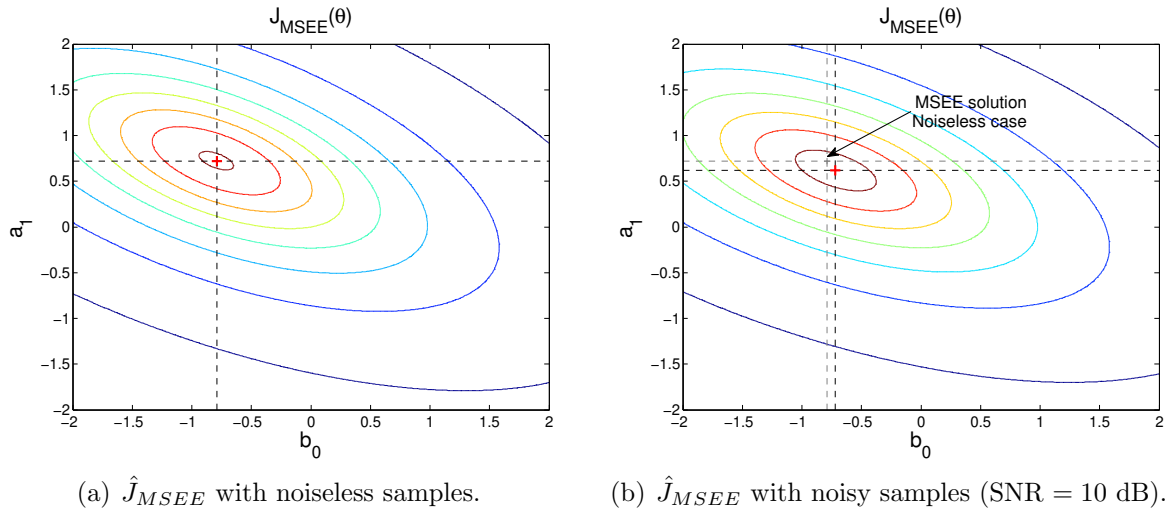


Figure 7.2: Equation-Error Formulation - Scenario 1 - MSEE Surface contours.

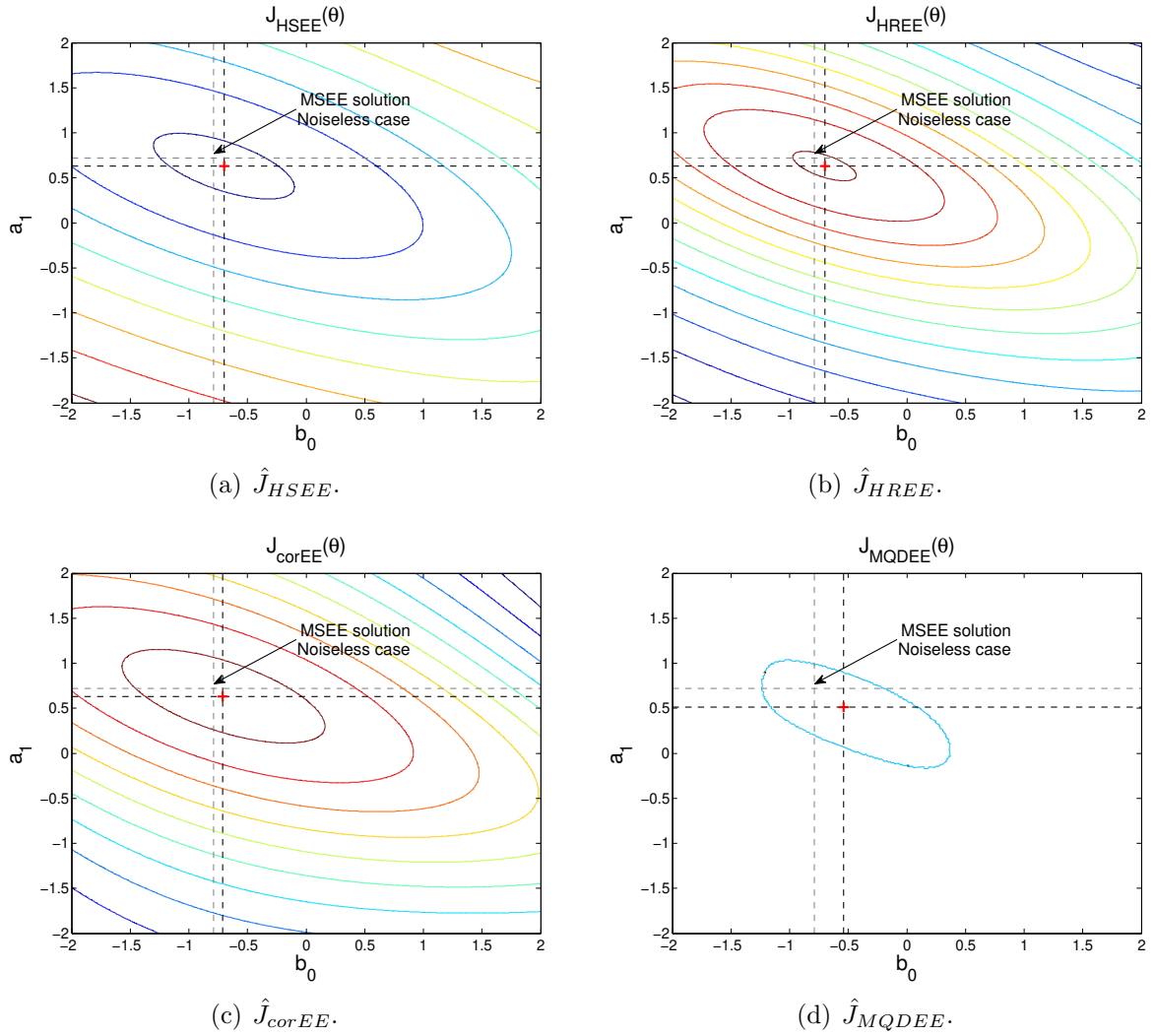


Figure 7.3: Equation-Error Formulation - Scenario 1 - ITL costs surface contours for $\sigma = 3$, $M = 0$ and SNR of 10 dB.

that the cost surfaces become more irregular, with a slight change on the optima positions. In general terms, the ITL criteria solutions, in comparison with the $\sigma = 3$ case, becomes closer to the MSEE solution with no noise, which indicates that low values of σ may improve the performance of the algorithms.

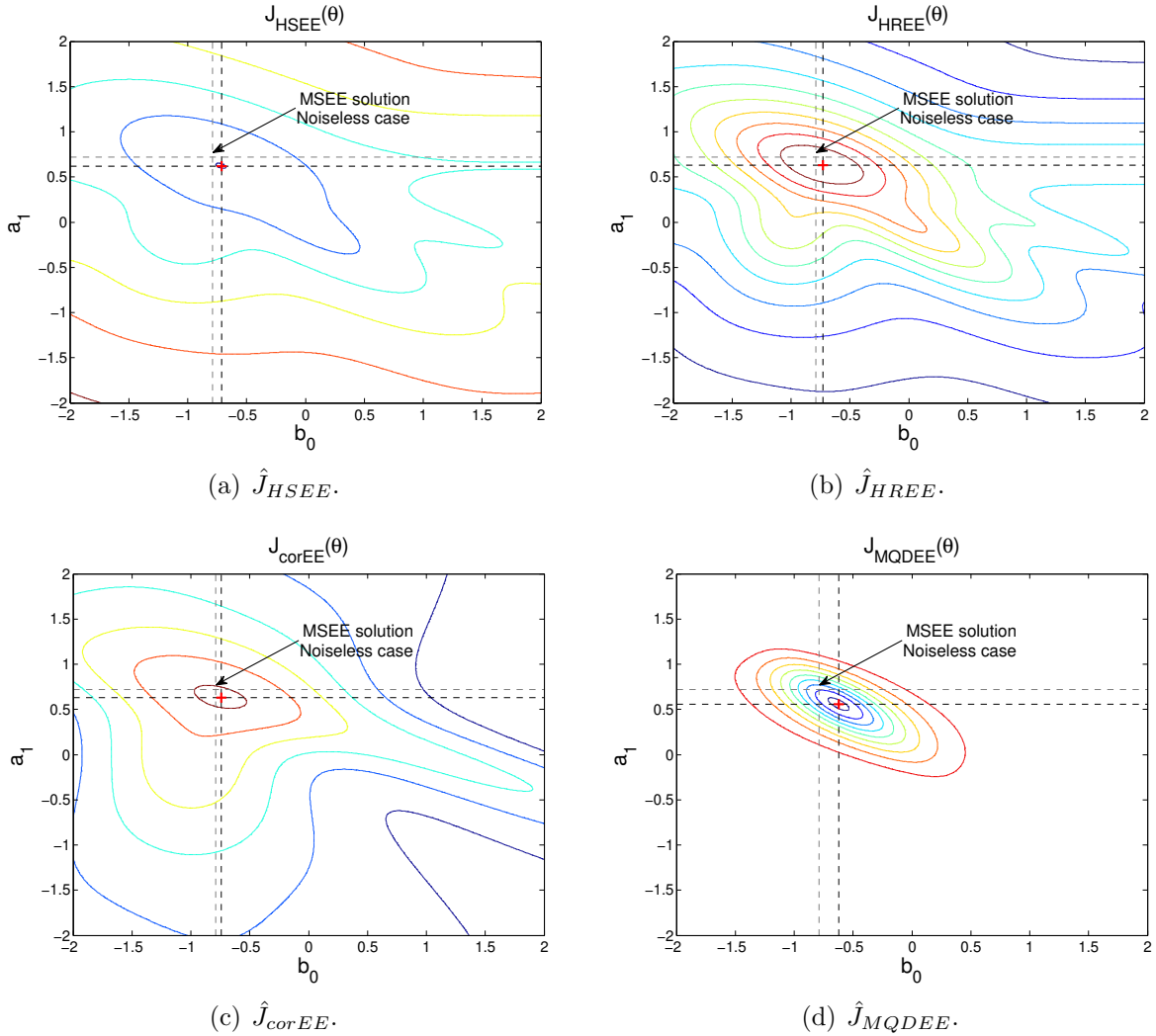


Figure 7.4: Equation-Error Formulation - Scenario 1: ITL costs surface contours for $\sigma = 0.7$, $M = 0$ and SNR of 10 dB.

In order to extract the error signal temporal information more effectively, we consider now the increment on the number of delays M . By adopting $M = 2$, the ITL criteria surface contours assumes the form displayed at Fig. 7.5. The temporal information of the error signal caused a smoothing effect on the surfaces, but also provoked a slightly change on the optima position: just like the kernel size smoothing effect, the increase of M caused a larger deviation when compared to the MSEE solution in the noiseless scenario. This indicates that, an increase in M may require a reduction of the kernel size σ in order to keep the smoothing effect balanced. These two parameters will be analyzed in more detail in the following, where we will also evaluate the criteria solutions via the

LMS-based algorithms.

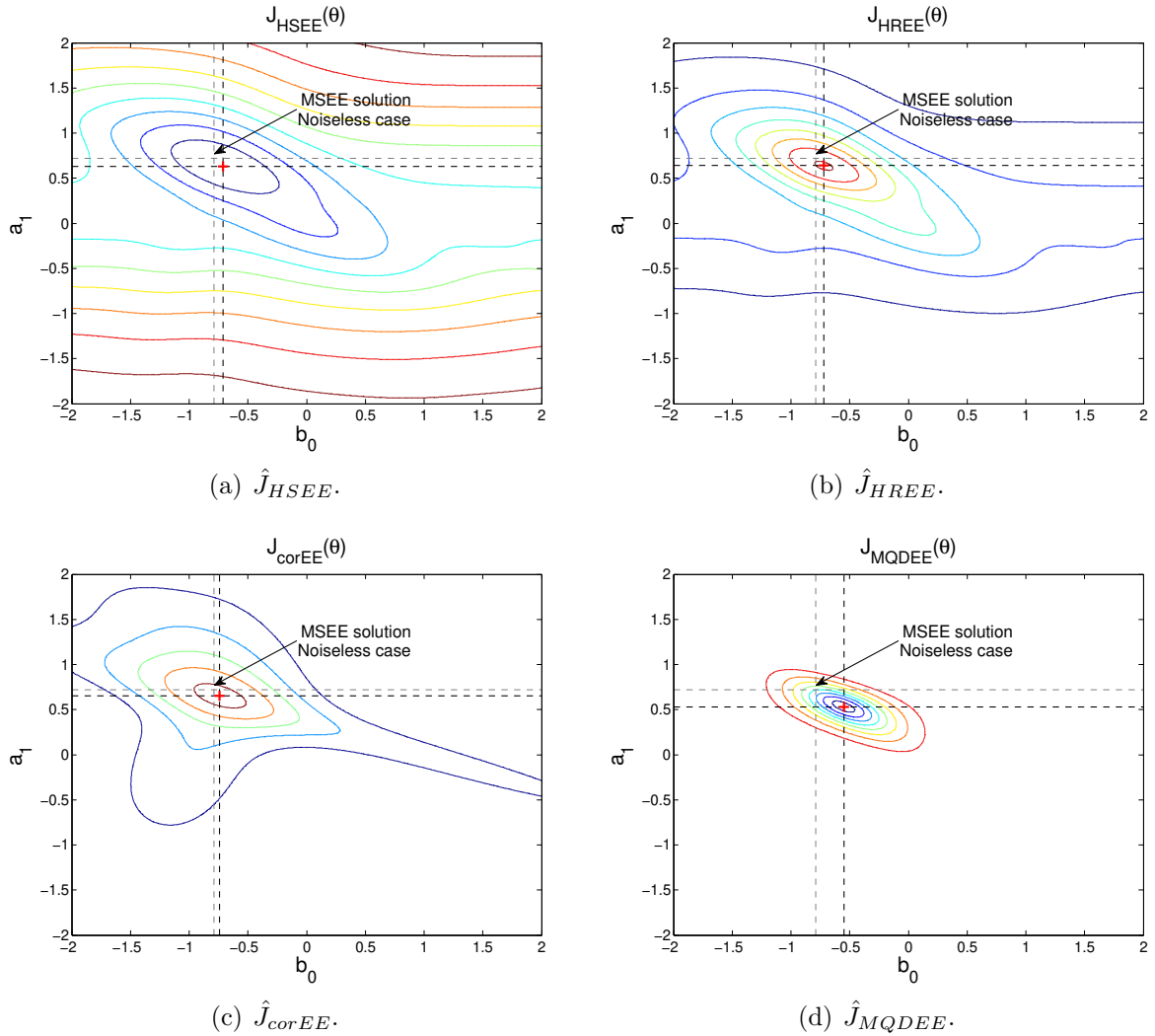


Figure 7.5: Equation-Error Formulation - Scenario 1: ITL costs surface contours for $\sigma = 0.7$, $M = 2$ and SNR of 10 dB.

LMS-Based Algorithms

As shown by the previous figures, the criteria surfaces present a single optimum, whose values can be satisfactorily reached through the use of a gradient-based algorithm. In this case, the LMS-based algorithms presented in Section 7.3 will be employed as optimization tools.

For the same scenario 1 (with SNR level of 10 dB), we adopted the following parameters: $N_e = 5$; $M = 0$; step sizes $\mu_{MSEE} = 0.004$, $\mu_{HSEE} = 0.004$, $\mu_{HREE} = 0.027$, $\mu_{corEE} = 0.015$ and $\mu_{MQDEE} = 0.006$; and kernel size $\sigma = 1$ for all kernel-based algorithms. After running the LMS-based algorithms, we obtained the mean QISI performance along iterations for 30 independent simulations, as displayed at Fig. 7.6(a). The measured mean displacement given by Eq. (7.32) was of $1.4e - 3$, being considered $N_{it} = 10000$

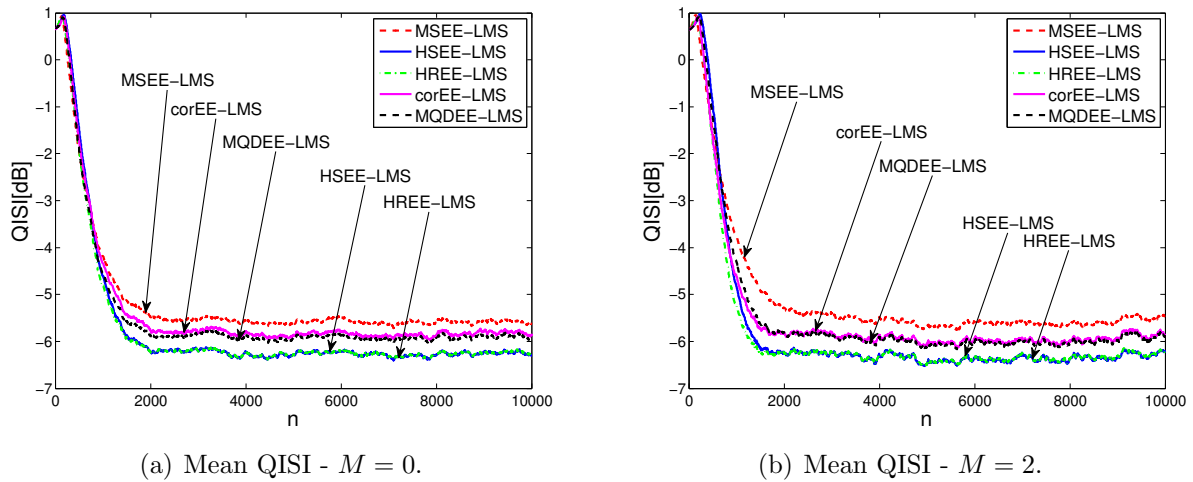


Figure 7.6: Equation-Error Formulation - Scenario 1: QISI Performance of the LMS-based algorithms for $M = 0$ and $M = 2$ and SNR of 10 dB.

(the maximum number of iterations) and $N_{conv} = 2000$ (the number of iterations required for convergence). We repeated this procedure for $M = 2$, adopting the parameters: $N_e = 5$; step sizes $\mu_{MSEE} = 0.0035$, $\mu_{HSEE} = 0.002$, $\mu_{HREE} = 0.2$, $\mu_{corEE} = 0.05$ and $\mu_{MQDEE} = 0.02$; and $\sigma = 1$ for all algorithms. The measured mean QISI performance is illustrated in Fig. 7.6(b). The measured mean displacement was of $1.4e - 3$. As can be noted, for $M = 0$, the HSEE-LMS and the HREE-LMS algorithms achieved together the lowest QISI performance, with about -6.35 dB of mean QISI after convergence, being followed by the MQDEE-LMS algorithm, with -6.02 dB, by the corEE-LMS, with -5.90 dB, and, at last, the classical MSEE-LMS algorithm, with -5.62 dB. The convergence speed is practically the same for all algorithms ($N_{conv} = 2000$). For $M = 2$, the QISI performance is slightly improved: the HSEE-LMS and the HREE-LMS algorithms achieved -6.43 dB of QISI, the MQDEE-LMS algorithm achieved -6.11 dB and the corEE-LMS algorithm -6.08 dB. This might indicate that the use of the temporal structure is not effective in this case, however, if the scenario conditions are changed, the effect of using more delays can be more significant, as we will see later.

To obtain a more accurate kernel size adjustment, we performed a linear sweep on σ for the $M = 0$ and $M = 2$ cases – keeping the same previous parameters – to investigate its influence on the solutions. After each execution of the LMS-based algorithms, the mean performance after convergence was evaluated in terms of QISI. For each considered value of σ , 30 independent experiments were considered, being their average QISI values displayed in Fig. 7.7. For $M = 0$, Fig. 7.7(a), it is possible to note that, for $\sigma < 0.5$, the ITL-based algorithms presented poor performance. For $\sigma = 0.6$ the corEE and the MQDEE algorithms attain their best performances. The HSEE algorithm presents the best QISI value for $\sigma \approx 0.9$ and gradually loses performance as σ increases; while the HREE algorithm shows practically constant QISI performance for $\sigma > 0.5$. However, this

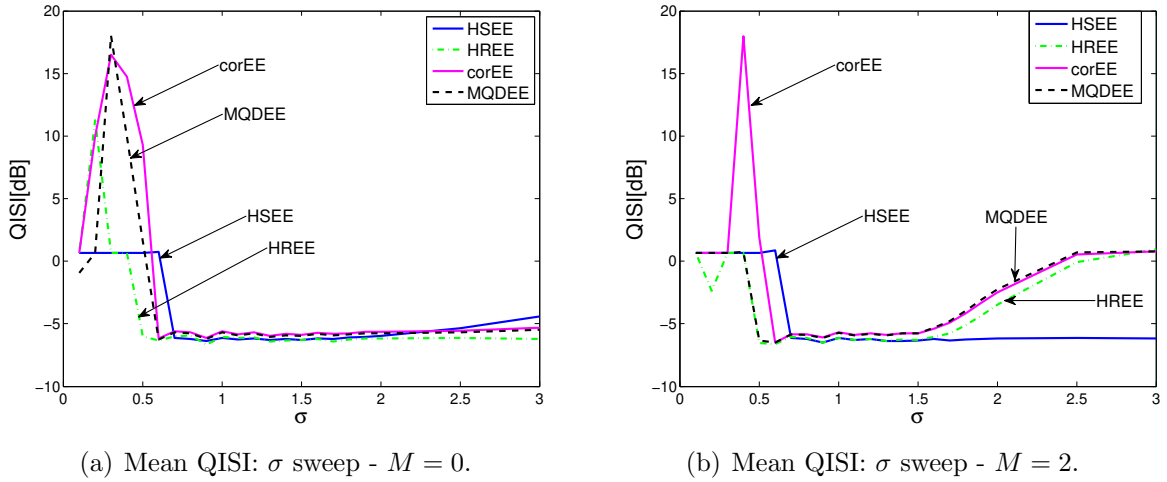


Figure 7.7: Equation-Error Formulation - Scenario 1: QISI Performance σ sweep.

behavior changes when M is increased to 2. Indeed, as shown in Fig. 7.7(b), for $\sigma > 1.5$, the HREE, the corEE and the MQDEE algorithms tend to perform poorer. The only exception is the HSEE, which now maintains its performance even for $\sigma > 1.5$. In view of this, one possible general σ choice for all criteria is $\sigma = 1$, which lies on an interval acceptable for both $M = 0$ and $M = 2$ (although this may cause a small reduction on the QISI performance for corEE and MQDEE whose best σ is 0.6, but, at least, it moves them away from the unstable region of $\sigma < 0.5$).

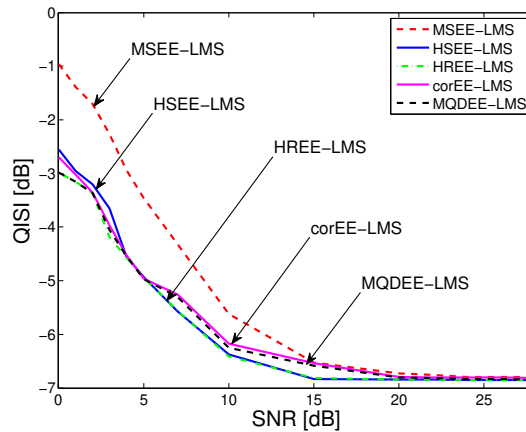


Figure 7.8: Equation Error - Scenario 1: QISI \times SNR ($M = 0$).

Hence, adjusting the kernel sizes to their optimal values for $M = 0$, i.e., $\sigma_{HSEE} = 0.9$, $\sigma_{HREE} = 0.6$, $\sigma_{corEE} = 0.6$ and $\sigma_{MQDEE} = 0.6$, we varied the SNR levels from 0 to 28 dB in order to obtain a QISI \times SNR curve. The mean QISI values were measured after the convergence of the algorithms for 30 independent experiments, whose average are shown at Fig. 7.8. As can be observed, the use of the ITL-based algorithms is especially useful for lower SNR levels (below 20 dB). For higher SNR levels, all the algorithms tend to

converge to the same QISI performance of ≈ -6.85 dB. For most SNR values, the HSEE-LMS and the HREE-LMS algorithms performed better and almost equivalently, staying behind the corEE-LMS and MQDEE-LMS only for SNR levels close to zero dB.

Moving our attention to the number of delays M , we considered three SNR values, i.e., 3 dB, 10 dB and 22 dB, and varied M from 0 to 3. The average performance in terms of QISI for 30 independent experiments is as exhibited in Tab. 7.1. Again, we observe

Table 7.1: Mean QISI performance for several number of delays M .

QISI [dB] - SNR 3 dB					
SNR 3 dB					
M	MSEE	HSEE	HREE	CorEE	MQDEE
0	-2.271	-3.648	-4.191	-3.971	-4.053
1	-	-3.667	-4.382	-3.983	-4.146
2	-	-3.883	-4.539	-4.192	-4.249
3	-	-4.023	-4.508	-4.298	-4.326
SNR 10 dB					
M	MSEE	HSEE	HREE	CorEE	MQDEE
0	-5.798	-6.377	-6.410	-6.176	-6.254
1	-	-6.414	-6.523	-6.338	-6.349
2	-	-6.485	-6.628	-6.506	-6.510
3	-	-6.495	-6.624	-6.483	-6.505
SNR 22 dB					
M	MSEE	HSEE	HREE	CorEE	MQDEE
0	-6.765	-6.851	-6.838	-6.784	-6.811
1	-	-6.811	-6.832	-6.794	-6.805
2	-	-6.836	-6.844	-6.782	-6.824
3	-	-6.844	-6.847	-6.799	-6.829

the particular efficiency of the ITL algorithms in the noisier conditions (i.e., for low SNR values). For an SNR of 3 dB, all the ITL algorithms take advantage of the number of delays M and are able to improve their performance as M increases. Among all of them, we highlight the performance of the HREE algorithm, which is better than that of other algorithms and twice as better than that of the MSEE for $M = 2$. Even though, the other ITL algorithms performance are not far from the HREE. For an SNR of 10 dB, increasing the number of delays only provokes slight improvements on the QISI performance, while, for 22 dB, the QISI performance is practically kept constant.

This first analysis suggests that the ITL-based approaches might be useful in the equation-error formulation, since they are able to exhibit good performance even on strong noise scenarios. But we remind the reader that the present scenario encompasses a simple IIR equalizer, and some features can be hidden due to structural limitations. In that sense, we analyze more complex cases in the following.

7.4.2 Equation-Error Formulation - Scenario 2

In the second scenario, we consider more complex channel and equalizer models. The source s_n is an *i.i.d.* BPSK modulated signal and the channel has the transfer function

$$H(z) = \frac{0.76 - 0.25z^{-1} + 0.44z^{-2} - 0.02z^{-3}}{1 + 0.2z^{-1} - 0.5z^{-2}}. \quad (7.35)$$

The IIR equalizer is of the type:

$$\Theta(z) = \frac{b_0 + b_1z^{-1}}{1 - a_1z^{-1} - a_2z^{-2} - a_3z^{-3}}. \quad (7.36)$$

Note that, in this case, the equalizer is not able to completely equalize the channel.

We consider two types of noise, the usual AWGN and the impulsive noise, whose PDF is given by

$$f_\eta(v) = \epsilon G_{\sigma_1^2}(v) + (1 - \epsilon)G_{\sigma_2^2}(v), \quad (7.37)$$

where we considered $\epsilon = 0.1$ and $\sigma_1/\sigma_2 = 30$, the same relation of the previous chapter. By varying the noise energy, it is possible for us to draw a QISI \times SNR curve.

We considered the LMS-based algorithms for optimization and assumed $M = 0$, $N_e = 5$ and the step sizes $\mu_{MSEE} = 0.0016$, $\mu_{HSEE} = 0.0015$, $\mu_{HREE} = 0.01$, $\mu_{corEE} = 0.0062$ and $\mu_{MQDEE} = 0.0025$, $N_{it} = 10000$ and $N_{conv} = 4000$, with mean displacement $disp_\theta = 1.1e-3$ for SNR of 10 dB (AWGN). The kernel sizes were chosen to be $\sigma = 1$ for all ITL-based criteria (a general choice, as previously discussed). The performance of the solutions of the algorithms were evaluated in terms of QISI – i.e., mean QISI after convergence – for 30 independent experiments, considering the Gaussian and the impulsive noise cases. The average QISI values along experiments can be verified in Fig. 7.9. For the Gaussian

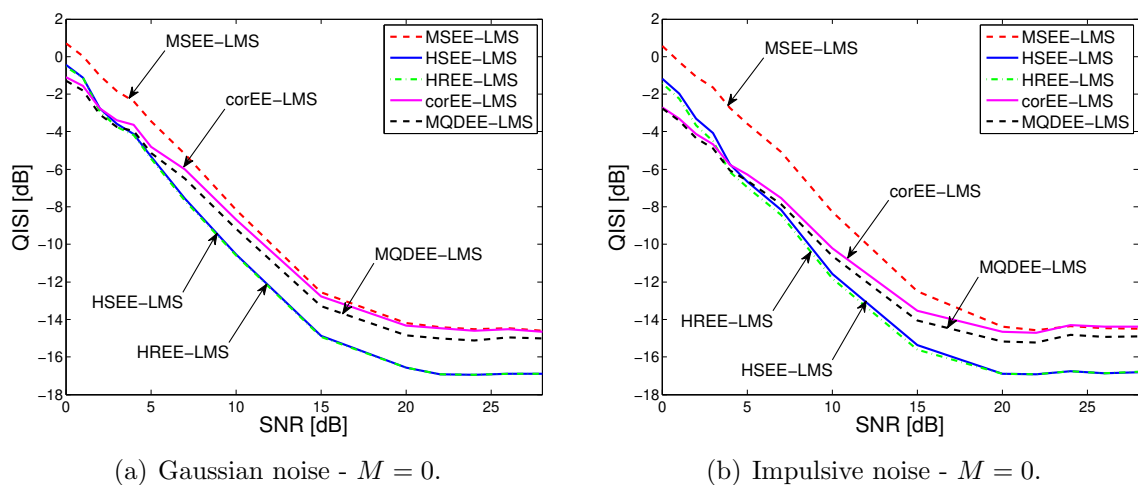


Figure 7.9: Equation-Error Formulation - Scenario 2: QISI \times SNR for $M = 0$.

noise, Fig. 7.9(a), it is possible to note that the ITL-based algorithms outperform the

MSEE-LMS algorithm for all SNR values. The performances of the corEE-LMS and of the MQDEE-LMS algorithms attain the best levels for low SNR values (SNR lower than 3 dB), however, above 5 dB, the HSEE-LMS and the HREE-LMS practically present the same performance and achieve the lowest QISI levels. Differently from scenario 1, the ITL-based algorithms outperform the MSEE-LMS algorithm even for greater SNR values (i.e., for SNR levels greater than 20 dB). In fact, this performance gain is mainly observed for the HSEE-LMS and the HREE-LMS algorithms, since the corEE-LMS algorithm converges to the same QISI level as the MSEE-LMS. The MQDEE-LMS algorithm, which can be viewed as a combination of the HREE-LMS and corEE-LMS algorithms, exhibits an intermediate performance. We emphasize that the good performance achieved by the HSEE-LMS and the HREE-LMS even on high SNR levels is a consequence of the higher degree of freedom of the IIR equalizer, which allows a more flexible processing of the data. For the impulsive noise, Fig. 7.9(b), we observe a similar behavior of the ITL-based algorithms. However, as the kernel estimators mitigate the impulsive effect of the noise, their performance is improved for lower SNR levels (less than 20 dB). Indeed, for an SNR of 5 dB, the ITL-algorithms outperform the MSEE-LMS by more than 3 dB.

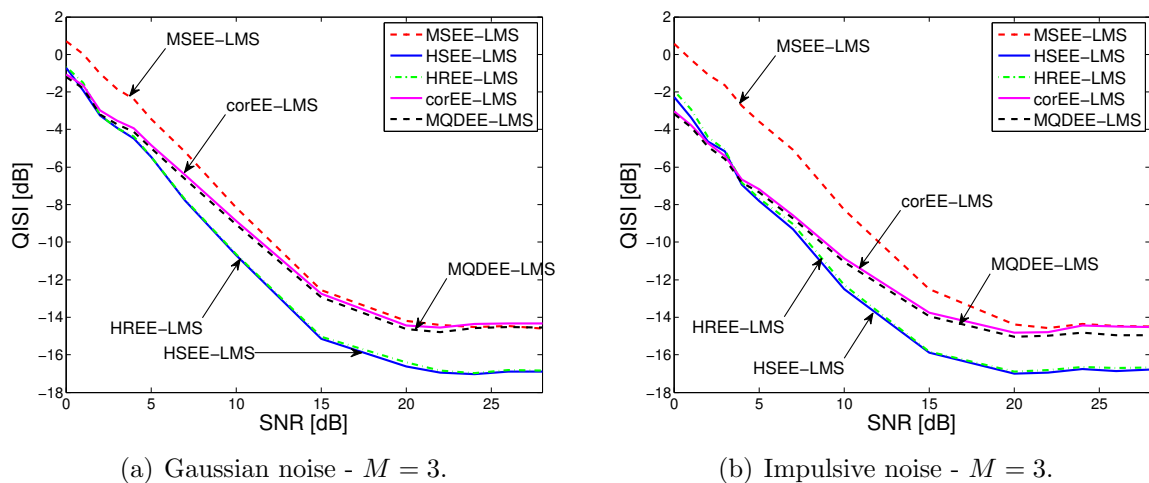


Figure 7.10: Equation-Error Formulation - Scenario 2: $\text{QISI} \times \text{SNR}$ for $M = 3$.

Regarding the multivariate case, we consider now $M = 3$ delays. The criteria parameters for this case were $M = 3$, $N_e = 5$ and the step sizes $\mu_{MSEE} = 0.0016$ (with $M = 0$ for MSEE), $\mu_{HSEE} = 0.0006$, $\mu_{HREE} = 0.22$, $\mu_{corEE} = 0.045$ and $\mu_{MQDEE} = 0.02$, $N_{it} = 10000$ and $N_{conv} = 4000$, with mean displacement $disp_{\theta} = 1.1e-3$ for SNR of 10 dB (AWGN). The $\text{QISI} \times \text{SNR}$ curves are as shown in Fig. 7.10. Comparing with the univariate case ($M = 0$), Fig. 7.9, we can observe a slight improvement on the performance: for instance, for SNR levels 3, 10 and 22 dB, the mean QISI performance is exhibited in Tab. 7.2 for $M = 0$ and $M = 3$, where it is clear that the gain on performance mostly occurs for lower SNR values. Under impulsive noise, the performance improvement is more pronounced, as can be verified in Tab. 7.3, mainly for lower SNR levels, in which

Table 7.2: Scenario 2: Mean QISI performance for Gaussian noise and for $M = 0$ and $M = 3$.

QISI [dB] - SNR 3 dB					
SNR 3 dB					
M	MSEE	HSEE	HREE	CorEE	MQDEE
0	-1.825	-3.571	-3.749	-3.397	-3.733
3	-	-3.905	-3.926	-3.516	-3.741
SNR 10 dB					
M	MSEE	HSEE	HREE	CorEE	MQDEE
0	-8.158	-10.537	-10.582	-8.673	-9.162
3	-	-10.690	-10.638	-8.879	-9.177
SNR 22 dB					
M	MSEE	HSEE	HREE	CorEE	MQDEE
0	-14.425	-16.913	-16.915	-14.464	-15.014
3	-	-16.965	-16.918	-14.559	-14.988

Table 7.3: Scenario 2: Mean QISI performance for impulsive noise and for $M = 0$ and $M = 3$.

QISI [dB] - SNR 3 dB					
SNR 3 dB					
M	MSEE	HSEE	HREE	CorEE	MQDEE
0	-1.632	-4.084	-4.508	-4.673	-4.884
3	-	-5.166	-5.087	-5.416	-5.571
SNR 10 dB					
M	MSEE	HSEE	HREE	CorEE	MQDEE
0	-8.262	-11.572	-11.835	-10.207	-10.626
3	-	-12.561	-12.293	-10.869	-11.042
SNR 22 dB					
M	MSEE	HSEE	HREE	CorEE	MQDEE
0	-14.591	-16.936	-16.922	-14.724	-15.229
3	-	-16.944	-16.926	-14.785	-15.234

the gain is up to 1 dB of QISI for SNR of 3 and 10 dB (for the HSEE-LMS algorithm). We highlight the performance of the HSEE-LMS and the HREE-LMS algorithms, which were similar and attained the best QISI values.

7.4.3 Equation-Error Formulation - Scenario 3

Within the same context of scenario 2, it is now assumed that the equalizer has the following transfer function

$$\Theta(z) = \frac{b_0 + b_1 z^{-1} + b_2 z^{-2}}{1 - a_1 z^{-1} - a_2 z^{-2} - a_3 z^{-3} - a_4 z^{-4}}, \quad (7.38)$$

being able to completely invert the channel and to achieve the ZF condition.

The algorithm parameters were chosen to be exactly the same of scenario 2 for $M = 0$ (which also leads the algorithms to the mean displacement of $disp_{\theta} = 1.1e-3$ for SNR level of 10 dB). The QISI \times SNR curves were obtained through the same procedure, as shown in Fig. 7.11. For Gaussian noise, Fig. 7.11(a), the performances in the neighbor-

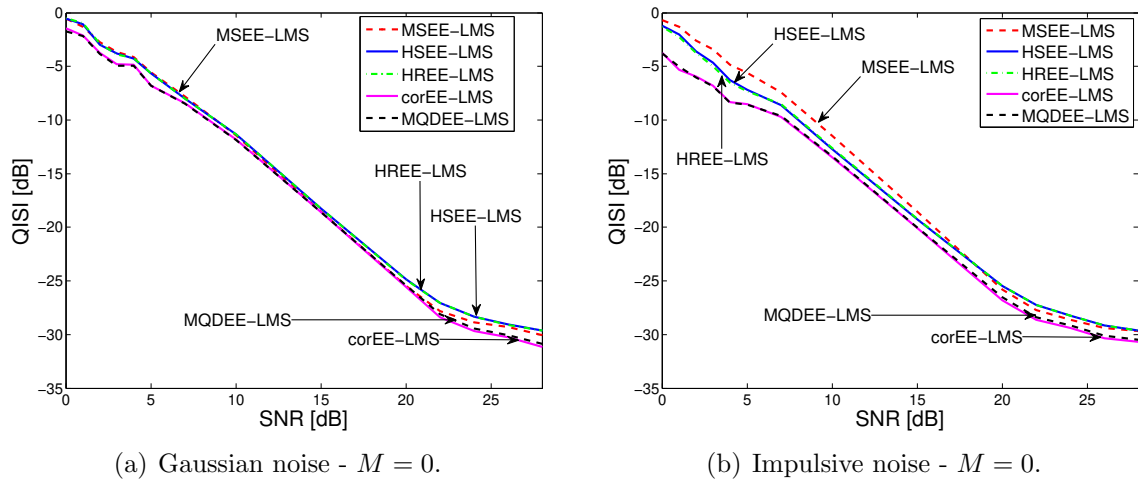


Figure 7.11: Equation-Error Formulation - Scenario 3: QISI \times SNR for $M = 0$.

hood of SNR level of 13 dB are similar among the algorithms. Curiously, the HSEE-LMS and the HREE-LMS algorithms – that achieved the best QISI performances in the previous scenarios – occupy now positions very close to the classical MSEE-LMS algorithm. This behavior suggests that, when the error can be substantially small (e.g., and the ZF condition is attainable) and the noise is Gaussian, the (Shannon’s and Rényi’s) error entropy becomes practically equivalent to the MSEE. On the other hand, the corEE-LMS and the MQDEE-LMS algorithms obtain now the best performances, specially for SNR values lower than 5 dB and higher than 20 dB. For the impulsive noise case, Fig. 7.11(b), the ITL-based algorithms show better QISI performance in comparison with the MSEE-LMS algorithms (due to their greater robustness against this type of noise), except for the HSEE-LMS and the HREE-LMS algorithms, whose performance above SNR of 17 dB becomes very close (and sometimes slightly worst) to the MSEE-LMS algorithm. The corEE-LMS and the MQDEE-LMS algorithms are about 4 dB of QISI better than the MSEE-LMS algorithm for SNR levels lower than 5 dB, and about 1 dB better for SNR values greater than 15 dB under impulsive noise.

By increasing the number of delays to $M = 3$, the resulting QISI performance is as shown in Fig. 7.12. In this case, the algorithms parameters were equal to those of the previous scenario for $M = 3$. For both noise cases, the gain in the QISI performance is mainly observed for SNR values higher than 20 dB in comparison with the $M = 0$ case. This becomes more evident from the QISI measures for SNR of 3, 10 and 26 dB, as shown in Tabs. 7.4 and 7.5 for the Gaussian and impulsive noise, respectively. More specifically, for the Gaussian noise, the HSEE-LMS and the HREE-LMS algorithms practically remain

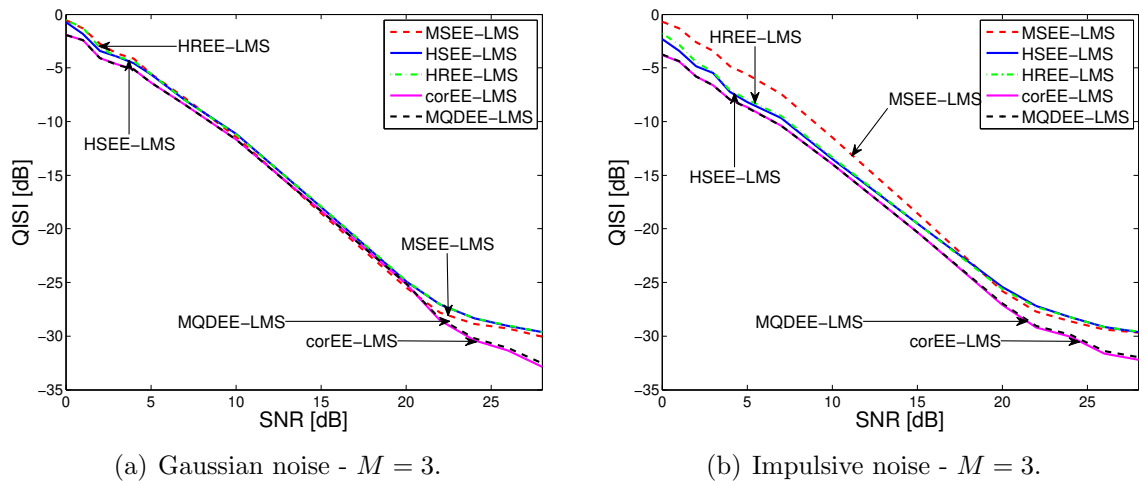


Figure 7.12: Equation-Error Formulation - Scenario 3: $\text{QISI} \times \text{SNR}$ for $M = 3$.

Table 7.4: Scenario 3: Mean QISI performance for Gaussian noise and for $M = 0$ and $M = 3$.

QISI [dB] - SNR 3 dB					
SNR 3 dB					
M	MSEE	HSEE	HREE	corEE	MQDEE
0	-3.657	-3.796	-3.887	-4.806	-4.959
3	-	-3.958	-3.944	-4.876	-4.995
SNR 10 dB					
M	MSEE	HSEE	HREE	CorEE	MQDEE
0	-11.412	-11.397	-11.408	-11.837	-11.855
3	-	-11.175	-11.213	-11.867	-11.872
SNR 26 dB					
M	MSEE	HSEE	HREE	CorEE	MQDEE
0	-29.314	-29.077	-29.061	-30.258	-30.052
3	-	-29.084	-29.039	-31.356	-31.118

unchanged by increasing M to 3. However, for the corEE-LMS and the MQDEE-LMS algorithms, the QISI performance is improved by approximately 1 dB for SNR of 26 dB. When the noise has impulsive behavior, the HSEE-LMS and the HREE-LMS algorithms can improve their performance for $M = 3$ and low SNR values (lower than 15 dB). Contrarily, for the corEE-LMS and the MQDEE-LMS algorithms, the increase of M leads to a performance improvement for higher SNR values (greater than 20 dB).

These results establish a clear disparity between the attainable and the non-attainable ZF condition, in which the corEE-LMS and the MQDEE-LMS algorithms switch places with the HSEE-LMS and HREE-LMS algorithms in occupying the best QISI performance position. In fact, Shannon's and Rényi's entropy-based algorithms show to be promising choices when the ZF condition is not attainable; for attainable ZF solutions, these entropy-based algorithms achieve a performance similar to that of the classical MSEE-

Table 7.5: Scenario 3: Mean QISI performance for impulsive noise and for $M = 0$ and $M = 3$.

QISI [dB] - SNR 3 dB					
SNR 3 dB					
M	MSEE	HSEE	HREE	CorEE	MQDEE
0	-3.416	-4.667	-4.969	-6.819	-6.835
3	-	-5.466	-5.384	-6.822	-6.838
SNR 10 dB					
M	MSEE	HSEE	HREE	CorEE	MQDEE
0	-11.531	-12.714	-12.615	-13.487	-13.458
3	-	-13.487	-13.352	-12.976	-13.972
SNR 26 dB					
M	MSEE	HSEE	HREE	CorEE	MQDEE
0	-29.369	-29.139	-29.164	-30.357	-30.121
3	-	-29.148	-29.167	-31.643	-31.386

LMS algorithm, but, on the contrary, the corEE-LMS and the MQDEE-LMS algorithms are able to reach the lowest QISI values, being preferable in these cases; however, the performance gain is more evident for SNR levels lower than 5 dB or higher than 20 dB. In fact, when the ZF solution is reached by an algorithm, the error PDF is equivalent to that of the noise, and, in the AWGN case, it is Gaussian distributed, a situation in which the SOS (or, in other words, the MSEE) is sufficient for equalization, hence the similarity in the performance. The error distribution tends to deviate from the Gaussian mainly for lower (below 5 dB) SNR levels, where the algorithms are more susceptible to the noise, and for higher (above 20 dB) SNR levels, in which the error distribution tends to an impulse at the origin. In these two cases, the corEE-LMS and the MQDEE-LMS algorithms performed better. When the noise is impulsive, the corEE-LMS and the MQDEE-LMS algorithms presented good performance for all SNR levels, and, since the error distribution is not Gaussian, the HSEE-LMS and HREE-LMS algorithms also outperform the MSEE-LMS algorithm for SNR under 20 dB.

7.5 Performance Analysis - Output-Error Formulation

In the output-error formulation, we compare the surfaces for each cost and the performance of the ITL algorithms based on the PLR and RPE approaches. Notwithstanding, since the algorithms assume approximations on the IIR structure to compute the gradient, it is expected that some divergences may arise on the optimal value. In that sense, we employ, as an alternative optimization method, the DE metaheuristic [Storn and Price, 1997].

7.5.1 Output-Error Formulation - Scenario 1

We assume that the source s_n is an *i.i.d.* BPSK modulated signal transmitted through the channel

$$H(z) = \frac{1 - 0.6z^{-1}}{1 + 0.2z^{-1}}, \quad (7.39)$$

and that the IIR equalizer is an all pole filter, with two free parameters a_1 and a_2 :

$$\Theta(z) = \frac{1}{1 + a_1z^{-1} + a_2z^{-2}}, \quad (7.40)$$

The presence of Gaussian noise with SNR level of 10 dB at the receiver input is also considered. Note that the equalizer structure is insufficient to completely compensate the channel.

The ITL Cost Surfaces

The reference approach is the MSOE, which, similarly to the equation-error formulation in the context of channel equalization, also suffers from the noise bias effect. This deficiency is also visible in the costs surfaces, as we intend to show.

We consider that there are $N_e = 200$ error samples available to estimate the MSOE cost and that the coefficients taps a_1 and a_2 vary from -2 to 2 . For the noiseless and noisy (SNR of 10 dB) cases, the obtained contours of the MSOE cost are illustrated in Fig. 7.13. Differently from the Equation-Error formulation, the surface cost is not a paraboloid, but

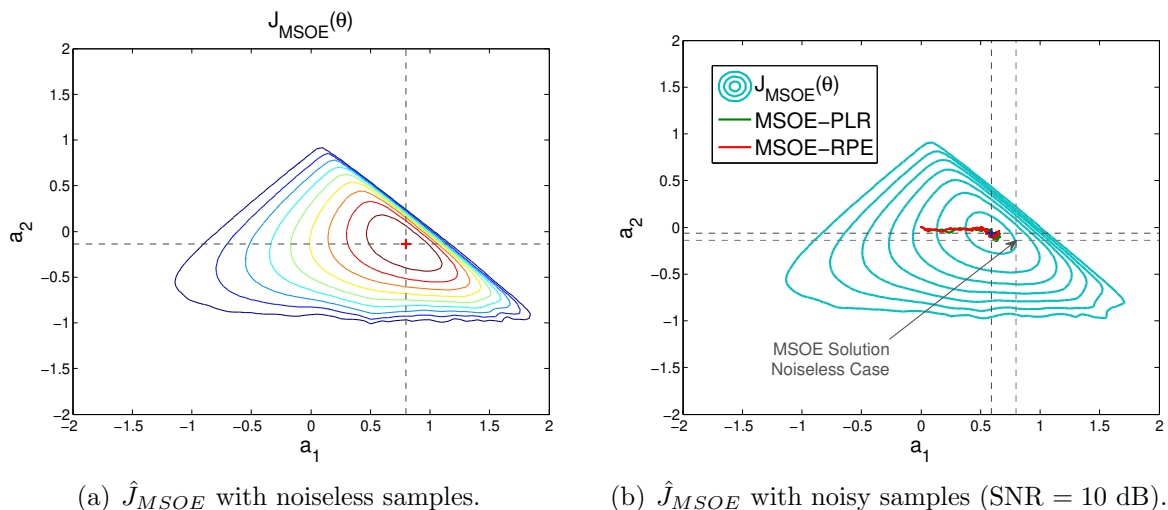


Figure 7.13: Output-Error Formulation - Scenario 1 - MSOE Surface contours.

still presents a single optimum (denoted by a cross ‘+’ sign). Interestingly, it is possible to clearly observe the shape of the stability triangle, the area where the IIR filter presents stable behavior (as shown in Section 1.1.1) in both noiseless and noisy cases. When there is noise, Fig. 7.13(b), it is possible to note that the solution becomes biased – as also

occurs in the equation-error formulation. Hence, the objective in using the ITL-based approaches here will also be to find methods that are more robust to noise. However, since the PLR and RPE algorithms make use of an approximate gradient, the conclusion might not be the same of the previous analysis. Fig. 7.13(b) also displays the evolution of the PLR- and RPE-based algorithms along the iterations for a certain configuration, but we will treat this topic later.

To start the investigation of the ITL criteria, we will observe their surfaces for certain parameters values. We first consider a kernel size of $\sigma = 3$, $N_e = 200$ and $M = 0$ delays, whose resulting contours for the HSOE, the HROE, the corOE and the MQDOE costs are illustrated in Fig. 7.14. With exception of the MQDOE, which presents a flatter surface and certain (non-minima) spikes, all the costs surfaces are similar to that of the MSOE, with a clearly defined solution (denoted by the cross ‘+’ sign). However, the noise bias

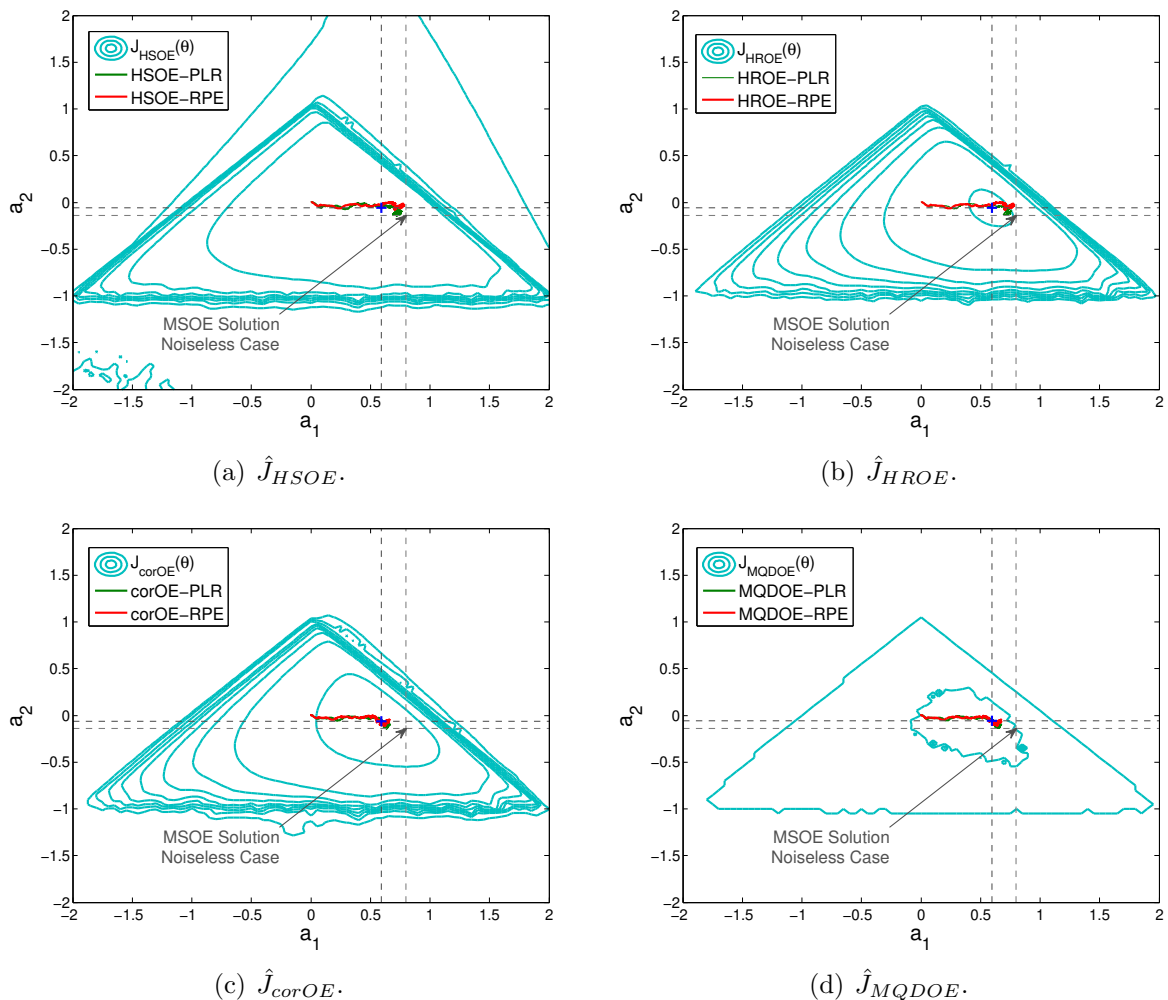


Figure 7.14: Output-Error Formulation - Scenario 1: ITL costs surface contours for $\sigma = 3$, $M = 0$ and SNR of 10 dB.

effect is still present and seems to be similar among the ITL costs.

Reducing the kernel size to $\sigma = 1.2$, we obtain the contours displayed at Fig. 7.15,

in which the surfaces smoothness are reduced for all ITL costs, but the impact on the solutions is very small, i.e., they practically do not change their positions. The MQDOE cost presents a larger number of non-minima spikes, which now concentrates closer to the solution.

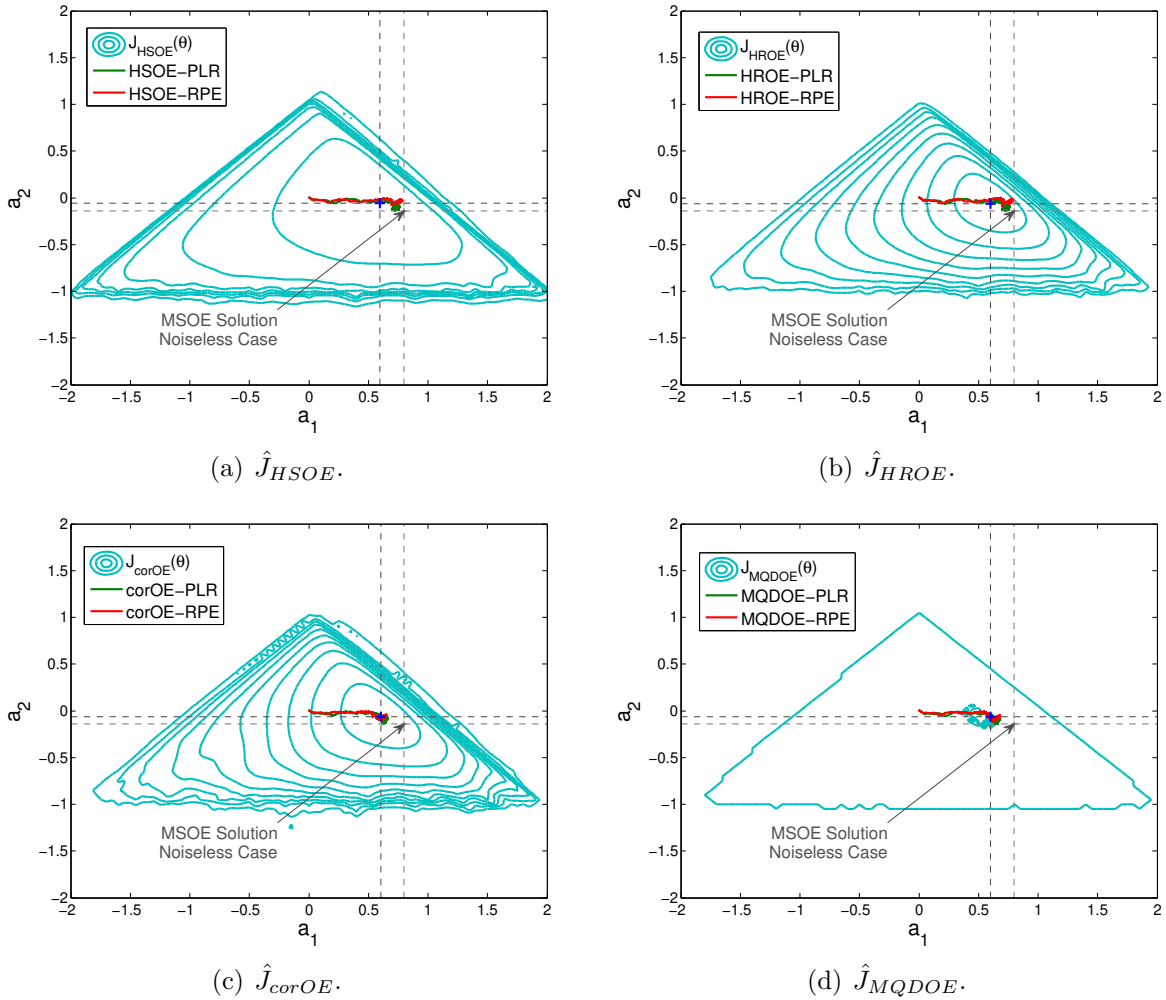


Figure 7.15: Output-Error Formulation - Scenario 1: ITL costs surface contours for $\sigma = 1.2$, $M = 0$ and SNR of 10 dB.

Now we vary the number of considered delays, increasing it to $M = 2$ (for the MSOE cost, the number of delays is fixed – $M = 0$). Keeping $\sigma = 1.2$, the resulting surface contours of the ITL costs are as displayed in Fig. 7.16. It is possible to note that the HROE and the corOE cost shapes change significantly, being the stability triangles not completely visible anymore. In addition, for all costs, the solutions have changed their position, being closer to the noiseless MSOE solution, which suggests that the performance of the ITL approaches might be improved through the use the temporal information about the error signal. However, the proper performance analysis will be held in the following.

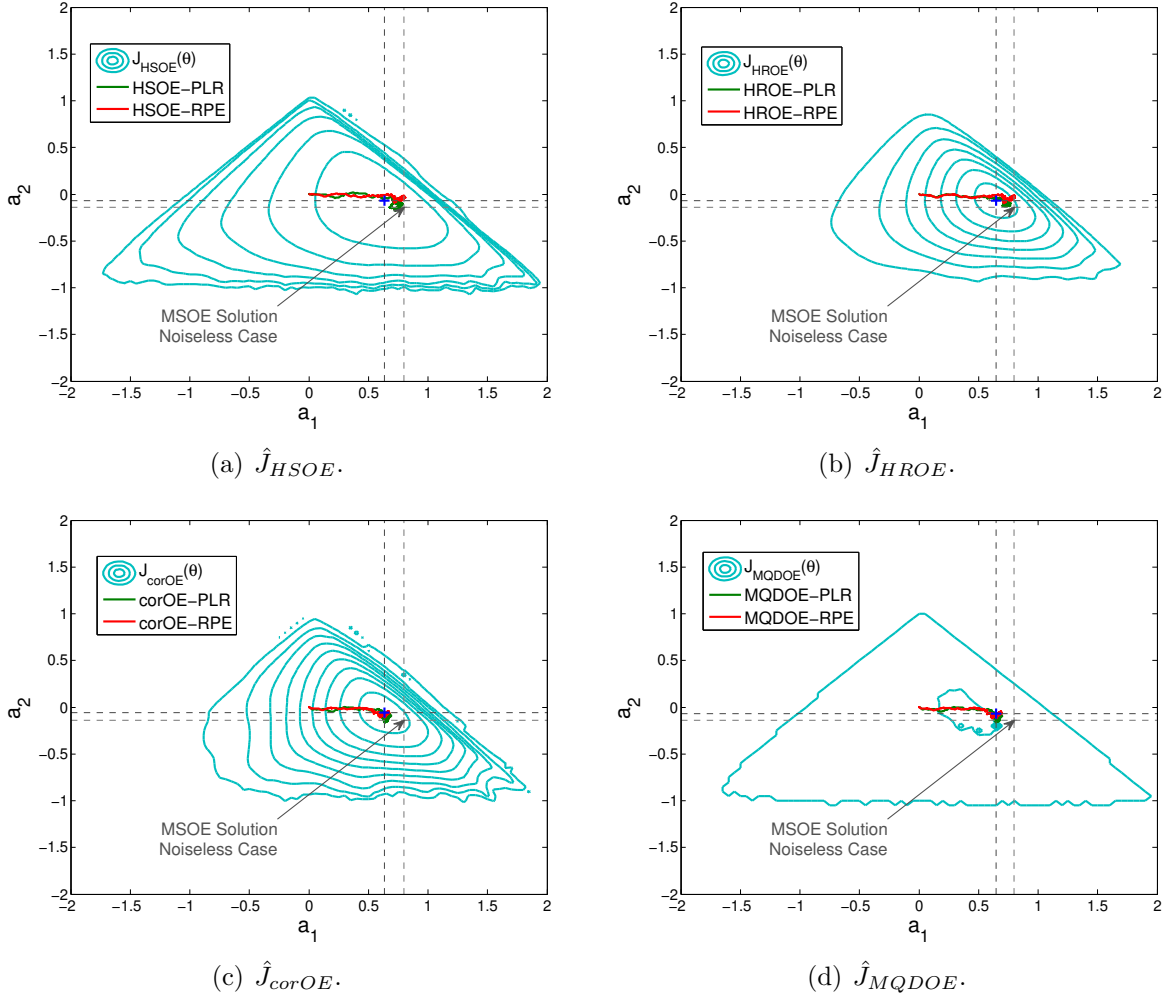
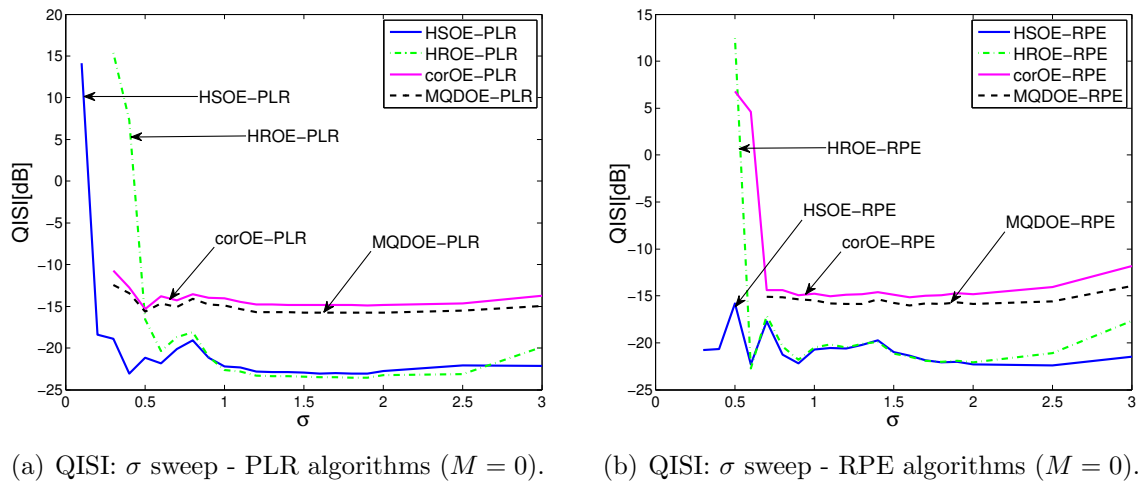


Figure 7.16: Output-Error Formulation - Scenario 1: ITL costs surface contours for $\sigma = 1.2$, $M = 2$ and SNR of 10 dB.

Gradient-Based Methods - The Kernel Size

To measure the performance of the ITL-based approaches, we will use the LPR- and RPE-based algorithms, as well as the DE metaheuristic to find the global optimum, since the algorithms might deviate from the solution due to the approximate gradient.

Starting with the gradient-based methods, we choose – for scenario 1 – the parameters: $N_e = 5$, $M = 0$, step sizes $\mu_{MSOE-PLR} = 0.003$, $\mu_{HSOE-PLR} = 0.0035$, $\mu_{HROE-PLR} = 0.03$, $\mu_{corOE-PLR} = 0.015$ and $\mu_{MQDOE-PLR} = 0.0065$, and $\mu_{MSOE-RPE} = 0.002$, $\mu_{HSOE-RPE} = 0.0027$, $\mu_{HROE-RPE} = 0.025$, $\mu_{corOE-RPE} = 0.01$ and $\mu_{MQDOE-RPE} = 0.005$. For the kernel size, we performed a linear sweep on σ , similarly to the previous section. The QISI performance of the algorithms after convergence was registered in 30 independent simulations, whose mean values are displayed in Fig. 7.17. For both type of algorithms, low σ values ($\sigma < 0.5$ for the PLR-based algorithms and $\sigma < 0.7$ for the RPE-based algorithms) may cause the algorithms to diverge, resulting in poor performance in some cases. For greater values of σ , the PLR- and RPE-based algorithms are able to



(a) QISI: σ sweep - PLR algorithms ($M = 0$). (b) QISI: σ sweep - RPE algorithms ($M = 0$).

Figure 7.17: Output-Error Formulation - Scenario 1: PLR and RPE algorithms Performance - σ sweep ($M = 0$).

improve their performances and, in the vicinity of $\sigma = 1.9$, all the algorithms attain their best performances. For larger σ values, the QISI tends to increase – more slowly for the PLR-based algorithms. Nonetheless, there is an acceptable range of σ between 1.2 and 2 that yields practically the same QISI performance for the PLR algorithms. For the RPE-based algorithms, this range is somehow valid for the corOE-RPE and the MQDOE-RPE algorithms, but, for the HSOE-RPE, the range goes from 1.9 to 2.5 and, for the HROE-RPE, from 1.7 to 2.2. In all cases, $\sigma = 1.9$ leads to a reasonably good performance and, for this reason, we choose this value for the kernel size when $M = 0$ – but other values of σ would result in similar performance, according to the Fig. 7.17. Under these conditions, the choice of the parameters yielded a mean displacement of $disp_{\theta} = 5e-4$ for $N_{it} = 10000$ and $N_{conv} = 4000$ for both PLR and RPE approaches.

For $M = 2$, we adopted the parameters: $N_e = 5$, step sizes $\mu_{HSOE-PLR} = 0.002$, $\mu_{HROE-PLR} = 0.19$, $\mu_{corOE-PLR} = 0.07$, $\mu_{MQDOE-PLR} = 0.03$, $\mu_{HSOE-RPE} = 0.002$, $\mu_{HROE-RPE} = 0.0012$, $\mu_{corOE-RPE} = 0.04$ and $\mu_{MQDOE-RPE} = 0.02$. The linear sweep on σ , in this case, resulted in the QISI performance shown in Fig. 7.18. Again, low SNR values (below 1 dB) may result in poor performance or make the algorithms diverge. For the HSOE-PLR and HROE-PLR algorithms (Fig. 7.18(a)), the range from 1.6 to 1.9 is a promising region, with minimum QISI at 1.8. For the corOE-PLR and MQDOE-PLR algorithms, there is a plateau from $\sigma = 1$ to $\sigma = 2$, with a minimum (almost imperceptible) at $\sigma = 1.4$, in both cases. For the HSOE-RPE algorithm (Fig. 7.18(b)), $\sigma = 1.3$ is the kernel size that leads to the best QISI performance, but the range of σ from 2 to 2.5 also leads to very close QISI levels. For HSOE-RPE algorithm, there is a clear minimum at $\sigma = 1.4$. For the corOE-RPE and MQDOE-RPE algorithms, the minimum QISI is achieved for $\sigma = 1.9$. Thus, for $M = 2$, the kernel sizes are chosen to be as shown in Tab. 7.6. These parameters yielded a mean displacement of $disp_{\theta} = 5e-4$ for $N_{it} = 10000$

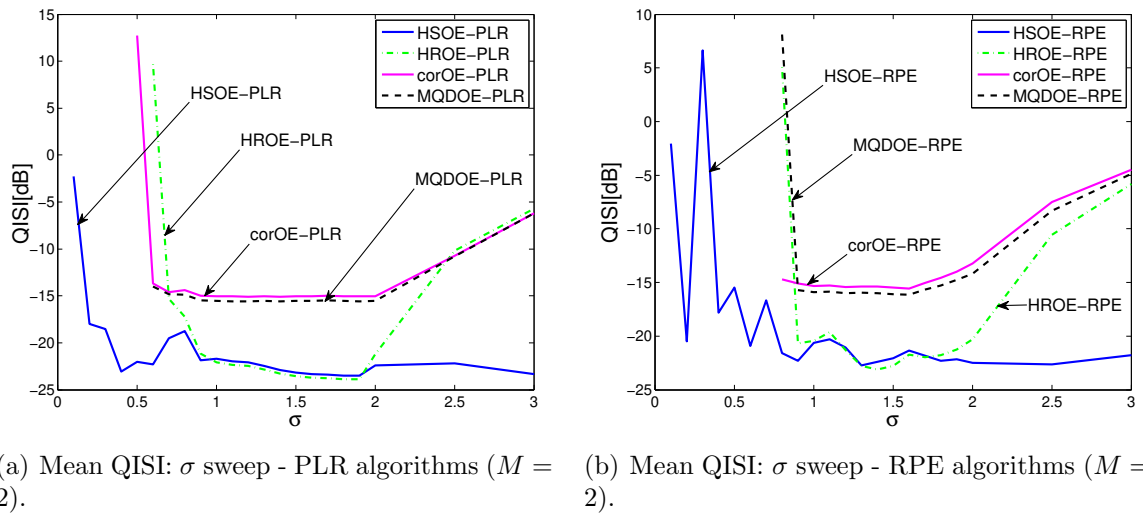


Figure 7.18: Output-Error Formulation - Scenario 1: PLR and RPE algorithms Performance - σ sweep ($M = 2$).

and $N_{conv} = 4000$ for both PLR and RPE approaches. Once the parameters are defined, we are able to proceed with the analysis of the algorithms.

Table 7.6: Output-Error Formulation: Algorithms Parameters for $M = 0$ and $M = 2$.

$M = 0$				
	PLR		RPE	
	step size μ	kernel size σ	step size μ	kernel size σ
MSOE	0.003	–	0.002	–
HSOE	0.0035	1.9	0.0027	1.9
HROE	0.03	1.9	0.025	1.9
corOE	0.015	1.9	0.01	1.9
MQDOE	0.0065	1.9	0.005	1.9
$M = 2$				
	PLR		RPE	
	step size μ	kernel size σ	step size μ	kernel size σ
MSOE	–	–	–	–
HSOE	0.002	1.8	0.002	1.3
HROE	0.19	1.8	0.0012	1.4
corOE	0.07	1.4	0.04	1.9
MQDOE	0.03	1.4	0.02	1.9

Optimization Methods

For the $M = 0$ case, the QISI performance was measured along iterations throughout 30 independent experiments, whose mean values are illustrated in Fig. 7.19 for the PLR- and the RPE-based algorithms (the parameters were adjusted as indicated in Tab. 7.6). The convergence speeds were very similar between the two approaches. It can also be seen that the MSOE algorithms presented the poorer QISI performance along with the corOE

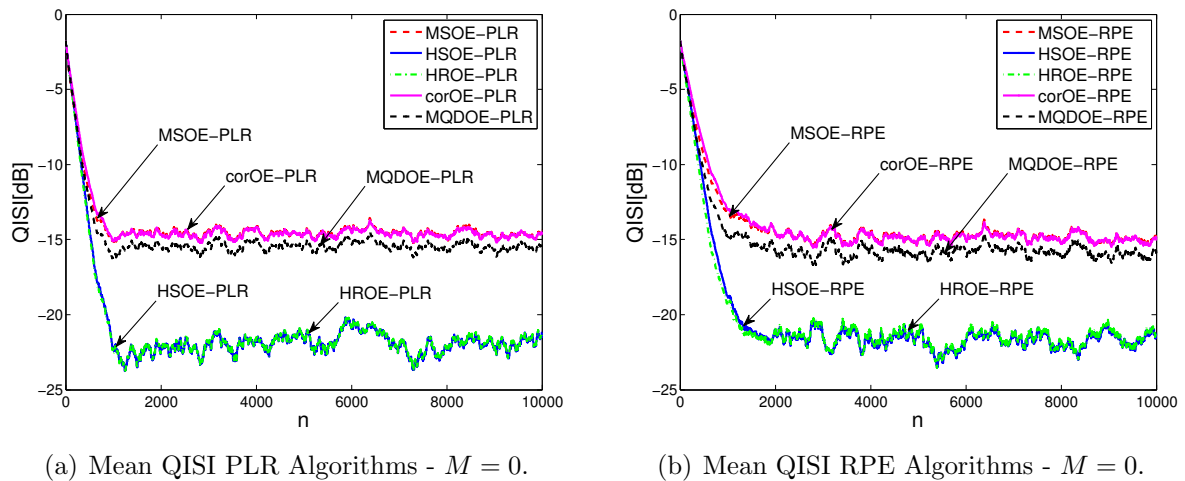


Figure 7.19: Output-Error Formulation - Scenario 1: QISI Performance of the PLR- and RPE-based algorithms for $M = 0$ and SNR of 10 dB.

approaches. The MQDOE algorithms present a slightly better performance for both PLR and RPE versions. With some advantage, the HSOE and the HROE algorithms attained the lowest values of QISI. To understand this behavior, we have plotted on the contours of Figs. 7.13(b), 7.14 and 7.15 the weight evolution along iterations for the PLR- and RPE-based algorithms in one of the experiments. Very interestingly, the convergence of the HSOE-PLR, HSOE-RPE, HROE-PLR and HROE-RPE algorithms do not match the cost optima. Indeed, as previously mentioned, the approximation carried out on the gradient by both PLR and RPE algorithms causes a deviation on the optima, which, in this case, seems to lead to improved solutions. This deviation also exists for the MSOE, corOE and MQDOE algorithms, but to a smaller degree.

For comparison purposes, we have also evaluated the performance of the solutions found by the DE metaheuristic, which are expected to be more ‘precise’ according to adopted criteria. For this, we have considered $N_e = 200$, the kernel sizes indicated in Tab. 7.6 (for the RPE algorithm and for $M = 0$) and the DE parameters $N_P = 100$, $F = 0.5$, $CR = 0.9$ and 100 iterations. The mean QISI performance for 30 independent experiments is displayed in Tab. 7.7 along with the QISI convergence values of the algorithms. It is possible to see that the DE solutions for the MSOE, corOE and MQDOE criteria presented similar performances to the solutions found by the PLR and RPE approaches. However, for the HSOE and HROE criteria, the DE solution remained distant from the QISI level of -21 dB obtained by the algorithms. This indicates that the PLR and RPE algorithms along with the entropy-based approaches might establish a particular and beneficial relationship.

Increasing M to 2, we observe the effect of the temporal information on the algorithms. We adopted the parameters: $N_e = 5$ and step sizes and kernel size according to Tab. 7.6. The mean QISI performance for 30 experiments throughout iterations is illustrated in

Fig. 7.20 for the PLR and the RPE-based algorithms. As can be noted, the algorithms

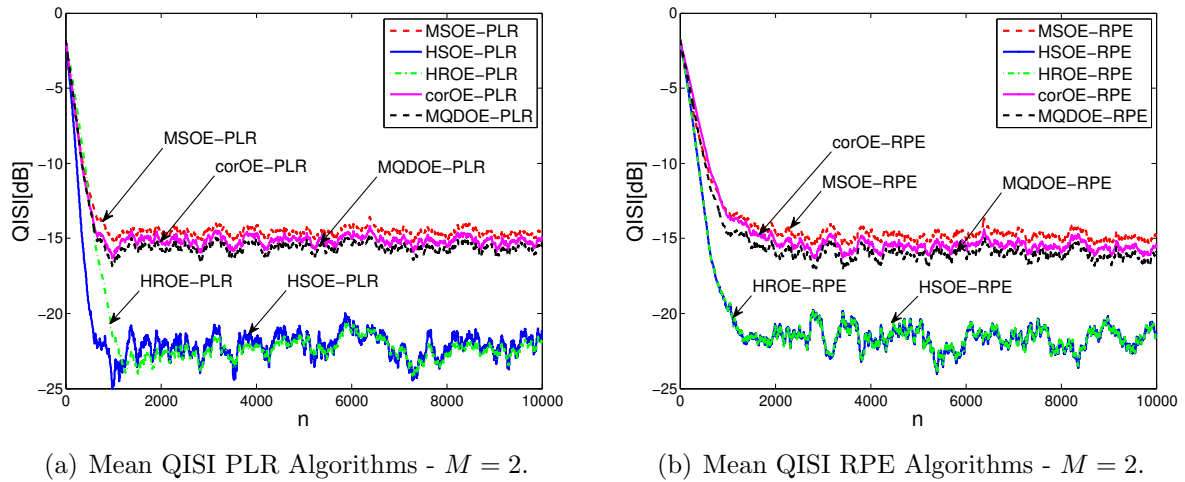


Figure 7.20: Output-Error Formulation - Scenario 1: QISI Performance of the PLR- and RPE-based algorithms for $M = 2$ and SNR of 10 dB.

behavior is very similar to the $M = 0$ case and the performance at convergence is only slightly improved for the corOE and the MQDOE algorithms (both PLR and RPE versions), as can be also verified from Tab. 7.7. For the HSOE and HROE algorithms, the performance is practically kept the same.

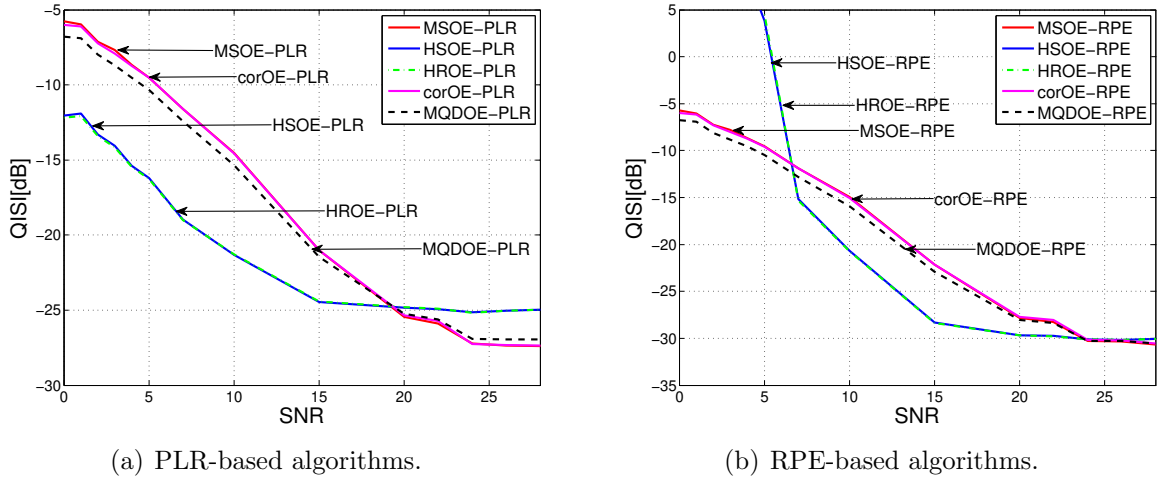
The performance associated with the solutions found by the DE metaheuristic for $M = 2$ can also be seen in Tab. 7.7. Interestingly, the QISI values were about 1 dB lower than that for $M = 0$, which indicates that the criteria are able to use the temporal information efficiently, but not the algorithms. This result is in accordance with the behavior observed in the surface analysis, in which, by increasing M , the solutions became closer to the desired noiseless solution case.

Other interesting topic to be analyzed is the effect of the SNR level. In that sense, by performing a sweep on the SNR values from 0 to 28, we obtained the $\text{QISI} \times \text{SNR}$ curves depicted in Fig. 7.21 for the PLR- and RPE-based algorithms in the $M = 0$ case, as well as the performance of the solution found by the DE metaheuristic (note, however, that

Table 7.7: Output-Error Formulation - Scenario 1: Mean QISI performance for $M = 0$ and $M = 2$ (SNR level of 10 dB).

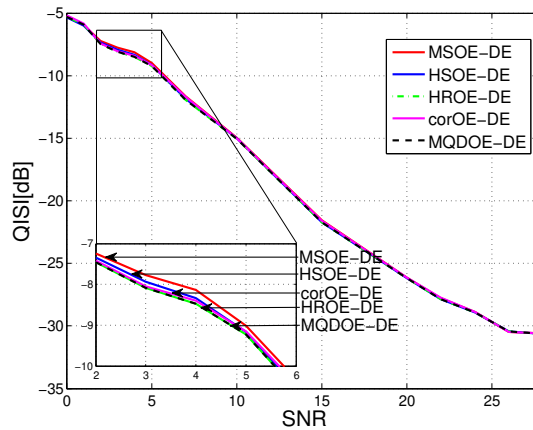
M	Otim.	QISI [dB]				
		MSOE	HSOE	HROE	corOE	MQDOE
0	PLR	-14.542	-21.407	-21.365	-14.624	-15.418
	RPE	-14.857	-21.362	-21.253	-14.964	-15.843
	DE	-14.198	-14.362	-14.335	-14.197	-14.335
2	PLR	-	-21.416	-21.767	-15.051	-15.518
	RPE	-	-21.363	-21.356	-15.576	-16.066
	DE	-	-15.301	-15.386	-14.7014	-15.386

we have used $N_e = 5$ for the algorithms while $N_e = 200$ for the DE; the other parameters were kept the same, according to Tab. 7.6). For the PLR-based algorithms performance,



(a) PLR-based algorithms.

(b) RPE-based algorithms.



(c) DE metaheuristic.

Figure 7.21: Output-Error Formulation - Scenario 1: $QISI \times SNR$ for $M = 0$.

Fig. 7.21(a), we are able to observe two distinct groups of similar performances: the first one is composed by the MSOE-PLR, corOE-PLR and MQDOE-PLR algorithms and the second group is the HSOE-PLR and the HROE-PLR algorithms. In the first group, the MSOE-PLR and the corOE-PLR algorithms perform very similarly, while the MQDOE-PLR algorithm is able to attain smaller QISI measures for SNR levels lower than 20 dB. For SNR values greater than 20 dB, the MQDOE-PLR algorithm is close to the MSOE-PLR, but with a slightly greater QISI value. On the second group, we observe the practically identical QISI performance of the HSOE-PLR and HROE-PLR algorithms. For SNR lower than 19 dB, the HSOE-PLR and HROE-PLR outperform all the other algorithms. For instance, for SNR level of 7 dB, the HSOE-PLR and HROE-PLR algorithms attain -20 dB of QISI, while the MSOE-PLR only -11 dB of QISI, i.e., a reduction of about 9 dB of QISI, which is an impressive performance gain. On the other

hand, for SNR greater than or equal to 20 dB, the QISI performance of the HSOE-PLR and HROE-PLR algorithms stagnates and the performance is worst than the classical MSOE-PLR algorithm.

Regarding the RPE-based algorithms performance, Fig. 7.21(b), we also observe the same two groups of the PLR case. In the first group (MSOE-RPE, corOE-RPE and MQDOE-RPE), for low SNR values, the performance is very similar to the PLR case, but for an SNR higher than 10 dB, the QISI performance is improved for all algorithms. For example, for an SNR equal to 25 dB, the QISI performance is about -30 dB, while the MSOE performance for the PLR case achieves about -27 dB. The second group – composed by the HSOE-RPE and HROE-RPE algorithms – presents poor performance for SNR lower than 7 dB, but, for SNR levels between 7 and 24 dB, their performances are the best among the RPE-based algorithms. In comparison with the PLR algorithms, the HSOE-RPE and HROE-RPE algorithms outperform their PLR counterparts for SNR higher than 10 dB, but, for an SNR lower than 10, the HSOE-PLR and HROE-PLR algorithms are preferred.

Finally, for the solutions found by the DE metaheuristic, Fig. 7.21(c), the criteria performances are worst than the PLR and RPE algorithms, but very similar among each other. The major difference occurs for SNR values from 2 to 6 dB (the zoomed area in Fig. 7.21(c)), where the MSOE is outperformed by the HSOE, the corOE, the HROE and the MQDOE algorithms.

Now, to investigate the effect of the temporal information, we perform the same analysis for the $M = 2$ case, whose parameters were adjusted according to Tab. 7.6. The resulting QISI \times SNR curves for the PLR- and RPE-based algorithms as well as for the DE metaheuristic are shown in Fig. 7.22. For the PLR-based algorithms, Fig. 7.22(a), the ITL-based approaches showed an improvement on the performance for SNR values lower than 20 dB in comparison with the $M = 0$ case. The corOE-PLR and the MQDOE-PLR experienced a more intense reduction on the QISI measures for lower SNR levels: for SNR of 0 dB, the corOE-PLR and MQDOE-PLR algorithms achieved, for $M = 2$, -7.4 and -7.6 dB, respectively; when $M = 0$, the QISI performances were -6.1 and -6.9 dB, respectively. This difference gradually diminishes as the SNR increases. The HSOE-PLR and the HROE-PLR algorithms expressed similar behavior, being able to achieve, for SNR of 0 dB and $M = 2$, approximately -15 dB of QISI, instead of -12 dB of QISI for $M = 0$. It is also worth mentioning that the HROE-PLR algorithm performed better than the HSOE-PLR for SNR values between 5 and 24 dB (out of this range, the performance was very similar). However, for SNR levels higher than 24 dB, the algorithms converged to the same QISI values of the $M = 0$ case.

In Fig. 7.22(b), the QISI curves for the RPE-based algorithms showed a similar effect for the corOE-RPE and the MQDOE-RPE algorithms, i.e., their QISI performance were improved mainly for lower SNR values in comparison with the $M = 0$ case. However, for

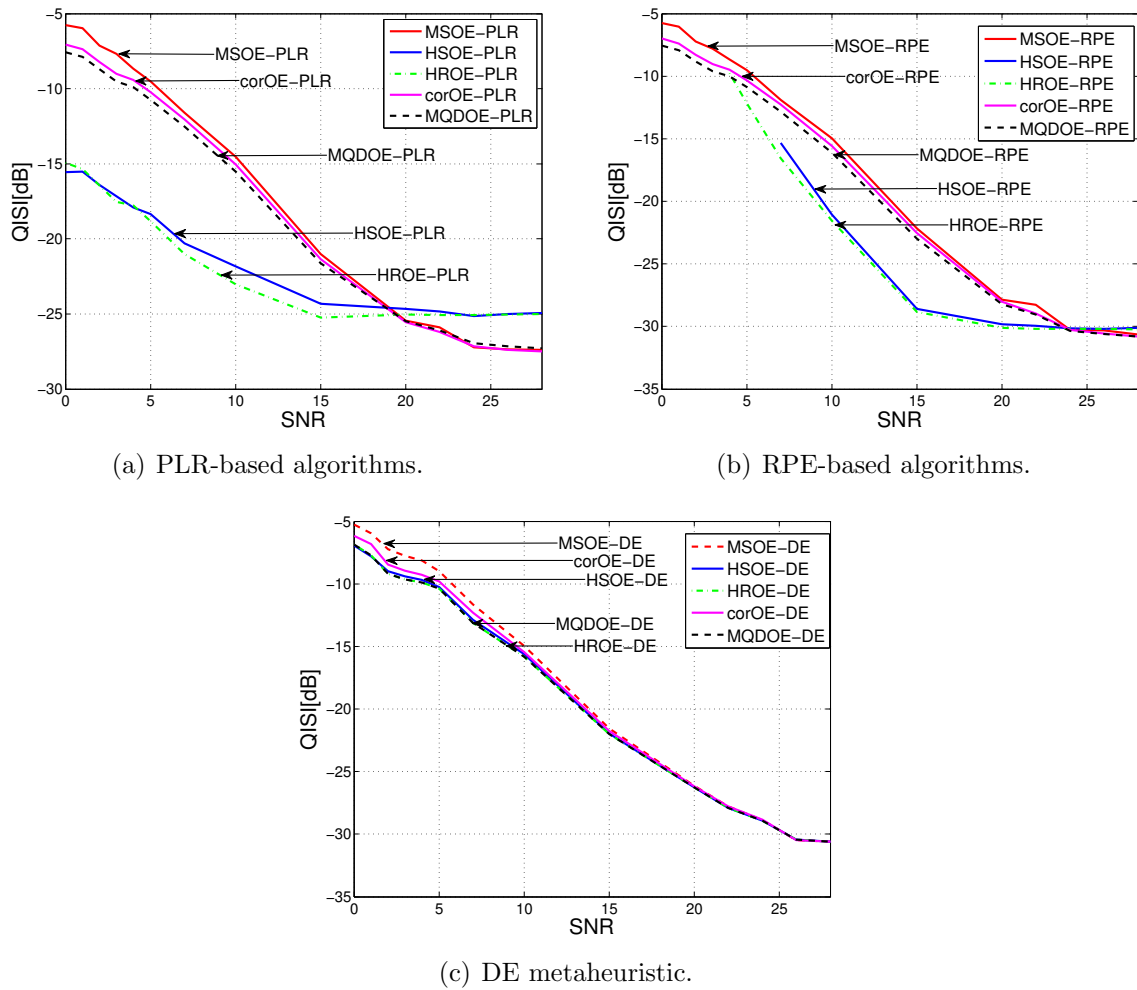


Figure 7.22: Output-Error Formulation - Scenario 1: $QISI \times SNR$ for $M = 2$.

the HSOE-RPE and the HROE-RPE algorithms, the attained QISI values were practically kept the same. For SNR values below 5 dB, these two algorithms may diverge, presenting QISI levels higher than the $M = 0$ case.

The QISI performance of the solutions found by the DE metaheuristic (Fig. 7.22(c)) also revealed that, by increasing M , an improvement on the performance of the ITL-based algorithms for lower SNR levels (less than 15 dB) can be observed. In fact, the MQDOE, the HROE and the HSOE criteria showed similar QISI values and achieved the best performance. After them, the corOE criterion showed an intermediate QISI performance, but still better than the MSOE criterion. For above 15 dB, the QISI performance is almost indistinguishable among the criteria.

In summary, considering this first scenario, we may say that the HSOE- and the HROE-based algorithms were able to achieve the best performances for SNR levels below 20 dB, although this does not hold for the HSOE-RPE and the HROE-RPE algorithm for SNR less than 7 dB. The corOE- and the MQDOE-based algorithms are able to perform better than the classical MSOE-based algorithms for SNR levels below 20 dB. For SNR

levels above 20 dB, the RPE-based algorithms presented better performances than their corresponding PLR counterpart. Interestingly, through the comparison made with the solutions found by the DE metaheuristic, we confirmed that the two PLR- and RPE-based algorithms deviate from the actual solution provided by the algorithms and, in this case, the deviation helped improving the QISI performance. The increase of the number of delays M also contributed for the performance improvement regarding the PLR, the RPE (with exception of the HSOE-RPE and HROE-RPE algorithms) and the DE solutions. Notwithstanding, to confirm that the deviations are not a mere coincidence, we investigate in the following section two scenarios encompassing more complex channel and equalizer models.

7.5.2 Output-Error Formulation - Scenario 2

In the second scenario, the source s_n is an *i.i.d.* BPSK modulated signal, which is transmitted through the channel with transfer function

$$H(z) = \frac{1 - 0.8z^{-1} + 0.2z^{-2} + 0.1z^{-3}}{1 + 0.2z^{-1}}. \quad (7.41)$$

and the IIR equalizer

$$\Theta(z) = \frac{b_0 + b_1z^{-1}}{1 - a_1z^{-1} - a_2z^{-2}}, \quad (7.42)$$

where b_0 , b_1 , a_1 and a_2 are free coefficients. It is important to remark that the ZF solution can not be attained in this case due to structural limitations of the equalizer. We also consider the presence of noise, that can be Gaussian or impulsive (the impulsive noise model is as described in Section 7.4.2).

For the $M = 0$ case, we considered the following parameters for the algorithms: $N_e = 5$, kernel sizes according to Tab. 7.6 and the step sizes $\mu_{MSOE-PLR} = 0.003$, $\mu_{HSOE-PLR} = 0.007$, $\mu_{HROE-PLR} = 0.09$, $\mu_{corOE-PLR} = 0.06$, $\mu_{MQDOE-PLR} = 0.022$, $\mu_{MSOE-RPE} = 0.003$, $\mu_{HSOE-RPE} = 0.008$, $\mu_{HROE-RPE} = 0.1$, $\mu_{corOE-RPE} = 0.052$ and $\mu_{MQDOE-RPE} = 0.022$, which resulted in mean displacement of $disp_\theta = 1.3e-3$ for SNR of 10 dB (AWGN), with $N_{it} = 10000$ and $N_{conv} = 4000$. The DE parameters were chosen to be $N_P = 300$, $F = 0.5$, $CR = 0.9$ and 300 iterations ($N_e = 200$ and the kernel sizes were the same of the RPE approach). For 30 independent experiments, the QISI×SNR curves considering the Gaussian and the impulsive noise cases are as displayed in Figs. 7.23 and 7.24, respectively.

For the Gaussian noise, Fig. 7.23, the observed performance for the PLR-based algorithms is similar to that of scenario 1 (Fig. 7.21(a)), where the HSOE-PLR and the HROE-PLR algorithms are more adequate for lower SNR levels (here, below 12 dB), but for higher SNR levels, they perform poorer than the MSOE-PLR algorithm. The corOE-PLR algorithm presents a QISI performance similar to that of the MSOE-PLR algorithm

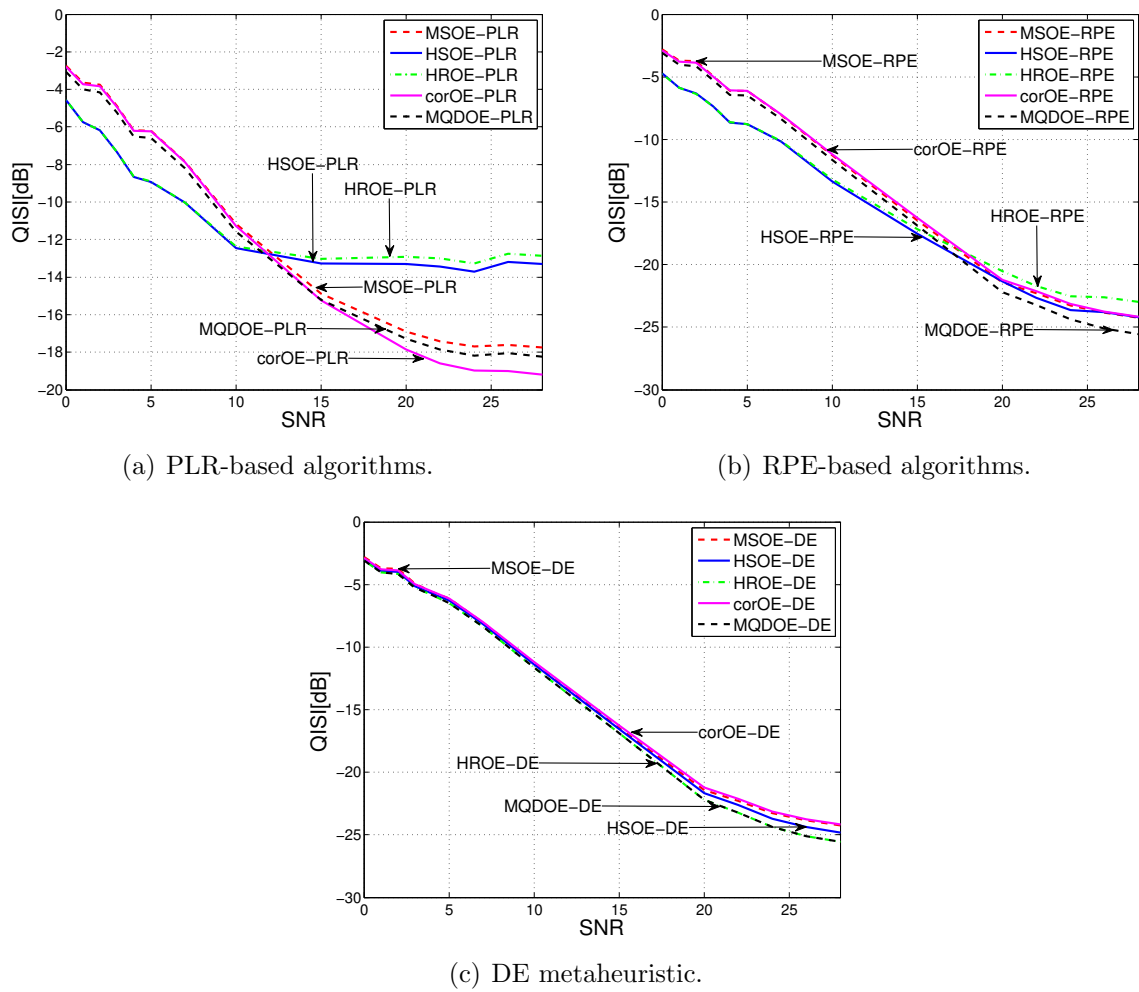


Figure 7.23: Output-Error Formulation - Scenario 2: $QISI \times SNR$ for Gaussian noise and $M = 0$.

for SNR values lower than 12 dB, but, as the SNR increases, it exhibits the best performance, with about 1.5 dB lower than the MSOE-PLR algorithm for SNR of 25 dB. The MQDOE-PLR algorithm presents the most consistent performance gain over all the SNR values, with about 0.4 dB less than MSOE-PLR algorithm (as can be seen in Tab. 7.8). From the RPE-based algorithms perspective, Fig. 7.23(b), the greater flexibility of the IIR structure allowed the HSOE-RPE and the HROE-RPE algorithms to obtain the best QISI performances even for lower SNR values (below 17 dB). The corOE-RPE algorithm, as before, performed very similarly to the MSOE-RPE algorithm, while the MQDOE-RPE algorithm was able to achieve the best QISI performance for higher SNR levels (above 17 dB) – for SNR of 26 dB, the MQDOE-RPE algorithm attained -25.1 dB of QISI and the classical MSOE-RPE algorithm achieved -23.8 dB: more than 1 dB of QISI performance gain. Finally, for the solutions found by the DE metaheuristic, Fig. 7.23(c), the performances of the HROE and HSOE criteria are impaired in comparison with their respective RPE-based algorithms for SNR levels below 20 dB (due to the mentioned approximate

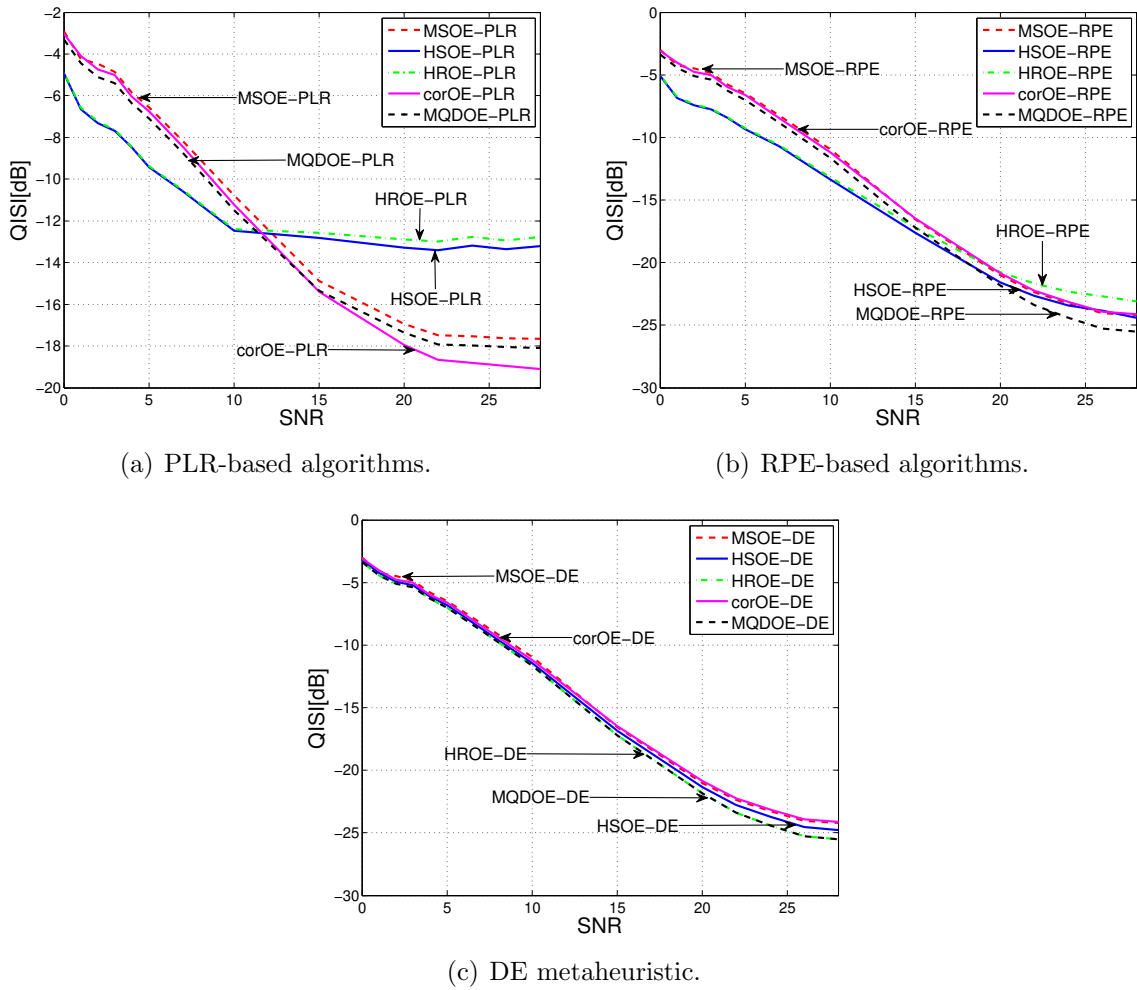


Figure 7.24: Output-Error Formulation - Scenario 2: $QISI \times SNR$ for impulsive noise and $M = 0$.

gradient). The performance gain is mainly observed for higher SNR levels, in which the HSOE and the MQDOE criteria achieve the best QISI performances. When there is additive impulsive noise, Fig. 7.24, the resulting performance is similar to that of the Gaussian noise case, but all the ITL-based approaches experience a slight improvement on the performance for lower SNR levels. For instance, for an SNR of 5 dB with Gaussian noise, the HSOE-PLR and the MQDOE-PLR algorithms achieved -8.9 dB and -6.6 dB of QISI, respectively, while, for impulsive noise, the performance was of -9.4 dB and -7.1 dB, respectively. Similarly, the HSOE-RPE and the MQDOE-RPE algorithms achieved -8.8 dB and -6.5 dB of QISI, respectively, for SNR of 5 dB with Gaussian noise, while, for impulsive noise, the performance was of -9.28 dB and -7.0 dB, respectively. This behavior can also be observed in Tab. 7.8 for the other algorithms.

By changing M to 2, we also evaluated the effect of the error temporal structure. In this case, the parameters were: $N_e = 5$, kernel sizes according to Tab. 7.6 and the step sizes $\mu_{MSOE-PLR} = 0.003$ ($M = 0$), $\mu_{HSOE-PLR} = 0.0025$, $\mu_{HROE-PLR} = 1.3$,

Table 7.8: Output-Error Formulation - Scenario 2: Mean QISI performance for $M = 0$.

		QISI [dB]					
$M = 0$		Gaussian Noise			Impulsive Noise		
		5 dB	15 dB	26 dB	5 dB	15 dB	26 dB
MSOE	PLR	-6.197	-14.865	-17.618	-6.546	-14.889	-17.617
	RPE	-6.113	-16.447	-23.845	-6.482	-16.540	-24.043
	DE	-6.327	-16.782	-24.021	-6.589	-16.801	-24.021
HSOE	PLR	-8.923	-13.294	-13.188	-9.436	-12.823	-13.376
	RPE	-8.796	-17.553	-23.794	-9.353	-17.617	-23.864
	DE	-6.296	-16.539	-24.370	-6.811	-16.832	-24.548
HROE	PLR	-8.910	-13.047	-12.762	-9.373	-12.575	-12.949
	RPE	-8.783	-17.179	-22.601	-9.285	-17.194	-22.680
	DE	-6.473	-16.874	-25.103	-7.002	-17.214	-25.265
corOE	PLR	-6.233	-15.256	-18.995	-6.742	-15.402	-18.961
	RPE	-6.127	-16.247	-23.754	-6.629	-16.494	-23.931
	DE	-6.243	-16.389	-23.809	-6.697	-16.538	-23.811
MQDOE	PLR	-6.595	-15.211	-18.063	-9.085	-15.336	-18.065
	RPE	-6.482	-16.870	-25.092	-7.014	-17.216	-25.271
	DE	-6.521	-16.923	-25.104	-7.081	-17.247	-25.293

$\mu_{corOE-PLR} = 0.13$, $\mu_{MQDOE-PLR} = 0.055$, $\mu_{MSOE-RPE} = 0.003$ ($M = 0$), $\mu_{HSOE-RPE} = 0.0018$, $\mu_{HROE-RPE} = 0.42$, $\mu_{corOE-RPE} = 0.45$ and $\mu_{MQDOE-RPE} = 0.2$, which resulted in mean displacement of $disp_{\theta} = 1.3e-3$ for SNR of 10 dB (AWGN), with $N_{it} = 10000$ and $N_{conv} = 4000$. The DE parameters were kept the same. The resulting QISI \times SNR curves for the Gaussian and impulsive noise cases are displayed in Figs. 7.25 and 7.26, respectively.

Table 7.9: Output-Error Formulation - Scenario 2: Mean QISI performance for $M = 2$.

		QISI [dB]					
$M = 2$		Gaussian Noise			Impulsive Noise		
		5 dB	15 dB	26 dB	5 dB	15 dB	26 dB
HSOE	PLR	-9.091	-14.071	-14.937	-9.818	-13.612	-15.073
	RPE	-9.126	-18.733	-30.158	-10.221	-19.267	-30.165
	DE	-7.047	-17.405	-26.512	-7.799	-17.903	-26.744
HROE	PLR	-9.023	-13.964	-14.810	-9.733	-13.528	-14.956
	RPE	-8.975	-17.843	-26.137	-9.903	-18.121	-26.179
	DE	-7.172	-17.549	-26.693	-7.922	-18.063	-26.894
corOE	PLR	-6.571	-15.902	-22.235	-7.680	-16.524	-22.080
	RPE	-6.297	-16.637	-25.711	-7.096	-17.169	-26.041
	DE	-6.926	-17.266	-26.334	-7.679	-17.750	-26.582
MQDOE	PLR	-6.761	-15.894	-21.547	-9.818	-13.615	-15.077
	RPE	-6.472	-16.842	-25.996	-7.272	-17.416	-26.248
	DE	-7.174	-17.552	-26.697	-7.924	-18.067	-26.898

When the noise is Gaussian, Fig. 7.25, the use of the temporal information in the

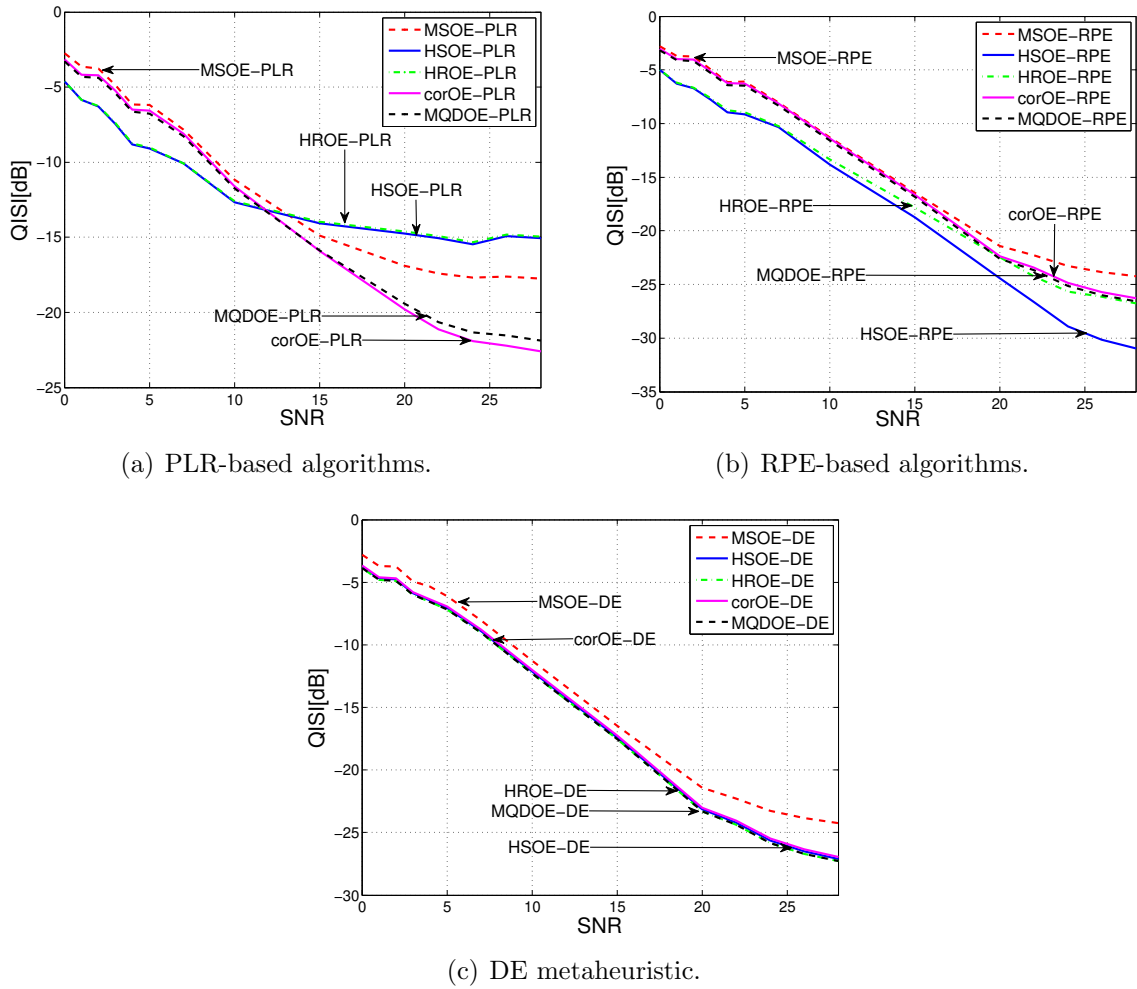


Figure 7.25: Output-Error Formulation - Scenario 2: $QISI \times SNR$ for Gaussian noise and $M = 2$.

PLR approach is particularly beneficial to the corOE-PLR and the MQDOE-PLR algorithms, whose performances improved in comparison with the $M = 0$ case mainly for higher SNR levels, as can be seen in Fig. 7.25(a) and Tab. 7.9. With respect to the RPE approach, Fig. 7.25(b), all the ITL-based algorithms experience an improvement on the QISI performance for higher SNR levels (specially the HSOE-RPE algorithm, which attains the best QISI performance for all considered SNR values, as shown in Tab. 7.9). With respect to the DE optimization, the HSOE and the HROE criteria do not show the same performances as the RPE-based algorithms, as previously observed, but it is also possible to note from Fig. 7.25(c) the performance gain for higher SNR levels (above 20 dB). When the noise presents impulsive behavior, the QISI is slightly improved for all optimization approaches, as shown in Fig. 7.26 and Tab. 7.9, with exception of the PLR-based algorithms for SNR values greater than 10 dB.

As conclusions for this scenario, we have seen that an IIR equalizer with greater flexibility (i.e., with more adjustable coefficients) is able to solve some limitations observed in scenario 1. For instance, both the PLR- and the RPE-based algorithms led to QISI

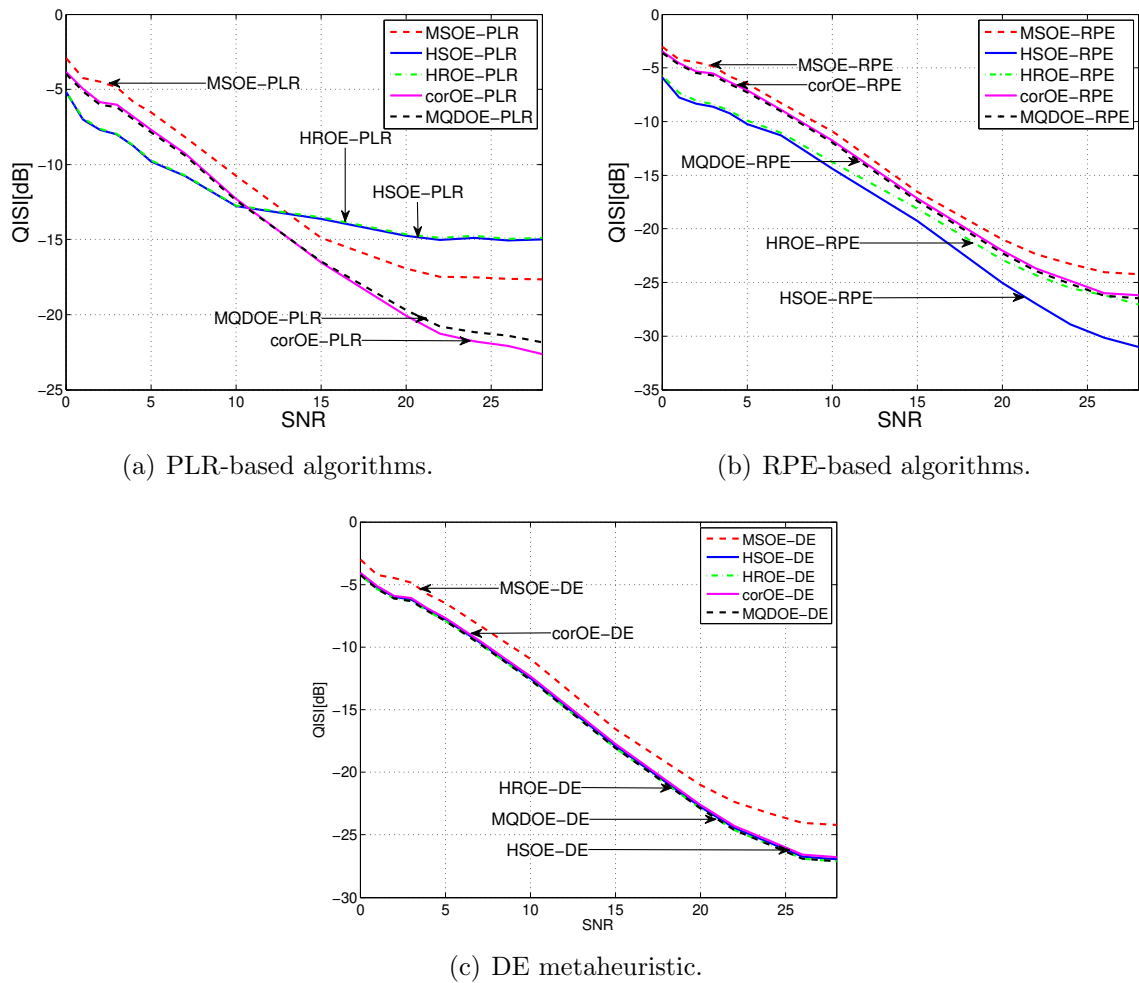


Figure 7.26: Output-Error Formulation - Scenario 2: $QISI \times SNR$ for impulsive noise and $M = 2$.

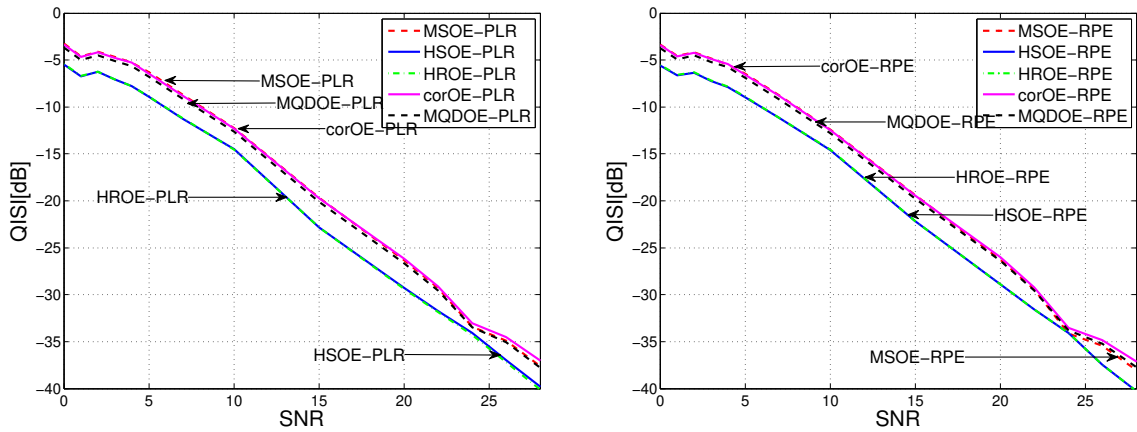
values very similar to the MSOE approach for high SNR levels (with exception to the HSOE-PLR and the HROE-PLR algorithms) in scenario 1, but, in scenario 2, the MSOE approach could be outperformed in several cases. As before, the approximate gradient led the algorithms to solutions different from that found by the DE metaheuristic, mainly for the HSOE and the HROE approaches. For higher SNR values (greater than 12 dB), the RPE-based algorithms performed better than their PLR counterparts. In all cases, the use of the HSOE-RPE algorithm allied to the use of the temporal structure presented the best QISI performance. The ITL-based algorithms showed to be more robust against impulsive noise, as was expected from the use of the kernel method for estimation. At last, the present scenario revealed that the use of the data temporal structure might also be beneficial to the ITL algorithms and the ITL criteria as well (through the DE metaheuristic).

7.5.3 Output-Error Formulation - Scenario 3

Keeping the same transmitted symbols and the transmission channel of scenario 2, we only change the IIR equalizer to

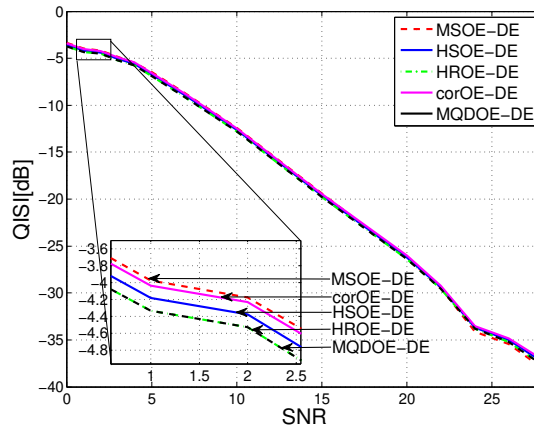
$$\Theta(z) = \frac{b_0 + b_1 z^{-1} + b_2 z^{-2}}{1 - a_1 z^{-1} - a_2 z^{-2} - a_3 z^{-3} - a_4 z^{-4}}, \quad (7.43)$$

which is now able to achieve the ZF condition.



(a) PLR-based algorithms.

(b) RPE-based algorithms.



(c) DE metaheuristic.

Figure 7.27: Output-Error Formulation - Scenario 3: $QISI \times SNR$ for Gaussian noise and $M = 0$.

For $M = 0$, the algorithm parameters were chosen to be: $N_e = 5$, kernel sizes according to Tab. 7.6 and the step sizes $\mu_{MSOE-PLR} = 0.003$, $\mu_{HSOE-PLR} = 0.0035$, $\mu_{HROE-PLR} = 0.03$, $\mu_{corOE-PLR} = 0.025$, $\mu_{MQDOE-PLR} = 0.009$, $\mu_{MSOE-RPE} = 0.002$, $\mu_{HSOE-RPE} = 0.0027$, $\mu_{HROE-RPE} = 0.025$, $\mu_{corOE-RPE} = 0.018$ and $\mu_{MQDOE-RPE} = 0.007$, which resulted in mean displacement of $disp_\theta = 1.6e-3$ for SNR of 10 dB (AWGN), with $N_{it} = 10000$ and $N_{conv} = 4000$. The DE parameters were chosen to be $N_P = 500$, $F = 0.5$, $CR = 0.9$ and 500 iterations (with $N_e = 200$ and kernel sizes equal of that

used in the RPE approach). Following the same procedure, the $QISI \times SNR$ curves were obtained for the Gaussian and impulsive noise cases, as illustrated in Figs. 7.27 and 7.28, respectively.

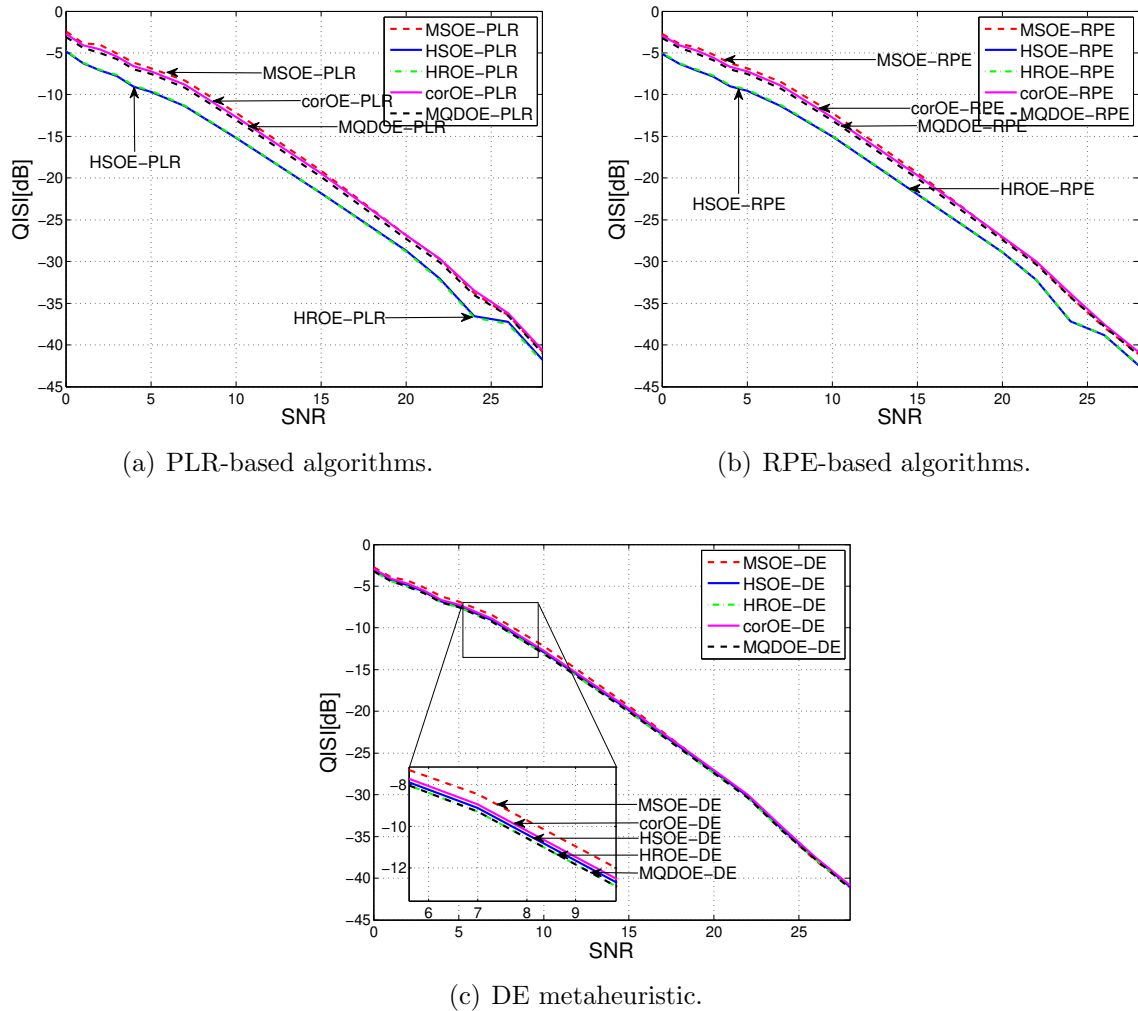


Figure 7.28: Output-Error Formulation - Scenario 3: $QISI \times SNR$ for impulsive noise and $M = 0$.

For Gaussian noise, Fig. 7.27, it is possible to see that both PLR and RPE approaches performed very similarly (Figs. 7.27(a) and 7.27(b)). In both cases, the corOE and the MQDOE methods achieved a QISI performance close to that of MSOE, as can be verified in Tab. 7.10. The HSOE- and the HROE-based algorithms presented very similar behavior and attained the lowest QISI levels for all SNR values. As in the previous scenarios, the HSOE and the HROE solutions found by the DE metaheuristic do not match the ones found by the algorithms and the performance is similar to the MSOE case, as shown in Fig. 7.27(c). When the noise presents impulsive behavior, Fig. 7.28, we observe the general tendencies of the Gaussian noise case plus a slight improvement on the performance for the ITL-based algorithms for SNR values less than 10 dB and greater than 20 dB, as can also be noted in Tab. 7.10.

Table 7.10: Output-Error Formulation - Scenario 3: Mean QISI performance for $M = 0$.

		QISI [dB]					
$M = 0$		Gaussian Noise			Impulsive Noise		
		5 dB	15 dB	26 dB	5 dB	15 dB	26 dB
MSOE	PLR	-6.294	-19.692	-34.884	-6.853	-19.148	-36.461
	RPE	-6.451	-19.416	-35.427	-6.815	-19.392	-37.930
	DE	-6.489	-19.436	-35.448	-6.847	-19.419	-37.986
HSOE	PLR	-8.915	-22.820	-37.215	-9.671	-21.804	-37.243
	RPE	-8.980	-22.163	-37.459	-9.569	-21.935	-38.867
	DE	-6.731	-19.607	-35.032	-7.382	-19.871	-37.689
HROE	PLR	-8.915	-22.824	-37.211	-9.547	-21.846	-37.472
	RPE	-8.942	-22.168	-37.446	-9.453	-21.903	-38.844
	DE	-6.898	-19.795	-35.250	-7.538	-20.062	-37.813
corOE	PLR	-6.451	-19.737	-34.492	-7.197	-19.457	-36.204
	RPE	-6.569	-19.431	-34.833	-7.227	-19.685	-37.556
	DE	-6.573	-19.439	-34.845	-7.239	-19.697	-37.602
MQDOE	PLR	-6.815	-20.128	-35.073	-7.516	-19.864	-36.515
	RPE	-6.906	-19.847	-35.267	-7.542	-20.071	-37.838
	DE	-6.911	-19.925	-35.274	-7.558	-20.084	-37.846

Increasing M to 2, we adjusted the algorithms parameters to $N_e = 5$, kernel sizes according to Tab. 7.6 and the step sizes to $\mu_{MSOE-PLR} = 0.003$ ($M = 0$), $\mu_{HSOE-PLR} = 0.0015$, $\mu_{HROE-PLR} = 0.3$, $\mu_{corOE-PLR} = 0.12$, $\mu_{MQDOE-PLR} = 0.055$, $\mu_{MSOE-RPE} = 0.002$ ($M = 0$), $\mu_{HSOE-RPE} = 0.001$, $\mu_{HROE-RPE} = 0.22$, $\mu_{corOE-RPE} = 0.08$ and $\mu_{MQDOE-RPE} = 0.04$, resulting in a mean displacement of $disp_\theta = 1.6e-3$ for SNR of 10 dB (AWGN), with $N_{it} = 10000$ and $N_{conv} = 4000$. For 30 independent simulations, the QISI \times SNR curves for Gaussian and impulsive noise are as displayed in Figs. 7.29 and 7.30, respectively.

The use of the data temporal information in the Gaussian noise case, for both PLR- and RPE-based algorithms, Figs. 7.29(a) and 7.29(b), contributed to the performance improvement of the ITL approaches in comparison with the $M = 0$ case for SNR values less than 10 dB and, mainly, greater than 20 dB, as can also be verified in Tab. 7.11. The solutions found by the DE metaheuristic were able to reduce the QISI levels for all considered SNR values in comparison with the $M = 0$ case. For the impulsive noise case, the ITL-based algorithms also showed to be more robust in comparison with the Gaussian noise case, mainly when the SNR level is lower. As an exception, for an SNR greater than 22 dB, the PLR-based approaches had worse performances, as shown in Tab. 7.11.

Summarizing this scenario where the ZF solution is attainable, we have observed that the HSOE- and the HROE-based algorithms can perform similarly and obtain the best QISI performance measures, but the RPE-based algorithms performance is slightly better than the PLR-based ones. Once more, we have observed that the HSOE and the HROE solutions found by the algorithms diverged from the solutions found by the DE

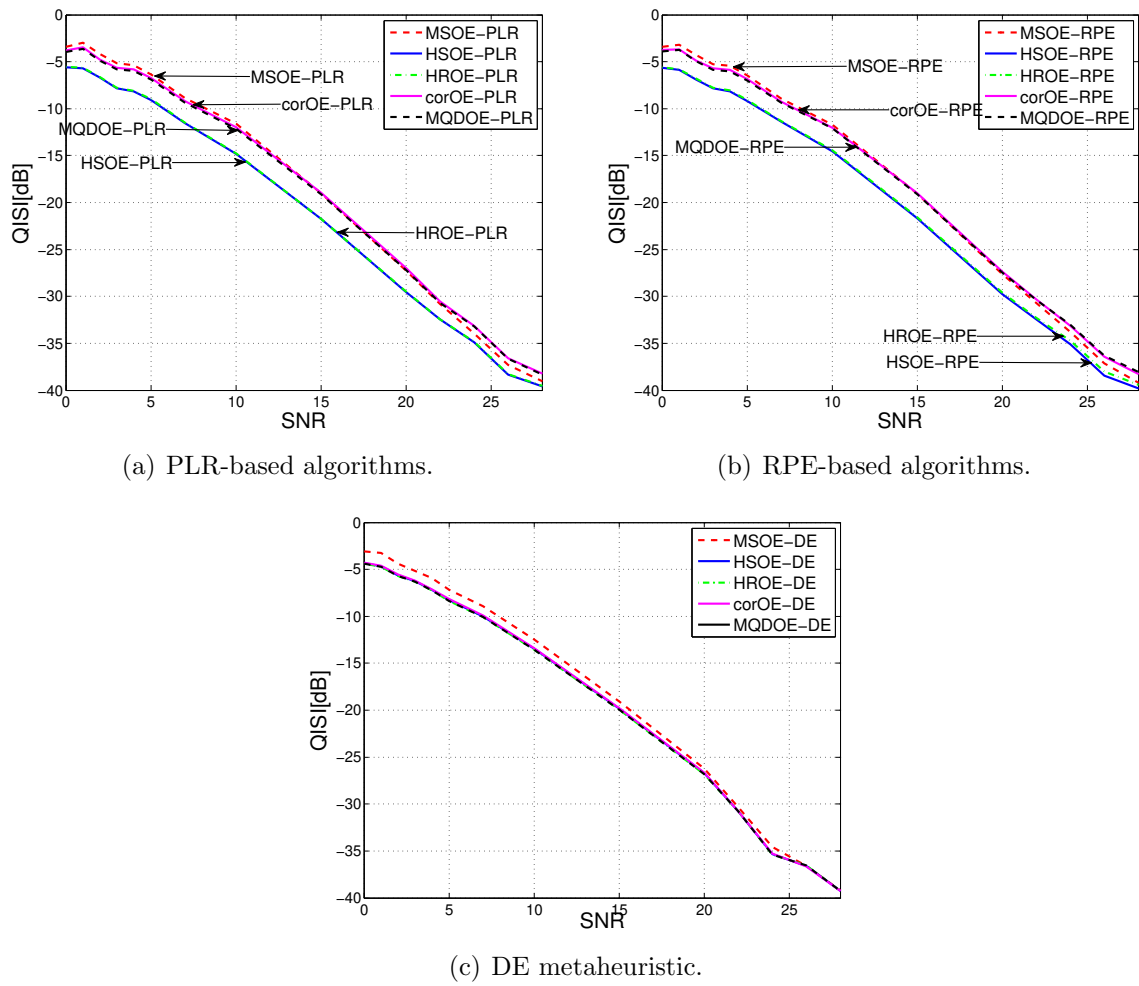


Figure 7.29: Output-Error Formulation - Scenario 3: $QISI \times SNR$ for Gaussian noise and $M = 2$.

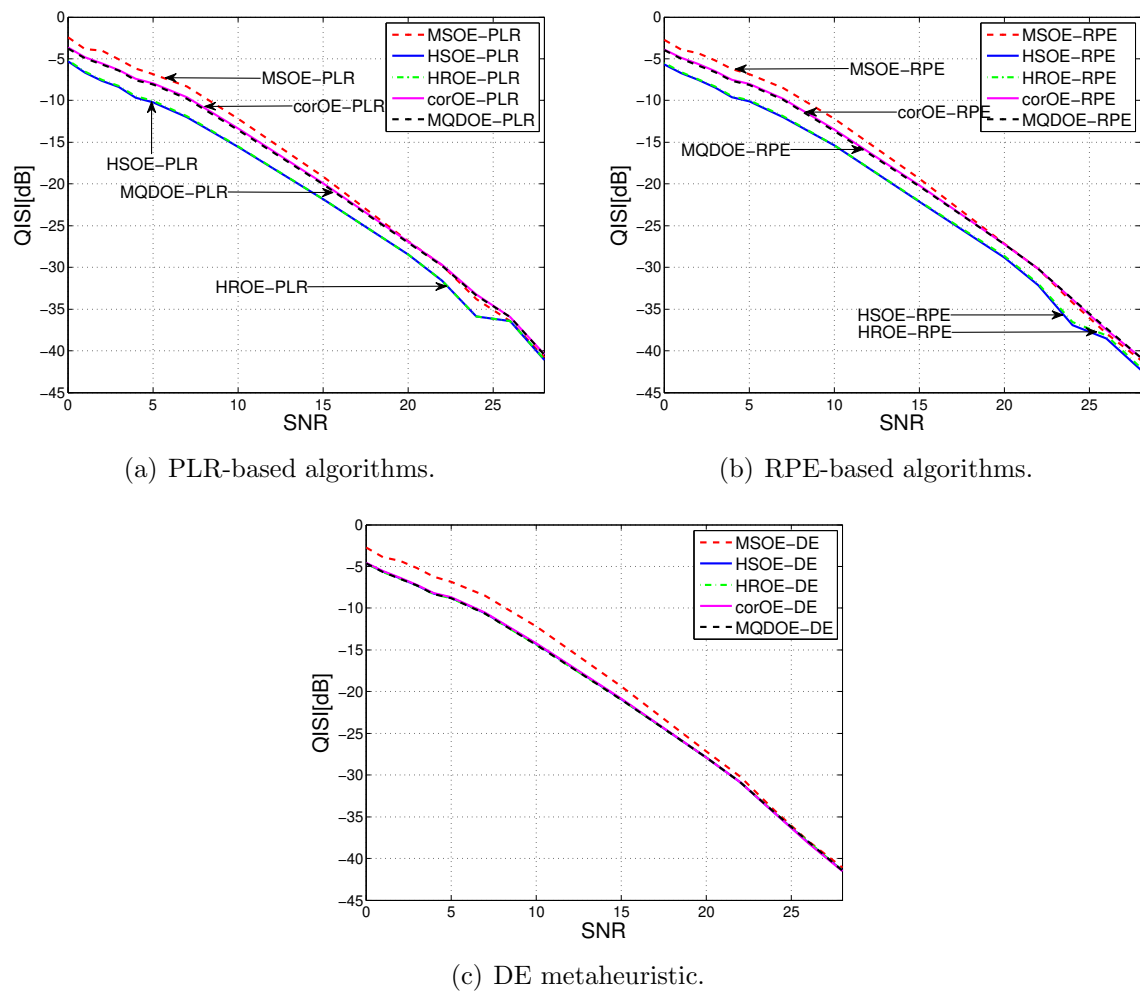


Figure 7.30: Output-Error Formulation - Scenario 3: $QISI \times SNR$ for impulsive noise and $M = 2$.

Table 7.11: Output-Error Formulation - Scenario 3: Mean QISI performance for $M = 2$.

		QISI [dB]					
$M = 2$		Gaussian Noise			Impulsive Noise		
		5 dB	15 dB	26 dB	5 dB	15 dB	26 dB
HSOE	PLR	-9.067	-21.765	-38.341	-10.203	-21.827	-36.450
	RPE	-9.171	-21.712	-38.446	-10.078	-22.156	-38.532
	DE	-8.267	-19.857	-36.573	-8.775	-20.934	-38.079
HROE	PLR	-8.996	-21.733	-38.274	-10.064	-21.842	-36.416
	RPE	-9.076	-21.601	-38.039	-9.960	-22.068	-38.137
	DE	-8.354	-19.946	-36.527	-8.839	-20.996	-37.981
corOE	PLR	-6.758	-18.954	-36.580	-7.949	-19.913	-35.968
	RPE	-6.871	-19.048	-36.442	-8.012	-20.160	-37.463
	DE	-8.182	-19.770	-36.621	-8.712	-20.864	-38.167
MQDOE	PLR	-6.887	-19.129	-36.661	-9.089	-20.062	-35.944
	RPE	-6.989	-19.152	-36.346	-8.139	-20.295	-37.282
	DE	-8.360	-19.949	-36.532	-8.846	-21.005	-37.985

metaheuristic. In general, the corOE and the MQDOE algorithms performed better than the MSOE algorithms but are still close to it. The use of the temporal structure of the error signal also contributed to increase the performance of ITL-based methods in this scenario, except for intermediate SNR values (in the vicinity of 15 dB).

7.6 Conclusions

In this chapter, we focused on the use of IIR filters for the supervised channel equalization problem. The study was based on the equation- and the output-error formulations, with special attention dedicated to their underlying algorithms: the LMS, the PLR and the (simplified) RPE algorithms. From the ITL framework, four criteria were chosen to be investigated in this context: Shannon's and Rényi's entropy, correntropy and matching of densities. The reason for this choice comes from their known capability of extracting the statistical information about the error signal and their extensibility to the multivariate case, which allows a more effective use of the error temporal structure. It is important to remark that the application of these ITL criteria in the IIR equalization problem as well as their extension to the multivariate case is a novelty introduced in our work.

In the equation-error formulation, the simplification on the IIR structure during the training step immensely aids the optimization task, since the MSEE cost surface is a paraboloid and the LMS algorithm is sufficient to find the single optimum. For the ITL criteria, the cost surfaces are not as regular as in the MSEE case, and their smoothness will depend on the kernel size and the number of considered delays. Nonetheless, the clear existence of the single optimum is also favorable to the adoption of the LMS-based algorithms for optimization. The performances of the algorithms were evaluated in terms

of QISI in different scenarios, where it was possible to identify two distinct behaviors, depending on the capability of the IIR structure to achieve the ZF condition. When the ZF solution could not be achieved due to limitations of the IIR equalizer, Shannon's and Rényi's entropy-based algorithms – HSEE-LMS and HREE-LMS, respectively – outperformed the classical MSEE-LMS, the correntropy-based (corEE-LMS) and the density matching-based (MQDEE-LMS) algorithms for almost all range of SNR values considered, specially for impulsive noise, whose ITL algorithms robustness are known to be very effective [Principe, 2010]. The use of the temporal structure also contributed significantly for the performance improvement. Notwithstanding, when the ZF condition is reachable, the corEE-LMS and the MQDEE-LMS algorithms are the ones who achieved the lowest QISI levels, but only for low (below 5 dB) or high SNR levels (above 20 dB).

For the output-error formulation, no simplification is made on the IIR structure, leading to important implications like the use of approximate gradients. In that sense, two approaches were considered: the LPR and the (simplified) RPE gradient approximation, which, combined with the ITL criteria, led to a set of LPR- and RPE-based algorithms. The analysis of the cost surfaces showed that they are more complex than the previous paraboloids, however, similarly to the equation-error formulation, there is only a single optimum in the supervised equalization problem, whose position might deviate depending on the noise intensity. For the ITL criteria, the cost surfaces can have their smoothness controlled by the kernel size and/or by the number of delays considered, which is an advantage in comparison with the classical MSOE cost. The performance of the PLR- and the RPE-based algorithms were evaluated in scenarios with non-attainable and attainable ZF solutions. Very interestingly, in both cases, the PLR and the RPE approximate gradient versions caused the algorithms to deviate from the solution observed in the costs, principally for Shannon's and Rényi's entropy-based (HSOE and HROE, respectively) algorithms. Due to this, the DE metaheuristic was also employed for optimization. For non-attainable ZF solutions, the Shannon's entropy-based RPE algorithm (HSOE-RPE) allied to the use of the temporal structure of the error presented the best QISI performance for all considered SNR values, outperforming even the solutions found by the DE metaheuristic. From a general perspective, the RPE-based algorithms performed better than the PLR-based ones. When the ZF condition is achievable, the performance of the PLR-based algorithms becomes closer to that based on the RPE, however, the RPE approach still led to slightly better QISI performance. More specifically, the HSOE-RPE and the HROE-RPE algorithms exhibited the best performances, in which the use of the temporal structure also contributed specially for SNR values out of the vicinity of 15 dB.

In general terms, the performed investigation revealed interesting features of the ITL-based algorithms in both equation- and output-error formulations, where we highlight the Shannon's and Rényi's entropy-based algorithms and their synergy with the error signals and with the approximate gradients (mainly in the RPE approach). Although the results

showed a performance improvement, a deeper investigation on the entropy properties that justify the observed behavior is still lacking, which will be left for future works. Other promising perspective is the application of these ITL methods in the identification problem.

Chapter 8

Blind Separation of Temporally Structured Sources in Post-Nonlinear Mixtures

In the context of Blind Source Separation (BSS) [Comon and Jutten, 2010; Romano et al., 2010], the use of the temporal information of the underlying signals is a well studied issue under the assumption of linear and instantaneous mixing models and mutually independent sources. In fact, the temporal structure of the signals showed to provide fundamental additional information to solve the problem, reducing the ICA requisites to the simple SOS [Comon and Jutten, 2010]. Within this scope, a wide range of SOS-based methods emerged, in which we cite the AMUSE [Hyvärinen et al., 2001], SOBI [Belouchrani et al., 1997], TDSEP method, among others [Comon and Jutten, 2010].

Notwithstanding, regarding their extension to the nonlinear mixing models, the use of the signals temporal structure is still incipient. In fact, it is known that, from a general standpoint, mutual independence may not be sufficient for performing separation, but a promising way to work around this issue is to use the temporal information [Jutten and Karhunen, 2004].

Due to the vastness and the inherent difficulties encompassed in general nonlinear models, the study on this topic is usually focused on a restricted set of models. Particularly, the Post-Nonlinear (PNL) models [Taleb and Jutten, 1999] are of practical interest in view of their application in several real world problems, such as hyperspectral imaging [Meganem et al., 2011], sensor arrays, microwave communications and biological models [Taleb and Jutten, 1999]. Furthermore, separation for the PNL mixing problem using ICA-based methods has already shown to be effective under certain constraints on the mixing/separating functions [Hosseini and Jutten, 2003]. However, its study in light of the sole use of the temporal structure of the sources and SOS is still incipient. An initial step in this direction was given for the two-stage approach [Deville and Duarte, 2015], where the nonlinearities are compensated in a first step via a Gaussianization method, leaving a linear BSS problem that can be solved using the temporal information via SOS-

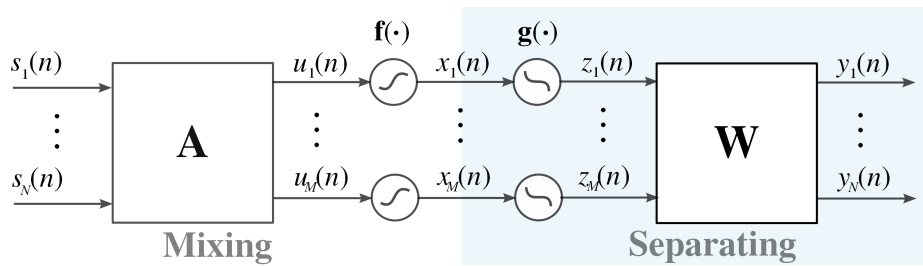


Figure 8.1: Mixing and separating systems in the PNL model.

based methods [Ziehe et al., 2003]. Nonetheless, the use of HOS is mandatory in the Gaussianization step. In view of this, in this chapter, we focus on the analysis of the sole use of the SOS in the PNL mixing problem, more specifically, for the case in which the nonlinearities belong to a class of cubic polynomials. The case study encompasses two important contributions, which are: a novel formulation of the PNL problem considering its extension to the temporal structure of the data and the proposition of a SOS-based criterion that is capable of performing source separation if a given number of time delays is considered. As we intend to show, the temporal-extended formulation allows the analytic computation of the SOS-based cost functions and contributes to a richer analysis of their performance.

Next, we present the temporal-extended formulation of the PNL mixtures in the case in which the nonlinearities are modeled as cubic polynomials. Based on this formulation, mutual information can be used under the hypothesis of colored (multivariate) Gaussian sources, which will result in an SOS-based criterion.

8.1 The Post-Nonlinear Mixing Model

Recalling the PNL structure presented in Section 4.4.2, the main objective is to recover the original sources $\mathbf{s}(n)$ from observed mixtures

$$\mathbf{x}(n) = \mathbf{f}(\mathbf{A}\mathbf{s}(n)), \quad (8.1)$$

being $\mathbf{x}(n) = [x_1(n) \cdots x_M(n)]^T$ the observation vector with M mixtures, $\mathbf{s}(n) = [s_1(n) \cdots s_N(n)]^T$ the vector with N source signals at time instant n^1 and $\mathbf{f}(\cdot)$ the set of M component-wise functions [Comon and Jutten, 2010], as shown in Fig. 8.1. The separation system is the mirrored version of the mixing system, with output given by

$$\mathbf{y}(n) = \mathbf{W}\mathbf{g}(\mathbf{x}(n)), \quad (8.2)$$

¹Note that, as customary in the BSS formulation, we have used a different notation in this chapter, in which the temporal index n is no longer in subscript, but inside parentheses

where \mathbf{W} is a $N \times M$ matrix and $\mathbf{g}(\cdot)$ is a set of M component-wise functions [Comon and Jutten, 2010].

Although the PNL structure engenders interesting features by itself, the additional supposition that the sources possess temporal statistical information is also valuable to us. Hence, in the following, we formulate a temporal-extended version of the PNL problem, which shall be useful to encompass the temporal information in a more organic manner.

8.1.1 Time-Dependent Sources in the PNL Model

The temporal structure of the sources is usually seen as the inherent result of the system which generates the sources. Notwithstanding, in some applications, it can be modeled as the result of independent and identically distributed (*i.i.d.*) signals processed by linear or nonlinear systems, whose signature is the temporal structure imprinted on the signals. For simplicity, as assumed in Chapters 5 and 6, to investigate the Second-Order Statistics (SOS) features in the PNL models, we restrain ourselves to the case in which the temporal structure is obtained by means of linear systems called pre-coders – here assumed to be unknown.

To suitably describe the temporal structure in the sources, we consider vectors with the N sources at time instant n concatenated with d delayed versions of them in the following form:

$$\begin{aligned} \underline{\mathbf{s}}(n) &= [s_1(n) \ \dots \ s_1(n-d) \ s_2(n) \ \dots \ s_2(n-d) \ \dots \ s_N(n) \ \dots \ s_N(n-d)]^T \\ &= [\underline{\mathbf{s}}_1(n) \ \underline{\mathbf{s}}_2(n) \ \dots \ \underline{\mathbf{s}}_N(n)]^T, \end{aligned} \quad (8.3)$$

where d is the maximum considered time delay and $\underline{\mathbf{s}}_i(n) = [s_i(n) \ \dots \ s_i(n-d)]^T$, for $i = \{1, \dots, N\}$. These vectors of Eq. (8.3) will be associated with the RV \underline{S} . We wish to express the sources (and its delays) $\underline{\mathbf{s}}(n)$ in function of *i.i.d* signals $\underline{\mathbf{r}}(n)$ (note that, similarly to $\underline{\mathbf{s}}(n)$ and $\mathbf{s}(n)$, all the underlined variables are the temporal-extended versions of the classical formulation). In order to do so, we consider a set of N FIR filters (or pre-coders) that are responsible to introduce correlation in the signals $\underline{\mathbf{s}}(n)$. The coefficients of each FIR filter is arranged in vectors \mathbf{p}_i , for $i = \{1, \dots, N\}$. Hence, for instance, a FIR filter with impulse response $P_i(z) = p_{i,0} + p_{i,1}z^{-1} + \dots + p_{i,L_{p_i}}z^{-L_{p_i}}$ is represented by the vector $\mathbf{p}_i = [p_{i,0} \ p_{i,1} \ \dots \ p_{i,L_{p_i}}]$. Based on this, we define

$$\mathbf{P}_i = \mathbf{p}_i \otimes \mathbf{I}_{d+1} = \begin{bmatrix} p_{i,0} & \cdots & p_{i,L_{p_i}} & 0 & 0 & \cdots & 0 \\ 0 & p_{i,0} & \cdots & p_{i,L_{p_i}} & 0 & \cdots & 0 \\ \vdots & \ddots & & \ddots & & \ddots & \vdots \\ 0 & \cdots & 0 & 0 & p_{i,0} & \cdots & p_{i,L_{p_i}} \end{bmatrix}, \quad (8.4)$$

which is a diagonal replication of the vector \mathbf{p}_i , being the resultant matrix \mathbf{P}_i of dimension

$(d+1) \times (L_{p_i}+d+1)$, and \mathbf{I}_{d+1} the identity matrix of size $d+1$.

For the sake of simplicity, we assume henceforth $N = 2$ sources without loss of generality. In this case, the sources $\underline{\mathbf{s}}(n)$ can be written as a function of $\underline{\mathbf{r}}(n)$:

$$\underline{\mathbf{s}}(n) = \underline{\mathcal{P}}\underline{\mathbf{r}}(n) = \begin{bmatrix} \mathbf{P}_1 & \mathbf{0} \\ \mathbf{0} & \mathbf{P}_2 \end{bmatrix} \underline{\mathbf{r}}(n), \quad (8.5)$$

where $\underline{\mathcal{P}}$ is a block-diagonal matrix with dimension $N(d+1) \times (\sum_{i=1}^N L_{p_i} + d+1)$ and $\underline{\mathbf{r}}(n) = [r_1(n) \ r_1(n-1) \ \dots \ r_1(n-L_{p_1}-d) \ r_2(n) \ r_2(n-1) \ \dots \ r_2(n-L_{p_2}-d)]^T$ is the temporal-extended *i.i.d.* vector with the original signals $r_1(n)$, $r_2(n)$ and its delayed versions. Note that the *i.i.d.* signals $r_i(n)$ will only be temporally mixed by $\underline{\mathcal{P}}$ and that there is no mixing between $r_1(n)$ and $r_2(n)$. Eq. (8.5) is important because it can express the sources $s_i(n)$ as function of an *i.i.d.* RV, which can be convenient to analytically compute certain statistical moments.

Proceeding with the PNL temporal-extended formulation, we can write the linear mixtures as $\underline{\mathbf{u}}(n) = \underline{\mathcal{A}}\underline{\mathbf{s}}(n)$, being $\underline{\mathcal{A}}$ the extended linear mixing matrix:

$$\underline{\mathcal{A}} = \begin{bmatrix} a_{11}\mathbf{I}_{d+1} & a_{12}\mathbf{I}_{d+1} \\ a_{21}\mathbf{I}_{d+1} & a_{22}\mathbf{I}_{d+1} \end{bmatrix}, \quad (8.6)$$

in which each element is replicated along a diagonal of a (sub)matrix of size $d+1$. The observations (nonlinear mixtures) $\underline{\mathbf{x}}(n)$ can be written as

$$\underline{\mathbf{x}}(n) = \underline{\mathcal{F}}(\underline{\mathbf{u}}(n)) = \underline{\mathcal{F}}(\underline{\mathcal{A}}\underline{\mathbf{s}}(n)), \quad (8.7)$$

where $\underline{\mathcal{F}}(\cdot)$ is a set of functions diagonally disposed as

$$\underline{\mathcal{F}}(\cdot) = \begin{bmatrix} f_1(\cdot)\mathbf{I}_{d+1} & \mathbf{0} \\ \mathbf{0} & f_2(\cdot)\mathbf{I}_{d+1} \end{bmatrix}. \quad (8.8)$$

The separating system is a mirrored version of the mixing one, with output

$$\underline{\mathbf{y}}(n) = \underline{\mathcal{W}}\underline{\mathcal{G}}(\underline{\mathbf{x}}(n)), \quad (8.9)$$

where $\underline{\mathcal{G}}(\cdot)$ and $\underline{\mathcal{W}}$ have structures similar to $\underline{\mathcal{F}}(\cdot)$ and $\underline{\mathcal{A}}$, respectively.

Interestingly, by combining Eqs. (8.9), (8.7) and (8.5), we are able to directly express the separated sources $\underline{\mathbf{y}}(n)$ in function of $\underline{\mathbf{r}}(n)$ as

$$\underline{\mathbf{y}}(n) = \underline{\mathcal{W}}\underline{\mathcal{G}}(\underline{\mathcal{F}}(\underline{\mathcal{A}}\underline{\mathcal{P}}\underline{\mathbf{r}}(n))). \quad (8.10)$$

Undoubtedly, in practical scenarios, the elements $\underline{\mathcal{F}}$, $\underline{\mathcal{A}}$, $\underline{\mathcal{P}}$ and $\underline{\mathbf{r}}(n)$ are considered unknown and the separation task may be performed relying on, for instance, some statistical

properties of the sources $\underline{\mathbf{s}}(n)$, like the mutual independence. Notwithstanding, Eq. (8.10) is of great theoretical importance, since it exposes a direct relation to an *i.i.d.* RV and opens way to analytical computations of the statistics involved in the separation process, as we intend to show. It is important to note that some additional assumptions may be necessary, for example, the definition of the type of the nonlinearities $\underline{\mathcal{F}}(\cdot)$ and $\underline{\mathcal{G}}(\cdot)$.

8.1.2 A Special Case: The Cubic Nonlinearity

In order to simplify our analysis, we make the assumption that the combined nonlinear function $\underline{\mathcal{F}} \circ \underline{\mathcal{G}}$ yields as output

$$\underline{\mathbf{z}}(n) = \underline{\mathcal{A}}\underline{\mathbf{s}}(n) + \underline{\mathbf{\Gamma}}(\underline{\mathcal{A}}\underline{\mathbf{s}}(n))^{\odot 3}, \quad (8.11)$$

where

$$\underline{\mathbf{\Gamma}} = \begin{bmatrix} \gamma_1 \mathbf{I}_{d+1} & \mathbf{0} \\ \mathbf{0} & \gamma_2 \mathbf{I}_{d+1} \end{bmatrix} \quad (8.12)$$

and $(\cdot)^{\odot 3}$ is the Hadamard power of 3 (i.e., an element wise cubic operator). This can be viewed as, for instance, a cubic nonlinearity $\underline{\mathcal{F}}(\underline{\mathbf{x}}(n)) = \underline{\mathbf{x}}^{\odot 3}(n)$ and with $\underline{\mathcal{G}}(\underline{\mathbf{x}}(n)) = \text{sgn}(\underline{\mathbf{x}}(n))(|\underline{\mathbf{x}}(n)|)^{\odot 1/3} + \underline{\mathbf{\Gamma}}\underline{\mathbf{x}}(n)$. Finally, based on Eq. (8.10), the system output can now be written as

$$\underline{\mathbf{y}}(n) = \underline{\mathcal{W}}\underline{\mathbf{z}}(n) = \underline{\mathcal{W}}\underline{\mathcal{A}}\underline{\mathcal{P}}\underline{\mathbf{r}}(n) + \underline{\mathcal{W}}\underline{\mathbf{\Gamma}}(\underline{\mathcal{A}}\underline{\mathcal{P}}\underline{\mathbf{r}}(n))^{\odot 3}. \quad (8.13)$$

Very interestingly, the nonlinear term can be expressed by means of a Volterra expansion [Mathews and Sicuranza, 2000] (see Section 1.1.2) of the type:

$$\begin{aligned} (\underline{\mathcal{A}}\underline{\mathcal{P}}\underline{\mathbf{r}}(n))^{\odot 3} &= \begin{bmatrix} (a_{11}p_{1,1})^3 r_1^3(n) + (a_{11}p_{1,2})^3 r_1^3(n-1) + \dots \\ \vdots \\ (a_{11}p_{1,1})^3 r_1^3(n-d+1) + (a_{11}p_{1,2})^3 r_1^3(n-d) + \dots \\ (a_{21}p_{1,1})^3 r_1^3(n) + (a_{21}p_{1,2})^3 r_1^3(n-1) + \dots \\ \vdots \\ (a_{21}p_{1,1})^3 r_1^3(n-d+1) + (a_{21}p_{1,2})^3 r_1^3(n-d) + \dots \end{bmatrix} \\ &= \begin{bmatrix} \theta_{11}^3 r_1^3(n) + \theta_{12}^3 r_1^3(n-1) + \dots \\ \vdots \\ \theta_{11}^3 r_1^3(n-d+1) + \theta_{12}^3 r_1^3(n-d) + \dots \\ \theta_{21}^3 r_1^3(n) + \theta_{22}^3 r_1^3(n-1) + \dots \\ \vdots \\ \theta_{21}^3 r_1^3(n-d+1) + \theta_{22}^3 r_1^3(n-d) + \dots \end{bmatrix} = \begin{bmatrix} \boldsymbol{\theta}_1 \otimes \mathbf{I}_{d+1} \\ \boldsymbol{\theta}_2 \otimes \mathbf{I}_{d+1} \end{bmatrix} \begin{bmatrix} \boldsymbol{\rho}(n) \\ \boldsymbol{\rho}(n-1) \\ \vdots \\ \boldsymbol{\rho}(n-d) \end{bmatrix} \\ &= \underline{\boldsymbol{\Theta}}\underline{\boldsymbol{\rho}}(n), \end{aligned} \quad (8.14)$$

where $\boldsymbol{\rho}(n) = [r_1^3(n) \ r_1^3(n-1) \ r_2^3(n) \ r_2^3(n-1) \ \dots]^T$ is the column vector with the L_v terms involving the signals $r_1(n)$, $r_2(n)$ and some of their delayed versions, θ_{ij} are the matrix elements of the product $\underline{\mathcal{A}}\underline{\mathcal{P}}$, for $i = 1, \dots, N$ and for $j = 1, \dots, L_v$, and $\boldsymbol{\theta}_i = [\theta_{i1} \ \theta_{i2} \ \dots \ \theta_{iL_v}]$; the number of elements L_v in $\boldsymbol{\rho}(n)$ is a combinatorial problem: assuming that all pre-coders have the same maximum length L_p , without loss of generality, we have that $L_v = (NL_p+2)!/(3!(NL_p-1)!)$. As we concatenate all the $d+1$ considered delays in the column vector $\underline{\boldsymbol{\rho}}(n)$, its length is $(d+1)(NL_p+2)!/(3!(NL_p-1)!)$; finally, $\underline{\boldsymbol{\Theta}}$ is a $N(d+1) \times (d+1)(NL_p+2)!/(3!(NL_p-1)!)$ matrix. Observe that the computational complexity can drastically increase, depending on the values of N (here chosen to be 2), d and L_p .

It is interesting to note in Eq. (8.14) that $\underline{\boldsymbol{\rho}}(n)$ encompasses elements of $\mathbf{r}(n)$ up to the power of 3 (due to the assumed cubic nonlinearity) but we have expressed the terms by means of a simple linear combination.

With the expanded Volterra terms at hand, it is possible to write a linear expression for the separated sources:

$$\underline{\mathbf{y}}(n) = \underline{\mathcal{W}}\underline{\mathcal{A}}\underline{\mathcal{P}}\mathbf{r}(n) + \underline{\mathcal{W}}\underline{\boldsymbol{\Gamma}}\underline{\boldsymbol{\Theta}}\underline{\boldsymbol{\rho}}(n). \quad (8.15)$$

Example

For illustration purposes, we consider the following pre-coders $\mathbf{p}_1 = [p_{1,0} \ p_{1,1}]$ and $\mathbf{p}_2 = [p_{2,0} \ p_{2,1}]$ and the mixtures

$$\mathbf{x}(n) = (\mathbf{A}\mathbf{s}(n))^{\odot 3}, \quad (8.16)$$

where $\mathbf{A} = [a_{11} \ a_{12} ; a_{21} \ a_{22}]$. The compensating nonlinearities are chosen to be $\mathbf{g}(\mathbf{x}(n)) = (\mathbf{x}(n))^{\odot 1/3} + \mathbf{x}(n)$, which results

$$\mathbf{z}(n) = \mathbf{A}\mathbf{s}(n) + \gamma (\mathbf{A}\mathbf{s}(n))^{\odot 3}. \quad (8.17)$$

In the temporal-extended domain, if we consider $d = 1$, the sources can be expressed as

$$\underline{\mathbf{s}}(n) = \begin{bmatrix} s_1(n) \\ s_1(n-1) \\ s_2(n) \\ s_2(n-1) \end{bmatrix} = \underline{\mathcal{P}}\mathbf{r}(n) = \begin{bmatrix} p_{1,0} & p_{1,1} & 0 & 0 & 0 & 0 \\ 0 & p_{1,0} & p_{1,1} & 0 & 0 & 0 \\ 0 & 0 & 0 & p_{2,0} & p_{2,1} & 0 \\ 0 & 0 & 0 & 0 & p_{2,0} & p_{2,1} \end{bmatrix} \begin{bmatrix} r_1(n) \\ r_1(n-1) \\ r_1(n-2) \\ r_2(n) \\ r_2(n-1) \\ r_2(n-2) \end{bmatrix}, \quad (8.18)$$

and the mixtures

$$\begin{aligned}
\underline{\mathbf{x}}(n) &= \mathcal{F}(\underline{\mathcal{A}}\mathbf{s}(n)) = (\underline{\mathcal{A}}\underline{\mathcal{P}}\mathbf{r}(n))^{\odot 3} \\
&= \left(\begin{bmatrix} a_{11} & 0 & a_{12} & 0 \\ 0 & a_{11} & 0 & a_{12} \\ a_{21} & 0 & a_{22} & 0 \\ 0 & a_{21} & 0 & a_{22} \end{bmatrix} \begin{bmatrix} p_{1,0} & p_{1,1} & 0 & 0 & 0 & 0 \\ 0 & p_{1,0} & p_{1,1} & 0 & 0 & 0 \\ 0 & 0 & 0 & p_{2,0} & p_{2,1} & 0 \\ 0 & 0 & 0 & 0 & p_{2,0} & p_{2,1} \end{bmatrix} \underline{\mathbf{r}}(n) \right)^{\odot 3} \\
&= \left(\begin{bmatrix} \psi_{1,1} & \psi_{1,2} & 0 & \psi_{1,3} & \psi_{1,4} & 0 \\ 0 & \psi_{1,1} & \psi_{1,2} & 0 & \psi_{1,3} & \psi_{1,4} \\ \psi_{2,1} & \psi_{2,2} & 0 & \psi_{2,3} & \psi_{2,4} & 0 \\ 0 & \psi_{2,1} & \psi_{2,2} & 0 & \psi_{2,3} & \psi_{2,4} \end{bmatrix} \begin{bmatrix} r_1(n) \\ r_1(n-1) \\ r_1(n-2) \\ r_2(n) \\ r_2(n-1) \\ r_2(n-2) \end{bmatrix} \right)^{\odot 3}, \tag{8.19}
\end{aligned}$$

being $\psi_{i,j}$ are the non-null elements resultant from the matrix product $\underline{\mathcal{A}}\underline{\mathcal{P}}$.

Proceeding with the Volterra expansion, as shown by Eq. (8.14), the vector $\boldsymbol{\rho}(n)$ has $L_v = (NL_p+2)!/(3!(NL_p-1)!) = 20$ elements, which are all possible triplets among $r_1(n)$, $r_1(n-1)$, $r_2(n)$ and $r_2(n-1)$, i.e.,

$$\begin{aligned}
\boldsymbol{\rho}(n) &= [r_1^3(n) \quad r_1^3(n-1) \quad r_2^3(n) \quad r_2^3(n-1) \quad \dots \\
&\quad r_1^2(n)r_1(n-1) \quad r_1^2(n)r_2(n) \quad r_1^2(n)r_2(n-1) \quad r_1(n)r_1^2(n-1) \quad \dots \\
&\quad r_1(n)r_2^2(n) \quad r_1(n)r_2^2(n-1) \quad r_1^2(n-1)r_2(n) \quad r_1^2(n-1)r_2(n-1) \quad \dots \\
&\quad r_1(n-1)r_2^2(n) \quad r_1(n)r_2^2(n-1) \quad r_2^2(n)r_2(n-1) \quad r_2(n)r_2^2(n-1) \quad \dots \\
&\quad r_1(n)r_1(n-1)r_2(n) \quad r_1(n)r_1(n-1)r_2(n-1) \quad r_1(n)r_2(n)r_2(n-1) \quad \dots \\
&\quad r_1(n-1)r_2(n)r_2(n-1)]^T; \tag{8.20}
\end{aligned}$$

and the vector $\boldsymbol{\theta}_i$ also has $L_v = 20$ elements:

$$\begin{aligned}
\boldsymbol{\theta}_i &= [\psi_{i,1}^3 \quad \psi_{i,2}^3 \quad \psi_{i,3}^3 \quad \psi_{i,4}^3 \quad \dots \\
&\quad 3\psi_{i,1}^2\psi_{i,2} \quad 3\psi_{i,1}^2\psi_{i,3} \quad 3\psi_{i,1}^2\psi_{i,4} \quad 3\psi_{i,1}\psi_{i,2}^2 \quad \dots \\
&\quad 3\psi_{i,1}\psi_{i,3}^2 \quad 3\psi_{i,1}\psi_{i,4}^2 \quad 3\psi_{i,2}^2\psi_{i,3} \quad 3\psi_{i,2}^2\psi_{i,4} \quad \dots \\
&\quad 3\psi_{i,2}\psi_{i,3}^2 \quad 3\psi_{i,1}\psi_{i,4}^2 \quad 3\psi_{i,3}^2\psi_{i,4} \quad 3\psi_{i,3}\psi_{i,4}^2 \quad \dots \\
&\quad 6\psi_{i,1}\psi_{i,2}\psi_{i,3} \quad 6\psi_{i,1}\psi_{i,2}\psi_{i,4} \quad 6\psi_{i,1}\psi_{i,3}\psi_{i,4} \quad \dots \\
&\quad 6\psi_{i,2}\psi_{i,3}\psi_{i,4}]^T; \tag{8.21}
\end{aligned}$$

for $i = 1, \dots, d+1$. Hence, the mixtures can be alternatively written as

$$\begin{aligned} \mathbf{x}(n) &= \gamma (\mathbf{A}\mathbf{s}(n))^{\odot 3} \\ &= \underline{\Theta} \underline{\rho}(n) = \begin{bmatrix} \boldsymbol{\theta}_1 & \mathbf{0} \\ \mathbf{0} & \boldsymbol{\theta}_1 \\ \boldsymbol{\theta}_2 & \mathbf{0} \\ \mathbf{0} & \boldsymbol{\theta}_2 \end{bmatrix} \begin{bmatrix} \boldsymbol{\rho}(n) \\ \boldsymbol{\rho}(n-1) \end{bmatrix}. \end{aligned} \quad (8.22)$$

As Eq. (8.22) shows, the cubic nonlinearity can be expressed by means of a linear matrix product of nonlinear elements, a property that shall be very useful for us.

Finally, the vector $\underline{\mathbf{z}}(n)$ becomes

$$\begin{aligned} \underline{\mathbf{z}}(n) &= \underline{\mathbf{A}}\mathbf{s}(n) + \underline{\mathbf{\Gamma}} (\underline{\mathbf{A}}\mathbf{s}(n))^{\odot 3} \\ &= \underline{\mathcal{A}}\underline{\mathcal{P}}\mathbf{r}(n) + \underline{\mathbf{\Gamma}}\underline{\Theta}\underline{\rho}(n) \\ &= \begin{bmatrix} a_{11} & 0 & a_{12} & 0 \\ 0 & a_{11} & 0 & a_{12} \\ a_{21} & 0 & a_{22} & 0 \\ 0 & a_{21} & 0 & a_{22} \end{bmatrix} \begin{bmatrix} p_{1,0} & p_{1,1} & 0 & 0 & 0 & 0 \\ 0 & p_{1,0} & p_{1,1} & 0 & 0 & 0 \\ 0 & 0 & 0 & p_{2,0} & p_{2,1} & 0 \\ 0 & 0 & 0 & 0 & p_{2,0} & p_{2,1} \end{bmatrix} \begin{bmatrix} r_1(n) \\ r_1(n-1) \\ r_1(n-2) \\ r_2(n) \\ r_2(n-1) \\ r_2(n-2) \end{bmatrix} \\ &\quad + \begin{bmatrix} \gamma_1 & 0 & 0 & 0 \\ 0 & \gamma_1 & 0 & 0 \\ 0 & 0 & \gamma_2 & 0 \\ 0 & 0 & 0 & \gamma_2 \end{bmatrix} \begin{bmatrix} \boldsymbol{\theta}_1 & \mathbf{0} \\ \mathbf{0} & \boldsymbol{\theta}_1 \\ \boldsymbol{\theta}_2 & \mathbf{0} \\ \mathbf{0} & \boldsymbol{\theta}_2 \end{bmatrix} \begin{bmatrix} \boldsymbol{\rho}(n) \\ \boldsymbol{\rho}(n-1) \end{bmatrix}, \end{aligned} \quad (8.23)$$

whose coefficients $\underline{\mathcal{A}}$, $\underline{\mathcal{P}}$ and $\underline{\Theta}$ are considered to be fixed, $\underline{\mathbf{r}}(n)$ and $\underline{\boldsymbol{\rho}}(n)$ can vary at each time instant and $\underline{\mathbf{\Gamma}}$ should be adjusted in the separation process (along with $\underline{\mathcal{W}}$).

Although we focus on the cubic nonlinearity, the idea of using the Volterra expansion is also valid for other polynomial functions. Such study will be left for future works. In the following, we present the SOS-based criteria to perform separation and its analytical form for the considered specific case.

8.2 Classical Joint Diagonalization of Correlation Matrices

The use of SOS in the linear BSS problem is known to be effective when it involves sources that present temporal structure [Comon and Jutten, 2010; Belouchrani et al., 1997]. In such case, the main idea is to jointly diagonalize the correlation matrices be-

tween separated sources for a given number of delays; in other words, the objective is to mutually decorrelate the outputs, but considering different time delays. There are several methods that perform the second-order separation, among which we cite the algorithms SOBI [Belouchrani et al., 1997], AMUSE and TDSEP [Hyvärinen et al., 2001; Comon and Jutten, 2010]. However, for PNL mixtures, the exclusive use of the SOS for separation has not been addressed yet. In that sense, the analytical formulation of the PNL case may give us important elements to help clarify certain theoretical aspects in this approach. In the following, we present a classical SOS-based criterion for separation [Belouchrani et al., 1997], but we pose it under the light of the temporal-extended formulation introduced in the previous section.

Given a number of time delays d , it is desired that the correlation matrix

$$\underline{\mathbf{R}}_{\underline{\mathbf{Y}}} = E [\underline{\mathbf{y}}(n)\underline{\mathbf{y}}^T(n)] = \begin{bmatrix} \underline{\mathbf{R}}_{y_1 y_1} & \underline{\mathbf{R}}_{y_1 y_2} \\ \underline{\mathbf{R}}_{y_2 y_1} & \underline{\mathbf{R}}_{y_2 y_2} \end{bmatrix}. \quad (8.24)$$

be block-diagonal, i.e., that the cross correlation matrices between outputs (red blocks in Eq. (8.24)) are all null, where $\underline{\mathbf{R}}_{y_i y_j} = E [\underline{\mathbf{y}}_i(n)\underline{\mathbf{y}}_j^T(n)]$, being $\underline{\mathbf{y}}_i(n) = [y_i(n) y_i(n-1) \cdots y_i(n-d)]^T$ and $\underline{\mathbf{y}}(n) = [\underline{\mathbf{y}}_1^T(n) \underline{\mathbf{y}}_2^T(n)]^T$. Hence, we can write the block-diagonalization (BD) criterion as

$$J_{BD} = \min_{\underline{\mathcal{W}}, \underline{\mathcal{G}}} \text{blkoff}(\underline{\mathbf{R}}_{\underline{\mathbf{Y}}}), \quad (8.25)$$

where $\text{blkoff}(\cdot)$ is the squared sum of all elements in the off-block-diagonal of a squared matrix. Additionally, a norm constraint can be applied to force the main diagonal of $\underline{\mathbf{R}}_{\underline{\mathbf{Y}}}$ to be unitary, e.g., by adding to the cost:

$$J_c = \min \sum_{i=1}^N (E [y_i^2(n)] - 1)^2, \quad (8.26)$$

This constraint is necessary in order to avoid the trivial solution. Note that, as the number of delays d increases, the larger the cross correlation matrices get, and more information can be considered by the criterion.

8.2.1 The Analytical BD Cost Function

As usual in SOS-based approaches, the main entity is the correlation matrix and, considering the mixing model given by Eq. (8.15), the expanded correlation matrix $\underline{\mathbf{R}}_{\underline{\mathbf{Y}}}$

can be computed analytically:

$$\begin{aligned}
\mathbf{R}_Y &= E [\mathbf{y}(n)\mathbf{y}^T(n)] \\
&= E [\mathcal{W}\mathcal{A}\mathcal{P}\mathbf{r}(n)\mathbf{r}^T(n)\mathcal{P}^T\mathcal{A}^T\mathcal{W}^T] + E [\mathcal{W}\mathcal{A}\mathcal{P}\mathbf{r}(n)\underline{\boldsymbol{\rho}}^T(n)\underline{\boldsymbol{\Theta}}^T\underline{\boldsymbol{\Gamma}}^T\mathcal{W}^T] \\
&\quad + E [\mathcal{W}\underline{\boldsymbol{\Gamma}}\underline{\boldsymbol{\Theta}}\underline{\boldsymbol{\rho}}(n)\mathbf{r}^T(n)\mathcal{P}^T\mathcal{A}^T\mathcal{W}^T] + E [\mathcal{W}\underline{\boldsymbol{\Gamma}}\underline{\boldsymbol{\Theta}}\underline{\boldsymbol{\rho}}(n)\underline{\boldsymbol{\rho}}^T(n)\underline{\boldsymbol{\Theta}}^T\underline{\boldsymbol{\Gamma}}^T\mathcal{W}^T] \quad (8.27) \\
&= \mathcal{W}\mathcal{A}\mathcal{P}\mathbf{R}_{rr}\mathcal{P}^T\mathcal{A}^T\mathcal{W}^T + \mathcal{W}\mathcal{A}\mathcal{P}\mathbf{R}_{r\rho}\underline{\boldsymbol{\Theta}}^T\underline{\boldsymbol{\Gamma}}^T\mathcal{W}^T + \mathcal{W}\underline{\boldsymbol{\Gamma}}\underline{\boldsymbol{\Theta}}\mathbf{R}_{\rho r}\mathcal{P}^T\mathcal{A}^T\mathcal{W}^T \\
&\quad + \mathcal{W}\underline{\boldsymbol{\Gamma}}\underline{\boldsymbol{\Theta}}\mathbf{R}_{\rho\rho}\underline{\boldsymbol{\Theta}}^T\underline{\boldsymbol{\Gamma}}^T\mathcal{W}^T,
\end{aligned}$$

where $\mathbf{R}_{rr} = E [\mathbf{r}(n)\mathbf{r}^T(n)]$, $\mathbf{R}_{r\rho} = E [\mathbf{r}(n)\underline{\boldsymbol{\rho}}^T(n)]$, $\mathbf{R}_{\rho r} = E [\underline{\boldsymbol{\rho}}(n)\mathbf{r}^T(n)]$ and $\mathbf{R}_{\rho\rho} = E [\underline{\boldsymbol{\rho}}(n)\underline{\boldsymbol{\rho}}^T(n)]$ are the correlation matrices in function of $\mathbf{r}(n)$ and $\underline{\boldsymbol{\rho}}(n)$ – being $\underline{\boldsymbol{\rho}}(n)$ the Volterra expansion of $\mathbf{r}(n)$. Since $\mathbf{r}(n)$ is an *i.i.d* vector, these covariance matrices can be easily computed (although this may demand an extensive effort due to the size of the matrices), but the statistical moments $E [r_i^2(n)]$, $E [r_i^4(n)]$ and $E [r_i^6(n)]$ must be known. It is important to note that, due to the nonlinearity, some HOS are encompassed in the correlation matrix, which might be essential to the nonlinear separation process.

In the BD cost function, only the off-block-diagonal elements are considered, so that the matrices $\mathbf{R}_{y_1y_2}$ and $\mathbf{R}_{y_2y_1}$ are the ones effectively used. Assuming stationary discrete-time stochastic processes, we have that $\mathbf{R}_{y_1y_2} = \mathbf{R}_{y_2y_1}^T$ (are Toeplitz) and, in this case, a single matrix provides all statistical information needed for the BD cost. Based on Eq. (8.27), we can write:

$$\begin{aligned}
\mathbf{R}_{y_iy_j} &= \mathcal{W}_i \left(\mathcal{A}\mathbf{P}\mathbf{R}_{rr}\mathcal{P}^T\mathcal{A}^T + \mathcal{A}\mathbf{P}\mathbf{R}_{r\rho}\underline{\boldsymbol{\Theta}}^T\underline{\boldsymbol{\Gamma}}^T \right. \\
&\quad \left. + \underline{\boldsymbol{\Gamma}}\underline{\boldsymbol{\Theta}}\mathbf{R}_{\rho r}\mathcal{P}^T\mathcal{A}^T + \underline{\boldsymbol{\Gamma}}\underline{\boldsymbol{\Theta}}\mathbf{R}_{\rho\rho}\underline{\boldsymbol{\Theta}}^T\underline{\boldsymbol{\Gamma}}^T \right) \mathcal{W}_j^T, \quad (8.28)
\end{aligned}$$

where \mathcal{W}_i is the i th block with $d+1$ rows of \mathcal{W} . It is possible to note that each of the $(d+1)^2$ elements of $\mathbf{R}_{y_iy_j}$ are quadratic polynomials in function of $\underline{\boldsymbol{\Gamma}}$ and \mathcal{W}_i – the separation coefficients – and can contribute with additional information for solving the system, as we will see ahead.

8.3 Second-Order Mutual Information Measure

Although it has already been shown that the joint diagonalization of covariance matrices is a solid approach for performing linear BSS, its study must not be limited to the cost given by Eq. (8.25), since the use of SOS can be employed in very diversified ways and lead to different perspectives of the problem at hand. Following this line of reasoning, we follow an alternative SOS-based separation measure that combines the temporal formulation – presented in Section 8.1.1 – with the mutual information measure [Comon and Jutten, 2010].

Basically, we aim at a mutual independence definition that is able to encompass the temporal structure of data, i.e.,

$$f_{\underline{\mathbf{Y}}}(\underline{\mathbf{v}}) = \prod_{i=1}^N f_{\underline{y}_i}(\underline{\mathbf{v}}_i), \quad (8.29)$$

being $f_{\underline{\mathbf{Y}}}(\underline{\mathbf{v}})$ and $f_{\underline{y}_i}(\underline{\mathbf{v}}_i)$ the multivariate probability density functions associated with $\underline{\mathbf{y}}(n)$ and $\underline{\mathbf{y}}_i(n)$, respectively (see Eq. (8.24)). The temporal structure, in this case, is inherently taken into account by the multivariate densities and the sources must be mutually independent for all considered delays.

In order to measure the mentioned independence, one can use the mutual information [Comon and Jutten, 2010]

$$I(\mathbf{y}(n), \dots, \mathbf{y}(n-d)) = -H^S(\underline{\mathbf{Y}}) + \sum_{i=1}^N H^S(\underline{y}_i), \quad (8.30)$$

where $H^S(\cdot)$ is Shannon's entropy, defined as

$$H^S(\underline{\mathbf{Y}}) = - \int_D f_{\underline{\mathbf{Y}}}(\underline{\mathbf{v}}) \log(f_{\underline{\mathbf{Y}}}(\underline{\mathbf{v}})) d\underline{\mathbf{v}}, \quad (8.31)$$

being $D \subseteq \mathbb{R}^{N(d+1)}$. When independence is reached for all delays, the mutual information is null. In its strict form, Eq. (8.30) is difficult to be calculated since it demands the estimation of the densities (which is critical in our case, where all densities are multivariate). Hence, to overcome this issue and also to restrain our analysis to the SOS – which are easier to be estimated –, we make the following assumption: the sources are jointly Gaussian distributed and present a time structure. Thus, it is expected that the recovered sources be Gaussian as well, i.e., $f_{\underline{\mathbf{Y}}}(\underline{\mathbf{v}}) \sim \mathcal{N}(\mathbf{0}, \underline{R}_{\underline{\mathbf{Y}}})$ or

$$f_{\underline{\mathbf{Y}}}(\underline{\mathbf{v}}) = \frac{1}{\sqrt{(2\pi)^{d+1} \det(\underline{R}_{\underline{\mathbf{Y}}})}} \exp\left(\frac{-1}{2} \underline{\mathbf{v}}^T \underline{R}_{\underline{\mathbf{Y}}}^{-1} \underline{\mathbf{v}}\right), \quad (8.32)$$

being $\underline{R}_{\underline{\mathbf{Y}}}$ as defined in Eq. (8.24).

It can be shown that, by combining Eq. (8.32) with (8.30), the mutual information reduces to the following criterion

$$J_{SOMI} = \min_{\underline{\mathcal{W}}, \underline{\mathcal{G}}} \frac{1}{2} \log\left(\frac{\prod_{i=1}^N \det(\underline{R}_{\underline{y}_i})}{\det(\underline{R}_{\underline{\mathbf{Y}}})}\right). \quad (8.33)$$

It is important to mention that a similar expression was already obtained through the spectral density of Gaussian sources, being named Gaussian Mutual Information (GMI) [Comon and Jutten, 2010; Pham, 2001; Pham and Cardoso, 2001], and the use of the temporal-

extended covariance matrices were used in the convolutive mixing problem [Buchner et al., 2005], however, its application on the PNL problem is novel. Hence, we refer to Eq. (8.33) as the Second-Order Mutual Information (SOMI). As the BD cost, Eq. (8.33) uses only the SOS information, but instead of using summation of quadratic terms (Eq. (8.25)), the determinant of matrices \underline{R}_{y_1} , \underline{R}_{y_2} and \underline{R}_Y is considered.

The objective of the SOMI criterion is to minimize the cost J_{SOMI} so that the mutual information be null. However, the direct minimization of Eq. (8.33) may point towards a null argument for the $\log(\cdot)$ function, most probably leading to null determinants. Hence, the norm constraint given by Eq. (8.26) might be essential for this criterion.

8.3.1 The Quadratic SOMI Cost

A closer observation of Eq. (8.33) reveals that it is, in fact, a matching between the determinant terms $\prod_{i=1}^N \det(\underline{R}_{y_i})$ and $\det(\underline{R}_Y)$. If equality is reached, the cost J_{SOMI} is equal to zero (i.e., the mutual information is null). In that sense, a similar cost can be written without relying on the logarithm properties, but on the simplicity of a quadratic difference:

$$J_{SOMIq} = \min_{\underline{W}, \underline{G}} \left(\prod_{i=1}^N \det(\underline{R}_{y_i}) - \det(\underline{R}_Y) \right)^2, \quad (8.34)$$

where the minimal (and desired) cost value is zero as well. Note that the norm constraint (Eq. (8.26)) is also necessary to avoid null determinants. This cost is named SOMIq due to its quadratic term.

When the correlation matrix \underline{R}_Y is block-diagonal, $\det(\underline{R}_Y) = \prod_{i=1}^N \det(\underline{R}_{y_i})$ and both the costs of SOMI and SOMIq will be null. In that sense, we expect that the solutions for SOMI and SOMIq be coincident, even though, the quadratic relation in SOMIq may be able to provide a more fruitful cost shape in the optimization process – we will discuss this point in more detail later.

Given Eqs. (8.27) and (8.28), the analytical costs of SOMI and SOMIq are straightforward.

8.4 Identifiability and Bounds

The three aforementioned criteria share a common feature when a solution is found: the extended correlation matrix of the output signals \underline{R}_Y is a block-diagonal matrix, i.e., all the off-block-diagonal elements are null. This observation allows us to write some general aspects involving the SOS-based costs in the context of the considered special PNL mixture case.

8.4.1 Blind Identifiability

In the linear BSS problem, the study of the blind identification conditions for the SOS-based approaches is a well studied topic [Belouchrani et al., 1997]: it is known that the linear mixing matrix \mathbf{A} can be identified, up to permutation and phase shifts, if the source signals have different spectral shapes. Generally, the demonstration for this linear problem is done by ensuring that the diagonalization process of the correlation matrix for different delays yields eigenvalues that are distinct. Translating this idea to our temporal-extended formulation, it is required that a block-diagonalized $\underline{\mathbf{R}}_Y$ present distinct eigenvalues.

The extension of this idea to the general PNL problem becomes more complex, since the identification conditions must be valid for \mathbf{A} and $\mathbf{f}(\cdot)$. In our particular case, i.e., for the cubic nonlinearity given by Eq. (8.11), the problem is simpler, since identification applies only to $\underline{\mathcal{W}}$ and $\underline{\mathbf{\Gamma}}$. In that sense, we can pose the conditions for identification as: based on Eq. (8.27), we have that $\underline{\mathcal{W}}$ must jointly block-diagonalize the matrices $\underline{\mathcal{A}}\underline{\mathbf{P}}\underline{\mathbf{R}}_{rr}\underline{\mathcal{P}}^T\underline{\mathcal{A}}^T$ (which is the linear part), $\underline{\mathcal{A}}\underline{\mathbf{P}}\underline{\mathbf{R}}_{r\rho}\underline{\Theta}^T\underline{\mathbf{\Gamma}}^T$ and $\underline{\mathbf{\Gamma}}\underline{\Theta}\underline{\mathbf{R}}_{\rho\rho}\underline{\mathcal{P}}^T\underline{\mathcal{A}}^T$ and $\underline{\mathbf{R}}_Y$ must yield distinct eigenvalues. To solve this problem, we consider two cases: (i) $\underline{\mathbf{\Gamma}}$ is null and (ii) $\underline{\mathbf{\Gamma}}$ has a non-null value.

In case (i), when $\underline{\mathbf{\Gamma}}$ is null, i.e., the case in which the nonlinear part is solved, $\underline{\mathcal{W}}$ must block-diagonalize only $\underline{\mathcal{A}}\underline{\mathbf{P}}\underline{\mathbf{R}}_{rr}\underline{\mathcal{P}}^T\underline{\mathcal{A}}^T$ and the conditions are the same as for the linear case, viz., the source signals must have different spectral shapes.

For case (ii), all terms in Eq. (8.27) must be block-diagonalized. To illustrate, we consider that the first term, $\underline{\mathcal{A}}\underline{\mathbf{P}}\underline{\mathbf{R}}_{rr}\underline{\mathcal{P}}^T\underline{\mathcal{A}}^T$, is block-diagonalized, where we have that $\underline{\mathcal{W}} = \underline{\mathcal{A}}^{-1}$. In this case,

$$\underline{\mathbf{R}}_Y = \underline{\mathcal{P}}\underline{\mathbf{R}}_{rr}\underline{\mathcal{P}}^T + \underline{\mathcal{P}}\underline{\mathbf{R}}_{r\rho}\underline{\Theta}^T\underline{\mathbf{\Gamma}}^T\underline{\mathcal{W}}^T + \underline{\mathcal{W}}\underline{\mathbf{\Gamma}}\underline{\Theta}\underline{\mathbf{R}}_{\rho\rho}\underline{\mathcal{P}}^T + \underline{\mathcal{W}}\underline{\mathbf{\Gamma}}\underline{\Theta}\underline{\mathbf{R}}_{\rho\rho}\underline{\Theta}^T\underline{\mathbf{\Gamma}}^T\underline{\mathcal{W}}^T, \quad (8.35)$$

and, by construction, the terms involving $\underline{\mathbf{\Gamma}}$ are not block-diagonal, regardless of the value of $\underline{\mathbf{\Gamma}}$. The only exception happens when $\underline{\mathcal{A}} = \mathbf{I}$, i.e., when the signals are not linearly mixed, and all the terms will be block-diagonal. In this case, the SOS-based methods are intended to fail. For other values of $\underline{\mathcal{W}}$, the linear term is not block-diagonal.

Thus, in short, the identifiability conditions are that the signals must present different spectral shapes and that the linear mixing part of the PNL model must effectively occur.

8.4.2 Bounds on the Number of Delays

As previously mentioned, each element in the off-block-diagonal of $\underline{\mathbf{R}}_Y$ forms a quadratic polynomial in function of $\underline{\mathbf{\Gamma}}$ and $\underline{\mathcal{W}}$, and, as we will see in this section, they will compose a system of quadratic equations. The unknown variables, in our studied case, are $\underline{\mathbf{\Gamma}}$ and $\underline{\mathcal{W}}$, which correspond to $N(N+1)$ variables.

Some elements (or equations) of $\underline{\mathbf{R}}_Y$, however, are redundant. For instance, the elements of the main diagonal of $\underline{\mathbf{R}}_{y_i y_j}$ form, from an statistical standpoint, the same equation and, hence, they only contribute as a single equation (new information) to the system. In addition, as we assume stationary signals, we have that $\underline{\mathbf{R}}_{y_i y_j} = \underline{\mathbf{R}}_{y_j y_i}^T$, which also reduces the effective number of equations in the system. In that sense, by removing the redundancy, we have $N(N-1)/2$ matrices $\underline{\mathbf{R}}_{y_i y_j}$, in which the number of effective equations are $d(d+1)+1$ each one, resulting in a total of $N(N-1)(d(d+1)+1)/2$ equations in the system.

Besides, the normalization given by Eq. (8.26) also performs a role as a constraint, and can contribute to the system with N equations. Finally, it is possible to state that the number of effective equations in the system is $N(N-1)(d(d+1)+1)/2 + N$, which must be equal to or higher than the number of unknown parameters. Considering, for example, the case of 6 unknown variables and $N=2$, it is necessary that $2(2-1)(d(d+1)+1)/2 + 2 \geq 6$, what implies in $d \geq 2$.

Notwithstanding, it is also possible that some of the off-diagonal elements of $\underline{\mathbf{R}}_{y_i y_j}$ be equivalent, depending on the temporal structure of the mixtures and, in that case, the number of valid equations might be reduced. In that sense, the expression $N(N-1)(d(d+1)+1)/2 + N$ is only an upper bound to the number of equations that can be valid to solve the system. Hence, in the previous example of 6 unknown variables and $N=2$, $d \geq 2$ is just a lower bound on the number of delays d , probably leading to the need of a higher value of d for a good quality separation.

In order to illustrate the system of equations, we consider a 2-source and 2-mixture case in which the linear mixing part of the PNL model is a rotation matrix, i.e.,

$$\mathbf{A} = \begin{bmatrix} \cos(\phi_a) & -\sin(\phi_a) \\ \sin(\phi_a) & \cos(\phi_a) \end{bmatrix}. \quad (8.36)$$

For the separation, based on Eq. (8.15), we have 2 unknown variables for the joint non-linear part, γ_1 and γ_2 , and 1 unknown variable, ϕ_w , for the linear separating matrix \mathbf{W} (which is a rotation matrix, similar to \mathbf{A}). Thus, we have that, for $N=2$ and $d=1$, the number of equations is, at most, $N(N-1)(d(d+1)+1)/2 + N = 5$. Fig. 8.2(a) shows the surface contour of each equation for given colored sources, with $\phi_a = 1.02$ rad. In this case, the off-diagonal elements of $\underline{\mathbf{R}}_{y_1 y_2}$ are coincident and we only have 4 equations. The intersection points of the surfaces will determine the regions where all equations are satisfied. Indeed, any of these points will be a valid solution for the BD, SOMI and SOMIq criteria.

Although the SOS-based criteria are intended to present the same solution, their costs shape may differ. We consider the same previous case, however, the linear part is assumed to be solved already, leaving just γ_1 and γ_2 to be adjusted. In Fig. 8.2(b), we show the

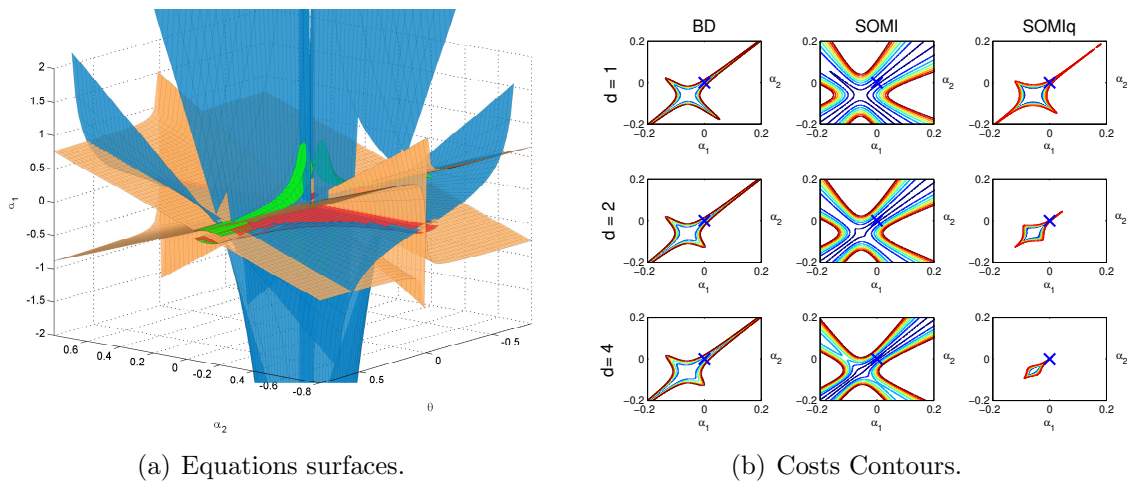


Figure 8.2: Number of delays: equations and solutions.

contours as a function of γ_1 and γ_2 and for d equal to 1, 2 and 4. In all cases, the global solution is $\gamma_1 = \gamma_2 = 0$ (denoted by an “X”), which is the desired solution, but local minima can also be seen. Very interestingly, as d increases, the “weight” of the local optima is reduced in the costs, being the global solution more evident. This effect is particularly more intense for the SOMIq cost, whose shape changes significantly.

In the next section, we will consider the case where $\underline{\Gamma}$ and $\underline{\mathcal{W}}$ have no constraints – which will drastically increase the space of solutions candidates – to evaluate the criteria performance.

8.5 Performance Analysis

So far, we verified that the SOS-based criteria share some features, but they might differ in their costs shapes and, when an optimization task is performed, its effect on the performance may be significant. In order to test this, we consider the two-source and two-mixture simulation scenarios encompassing the SOS-cost obtained via the analytical formulation and via samples estimation.

For the optimization of the weights (nonlinear and linear), we adopt, as in the previous chapters, the DE metaheuristic to avoid convergence to local optima [Price et al., 2005]. Since we consider $N=2$ sources, it implies that, according to our particular cubic nonlinearity case, 6 coefficients must be adapted: 2 for $\underline{\Gamma}$ and 4 for $\underline{\mathcal{W}}$. In this case, the 6-dimensional search space is considerably large, but the DE metaheuristic can be adjusted to use more resources and perform a more extensive search for the global optima. With that in mind, the DE parameters were chosen to be $N_P = 500$ (population size), $F = 0.5$, $CR = 0.9$ and 5000 iterations. These DE parameters were constant for all simulation cases.

With the DE solution at hand, the performance of the SOS-based methods can be measured in terms of the Signal-to-Interference Ratio (SIR) (after permutation, sign and variance correction), which is defined as

$$\text{SIR} = 10 \log \left(\frac{E[y_i(n)^2]}{E[(s_i(n) - y_i(n))^2]} \right). \quad (8.37)$$

In that sense, higher SIR values means better performance solutions.

8.5.1 Performance Using the Analytical Costs

In the first scenario, we wish to investigate the analytical costs and the effect of the number of delays d considered. For the sources, two *i.i.d.* Gaussian signals ($r_1(n)$ and $r_2(n)$) are generated and temporally colored by the pre-coders $\mathbf{p}_1 = [1 \ 0.6 \ -0.3 \ 0.1 \ 0.4 \ 0.3 \ -0.22 \ 0.18 \ 0.5]$ and $\mathbf{p}_2 = [1 \ -0.2 \ -0.8 \ 0.2 \ 0.1 \ -0.41 \ 0.5 \ 0.1]$, separately. Note that the temporal structures provided by \mathbf{p}_1 and \mathbf{p}_2 are of finite length and, hence, there is a limited amount of temporal information to be extracted. The linear mixing matrix is $\mathbf{A} = [0.25 \ 0.86; -0.86 \ 0.25]$ and we wish to adapt $\underline{\Gamma}$ and $\underline{\mathcal{W}}$, according to Eq. (8.15). Supposing that the pre-coders \mathbf{p}_1 and \mathbf{p}_2 as well as the mixing coefficients are known, the BD, SOMI and SOMIq costs can be analytically computed without the necessity of using samples for their estimation, as discussed in Sections 8.2, 8.3 and 8.3.1.

We considered that the number of delays d can vary from 1 to 7 and, for each value of d , we performed 50 independent runs of the DE, whose solutions were evaluated in terms of SIR for 700,000 test samples. Fig. 8.3(a) shows the mean SIR values for each delay considered, while Fig. 8.3(b) shows the SIR values for the best solution found by DE throughout the 50 runs. In the first case, one can note that the solutions found for the

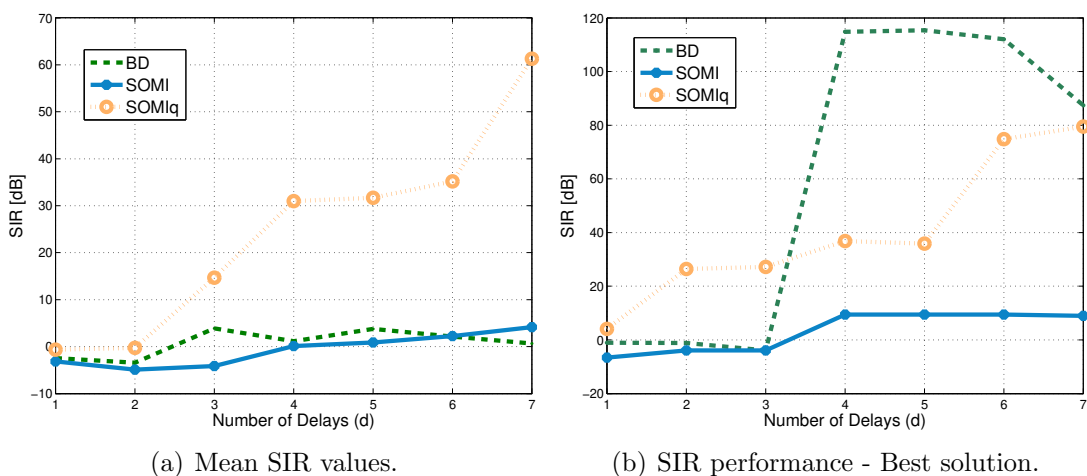


Figure 8.3: Mean and Best Performance - Analytical Costs.

BD and SOMI criteria led to a low value of SIR for all considered delays, indicating

that their solutions might not be adequate for performing BSS. Notwithstanding, for the best solution found, the BD criterion shows an intriguing result: for $d \geq 4$, the solutions for the BD are able to separate the sources with a higher level of SIR. This indicates that, although we have employed a huge search resource for the DE, it has presented difficulties in finding the best solution for BD. On the other hand, for the SOMIq criterion, the DE found good results more easily, without great discrepancies between Figs. 8.3(a) and 8.3(b), and, from a general perspective, it is possible to say that the solutions SIR level tends to increase with d , being the sources successfully separated. Note that, for $d = 2$, the SOMIq best solution found by DE is already able to separate the sources, which is in accordance with the bound on the number of delays.

In order to clarify the obtained results, we compare in Fig. 8.4(a) the costs values of BD, SOMI and SOMIq for one of the 50 runs of the DE (that we will refer to as ‘regular’) and its best solution (i.e., the lowest cost found throughout the 50 runs), all for $d = 4$. It

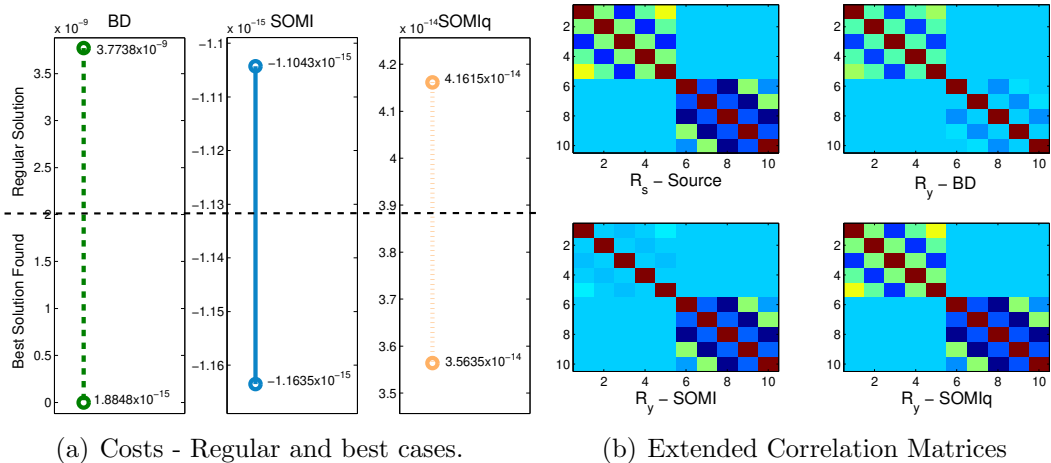


Figure 8.4: Cost Comparison and Correlation matrices.

is possible to note that, for the BD cost, the difference between the two cases is larger, being clear that the DE is presenting difficulties to find the global optima, differently from the other costs, where the differences were relatively small. This can be seen as an evidence that the BD cost suffers from low distinguishability of the global optima, being necessary to increase the search power of the DE metaheuristic. For the SOMI, the minimization of Eq. (8.33) led to negative values of the cost, which means that the MI does not achieve its desired (null) value. The SOMIq cost, on the other hand, solves the drawback of SOMI and converges to positive small values.

A more intuitive comparison can be obtained from Fig. 8.4(b), where we illustrate a colored version of the extended correlation matrix of the sources $\underline{\mathbf{R}}_S$ and of the outputs $\underline{\mathbf{R}}_Y$ for the BD, SOMI and SOMIq solutions in one of the executions (the same ‘regular’ run) of the DE metaheuristic, all for $d=4$. It is possible to note that, for $\underline{\mathbf{R}}_S$, the main block-diagonal is colored in different patterns, which reveals the temporal structure of

the sources, while the off-block-diagonal are uncorrelated and presents a single color. Ideally, the objective is to obtain $\underline{\mathbf{R}}_Y$ as close as possible to $\underline{\mathbf{R}}_S$. For the BD output, the temporal structure of only one of the sources was preserved, while the other source was temporally uncorrelated. A similar result also applies to SOMI, while, for the SOMIq output, the solution found was the desired one, whose sources are uncorrelated and with their temporal structure preserved. Although not visible, the residual correlation of the off-block-diagonal for the BD and SOMI solutions are higher than that of SOMIq, which indicates they converged to local minima in the regular run.

8.5.2 Performance Using Estimated Costs

When using an analytical formulation, the evaluation of the costs might gain infinite precision. However, for real-world problems, the costs are generally estimated from samples, which certainly lead to approximated costs with reduced accuracy. This could be determinant in the performance of the algorithms when local solutions are not too distinct from the global ones, which, as indicated in the previous analysis, is the case of the BD cost.

With the objective of measuring the SIR performance in more realistic scenarios, we consider now the estimated costs of BD, SOMI and SOMIq, where the extended covariance matrices are estimated via sample mean. Besides that, it is also desired to evaluate the performance for the case in which the sources are not Gaussian. Since the costs only depend on the SOS and the temporal structure, we expect that the distribution of the sources cause no impact on the performance (even on the SOMI and SOMIq costs, whose formulations are based on the assumption of Gaussian sources).

We consider a 2-source \times 2-mixture case, being the linear mixing matrix

$$\mathbf{A} = \begin{bmatrix} 0.55 & -0.92 \\ -0.82 & 0.38 \end{bmatrix} \quad (8.38)$$

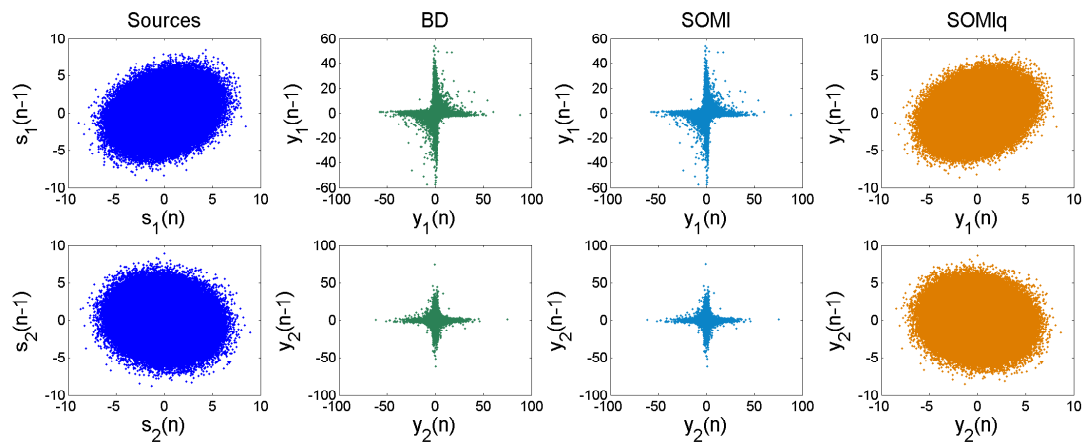
and the cubic nonlinearity, Eq. (8.11), as adopted throughout this chapter. Again, the temporal coloration is obtained through FIR filters as pre-coders, here chosen to be $\mathbf{p}_1 = [1 \ 0.6 \ -0.3 \ 0.1 \ 0.4]$ and $\mathbf{p}_2 = [1 \ -0.2 \ -0.8 \ 0.2 \ 0.1]$. Now, we assume two types of distribution for $r_1(n)$ and $r_2(n)$: in the first case, $r_1(n)$ and $r_2(n)$ are two *i.i.d.* Gaussian signals with zero mean and variance equal to 2 and, in the second case, they are two *i.i.d.* signals uniformly distributed between -1 and $+1$. In an attempt to avoid precision issues when estimating the costs, mainly the BD cost, we consider we have a large set of 50,000 samples for estimation. A test set with 700,000 samples will be used to estimate the SIR. The number of considered delays is $d = 4$.

To adapt the coefficients $\underline{\mathbf{I}}$ and $\underline{\mathcal{W}}$, we use the DE metaheuristic with the same previously defined parameters, but just perform a single run to search for the solution. The

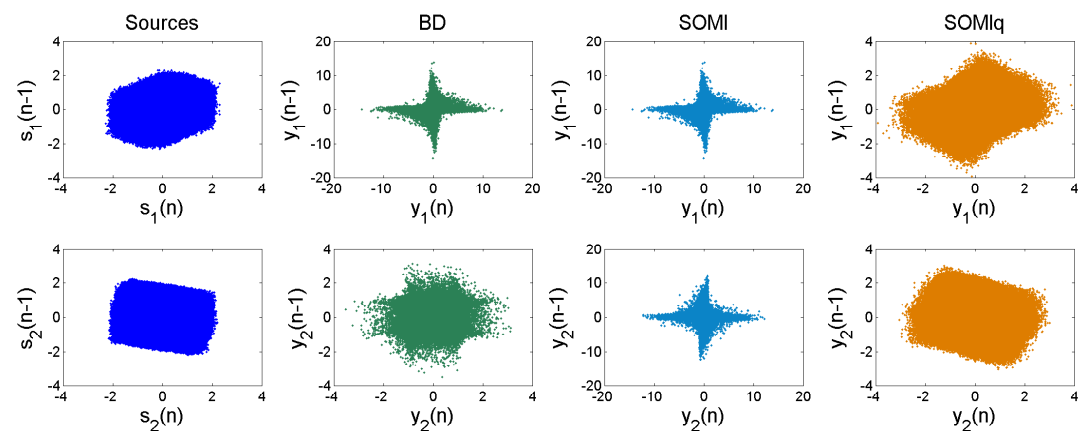
Table 8.1: Performance in terms of SIR [dB]

Scenario		BD	SOMI	SOMIq
Gaussian	Source 1	-0.021	0.259	68.432
	Source 2	-5.436	-5.400	65.060
Uniform	Source 1	-6.909	-3.404	42.421
	Source 2	9.639	-6.900	47.927

resulting performance for the BD, SOMI and SOMIq solutions found by the DE are exhibited in Tab. 8.1, for the Gaussian and uniform sources. It is possible to note that the BD and the SOMI solutions presented similar but lower values of SIR, for both Gaussian and uniform sources, while the SOMIq solutions achieved good performance: for the Gaussian sources, an impressive high SIR level was obtained, however, for the uniform sources, the SIR is lower, but still of high quality (above 30 dB). Note that this result is compatible to what was observed in the analytical scenario.

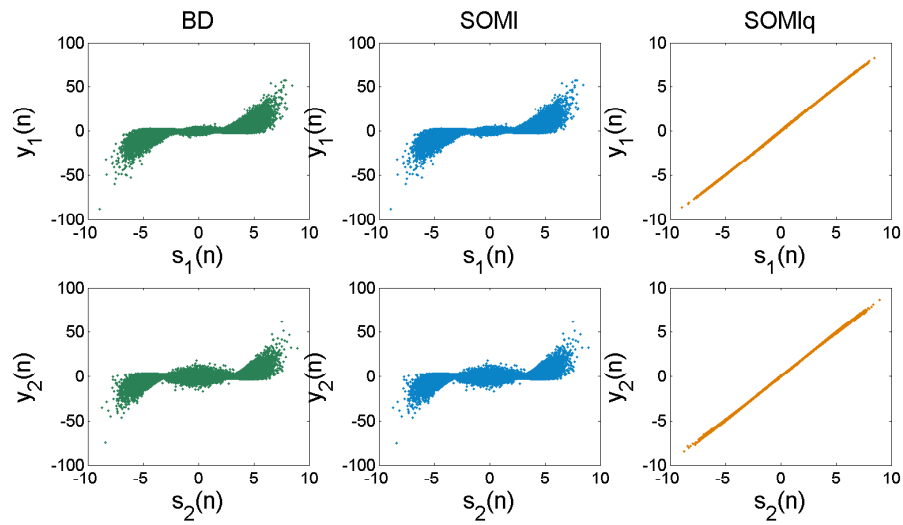


(a) Gaussian sources.

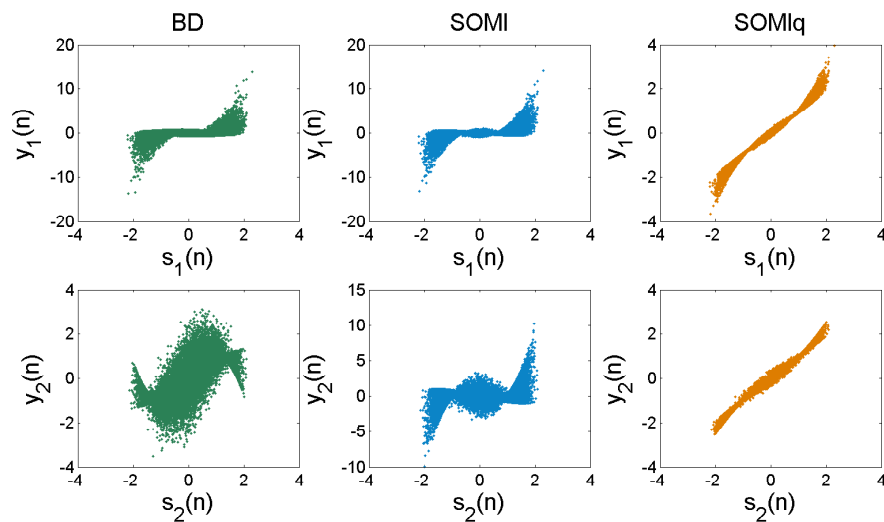


(b) Uniform sources.

Figure 8.5: Estimated Costs: Scatter plots.



(a) Gaussian sources.



(b) Uniform sources.

Figure 8.6: Estimated Costs: $s(n) \times y(n)$ plots.

In Fig. 8.5, we show the temporal scatter plots of the sources and its estimates via BD, SOMI and SOMIq (after sign, mean and variance correction); in addition, in Fig. 8.6, we show the $s(n) \times y(n)$ plots, in which a diagonal line will indicate that the source was correctly recovered. The outputs for BD and SOMI are almost equivalent, indicating that they might share the same local minimum – where the DE metaheuristic remained trapped without finding the global optima – and that the type of the sources was indifferent in this case. Due to the greater solution distinguishability of SOMIq, the solution found was the desired one (or close enough to it). For the Gaussian sources case, Figs. 8.5(a) and 8.6(a), the SOMIq output is practically the sources themselves and, for the uniform case, Figs. 8.5(b) and 8.6(b), the SOMIq solution is somehow similar to the sources, with SIR value similar to the average SIR obtained in the analytical simulations.

8.6 Conclusion

In this chapter, the problem of BSS was investigated in the context of PNL mixtures from an SOS-based perspective. In order to extract the signals temporal structure in a more extensive manner, an alternative formulation of the problem was presented, which allowed us to write the classical SOS-based cost functions from a temporal-extended standpoint, resulting in the BD (based on SOBI cost) and SOMI (based on GMI) costs. In addition, to overcome some minimization problems with SOMI, a quadratic-like modification was proposed and named SOMIq.

The temporal-extended formulation allowed the analytic computation of the SOS-based costs by assuming the specific case in which the PNL nonlinearity is a cubic polynomial (and using its Volterra expansion). Based on this, a simple analysis on the costs defined some identifiability conditions and a lower bound on the number of delays that must be considered for separation. To evaluate the performance of the criteria in the PNL model with cubic nonlinearities, some simulations were held in scenarios using analytical and estimated versions of the costs, being the optimization made by the DE metaheuristic. In the analytical case, the extended correlation matrices could be obtained without the use of samples (and were independent of the distribution of the sources). The results indicated that the BD criterion was able to perform source separation, however, due to its optima low distinguishability, the DE metaheuristic found difficulties during the solution search process and led to poor SIR performance; the SOMI criterion presented some problems since its cost led to solutions that were not able to establish mutually independent sources with the desired precision; on the other hand, the SOMIq criterion presented more distinguishable optima when compared to BD and led the DE to solutions that preserved the mutual independence (from a SOS point of view) and the temporal structure of the data – also, by increasing the number of delays above the lower bound, we observed an improvement of the performance in terms of SIR. For the estimated costs, a large number of samples was necessary in order to increase the precision in the estimation step. The obtained results corroborated with the performance analysis held in the analytical case and revealed a good performance for Gaussian and for uniformly distributed sources.

Although the present analysis focus on a specific case of the PNL mixtures, i.e., for cubic nonlinearities, we consider it an important step towards the use of the SOS framework in the nonlinear BSS problem. In that sense, for future works, we consider the extension of this analysis to other polynomial nonlinearities and other nonlinear mixing models.

Chapter 9

Conclusions

In this Ph.D. thesis, the efforts were aimed at a more extensive extraction of the information on the temporal structure of the signals, which was possible via the use of the ITL-based methods allied to a multivariate perspective. This approach was applied to three important problems within the signal processing area: (i) blind channel equalization with temporally structured sources, (ii) supervised equalization using IIR filtering structures, and (iii) nonlinear BSS problems. In each case, the results led to relevant contributions, extending the ITL paradigm to the multivariate approach and also to the use of metaheuristics as optimization strategy, instead of the traditional gradients.

Throughout the presented work, several concepts from statistics, signal processing, information theory, adaptive filtering and machine learning were used, as recapitulated in the following.

It was shown that performing a task within the signal processing area necessarily involves the use of three basic elements: the filtering structure, the criterion and the optimization method, whose main features were presented in Chapters 1, 2 and 3, respectively. More specifically, in Chapter 1 the linear FIR and IIR filters as well as the nonlinear polynomial filters and the RBF neural networks were presented. The concepts of the Information Theory and their contribution to the emergence of the ITL field were presented in Chapter 2, which also included the discussion of the main uncertainty and similarity measures and how to estimate them via the Parzen window method. At last, Chapter 3 describes the gradient-based methods – with special attention the to stochastic gradient approach – and the main concepts behind the DE metaheuristic for optimization.

Chapter 4 provided a brief overview on the methods for the channel equalization – for both supervised and unsupervised perspectives – and the BSS problems. Regarding the supervised channel equalization, the Wiener paradigm and the LMS algorithm derivation were described, being followed by the ITL trends on this topic: the Rényi's entropy and the correntropy. For the IIR structures, the equation-error and output-error formulations were considered, thus describing the LMS, PLR and RPE-based algorithms. Next, for the

blind channel equalization, the theoretical basis provided by the BGR and SW theorems were presented, being of fundamental importance to the justification of the HOS use in the described Bussgang techniques, SW criterion and blind ITL-based approaches, such as the distribution matching and correntropy approaches. For the BSS problem, the linear case was presented with special emphasis on the MI-based approaches and on the SOS-based ones – since they make use of the temporal structure of the sources –, while the nonlinear case encompassed the PNL model and its joint or two-stage approaches for adaptation. For each topic, the promising investigative lines were pointed out to motivate the contributions of this work.

As for the contributions, Chapter 5 established the statistical conditions for the colored blind channel equalization problem based on novel extensions of the BGR and SW theorems, which, through antique theorems found in the literature and some empirical results, revealed the necessity of the manipulation of multivariate distributions in order to achieve the ZF condition. It was also pointed out that, under certain conditions on the filtering structures, the multivariate statistical requirement can be relaxed and even a SOS-based approach was sufficient to ensure equalization.

Following the results presented in Chapter 5, four criteria based on the notion of statistics matching were considered in Chapter 6 due to their capabilities of extracting the temporal structure of the signals: the matching of correlation, of cross-kurtosis, of correntropies (state-of-the-art) and of multivariate distributions, being the matching of cross-kurtosis and of multivariate distributions contributions of this work. The derivation of special analytical cases and the gradient-based algorithms were presented as well as some estimation issues. The performance of the criteria were evaluated in a set of representative scenarios with results very favorable to the multivariate distributions matching approach, being equivalent or superior than the correntropy-based approach.

In Chapter 7, the supervised channel equalization problem using IIR filters was considered from the perspective of the equation-error and output-error formulations. For each case, the ITL-based Shannon's and Rényi's entropy as well as the correntropy were extended to the multivariate perspective in order to extract the temporal dependence of the signals more efficiently. The derivation of these multivariate ITL methods applied to the supervised channel equalization problem is one of the contributions of this work. For comparison purposes, the multivariate distribution matching criterion of the previous Chapter were also considered. For each criterion, versions of the LMS, PLR and RPE algorithms were derived. In the simulated scenarios, the multivariate Shannon's entropy RPE-based algorithm presented the best performance results, but, in general, all ITL-based algorithms performed better than the classical MSE-based approaches.

Finally, in Chapter 8, the PNL model with cubic nonlinear function was investigated. Using a temporal-extended formulation, an SOS-based criterion was obtained from the MI measure applied to multivariate Gaussian sources, but the method was not limited to these

distributions. Indeed, the comparison with other classical SOS methods in BSS revealed that the proposition was particularly useful in conjunction with the DE metaheuristic, with much higher convergence rate for BSS solutions than the other methods.

Future Perspectives

From the obtained results, there emerges a number of interesting possibilities that can be explored in future works:

- The colored blind channel equalization problem opens way to the use of coding schemes at the symbol level in communications, being possible, for instance, to extend the Viterbi coder/decoders to the continuous domain. In addition, following an approach similar to that of Shannon's, it would be interesting to investigate if this approach can lead to an increase of the practical channel capacity.
- A promising idea is the application of the distribution matching criterion in within Galois Fields. This would allow the equalization in corrupted digital data and genomic databases.
- The notion of the correlation matching may establish important connections with the predictive approach, since, in essence, the predictive methods only rely on the correlation through a constrained filter adaptation.
- The methods considered in the colored blind equalization problem and in the supervised IIR equalization can be easily extended to the unsupervised/supervised system identification problem, which certainly will contribute to the development of this problem.
- The combination of the ITL-based methods and the LMS/RPE-based approaches for IIR filters revealed a particular synergy that might be also valid in unsupervised scenarios. In that sense an investigation on the unsupervised methods can also be promising.
- An investigation on the efficiency of the proposed SOS-based criterion in other types of nonlinear mixtures and models.

Bibliography

- Achard, S. and Jutten, C. Identifiability of Post-Nonlinear Mixtures. *IEEE Signal Processing Letters*, 12(5):423–426, 2005.
- Agazzi, O., Messerschmitt, D., and Hodges, D. Nonlinear echo cancellation of data signals. *IEEE Transactions on Communications*, 30(11):2421–2433, 1982.
- Ahmad, I. and Lin, P.-E. A Nonparametric Estimation of the Entropy for Absolutely Continuous Distributions. *IEEE Transactions on Information Theory*, 22(3):372–375, 1976.
- Aronszajn, N. The Theory of Reproducing Kernels and Their Applications. *Cambridge Philos. Soc. Proc*, 39:133–153, 1943.
- Attux, R. R. F., Boccato, L., Fantinato, D. G., Montalvão Filho, J. R., Neves, A., Suyama, R., Nose Filho, K., and Silva, D. G. *Signals and Images: Advances and Results in Speech, Estimation, Compression, Recognition, Filtering, and Processing*, chapter Bio-Inspired and Information-Theoretic Signal Processing. CRC Press, 2015.
- Axford, R. A., Milstein, L. B., and Zeidler, J. R. The Effects of PN Sequences on the Misconvergence of the Constant Modulus Algorithm (CMA). *IEEE Transactions on Signal Processing*, 46(2):519–523, 1998.
- Bellini, S. and Rocca, F. Blind Deconvolution: Polyspectra or Bussgang Techniques? *Elsevier Science Publishers*, pages 251–263, 1986.
- Belouchrani, A., Abed-Meraim, K., Cardoso, J., and Moulines, E. A Blind Source Separation Technique Using Second-Order Statistics. *IEEE Trans. on Signal Processing*, 45(2):434–444, 1997.
- Benedetto, S., Biglieri, E., and Daffara, R. Modeling and Performance Evaluation of Nonlinear Satellite Links-A Volterra Series Approach. *IEEE Transactions on Aerospace and Electronic Systems*, AES-15(4):494–507, 1979.

-
- Benveniste, A., Bonnet, M., Goursat, M., Macchi, C., and Ruget, G. Report 325. *IRIA LABORIA*, September 1978.
- Benveniste, A., Goursat, M., and Ruget, G. Robust Identification of a Nonminimum Phase System: Blind Adjustment of a Linear Equalizer in Data Communications. *IEEE Trans. on Automatic Control*, AC-25(3):385–399, 1980.
- Biglieri, E., Gersho, A., Gitlin, R., and Lim, T. Adaptive cancellation of nonlinear intersymbol interference for voiceband data transmission. *IEEE Journal on Selected Areas in Communications*, 2(5):765–777, 1984.
- Blum, C. and Roli, A. Metaheuristics in Combinatorial Optimization: Overview and Conceptual Comparison. *ACM Computing Surveys (CSUR)*, 35(3):268–308, 2003.
- Bocato, L., Fantinato, D. G., Silva, D. G., Ferrari, R., Neves, A., and Attux, R. Analysis of ITL Criteria in the Context of FIR Channel Equalization. *Journal of Communication and Information Systems*, 31(1), 2016. doi: 10.14209/jcis.2016.1.
- Bourbaki, N. *Commutative algebra*, volume 8. Hermann Paris, 1972.
- Boussaïd, I., Lepagnot, J., and Siarry, P. A Survey on Optimization Metaheuristics. *Information Sciences*, 237:82–117, 2013.
- Broomhead, D. S. and Lowe, D. Multi-variable functional interpolation and adaptive networks. *Complex Systems*, 2:321–355, 1988.
- Buchner, H., Aichner, R., and Kellermann, W. A Generalization of Blind Source Separation Algorithms for Convolutional Mixtures Based on Second-Order Statistics. *IEEE Transactions on Speech and Audio Processing*, 13(1):120–134, 2005.
- Cacoullos, T. Estimation of a Multivariate Density. *Annals of the Institute of Statistical Mathematics*, 18(1):179–189, 1966.
- Calhoun, V., Adali, T., and Pearlson, G. Independent Component Analysis Applied to fMRI Data: A Generative Model for Validating Results. In *Neural Networks for Signal Processing XI, 2001. Proceedings of the 2001 IEEE Signal Processing Society Workshop*, pages 509–518. IEEE, 2001.
- Cavalcante, C. C. and Romano, J. M. T. Multi-User PDF Estimation Based Criteria for Adaptive Blind Separation of Discrete Sources. *Signal Processing*, 85(5):1059–1072, 2005.
- Chen, S. IIR Model Identification Using Batch-Recursive Adaptive Simulated Annealing Algorithm. *Proc. of 6th Annu. Chinese Autom. Comput. Sci. Conf., Loughborough, U.K.*, pages 151–155, 2000.

-
- Chen, S. and Luk, B. L. Digital IIR Filter Design Using Particle Swarm Optimisation. *International Journal of Modelling, Identification and Control*, 9(4):327–335, 2010.
- Chen, S. and Wu, Y. Maximum Likelihood Joint Channel and Data Estimation Using Genetic Algorithms. *IEEE Transactions on Signal Processing*, 46(5):1469–1473, 1998.
- Chen, S., Mulgrew, B., and Grant, P. M. A Clustering Technique for Digital Communications Channel Equalization Using Radial Basis Function Networks. *IEEE Transactions on Neural Networks*, 4(4):570–590, 1993.
- Coelho, R. F., Nascimento, V. H., de Queiroz, R. L., Romano, J. M. T., and Cavalcante, C. C. *Signals and Images: Advances and Results in Speech, Estimation, Compression, Recognition, Filtering, and Processing*. CRC Press, 2015.
- Comon, P. Independent Component Analysis, A New Concept? *Signal processing*, 36(3): 287–314, 1994.
- Comon, P. and Jutten, C. *Handbook of Blind Source Separation: Independent Component Analysis and Applications*. Academic Press, 2010.
- Cover, T. M. and Thomas, J. A. *Elements of Information Theory*. John Wiley, 1991.
- Cramér, H. Über eine Eigenschaft der normalen Verteilungsfunktion. *Mathematische Zeitschrift - Springer*, 41:405–414, 1936.
- De Castro, L. N. and Von Zuben, F. J. *Recent Developments in Biologically Inspired Computing*. Igi Global, 2005.
- Deville, Y. and Duarte, L. T. An Overview of Blind Source Separation Methods for Linear-Quadratic and Post-Nonlinear Mixtures. In *International Conference on Latent Variable Analysis and Signal Separation*, pages 155–167. Springer, 2015.
- Ding, Z., Kennedy, R., Anderson, B., and Johnson, C. Ill-Convergence of Godard Blind Equalizers in Data Communication Systems. *IEEE Trans. on Signal Processing*, 39: 1313–1327, 1991.
- Ding, Z., Kennedy, R. A., and Anderson, B. D. O. Local Convergence of Sato Blind Equalizer and Generalizations Under Practical Constraints. *IEEE Trans. on Information Theory*, 39(1):129–144, 1993.
- Duarte, L. T., Jutten, C., and Moussaoui, S. A Bayesian Nonlinear Source Separation Method for Smart Ion-Selective Electrode Arrays. *IEEE Sensors Journal*, 9(12):1763–1771, 2009.

-
- Duarte, L. T., Suyama, R., Rivet, B., Attux, R., Romano, J. M., and Jutten, C. Blind Compensation of Nonlinear Distortions: Application to Source Separation of Post-Nonlinear Mixtures. *IEEE Transactions on Signal Processing*, 60(11):5832–5844, 2012.
- Duda, R. O., Hart, P. E., and Stork, D. G. *Pattern Classification*. John Wiley & Sons, 2012.
- Erdogmus, D. and Principe, J. C. An Error-Entropy Minimization Algorithm for Supervised Training of Nonlinear Adaptive Systems. *IEEE Transactions on Signal Processing*, 50(7):1780 – 1786, 2002a.
- Erdogmus, D. and Principe, J. C. Generalized Information Potential Criterion for Adaptive System Training. *IEEE Transactions on Neural Networks*, 13(5):1035–1044, 2002b.
- Erdogmus, D. and Principe, J. C. From Linear Adaptive Filtering to Nonlinear Information Processing. *IEEE Signal Processing Magazine*, 23(2):14–33, 2006.
- Even, J. *Contributions à la Séparation de Sources à l'Aide de Statistiques d'Ordre*. PhD thesis, Université Joseph Fourier, Grenoble, 2003.
- Fantinato, D., Boccatto, L., Neves, A., and Attux, R. Multivariate PDF Matching via Kernel Density Estimation. *Proc. of the Symposium Series on Computational Intelligence (SSCI)*, 2014.
- Fantinato, D. G., Attux, R., Neves, A., Suyama, R., and Romano, J. M. T. Blind Deconvolution of Correlated Sources Based on Second-Order Statistics. *XXXI Simpósio Brasileiro de Telecomunicações*, 2013.
- Feintuch, P. L. An Adaptive Recursive LMS Filter. *Proceedings of the IEEE*, 64(11):1622–1624, 1976.
- Foschini, G. Equalization Without Altering or Detecting Data. *AT&T Technical Journal*, 64(8):1885–1911, 1985.
- Gauss, C. F. *Theoria Motus Corporum Coelestium in Sectionibus Conicis Solem Ambientium*. Hamburgi: sumtibus Frid. Perthes et I.H. Besser, 1809.
- Godard, D. Channel equalization using a kalman filter for fast data transmission. *IBM journal of Research and Development*, 18(3):267–273, 1974.
- Godard, D. Self-Recovering Equalization and Carrier Tracking in Two-Dimensional Data Communication Systems. *IEEE Trans. on Communications*, COM-28(11):1867–1875, 1980.

-
- Godfrey, R. and Rocca, F. Zero Memory Non-Linear Deconvolution. *Geophysical Prospecting*, 29:189–228, 1981.
- Goodwin, G. C. and Sin, K. S. *Adaptive Filtering Prediction and Control*. Prentice-Hall, Englewood Cliffs, NJ, 1984.
- Gunduz, A. and Principe, J. C. Correntropy as a Novel Measure for Nonlinearity Tests. *Signal Processing*, 89(1):14–23, 2009.
- Haykin, S. *Adaptive Filter Theory*. Prentice Hall, 3a. edition, 1996.
- Haykin, S. *Neural Networks: A Comprehensive Foundation*. Prentice Hall, 2a. edition, 1998.
- Haykin, S. *Communication Systems*. Wiley, 4th edition, 2001.
- Hérault, J., Jutten, C., and Ans, B. Détection de Grandeurs Primitives Dans Un Message Composite par Une Architecture de Calcul Neuromimétique en Apprentissage Non Supervisé. *Actes du Xème Colloque GRETSI*, pages 1017–1022, 1985.
- Horvath Jr., S. Adaptive IIR Digital Filters for On-Line Time-Domain Equalization and Linear Prediction. *IEEE Arden House Workshop on Digital Signal Processing*, 1976.
- Hosseini, S. and Jutten, C. On the Separability of Nonlinear Mixtures of Temporally Correlated Sources. *IEEE Signal Processing Letters*, 10(2):43–46, 2003.
- Hyvärinen, A., Karhunen, J., and Oja, E. *Independent Component Analysis*. Wiley, 2001.
- Johnson Jr., C. R. Adaptive IIR Filtering: Current Results and Open Issues. *IEEE Transactions on Information Theory*, 30(2):237–250, 1984.
- Jutten, C. and Karhunen, J. Advances in Blind Source Separation (BSS) and Independent Component Analysis (ICA) for Nonlinear Mixtures. *International Journal of Neural Systems*, 14(05):267–292, 2004.
- Jutten, C., Moussaoui, S., and Schmidt, F. How to Apply ICA on Actual Data? Example of Mars Hyperspectral Image Analysis. In *Digital Signal Processing, 2007 15th International Conference on*, pages 3–12. IEEE, 2007.
- Kakosyan, A., Klebanov, L., and Melamed, J. *Characterization of Distributions by the Method of Intensively Monotone Operators*, volume 1088 of *Lecture Notes in Mathematics*. Springer, 1984.
- Kolmogorov, A. N. Sur l'Interpolation et Extrapolation des Suites Stationnaires. *CR Acad. Sci*, 208:2043–2045, 1939.

-
- Kraskov, A., Stögbauer, H., and Grassberger, P. Estimating Mutual Information. *Physical Review E*, 69(6):066138, 2004.
- Krusienski, D. J. and Jenkins, W. K. Particle Swarm Optimization for Adaptive IIR Filter Structures. In *Congress on Evolutionary Computation*, volume 1, pages 965–970. IEEE, 2004.
- Lai, C.-A. *Global Optimization Algorithms for Adaptive Infinite Impulse Response Filters*. PhD thesis, Citeseer, 2002.
- Lai, C.-A. Global Optimization of Adaptive IIR Filters Using Renyi’s Quadratic Entropy. *Journal of Advanced Engineering*, 1(2):67–72, 2006.
- Lai, C.-A., Erdogmus, D., and Principe, J. C. Echo Cancellation by Global Optimization of Kautz Filters Using an Information Theoretic Criterion. In *Acoustics, Speech, and Signal Processing, 2003. Proceedings.(ICASSP’03). 2003 IEEE International Conference on*, volume 6, pages VI–197. IEEE, 2003.
- Lázaro, M., Santamaría, I., Pantaleón, C., Erdogmus, D., and Principe, J. Matched PDF-Based Blind Equalization. *IEEE Intern. Conf. on Acoustics, Speech, and Signal Proc.*, 4:IV – 297–300, 2003a.
- Lázaro, M., Santamaría, I., Pantaleón, C., Erdogmus, D., and Principe, J. C. Matched PDF-Based Blind Equalization. *IEEE Intern. Conf. on Acoustics, Speech, and Signal Proc.*, 4:IV – 297–300, 2003b.
- Lázaro, M., Santamaría, I., Erdogmus, D., Hild, K., Pantaleón, C., and Principe, J. Stochastic Blind Equalization Based on PDF Fitting Using Parzen Estimator. *IEEE Trans. on Signal Processing*, 53(2):696–704, 2005.
- LeBlanc, J. P., Dogancay, K., Kennedy, R. A., and Johnson, C. R. Effects of Input Data Correlation on the Convergence of Blind Adaptive Equalizers. In *IEEE International Conference on Acoustics, Speech, and Signal Processing*, volume 3, pages III–313. IEEE, 1994.
- Li, R., Liu, W., and Principe, J. C. A Unifying Criterion for Instantaneous Blind Source Separation Based on Correntropy. *Signal Processing*, 87(8):1872–1881, 2007.
- Liu, W., Pokharel, P. P., and Principe, J. C. Correntropy: A Localized Similarity Measure. In *Neural Networks, 2006. IJCNN’06. International Joint Conference on*, pages 4919–4924. IEEE, 2006.
- Ljung, L. *System Identification*. Springer, 1998.

-
- Ljung, L. and Söderström, T. *Theory and Practice of Recursive Identification*. Cambridge MIT Press, 1983.
- Long, G., Shwed, D., and Falconer, D. D. Study of a Pole-Zero Adaptive Echo Canceller. *IEEE Transactions on Circuits and Systems*, 34(7):765–769, 1987.
- Lucky, R. Automatic Equalization for Digital Communication. *Bell Systems Technical Journal*, 44:547–588, 1965.
- Macchi, O. *Adaptive Processing*. Jhon Wiley & Sons, 1996.
- Macchi, O. and Eweda, E. Convergence Analysis of Self-Adaptive Equalizers. *IEEE Trans. on Information Theory*, IT-30(2):161–176, 1984. Special Issue on Linear Adaptive Filtering.
- Makino, S., Sawada, H., Mukai, R., and Araki, S. Blind Source Separation of Convolutional Mixtures of Audio Signals in Frequency Domain. *Topics in Acoustic Echo and Noise Control Springer*, 2006.
- Marcinkiewicz, J. Sur Une Propriété de La Loi de Gauß. *Mathematische Zeitschrift - Springer*, 44:612–618, 1939.
- Mathews, V. J. and Sicuranza, G. L. *Polynomial Signal Processing*. Wiley, 2000.
- McCulloch, W. S. and Pitts, W. A logical calculus of the ideas immanent in nervous activity. *The bulletin of mathematical biophysics*, 5(4):115–133, 1943.
- Meganem, I., Deville, Y., Hosseini, S., Déliot, P., Briottet, X., and Duarte, L. T. Linear-Quadratic and Polynomial Non-Negative Matrix Factorization; Application to Spectral Unmixing. In *Signal Processing Conference, 2011 19th European*, pages 1859–1863. IEEE, 2011.
- Mendel, J. M. *Discrete Techniques of Parameter Estimation: The Equation Error Formulation*. Marcel Dekker, New York, 1973.
- Murray, W. A. *Numerical Methods for Unconstrained Optimization*. New York, Academic Press, 1972.
- Neves, A., Wada, C., Suyama, R., Attux, R., and Romano, J. M. T. An Analysis of Unsupervised Signal Processing Methods in the Context of Correlated Sources. *Lect. Notes in Computer Science*, 5441:82–89, 2009.
- Nose-Filho, K., Fantinato, D. G., Attux, R., Neves, A., and Romano, J. M. T. A Novel Entropy-based Equalization Performance Measure and Relations to L_p -Norm Deconvolution. In *XXXI Simpósio Brasileiro de Telecomunicações*, 2013.

-
- Oppenheim, A. V., Willsky, A. S., and Nawab, S. H. *Signals and Systems*. Prentice-Hall Signal Processing Series, 2nd edition, 1997.
- Papoulis, A. *Probability, Random Variables and Stochastic Processes*. Electrical & Electronic Engineering Series. McGraw-Hill International, New York, 3rd edition, 1991.
- Park, J. and Sandberg, I. W. Universal approximation using radial-basis-function networks. *Neural computation*, 3(2):246–257, 1991.
- Parzen, E. On the Estimation of a Probability Density Function and the Mode. *Ann. Math. Statist.*, 33:1065–1067, 1962.
- Pham, D. Blind Separation of Instantaneous Mixture of Sources Based on Order Statistics. *Signal Processing, IEEE Transactions on*, 48(2):363–375, 2000.
- Pham, D. Blind Separation of Instantaneous Mixture of Sources Via the Gaussian Mutual Information Criterion. *IEEE Transactions on Signal Processing*, 81:855–870, 2001.
- Pham, D. and Cardoso, J. Blind Separation of Instantaneous Mixtures of Non-Stationary Sources. *Signal Processing, IEEE Transactions on*, 49:1837–1848, 2001.
- Price, K., Storn, R. M., and Lampinen, J. A. *Differential Evolution: A Practical Approach to Global Optimization*. Springer, 2005.
- Principe, J. C. *Information Theoretic Learning Renyi's Entropy and Kernel Perspectives*. Springer, 2010.
- Principe, J. C., Xu, D., and Fisher, J. Information theoretic learning. *Unsupervised adaptive filtering*, 1:265–319, 2000.
- Proakis, J. G. and Manolakis, D. G. *Digital Signal Processing: Principles, Algorithms, and Application*. Prentice Hall, 1996.
- Regalia, P. *Adaptive IIR Filtering in Signal Processing and Control*, volume 90. CRC Press, 1994.
- Regalia, P. A. On the Equivalence Between the Godard and Shalvi-Weinstein Schemes of Blind Equalization. *Signal Processing*, 73(1-2):185–190, 1999.
- Rényi, A. Some Fundamental Questions of Information Theory. *Selected Papers of Alfred Rényi*, 2:526–552, 1976.
- Robbins, H. and Monro, S. A Stochastic Approximation Method. *The Annals of Mathematical Statistics*, 22:400–407, 1951.

-
- Romano, J. M. T., Attux, R. R. F., Cavalcante, C. C., and Suyama, R. *Unsupervised Signal Processing: Channel Equalization and Source Separation*. CRC Press, 2010.
- Rosenblatt, F. The perceptron: A probabilistic model for information storage and organization in the brain. *Psychological review*, 65(6):386, 1958.
- Ruggiero, M. A. G. and Lopes, V. L. d. R. *Cálculo numérico: aspectos teóricos e computacionais*. Makron Books do Brasil, 1997.
- Sala-Alvarez, J. and Vázquez-Grau, G. Statistical Reference Criteria for Adaptive Signal Processing in Digital Communications. *IEEE Transactions on Signal Processing*, 45(1):14–31, 1997.
- Santamaría, I., Erdogmus, D., and Principe, J. C. Entropy Minimization for Supervised Digital Communications Channel Equalization. *IEEE Transactions on Signal Processing*, 50(5):1184–1192, 2002.
- Santamaría, I., Pantaleón, C., Vielva, L., and Principe, J. C. A Fast Algorithm for Adaptive Blind Equalization Using Order- α Renyi's Entropy. *Proceedings of the International Conference on Acoustics*, 3:III–2657–III–2660, 2002a.
- Santamaría, I., Pantaleón, C., Vielva, L., and Principe, J. C. Adaptive Blind Equalization Through Quadratic PDF Matching. *Proc. Eur. Signal Process. Conf.*, II:289–292, 2002b.
- Santamaría, I., Pokharel, P., and Principe, J. Generalized Correlation Function: Definition, Properties and Application to Blind Equalization. *IEEE Trans. on Signal Processing*, 54:2187–2197, 2006.
- Sato, Y. A Method of Self-Recovering Equalization for Multilevel Amplitude-Modulation Systems. *IEEE Trans. on Communications*, 23(6):679–682, 1975.
- Scott, D. W. *Multivariate Density Estimation: Theory, Practice, and Visualization*. John Wiley & Sons, 1992.
- Scott, D. W. *Multivariate Density Estimation: Theory, Practice, and Visualization*. Wiley Series in Probability and Statistics. Wiley, 2 edition, 2015.
- Shalvi, O. and Weinstein, E. New Criteria for Blind Deconvolution of Nonminimum Phase Systems (Channels). *IEEE Trans. on Information Theory*, 36(2):312–321, 1990.
- Shalvi, O. and Weinstein, E. Super-Exponential Methods for Blind Deconvolution. *IEEE Trans. on Information Theory*, 39:504–519, 1993.

-
- Shannon, C. E. A Mathematical Theory of Communications. *Bell Systems Technical Journal*, 27:623–656, 1948.
- Shynk, J. J. Adaptive IIR Filtering. *IEEE ASSP Magazine*, 6(2):4–21, 1989.
- Silva, D., Fantinato, D., Canuto, J., Duarte, L., Neves, A., Suyama, R., Montalvão, J., and Attux, R. An Introduction to Information Theoretic Learning, Part I: Foundations. *Journal of Communication and Information Systems*, 31(1), 2016. doi: 10.14209/jcis.2016.6.
- Silva, L. M., de Sá, J. M., and Alexandre, L. A. Neural Network Classification Using Shannon's Entropy. In *European Symposium on Artificial Neural Networks*, pages 217–222, 2005.
- Silverman, B. W. Density Ratios, Empirical Likelihood and Cot Death. *Applied Statistics*, pages 26–33, 1978.
- Silverman, B. W. *Density Estimation for Statistics and Data Analysis*, volume 26. CRC Press, 1986.
- Singh, A. and Príncipe, J. Using Correntropy as a Cost Function in Linear Adaptive Filters. In *Proc. Of International Joint Conference on Neural Networks, Atlanta, USA*, pages 2950–2955, 2009.
- Steuer, R., Kurths, J., Daub, C. O., Weise, J., and Selbig, J. The Mutual Information: Detecting and Evaluating Dependencies Between Variables. *Bioinformatics*, 18(suppl 2):S231–S240, 2002.
- Storn, R. and Price, K. Differential Evolution - A Simple and Efficient Heuristic for Global Optimization over Continuous Spaces. *Journal of Global Optimization*, 11:341–359, 1997.
- Taleb, A. and Jutten, C. Source Separation in Post-Nonlinear Mixtures. *IEEE Transactions on signal Processing*, 47(10):2807–2820, 1999.
- Thomas, E. Some considerations on the application of the volterra representation of nonlinear networks to adaptive echo cancellers. *Bell System Technical Journal*, 50(8): 2797–2805, 1971.
- Tong, L., Liu, R.-W., Soon, V. C., and Huang, Y.-F. Indeterminacy and Identifiability of Blind Identification. *IEEE Transactions on circuits and systems*, 38(5):499–509, 1991.
- Treichler, J. and Agee, B. New Approach to Multipath Correction of Constant Modulus Signals. *IEEE Trans. Acoust., Speech and Signal Processing*, ASSP-31(2):459–472, 1983.

-
- Treichler, J. R. Adaptive Algorithms for Infinite Impulse Response Filters. In Cowen, C. F. N. and Grant, P. M., editors, *Adaptive Filters*, chapter 4, pages 60–90. Englewood Cliffs, NJ: Prentice-Hall, 1985.
- Vapnik, V. *The Nature of Statistical Learning Theory*. Springer Verlag, New York, 1995.
- Wang, Z. and Bovik, A. C. Mean Squared Error: Love It or Leave It? A New Look at Signal Fidelity Measures. *IEEE signal processing magazine*, 26(1):98–117, 2009.
- Werbos, P. J. *Beyond Regression: New Tools for Prediction and Analysis in the Behavioral Sciences*. PhD thesis, Ph. D Dissertation, Harvard University, Department of Applied Mathematics, 1974.
- White, S. A. Restoration of Nonlinearly Distorted Audio by Histogram Equalization. *Journal of the Audio Engineering Society*, 30(11):828–832, 1982.
- Widrow, B. Adaptive filters. *Aspects of network and system theory*, pages 563–587, 1971.
- Widrow, B., McCool, J., and Ball, M. The Complex LMS Algorithm. *Proc. IEEE*, 63: 719–720, 1975.
- Widrow, B., McCool, J. M., Larimore, M. G., and Johnson Jr., C. R. Stationary and Nonstationary Learning Characteristics of the LMS Adaptive Filter. *Proceedings of the IEEE*, 64(8):1151–1162, 1976.
- Wiener, N. *Extrapolation, interpolation, and smoothing of stationary time series*, volume 2. MIT press Cambridge, 1949.
- Yang, Z., Walden, A. T., and McCoy, E. J. Correntropy: Implications of nonGaussianity for the moment expansion and deconvolution. *Signal Processing*, 91(4):864–876, 2011.
- Yu, G., Sapiro, G., and Mallat, S. Solving Inverse Problems with Piecewise Linear Estimators: From Gaussian Mixture Models to Structured Sparsity. *IEEE Transactions on Image Processing*, 21(5):2481–2499, 2012.
- Ziehe, A. and Müller, K.-R. TDSEP-An efficient Algorithm for Blind Separation Using Time Structure. In *ICANN 98*, pages 675–680. Springer, 1998.
- Ziehe, A., Kawanabe, M., Harmeling, S., and Müller, K.-R. Blind Separation of Post-Nonlinear Mixtures Using Linearizing Transformations and Temporal Decorrelation. *Journal of Machine Learning Research*, 4(Dec):1319–1338, 2003.